TABLE OF CONTENTS

Page intentionally left blank.

LIST OF TABLES

LIST OF TABLES (CONT.)

LIST OF FIGURES

LIST OF FIGURES (CONT.)

LIST OF FIGURES (CONT.)

LIST OF FIGURES (CONT.)

LIST OF FIGURES (CONT.)

Page intentionally left blank.

2.5.2 Vibratory Ground Motion

This section provides a detailed description of the vibratory ground motion assessment that was carried out for the VEGP ESP site resulting in the development of the VEGP ESP site Ground Motion Response Spectrum (GMRS). This assessment was performed to address seismic hazard update guidance in Regulatory Guide 1.165, Identification and Characterization of Seismic Sources and Determination of Safe Shutdown Earthquake Ground Motion, Rev. 0, March 1997 (RG 1.165), and meet the SSE requirements in paragraph (d) of 10CFR 100.23. The starting point for this site assessment is the EPRI-SOG probabilistic seismic hazard analysis (PSHA) evaluation **(EPRI NP-6395-D 1989)**.

Section 2.5.2.1 through Section 2.5.2.4 document the review and update of the available EPRI seismicity, seismic source, and ground motion models. Section 2.5.2.5 summarizes information about the seismic wave transmission characteristics of the ESP site with reference to more detailed discussion of all engineering aspects of the subsurface in Section 2.5.4.

Section 2.5.2.6 describes the development of the horizontal GMRS for the VEGP ESP site. The selected ground motion is based on the risk-consistent/performance-based approach from NUREG/CR-6728 **(McGuire et al. 2001)** and ASCE 43-05 **(ASCE 2005)**. Site-specific horizontal ground motion amplification factors are developed using site-specific estimates of near-surface rock, soil, and engineered backfill properties. These amplification factors are then used to scale the hard rock spectra to develop Uniform Hazard Spectra (UHS) accounting for site-specific conditions using Approach 2A of NUREG/CR-6769. Horizontal GMRS spectra are developed from these ground surface Uniform Hazard Spectra (UHS) using the performance-based approach of ASCE 43-05. Companion outcrop motions are defined in Section 2.5.2.6 for the highest competent in situ layer and at the depth of the bottom of the Nuclear Island basemat. The highest competent in situ layer is at the top of the Blue Bluff Marl, at a depth of 86 ft. The bottom of the Nuclear Island basemat is at a depth of 40 ft. See Sections 2.5.4 and 2.5.2.5 for further discussion of the subsurface conditions.

Ratios of vertical to horrizontal motions appropriate to the site area are developed in Section 2.5.2.7 and applied to the horizontal spectra to derive recommended vertical spectra.

The GMRS described in this section are considered performance goal-based (risk-informed) site-specific response spectra. The spectra at the top of the Blue Bluff Marl reflect the seismic hazard in terms of a PSHA and **in situ** geologic characteristics of the site. The spectra at the bottom of the Nuclear Island basemat are used to define the Foundation Input Response Spectra (FIRS) used to help confirm the adequacy of the Certified Seismic Design Response Spectra (CSDRS) design basis of the Nuclear Island.

The site-specific SSE motion of Section 3.7.1 of the COLA is consistent with the description of the free-field ground motion at the site provided in this Section 2.5.2. The OBE is discussed in Section 2.5.2.8.

Finally, two complementary sensitivity studies, incorporating information from supplemental site-specific subsurface investigations, are discussed in Section 2.5.2.9.

2.5.2.1 Seismicity

The seismic hazard analysis conducted by EPRI (NP-6395-D 1989) relied on an analysis of historical seismicity in the Central and Eastern United States (CEUS) to estimate seismicity parameters (rates of activity and Richter b-values) for individual seismic sources. The historical earthquake catalog used in the EPRI analysis was complete through 1984. The earthquake data for the site region occurring since 1984 was reviewed and used to update the EPRI catalog.

2.5.2.1.1 Regional Seismicity Catalog Used for 1989 EPRI Seismic Hazard Analysis Study

Many seismic networks record earthquakes in the CEUS. A large effort was made during the EPRI seismic hazard analysis study to combine available data on historical earthquakes and to develop a homogeneous earthquake catalog that contained all recorded earthquakes for the region. "Homogeneous" means that estimates of body-wave magnitude, m_b, for all earthquakes are consistent, that duplicate earthquakes have been eliminated, that non-earthquakes (e.g., mine blasts and sonic booms) have been eliminated, and that significant events in the historical record have not been missed. Thus, the EPRI catalog **(EPRI NP-4726-A 1988)** forms a strong basis on which to estimate seismicity parameters.

2.5.2.1.2 Updated Seismicity Data

NRC Regulatory Guide 1.165, Identification and Characterization of Seismic Sources and Determination of Safe Shutdown Earthquake Ground Motion, Revision 0, March 1997 (RG 1.165) specifies that earthquakes of Modified Mercalli Intensity (MMI) greater than or equal to IV or magnitude greater than or equal to 3.0 should be listed for seismic sources "any part of which is within a radius of 200 mile (320 km) of the site (the site region)." In updating the EPRI catalog a latitude-longitude window of 30° to 37° N, 78° to 86° W was used. This window incorporates the 200 mi (320 km) radius "site region" and all seismic sources contributing significantly to VEGP ESP site earthquake hazard Figure 2.5.1-1 shows the VEGP ESP site and its associated site region. Figures 2.5.2-1 through 2.5.2-6 show this site region and the defined latitude-longitude window.

The updated catalog was compiled from the following sub-catalogs:

EPRI Catalog. The various data fields of the EPRI catalog are described in EPRI NP-4726-A 1988.

SEUSSN Catalog. The SEUSSN catalog is available from the Virginia Tech Seismological Observatory FTP site **(SEUSSN 2005)**. On the June 3, 2005 date of the catalog update, the SEUSSN catalog had 2,483 records dating from March 1698 to December 2003 within the site region latitude-longitude window. Of these, 1,355 records occurred in 1985 or later.

ANSS Catalog. The ANSS catalog **(ANSS 2005)** was searched on June 3, 2005, for all records within the site region latitude-longitude window, resulting in 1,710 records from 1928 to April 14, 2005. Of these, 1,375 records occurred in 1985 or later.

The Southeastern US Seismic Network (SEUSSN) and Advanced National Seismic System (ANSS) catalogs were used for the temporal update (1985 to present) of the EPRI seismicity catalog. The SEUSSN has coverage over the entire site region (defined above) and is the primary catalog used to compile the national ANSS seismicity catalog. While the SEUSSN catalog is taken as the preferred catalog, some additional events listed only in the ANSS catalog are also included in the update.

The magnitudes given in both catalogs were converted to best or expected estimate of m_b magnitude ($E[m_b]$, also called Emb), using the conversion factors given as equation 4-1 and Table 4-1 in EPRI NP-4726-A 1988:

$$Emb = 0.253 + 0.907 \cdot Md \qquad \text{(Equation 2.5.2-1)}$$

$$Emb = 0.655 + 0.812 \cdot ML \qquad \text{(Equation 2.5.2-2)}$$

where Md is duration or coda magnitude and ML is “local” magnitude.

Equation 4-2 of EPRI (NP-4726-A 1988) indicates that the equation from which mb* or Rmb is estimated from the best estimate of magnitude $E[m_b]$ or Emb and the variance of m_b, σ^2_{mb}, or Smb^2 is :

$$m_b^* = E[m_b] + (1/2) \cdot ln(10) \cdot b \cdot \sigma^2_{mb} \qquad \text{(Equation 2.5.2-3)}$$

where b = 1.0.

Values for σ^2_{mb} or Smb were estimated for the two catalogs, and m_b [Rmb] was assigned to each event added to the updated catalog.

The result of the above process was a catalog of 61 earthquakes shown in Table 2.5.2-1 as the update of the EPRI NP-4726-A seismicity catalog recommended for the site region. For the purpose of recurrence analysis, these should be considered independent events.

The 61 events in the 30° to 37° N, 78° to 86° W latitude-longitude window, incorporating the 200 mi (320 km) radius site region, from 1985 to April 2005 with Emb magnitude 3.0 or greater have been incorporated into a number of figures, including tectonic features discussed in Section 2.5.1 and EPRI Earth Science Team source maps in this section.

2.5.2.2 Geologic Structures and EPRI Seismic Source Model for the Site Region

As described in Section 2.5.1, a comprehensive review of available geological, seismological, and geophysical data has been performed for the VEGP ESP site region and adjoining areas. The following sections summarize seismic source interpretations from the 1989 EPRI probabilistic seismic hazard analysis (PSHA) study **(EPRI NP-6395-D 1989)** and from relevant

post-EPRI seismic source characterization studies and the updated interpretations of new and existing sources based on more recent data.

Since publication of the EPRI seismic source model, significant new information has been developed for assessing the earthquake source that produced the 1886 Charleston earthquake. This new information shows that the Charleston seismic source should be updated according to RG 1.165. Paleoliquefaction features and other new information published since the 1986 EPRI project **(EPRI NP-4726 1986)** have significant implications regarding the geometry, M_{max}, and recurrence of M_{max} in the Charleston seismic source. Results from the 1989 EPRI study also show that the Charleston seismic source is the most significant contributor to seismic hazard at the VEGP ESP site **(EPRI NP-6395-D 1989)**. Thus, an update of the Charleston seismic source has been developed as part of the work performed for this ESP application. Details of the Updated Charleston Seismic Source (UCSS) model are presented in Section 2.5.2.2.2.4 and in a separate Engineering Study Report **(Bechtel 2006d)**.

Sensitivity studies were performed to evaluate the potential significance of the UCSS model to seismic hazard at the VEGP ESP site, as described in detail in Section 2.5.2.4. Based on this analysis, it is found that the UCSS interpretations for the Charleston area show that the Charleston seismic source still dominates the seismic hazard at the VEGP ESP site. These new interpretations of the possible locations, sizes, and recurrence intervals of large earthquakes in the Charleston area form a strong basis with which to calculate the seismic ground motion hazard for the site.

2.5.2.2.1 Summary of EPRI Seismic Sources

This section summarizes the seismic sources and parameters used in the 1986 EPRI project (**EPRI NP-4726 1986)**. The description of seismic sources is limited to those sources within 200 mi of the VEGP ESP site (i.e., the site region) and those at distances greater than 200 mi that may affect the hazard at the VEGP ESP site.

In the 1986 EPRI project, six independent Earth Science Teams (ESTs) evaluated geological, geophysical, and seismological data to develop a model of seismic sources in the CEUS. These sources were used to model the occurrence of future earthquakes and evaluate earthquake hazards at nuclear power plant sites across the CEUS.

The six ESTs involved in the 1986 EPRI project were Bechtel Group, Dames & Moore, Law Engineering, Rondout Associates, Weston Geophysical Corporation, and Woodward-Clyde Consultants. Each team produced a report (volumes 5 through 10 of EPRI NP-4726) providing detailed descriptions of how they identified and defined seismic sources. The results were implemented into a PSHA study **(EPRI NP-6395-D 1989)**. For the computation of hazard in the 1989 study, a few seismic source parameters were modified or simplified from the original parameters determined by the six ESTs. EPRI NP-6452-D (1989) summarized the parameters used in the final PSHA calculations, and this reference is the primary source for the seismicity

parameters used in this current ESP application. Each EST provides more detailed descriptions of the rationale and methodology used in evaluating tectonic features and establishing the seismic sources (refer to volumes 5 through 10 of EPRI NP-4726).

The most significant seismic sources **(EPRI NP-6395-D 1989)** developed by each EST are shown in Figures 2.5.2-1 through 2.5.2-6. For the 1989 EPRI seismic hazard calculations, a screening criterion was implemented to identify those sources whose combined hazard exceeded 99 percent of the total hazard from all sources, for two ground motions measures **(EPRI NP-6395-D 1989)**. These sources are identified in the descriptions below as "primary" seismic sources. Other sources, which together contributed less than one percent of the total hazard from all sources for the two ground motion measures, are identified in the descriptions below as "additional" seismic sources. Earthquakes with body-wave magnitude m_b 3.0 are also shown in Figures 2.5.2-1 through 2.5.2-6 to show the spatial relationships between seismicity and seismic sources. Earthquake epicenters include both events from the EPRI earthquake catalog and for the period between 1985 and April 2005 as described in Section 2.5.2.1.2.

The maximum magnitude, interdependencies, and probability of activity for each EPRI EST's seismic sources are presented in Tables 2.5.2-2 through 2.5.2-7. These tables present the parameters assigned to each source within 200 mi of the VEGP ESP site and include primary and additional seismic sources as defined above. The tables also indicate whether new information has been identified that would lead to a revision of the source's geometry, maximum magnitude, or recurrence parameters. The seismicity recurrence parameters (a- and b-values) used in the seismic hazard studies were computed for each 1° latitude and longitude cell that intersects any portion of a seismic source.

The nomenclature used by each EST to describe the various seismic sources in the CEUS varies from team to team. In other words, a number of different names may have been used by the EPRI teams to describe the same or similar tectonic features or sources, or one team may describe seismic sources that another team does not. For example**,** the Charleston seismic source was modeled by each team but was called the Charleston Area and Charleston Faults by the Bechtel Group team; the Charleston Seismic Zone by the Dames & Moore, Law, and Weston teams; and Charleston by the Rondout and Woodward-Clyde teams. Each team's source names, data, and rationale are included in its team-specific documentation (volumes 5 through 10 of EPRI NP-4726).

The EPRI PSHA study expressed maximum magnitude (M_{max}) values in terms of body-wave magnitude (m_b), whereas most modern seismic hazard analyses describe M_{max} in terms of moment magnitude (**M**). To provide a consistent comparison between magnitude scales, this study relates body-wave magnitude to moment magnitude using the arithmetic average of three equations, or their inversions, presented in Atkinson and Boore (1995), Frankel et al (1996), and EPRI TR-102293 (1993). The conversion relations are very consistent for magnitudes 4.5 and greater and begin to show divergence at lower magnitudes. (Table 2.5.2-23 lists m_b and **M**

equivalences developed from these relations over the range of interest for this study.) Throughout this section, the largest assigned values of M_{max} distributions assigned by the ESTs to seismic sources are presented for both magnitude scales (m_b and **M**) to give perspective on the maximum earthquakes that were considered possible in each seismic source. For example, EPRI m_b values of M_{max} are followed by the equivalent **M** value.

The following sections describe the most significant EPRI sources (both primary and additional seismic sources) for each EST with respect to the VEGP ESP site. Assessment of these and other EPRI sources within the site region shows that the EPRI source parameters (M_{max}, geometry, and recurrence) are sufficient to capture the current understanding of the seismic hazard in the site region.

Except for the Charleston seismic source, no new geological, geophysical, or seismological information in the literature published since the EPRI NP-6395-D source model suggests that these sources should be modified. Each EST's characterization of the Charleston seismic source was replaced by four alternative source geometries. For each geometry, large earthquake occurrences (**M** 6.7 to 7.5) were modeled with a range of mean recurrence rates, and smaller earthquakes (m_b 5 to 6.7) were modeled with an exponential magnitude distribution, with rates and b-values determined from historical seismicity. Also, all surrounding sources for each team were redrawn so that the new Charleston source geometries were accurately represented as a "hole" in the surrounding source, and seismic activity rates and b-values were recalculated for the modified surrounding sources, based on historical seismicity. Further details and the results of sensitivity analyses performed on the modified seismic sources are presented in Section 2.5.2.4.

2.5.2.2.1.1 Sources Used for EPRI PSHA – Bechtel Group

Bechtel Group identified and characterized six primary seismic sources. All six of these primary seismic sources are located within the site region (200 mi); they are:

- Charleston Area (H)
- Charleston Faults (N3)
- Atlantic Coastal Region (BZ4)
- S Appalachians (BZ5)
- SE Appalachians (F)
- NW South Carolina (G)

Bechtel Group also characterized four additional seismic sources. These additional seismic sources are:

- Eastern Mesozoic Basins (13)
- Bristol Trends (24)

- Rosman Fault (15)
- Belair Fault (16)

Primary and additional seismic sources characterized by the Bechtel Group team within the site region are listed in Table 2.5.2-2. A map showing the locations and geometries of the Bechtel primary seismic sources is provided in Figure 2.5.2-1. Following is a brief discussion of each of the primary seismic sources characterized by the Bechtel Group team.

Charleston Area (H). The Charleston Area source (H) is located about 60 mi from the VEGP ESP site. This oblong combination source area is defined based on the historic earthquake pattern (including the Middleton Place-Summerville and Bowman seismic zones), is elongated northwest-southeast, and encompasses all of source zone N3 (described below). Sources H and N3 are interdependent; if N3 is active, it is unlikely that H is active, and vice versa. The largest M_{max} assigned by Bechtel Group to this zone is m_b 7.4 (**M** 7.9), reflecting its assumption that Charleston-type earthquakes are produced within this zone.

Charleston Faults (N3). The Charleston Faults (N3) source zone is a small area set within the Charleston Area (H) source zone and encompassing a number of identified and postulated faults in the Charleston, South Carolina, area, including the Ashley River, Charleston, and Woodstock faults. Source N3 is located approximately 85 mi from the VEGP ESP site. Sources H and N3 are interdependent; if N3 is active, it is unlikely that H is active, and vice versa. According to EPRI NP-4726, this combination was created for computational simplicity. The largest M_{max} assigned by the Bechtel Group team to this zone is m_b 7.4 (**M** 7.9), reflecting its assumption that Charleston-type earthquakes are produced within this zone.

Atlantic Coastal Region (BZ4). The VEGP ESP site is located within the Atlantic Coastal Region background source (BZ4). Source BZ4 is a large background zone that extends from offshore New England to Alabama and encompasses portions of the Coastal Plain from Georgia to southern Virginia. The largest M_{max} assigned by the Bechtel Group team to this zone is m_b 7.4 (**M** 7.9), reflecting its assumption that there is a small probability that a Charleston-type earthquake could occur within this region.

S Appalachians (BZ5). The Southern Appalachians background source (BZ5) is located about 10 mi from the VEGP ESP site. This source is a large background region that extends from New York to Alabama, including portions of the Southern Appalachians, Piedmont, and Coastal Plain. The largest M_{max} assigned by the Bechtel Group team to this zone is m_b 6.6 (**M** 6.5).

SE Appalachians (F). The VEGP ESP site is located about 10 mi from the Southeastern Appalachians source (F), a combination source zone that includes parts of Georgia and the Carolinas and flanks the southwest and northeast borders of Zone G (described below). Source Zone F is mutually exclusive with Zone G; if F is active, G is inactive, and vice versa. The largest M_{max} assigned by the Bechtel Group team to this zone is m_b 6.6 (**M** 6.5).

NW South Carolina (G). The VEGP ESP site is located about 10 mi from the Northwestern South Carolina combination source (G). Source Zone G is mutually exclusive with Zone F; if G is active, F is inactive, and vice versa. The largest M_{max} assigned by the Bechtel Group team to this zone is m_b 6.6 (**M** 6.5).

2.5.2.2.1.2 Sources Used for EPRI PSHA – Dames & Moore

Dames & Moore identified and characterized five primary seismic sources. All five of these seismic sources are located within the site region; they are:

- Charleston Seismic Zone (54)
- Charleston Mesozoic Rift (52)
- S Appalachian Mobile Belt (Default Zone) (53)
- S Cratonic Margin (Default Zone) (41)
- S Coastal Margin (20)

Dames & Moore also identified seven additional seismic sources within the site region. These sources are:

- Appalachian Fold Belts (4)
- Kink in Fold Belt (4A)
- Jonesboro Basin (49)
- Buried Triassic Basins (50)
- Florence Basin (51)
- Dunbarton Triassic Basin (65)
- Combination Zone 4A-4B-4C-4D (C01)

Primary and additional seismic sources characterized by the Dames & Moore team within the site region are listed in Table 2.5.2-3. A map showing the locations and geometries of the Dames & Moore primary seismic sources is provided in Figure 2.5.2-2. Following is a brief discussion of these primary seismic sources.

Charleston Seismic Zone (54). The Charleston Seismic Zone (54) is a northwest-southeast oriented polygon located about 45 mi from the VEGP ESP site. This source includes the Ashley River, Woodstock, Helena Banks, and Cooke faults, as well as the Bowman and Middleton Place-Summerville seismic zones and was designed to capture the occurrence of Charleston-type earthquakes. The largest M_{max} assigned by the Dames & Moore team to this zone is m_b 7.2 (**M** 7.5).

Charleston Mesozoic Rift (52). The Charleston Mesozoic Rift source (52) is a large polygon located less than 5 mi from the VEGP ESP site. This source extends from offshore South

Carolina to Gulf Shore Florida, including portions of the South Carolina and Georgia Coastal Plain. The largest M_{max} assigned by the Dames & Moore team to this zone is m_b 7.2 (**M** 7.5).

S Appalachian Mobile Belt (Default Zone) (53). The VEGP ESP site is located within the Southern Appalachian Mobile Belt (Default Zone) source (53). This default zone comprises crustal rocks that have undergone several periods of divergence and convergence. The source is bounded on the east by the East Coast magnetic anomaly and on the west by the westernmost boundary of the Appalachian gravity gradient. The largest M_{max} assigned by the Dames & Moore team to this zone is m_b 7.2 (**M** 7.5).

S Cratonic Margin (Default Zone) (41). The Southern Cratonic Margin (Default Zone) source is located about 65 mi from the VEGP ESP site. This large default zone is located between the Appalachian Fold Belt (4) and the Southern Appalachian Mobile Belt (53) and includes the region of continental margin deformed during Mesozoic rifting. Located within this default zone are many Triassic basins and border faults. The largest M_{max} assigned by the Dames & Moore team to this zone is m_b 7.2 (**M** 7.5).

S Coastal Margin (20). The Southern Coastal Margin regional source (20) is located approximately 90 mi from the VEGP ESP site. This zone is roughly parallel to the rifted continental margin from Texas to Alabama and incorporates a region of diffuse seismicity. Located within this source is a down-warped wedge of miogeosynclinal sediments of Cretaceous age and younger. The largest M_{max} assigned by the Dames & Moore team to this zone is m_b 7.2 (**M** 7.5).

2.5.2.2.1.3 Sources Used for EPRI PSHA – Law Engineering

Law Engineering identified and characterized 15 primary seismic sources all within the site region; They are:

- Charleston Seismic Zone (35)
- Eastern Basement (17)
- Reactivated E Seaboard Normal (22)
- Brunswick, NC Background (108)
- Mesozoic Basins (8 – Bridged) (C09)
- 8 – 35 (C10)
- 22 – 35 (C11)
- Eight mafic pluton sources (M33 and M36 through M42)

Law Engineering also characterized five additional seismic sources within the site region that do not contribute to 99 percent of the hazard at the VEGP ESP site. These are:

- Eastern Basement Background (217)

- Eastern Piedmont (107)
- 22 – 24 – 35 (GC13)
- 22 – 24 (GC12)
- Mesozoic Basins (8)

Primary and additional seismic sources characterized by the Law Engineering team within the site region are listed in Table 2.5.2-4. A map showing the locations and geometries of the Law Engineering primary seismic sources is provided in Figure 2.5.2-3. Following is a brief discussion of Law's primary seismic sources

Charleston Seismic Zone (35). The Charleston Seismic Zone source (35) is a northeast-southwest elongated polygon that includes the Charleston, Ashley River, and Woodstock faults, as well as parts of the offshore Helena Banks fault and most of the more recently discovered liquefaction features identified by Amick (1990). This source was designed to capture the occurrence of Charleston-type earthquakes. This source is located about 75 mi from the VEGP ESP site and overlaps with the Reactivated E Seaboard Normal (22; described below) and Buried Mesozoic Basins (8; not a 99 percent contributor) sources. The largest M_{max} assigned by the Law Engineering team to this zone is m_b 6.8 (**M** 6.8).

Eastern Basement (17). The VEGP ESP site is located 90 mi from the Eastern Basement (17) source. This source was defined as an area containing pre-Cambrian and Cambrian normal faults, developed during the opening of the proto-Atlantic Ocean, in the basement rocks beneath the Appalachian decollement. The Giles County and eastern Tennessee zones of seismicity are included in this source. The largest M_{max} assigned by the Law Engineering team to this zone is m_b 6.8 (**M** 6.8).

Reactivated E Seaboard Normal (22). The VEGP ESP site is located within the Reactivated Eastern Seaboard Normal (22) source. This source was characterized as a region along the eastern seaboard in which Mesozoic normal faults are reactivated as high-angle reverse faults. The Law Engineering team assigned a single M_{max} of m_b 6.8 (**M** 6.8) to this zone.

Brunswick, NC Background (108). The VEGP ESP site is located within the Brunswick NC Background source zone (108). The source 108 site represents a zone defined by a low-amplitude, long-wavelength magnetic anomaly pattern. The Law Engineering team interpreted this pattern as possibly indicating a zone of Mesozoic extended crust. The largest M_{max} assigned by the Law Engineering team to this zone is m_b 6.8 (**M** 6.8).

Mesozoic Basins (8 – Bridged) (C09). The VEGP ESP site is located within the Mesozoic Basins (C09) source, which comprises eight bridged basins. This source was defined based on northeast-trending sediment-filled troughs in basement rock bounded by normal faults. The largest M_{max} assigned by the Law Engineering team to this zone is m_b 6.8 (**M** 6.8).

8 – 35 (C10). The VEGP ESP site is located within the 8 – 35 combination source (C10). The largest M_{max} assigned by the Law Engineering team to this zone is m_b 6.8 (**M** 6.8).

22 – 35 (C11). The VEGP ESP site is located within the 22 – 35 combination source (C11). The largest M_{max} assigned by the Law Engineering team to this zone is m_b 6.8 (**M** 6.8).

Eight Mafic Pluton Sources (M33 and M36 through M42). The Law Engineering team identified a number of mafic pluton sources, eight of which are located within about 130 mi of the VEGP ESP site. The Law Engineering team considered pre- and post-metamorphic plutons in the Appalachians to be stress concentrators and, thus, earthquake sources. Law Engineering assigned a single M_{max} of m_b 6.8 (**M** 6.8) to all mafic pluton sources.

2.5.2.2.1.4 Sources Used for EPRI PSHA – Rondout Associates

Rondout Associates characterized two primary seismic sources both within the site region; they are:

- Charleston (24)
- South Carolina (26)

Rondout Associates also identified eight additional seismic sources within the site region. These are:

- Appalachian (49)
- Background 49 (C01)
- 49 + 32 (C09)
- Grenville (50)
- Background 50 (C02)
- 50 (02) + 12 (C07)
- Southern Appalachians (25)
- Tennessee-VA Border Zone (27)

Primary and additional seismic sources characterized by the Rondout Associates team within the site region are listed in Table 2.5.2-5. A map showing the locations and geometries of the Rondout Associates primary seismic sources is provided in Figure 2.5.2-4. Following is a brief discussion of both of these primary seismic sources.

Charleston (24). The Charleston source is a northwest-southeast-oriented area set within the larger South Carolina (26) source and located about 35 mi from the VEGP ESP site. Source 24 includes the Helena Banks, Charleston, Ashley River, and Woodstock faults, as well as the Bowman and Middleton Place-Summerville seismic zones, and was designed to capture the occurrence of Charleston-type earthquakes. The largest M_{max} assigned by the Rondout Associates team to this zone is m_b 7.0 (**M** 7.2).

South Carolina (26). The VEGP ESP site is located within the South Carolina source (26). The South Carolina source (26) is a northwest-southeast elongated area that surrounds, but does not

include, Source 24 (described above). Source 26 includes most of South Carolina except the Charleston area. The largest M_{max} assigned by the Rondout Associates team to this zone is m_b 6.8 (**M** 6.8).

2.5.2.2.1.5 Sources Used for EPRI PSHA – Weston Geophysical

Weston Geophysical identified and characterized 12 primary seismic sources, all within the site region; they are:

- Charleston Seismic Zone (25)
- South Carolina (26)
- Southern Coastal Plain (104)
- 103 – 23 – 24 (C19)
- 104 – 22 (C20)
- 104 – 25 (C21)
- 104 – 22 – 26 (C23)
- 104 – 22 – 25 (C24)
- 104 – 28BCDE – 22 (C26)
- 104 – 28BCDE – 22 – 25 (C27)
- 26 – 25 (C33)
- 104 – 28BE – 25 (C35)

Weston Geophysical also characterized 13 additional seismic sources within the site region. These sources are:

- 104 – 26 (C22)
- 104 – 28BE – 26 (C34)
- 104 – 28BCDE (C25)
- 104 – 28BCDE – 22 – 26 (C28)
- Zone of Mesozoic Basin (28B)
- 28A through E (C01)
- Southern Appalachians (103)
- 103 – 23 (C17)
- 103 – 24 (C18)
- Zone of Mesozoic Basin (28D)
- Zone of Mesozoic Basin (28E)
- Appalachian Plateau (102)

- New York-Alabama-Clingman (24)

Primary and additional seismic sources characterized by the Weston Geophysical team are listed in Table 2.5.2-6. A map showing the locations and geometries of the Weston Geophysical primary seismic sources is provided in Figure 2.5.2-6. Following is a brief discussion of each of the Weston Geophysical team's primary seismic sources.

Charleston Seismic Zone (25). The Charleston Seismic Zone source is an irregularly shaped hexagon centered just northeast of Charleston, South Carolina, and located about 60 mi from the VEGP ESP site. This source includes the Helena Banks, Charleston, Ashley River, and Woodstock faults, but does not include the Bowman seismic zone. This source was designed to capture the occurrence of Charleston-type earthquakes. The largest M_{max} assigned by the Weston Geophysical team to this zone is m_b 7.2 (**M** 7.5).

South Carolina (26). The South Carolina source (26) is a large area covering most of South Carolina and the VEGP ESP site. The largest M_{max} assigned by the Weston Geophysical team to this zone is m_b 7.2 (**M** 7.5).

Southern Coastal Plain (104). The Southern Coastal Plain source (104) extends from New York to Alabama and from the Towaliga-Lowdenville-Kings Mountain fault trends on the west to the offshore East Coast magnetic anomaly on the east. Source 104 was designed to include the Central Virginia seismic zone, the Charleston seismic zone, and a number of Mesozoic basins. The largest M_{max} assigned by the Weston Geophysical team to this zone is m_b 6.6 (**M** 6.5).

Nine Combination Zones: (103 – 23 – 24 (C19); 104 – 22 (C20); 104 – 25 (C21); 104 – 22 – 26 (C23); 104 – 22 – 25 (C24); 104 – 28BCDE – 22 (C26); 104 – 28BCDE – 22 – 25 (C27); 26 – 25 (C33); and 104 – 28BE – 25 (C35)). Weston Geophysical specified a number of combination seismic source zones, nine of which are primary sources for the VEGP ESP site. The largest M_{max} assigned by the Weston Geophysical team to these combination zones is m_b 6.6 (**M** 6.5).

2.5.2.2.1.6 Sources Used for EPRI PSHA – Woodward-Clyde Consultants

Woodward-Clyde Consultants identified and characterized five primary seismic sources, all five located within the site region; they are:

- Charleston (includes "none of the above," NOTA) (30)
- S Carolina Gravity Saddle (Extended) (29)
- SC Gravity Saddle No. 2 (Combo C3) (29A)
- SC Gravity Saddle No. 3 (NW Portion) (29B)
- Vogtle Background

Woodward-Clyde Consultants also identified two additional seismic sources within the site region. These sources are:

- Blue Ridge Combo (31)

- Blue Ridge Combination – Alternate Configuration (31A)

Primary and additional seismic sources characterized by the Woodward-Clyde team within the site region are listed in Table 2.5.2-7. A map showing the locations and geometries of the Woodward-Clyde primary seismic sources is provided in Figure 2.5.2-5. Following is a brief discussion of each of the primary seismic sources identified by the Woodward-Clyde team.

Charleston (includes NOTA) (30). The Charleston seismic source (30) is a northeast-southwest-oriented rectangle that includes most of the Charleston earthquake MMI IX and X area and the Charleston Ashley River and Woodstock faults. Source 30 is located about 70 mi from the VEGP ESP site and was designed to capture the occurrence of Charleston-type earthquakes. The Charleston source (30) is mutually exclusive with Sources 29, 29A, and 29B; if 30 is active, the other three are inactive, and vice versa. The largest M_{max} assigned by the Woodward-Clyde Consultants team to this zone is m_b 7.5 (**M** 8.0).

S Carolina Gravity Saddle (Extended) (29). The South Carolina Gravity Saddle (Extended) source (29) covers most of South Carolina and parts of Georgia, including the VEGP ESP site. The South Carolina Gravity Saddle source (29) is mutually exclusive with Sources 29A, 29B, and 30; if 29 is active, the other three are inactive, and vice versa. The largest M_{max} assigned by the Woodward-Clyde Consultants team to this zone is m_b 7.4 (**M** 7.9), reflecting its assumption that Charleston-type earthquakes can occur in this zone.

SC Gravity Saddle No. 2 (Combo C3) (29A). The South Carolina Gravity Saddle No. 2 source (29A) is an irregularly shaped polygon set within the larger area of Source 29. The SC Gravity Saddle No. 2 source (29A) is mutually exclusive with Sources 29, 29B, and 30; if 29A is active, the other three are inactive, and vice versa. The largest M_{max} assigned by the Woodward-Clyde Consultants team to this zone is m_b 7.4 (**M** 7.9), reflecting its assumption that Charleston-type earthquakes can occur in this zone.

SC Gravity Saddle No. 3 (NW Portion) (29B). The South Carolina Gravity Saddle No. 3 source (29B) is an irregularly shaped polygon set within the larger area of Source 29 and includes the VEGP ESP site. The SC Gravity Saddle No. 3 source (29B) is mutually exclusive with Sources 29, 29A, and 30; if 29B is active, the other three are inactive, and vice versa. The largest M_{max} assigned by the Woodward-Clyde Consultants team to this zone is m_b 7.0 (**M** 7.2).

Vogtle Background. The VEGP ESP Background source is a large box containing the VEGP ESP site and covering most of South Carolina and Georgia as well as parts of adjoining states and extending offshore. This source is a background zone defined as a rectangular area surrounding the VEGP ESP site and is not based on any geological, geophysical, or seismological features. The largest M_{max} assigned by the Woodward-Clyde Consultants team to this zone is m_b 6.6 (**M** 6.5).

2.5.2.2.2 Post-EPRI Seismic Source Characterization Studies

Since the EPRI (NP-4726 1986, NP-6395-D 1989) seismic hazard project, three recent studies have been performed to characterize seismic sources within the VEGP ESP site region for PSHAs. These studies include the US Geological Survey's (USGS) National Seismic Hazard Mapping Project **(Frankel et al. 1996, 2002)**, the South Carolina Department of Transportation's seismic hazard mapping project **(Chapman and Talwani 2002)**, and the Nuclear Regulatory Commission's Trial Implementation Project (TIP) study **(Savy et al. 2002)**. These three studies are described below (i.e., Section 2.5.2.2.2.1 through 2.5.2.2.2.3). Based on review of recent studies it was determined that an update of the Charleston seismic source for the EPRI (NP-4726 1986, NP-6395-D 1989) seismic hazard project was required. This update is presented in Section 2.5.2.2.2.4. In addition, at the perimeter of the VEGP ESP site region is what is now identified as the Eastern Tennessee Seismic Zone (ETSZ). The significance of the ETSZ on the VEGP ESP seismic hazard is discussed in Section 2.5.2.2.2.5.

2.5.2.2.2.1 US Geological Survey Model **(Frankel et al. 2002)**

In 2002, the USGS produced updated seismic hazard maps for the conterminous United States based on new seismological, geophysical, and geological information **(Frankel et al. 2002)**. The 2002 maps reflect changes to the source model used to construct the previous version of the national seismic hazard maps **(Frankel et al. 1996)**. The most significant modifications to the CEUS portion of the source model include changes in the recurrence, M_{max}, and geometry of the Charleston and New Madrid sources.

Unlike the EPRI models that incorporate many local sources, the USGS source model in the CEUS includes only five sources: the Extended Margin background, Stable Craton background, Charleston, Eastern Tennessee, and New Madrid (Table 2.5.2-8). Except for the Charleston and New Madrid zones, where earthquake recurrence is modeled by paleoliquefaction data, the hazard for the large background or "maximum magnitude" zones is largely based on historical seismicity and the variation of that seismicity. The USGS source model defines the M_{max} distribution for the Extended Margin background source zone as a single magnitude of **M** 7.5 with a weight of 1.0. The EPRI model, however, includes multiple source zones for each of the six ESTs for this region containing the eastern seaboard and the Appalachians. The EPRI M_{max} distributions for these sources capture a wide range of magnitudes and weights, reflecting considerable uncertainty in the assessment of M_{max} for the CEUS. An **M** 7.5 M_{max} is captured in most of the EPRI source zones, although at a lower weight than assigned by the USGS model.

As part of the 2002 update of the National Seismic Hazard Maps, the USGS developed a model of the Charleston source that incorporates available data regarding recurrence, M_{max}, and geometry of the source zone. The USGS model uses two equally weighted source geometries, one an areal source enveloping most of the tectonic features and liquefaction data in the greater Charleston area and the second a north-northeast-trending elongated areal source enveloping

the southern half of the southern segment of the East Coast fault system (ECFS) (Table 2.5.2-8 and Figure 2.5.2-7). The Frankel et al. (2002) report does not specify why the entire southern segment of the ECFS is not contained in the source geometry. For M_{max}, the study defines a distribution of magnitudes and weights of **M** 6.8 [.20], 7.1 [.20], 7.3 [.45], 7.5 [.15]. For recurrence, Frankel et al. (2002) adopt a mean paleoliquefaction-based recurrence interval of 550 years and represent the uncertainty with a continuous lognormal distribution.

2.5.2.2.2.2 South Carolina Department of Transportation Model **(Chapman and Talwani 2002)**

Chapman and Talwani (2002) created probabilistic seismic hazard maps for the South Carolina Department of Transportation (SCDOT). In the SCDOT model, treatment of the 1886 Charleston, South Carolina, earthquake and similar events dominates estimates of hazard statewide.

The SCDOT model employs a combination of line and area sources to characterize Charleston-type earthquakes in three separate geometries and uses a slightly different M_{max} range (**M** 7.1 to 7.5) than the USGS 2002 model (Table 2.5.2-9 and Figure 2.5.2-8). Three equally-weighted source zones defined for this study include (1) a source capturing the intersection of the Woodstock and Ashley River faults, (2) a larger Coastal South Carolina zone that includes most of the paleoliquefaction sites, and (3) a southern ECFS source zone. The respective magnitude distributions and weights used for M_{max} are **M** 7.1 [.20], 7.3 [.60], 7.5 [.20]. The mean recurrence interval used in the SCDOT study is 550 years, based on the paleoliquefaction record.

2.5.2.2.2.3 The Trial Implementation Project Study **(Savy et al. 2002)**

The purpose of the Lawrence Livermore National Laboratory Trial Implementation Project (TIP) study is to "test and implement the guidelines developed by the Senior Seismic Hazard Analysis Committee (SSHAC) developed under FIN L2503 (NRC 1997)" **(Savy et al. 2002, p. 1)**. To test the SSHAC PSHA methodology, the TIP study focuses on seismic zonation and earthquake recurrence models for the Watts Bar site in Tennessee and the VEGP site. The TIP study uses an expert elicitation process to characterize the Charleston seismic source, considering published data through 1996. The TIP study identifies multiple alternative zones for the Charleston source and for the South Carolina–Georgia seismic zone, as well as alternative background seismicity zones for the Charleston region. However, the TIP study focuses primarily on implementing the Senior Seismic Hazard Advisory Committee (SSHAC) PSHA methodology **(SSHAC 1997)** and was designed to be as much of a test of the methodology as a real estimate of seismic hazard. As a result, its findings are not included explicitly in this report.

2.5.2.2.2.4 Updated Charleston Seismic Source (UCSS) Model **(Bechtel 2006d)**

It has been nearly 20 years since the six EPRI ESTs evaluated hypotheses for earthquake causes and tectonic features and assessed seismic sources in the CEUS **(EPRI NP-4726 1986)**. The EPRI Charleston source zones developed by each EST are shown in Figure 2.5.2-10 and summarized in Table 2.5.2-10. Several studies that post-date the 1986 EPRI EST assessments have demonstrated that the source parameters for geometry, M_{max}, and recurrence of M_{max} in the Charleston seismic source need to be updated to capture a more current understanding for both the 1886 Charleston earthquake and the seismic source that produced this earthquake. In addition, recent PSHA studies of the South Carolina region **(Savy et al. 2002; Chapman and Talwani 2002)** and the southeastern United States (**Frankel et al. 2002)** have developed models of the Charleston seismic source that differ significantly from the earlier EPRI characterizations. Therefore, the Charleston seismic source was updated as part of this ESP application.

The UCSS model is summarized below and presented in detail in Bechtel (2006d). Methods used to update the Charleston seismic source follow guidelines provided in RG 1.165. An SSHAC Level 2 study was performed to incorporate current literature and data and the understanding of experts into an update of the Charleston seismic source model. This level of effort is outlined in the SSHAC (1997) report, which provides guidance on incorporating uncertainty and the use of experts in PSHA studies.

The UCSS model incorporates new information to re-characterize geometry, M_{max}, and recurrence for the Charleston seismic source. These components are discussed in the following sections. Paleoliquefaction data imply that the Charleston earthquake process is defined by repeated, relatively frequent, large earthquakes located in the vicinity of Charleston, indicating that the Charleston source is different from the rest of the eastern seaboard.

2.5.2.2.2.4.1 UCSS Geometry

The UCSS model includes four mutually exclusive source zone geometries (A, B, B', and C; Figure 2.5.2-9). The latitude and longitude coordinates that define these four source zones are presented in Table 2.5.2-11. Details for each source geometry are given below. The four geometries of the UCSS are defined based on current understanding of geologic and tectonic features in the 1886 Charleston earthquake epicentral region; the 1886 Charleston earthquake shaking intensity; distribution of seismicity; and geographic distribution, age, and density of liquefaction features associated with both the 1886 and prehistoric earthquakes. These features, shown in Figures 2.5.1-18 and 2.5.1-19, strongly suggest that the majority of evidence for the Charleston source is concentrated in the Charleston area and is not widely distributed throughout South Carolina. Table 2.5.2-10 provides a subset of the Charleston tectonic features differentiated by pre- and post-EPRI **(EPRI NP-4726 1986)** information. In addition, pre- and post-1986 instrumental seismicity, $m_b \geq 3$, are shown on Figures 2.5.1-18 and 2.5.1-19. Seismicity continues to be concentrated in the Charleston region in the Middleton Place–

Summerville seismic zone (MPSSZ), which has been used to define the intersection of the Woodstock and Ashley River faults **(Tarr et al. 1981; Madabhushi and Talwani 1993)**. Notably, two earthquakes in 2002 (m_b 3.5 and 4.4) are located offshore of South Carolina along the Helena Banks fault zone in an area previously devoid of seismicity of $m_b > 3$. A compilation of the EPRI EST Charleston source zones is provided in Figure 2.5.2-10 as a comparison to the UCSS geometries shown in Figure 2.5.2-9.

Geometry A - Charleston

Geometry A is an approximately 100 x 50 km, northeast-oriented area centered on the 1886 Charleston meizoseismal area (Figure 2.5.2-9). Geometry A is intended to represent a localized source area that generally confines the Charleston source to the 1886 meizoseismal area (i.e., a stationary source in time and space). Geometry A completely incorporates the 1886 earthquake MMI X isoseismal **(Bollinger 1977)**, the majority of identified Charleston-area tectonic features and inferred fault intersections, and the majority of reported 1886 liquefaction features. Geometry A excludes the northern extension of the southern segment of the East Coast fault system because this system extends well north of the meizoseismal zone and is included in its own source geometry (Geometry C). Geometry A also excludes outlying liquefaction features, because liquefaction occurs as a result of strong ground shaking that may extend well beyond the areal extend of the tectonic source. Geometry A also envelopes instrumentally located earthquakes spatially associated with the MPSSZ **(Tarr et al. 1981; Tarr and Rhea 1983; Madabhushi and Talwani 1993)**.

The preponderance of evidence strongly supports the conclusion that the seismic source for the 1886 Charleston earthquake is located in a relatively restricted area defined by Geometry A. Geometry A envelopes (1) the meizoseismal area of the 1886 earthquake, (2) the area containing the majority of local tectonic features (although many have large uncertainties associated with their existence and activity, as described earlier), (3) the area of ongoing concentrated seismicity, and (4) the area of greatest density of 1886 liquefaction and prehistoric liquefaction. These observations show that future earthquakes having magnitudes comparable to the Charleston earthquake of 1886 most likely will occur within the area defined by Geometry A. A weight of 0.70 is assigned to Geometry A (Figure 2.5.2-11). To confine the rupture dimension to within the source area and to maintain a preferred northeast fault orientation, Geometry A is represented in the model by a series of closely spaced, northeast-trending faults parallel to the long axis of the zone.

Geometries B, B', and C

While the preponderance of evidence supports the assessment that the 1886 Charleston meizoseismal area and Geometry A define the area where future events will most likely be

centered, it is possible that the tectonic feature responsible for the 1886 earthquake either extends beyond or lies outside Geometry A. Therefore, the remaining three geometries (B, B', and C) are assessed to capture the uncertainty that future events may not be restricted to Geometry A. The distribution of liquefaction features along the entire coast of South Carolina and observations from the paleoliquefaction record that a few events were localized (moderate earthquakes to the northeast and southwest of Charleston), suggest that the Charleston source could extend well beyond Charleston proper. Geometries B and B' are assessed to represent a larger source zone, while Geometry C represents the southern segment of the East Coast fault system as a possible source zone. The combined geometries of B and B' are assigned a weight of 0.20, and Geometry C is assigned a weight of 0.10. Geometry B' a subset of B, formally defines the onshore coastal area as a source (similar to the SCDOT coastal source zone) that would restrict earthquakes to the onshore region. Geometry B, which includes the onshore and offshore regions, and Geometry B' are mutually exclusive and given equal weight in the UCSS model. Therefore, the resulting weights are 0.10 for Geometries B and B'.

Geometry B - Coastal and Offshore Zone

Geometry B is a coast-parallel, approximately 260 x 100 km source area that (1) incorporates all of Geometry A, (2) is elongated to the northeast and southwest to capture other, more distant liquefaction features in coastal South Carolina **(Amick 1990; Amick et al. 1990a, 1990b; Talwani and Schaeffer 2001)**, and (3) extends to the southeast to include the offshore Helena Banks fault zone (**Behrendt and Yuan 1987**; Figure 2.5.2-9). The elongation and orientation of Geometry B is roughly parallel to the regional structural grain as well as roughly parallel to the elongation of 1886 isoseismals. The northeastern and southwestern extents of Geometry B are controlled by the mapped extent of paleoliquefaction features [e.g., (**Amick 1990; Amick et al. 1990a, 1990b; Talwani and Schaeffer 2001**)].

The location and timing of paleoliquefaction features in the Georgetown and Bluffton areas to the northeast and southwest of Charleston have suggested to some researchers that the earthquake source may not be restricted to the Charleston area **(Obermeier et al. 1989; Amick et al. 1990a; Talwani and Schaeffer 2001)**. A primary reason for defining Geometry B is to account for the possibility that there may be an elongated source or multiple sources along the South Carolina coast. Paleoliquefaction features in the Georgetown and Bluffton areas may be explained by an earthquake source both northeast and southwest of Charleston, as well as possibly offshore.

Geometry B extends southeast to include an offshore area and the Helena Banks fault zone. The Helena Banks fault zone is clearly shown by multiple seismic reflection profiles and has demonstrable late Miocene offset **(Behrendt and Yuan 1987)**. Offshore earthquakes in 2002 (m_b 3.5 and 4.4) suggest a possible spatial association of seismicity with the mapped trace of the Helena Banks fault system (Figures 2.5.2-9 and 2.5.1-19). Whereas these two events in the vicinity of the Helena Banks fault system do not provide a positive correlation with seismicity or demonstrate recent fault activity, these small earthquakes are considered new data since the

EPRI studies. The EPRI earthquake catalog **(EPRI NP-4726-A 1988)** was devoid of any events ($m_b \geq 3.0$) offshore from Charleston. The recent offshore seismicity also post-dates the development of the USGS and SCDOT source models that exclude any offshore Charleston source geometries.

A low weight of 0.10 is assigned to Geometry B (Figure 2.5.2-11), because the preponderance of evidence indicates that the seismic source that produced the 1886 earthquake lies onshore in the Charleston meizoseismal area and not in the offshore region. To confine the rupture dimension to within the source area and to maintain a preferred northeast fault orientation, Geometry B is represented in the model by a series of closely spaced, northeast-trending faults parallel to the long axis of the zone.

Geometry B' - Coastal Zone

Geometry B' is a coast-parallel, approximately 260 x 50 km source area that incorporates all of Geometry A, as well as the majority of reported paleoliquefaction features **(Amick 1990; Amick et al. 1990a, 1990b; Talwani and Schaeffer 2001)**. Unlike Geometry B, however, Geometry B' does not include the offshore Helena Banks fault zone (Figure 2.5.2-9).

The Helena Banks fault system is excluded from Geometry B' to recognize that the preponderance of the data and evaluations support the assessment that the fault system is not active and because most evidence strongly suggests that the 1886 Charleston earthquake occurred onshore in the 1886 meizoseismal area and not on an offshore fault. Whereas there is little uncertainty regarding the existence of the Helena Banks fault, there is a lack of evidence that this feature is still active. Isoseismal maps documenting shaking intensity in 1886 indicate an onshore meizoseismal area (the closed bull's eye centered onshore north of downtown Charleston, Figure 2.5.1-19). An onshore source for the 1886 earthquake as well as the prehistoric events is supported by the instrumentally recorded seismicity in the MPSSZ and the corresponding high density cluster of 1886 and prehistoric liquefaction features.

Similar to Geometry B above, a weight of 0.10 is assigned to Geometry B' and reflects the assessment that Geometry B' has a much lower probability of being the source zone for Charleston-type earthquakes than Geometry A (Figure 2.5.2-11). To confine the rupture dimension to within the source area and to maintain a preferred northeast fault orientation, Geometry B' is represented in the model by a series of closely spaced, northeast-trending faults parallel to the long axis of the zone.

Geometry C - East Coast Fault System - South (ECFS-s)

Geometry C is an approximately 200 x 30 km, north-northeast-oriented source area enveloping the southern segment of the proposed East Coast fault system (ECFS-s) shown in Figure 3 of Marple and Talwani (2000) (Figures 2.5.2-9 and 2.5.2-12). The USGS hazard model **(Frankel et al. 2002)** (Figure 2.5.2-7) incorporates the ECFS-s as a distinct source geometry (also known as the zone of river anomalies [ZRA]); however, as described earlier, the USGS model truncates the

northeastern extent of the proposed fault segment. The South Carolina Department of Transportation hazard model **(Chapman and Talwani 2002)** also incorporates the ECFS-s as a distinct source geometry; however, this model extends the southern segment of the proposed East Coast fault system farther to the south than originally postulated by Marple and Talwani (2000) to include, in part, the distribution of liquefaction in southeastern South Carolina **(Chapman 2005b)** (Figure 2.5.2-9).

In this ESP evaluation the area of Geometry C is restricted to envelope the original depiction of the ECFS-s by Marple and Talwani (2000). Truncation of the zone to the northeast as shown by the 2002 USGS model is not supported by available data, and the presence of liquefaction in southeastern South Carolina is best captured in Geometries B and B', rather than extending the ECFS-s farther to the south than defined by the data of Marple and Talwani (2000).

A low weight of 0.10 is assigned to Geometry C to reflect the assessment that Geometries B, B', and C all have equal, but relatively low, likelihood of producing Charleston-type earthquakes (Figure 2.5.2-11). As with the other UCSS geometries, Geometry C is represented as a series of parallel, vertical faults oriented northeast-southwest and parallel to the long axis of the narrow rectangular zone. The faults and extent of earthquake ruptures are confined within the rectangle depicting Geometry C.

UCSS Model Parameters

Based on studies by Bollinger et al. (1985, 1991) and Bollinger (1992), a 20-km-thick seismogenic crust is assumed for the UCSS. To model the occurrence of earthquakes in the characteristic part of the Charleston distribution (**M** > 6.7), the model uses a series of closely-spaced, vertical faults parallel to the long axis of each of the four source zones (A, B, B', and C). Faults and earthquake ruptures are limited to within each respective source zone and are not allowed to extend beyond the zone boundaries, and ruptures are constrained to occur within the depth range of 0 to 20 km. Modeled fault rupture areas are assumed to have a width-to-length aspect ratio of 0.5, conditional on the assumed maximum fault width of 20 km. To obtain Mmax earthquake rupture lengths from magnitude, the Wells and Coppersmith (1994) empirical relationship between surface rupture length and **M** for earthquakes of all slip types is used.

To maintain as much similarity as possible with the original EPRI model, the UCSS model treats earthquakes in the exponential part of the distribution (**M** < 6.7) as point sources uniformly distributed within the source area (full smoothing), with a constant depth fixed at 10 km.

2.5.2.2.2.4.2 UCSS Maximum Magnitude

The six EPRI ESTs developed a distribution of weighted M_{max} values and weights to characterize the largest earthquakes that could occur on Charleston seismic sources. On the low end, the Law Engineering team assessed a single M_{max} of m_b 6.8 to seismic sources it considered

capable of producing earthquakes comparable in magnitude to the 1886 Charleston earthquake. On the high end, four teams defined M_{max} upper bounds ranging between m_b 7.2 and 7.5. For this ESP application, the m_b magnitude values have been converted to moment magnitude (**M**) as described previously. The m_b value and converted moment magnitude value for each team are shown below. The range in **M** for the six ESTs is 6.5 to 8.0.

Team	Charleston M_{max} range
Bechtel Group	m_b 6.8 to 7.4 (**M** 6.8 to 7.9)
Dames & Moore	m_b 6.6 to 7.2 (**M** 6.5 to 7.5)
Law Engineering	m_b 6.8 (**M** 6.8)
Rondout	m_b 6.6 to 7.0 (**M** 6.5 to 7.2)
Weston Geophysical	m_b 6.6 to 7.2 (**M** 6.5 to 7.5)
Woodward-Clyde Consultants	m_b 6.7 to 7.5 (**M** 6.7 to 8.0)

The **M** equivalents of EPRI m_b estimates for Charleston M_{max} earthquakes show that the upper bound values are similar to, and in two cases exceed, the largest modern estimate of **M** 7.3 ± 0.26 **(Johnston 1996)** for the 1886 earthquake. The upper bound values for five of the six ESTs also exceed the preferred estimate of **M** 6.9 by Bakun and Hopper (2004) for the Charleston event. The EPRI M_{max} estimates are more heavily weighted toward the lower magnitudes, with the upper bound magnitudes given relatively low weights by several ESTs (Tables 2.5.2-2 through 2.5.2-7). Therefore, updating the M_{max} range and weights to reflect the current range of technical interpretations is warranted for the UCSS.

Based on assessment of the currently available data and interpretations regarding the range of modern M_{max} estimates (Table 2.5.2-12), the UCSS model modifies the USGS magnitude distribution **(Frankel et al. 2002)** to include a total of five discrete magnitude values, each separated by 0.2 **M** units (Figure 2.5.2-11). The UCSS M_{max} distribution includes a discrete value of **M** 6.9 to represent the Bakun and Hopper (2004) best estimate of the 1886 Charleston earthquake magnitude, as well as a lower value of **M** 6.7 to capture a low probability that the 1886 earthquake was smaller than the Bakun and Hopper (2004) mean estimate of **M** 6.9. Bakun and Hopper (2004) do not explicitly report a 1-sigma range in magnitude estimate of the 1886 earthquake, but do provide a 2-sigma range of **M** 6.4 to **M** 7.2.

The UCSS magnitudes and weights are as follows:

M	Weight	
6.7	0.10	
6.9	0.25	Bakun and Hopper (2004) mean
7.1	0.30	
7.3	0.25	Johnston (1996) mean
7.5	0.10	

This results in a weighted M_{max} mean magnitude of **M** 7.1 for the UCSS, which is slightly lower than the mean magnitude of **M** 7.2 in the USGS model **(Frankel et al. 2002)**.

2.5.2.2.2.4.3 UCSS Recurrence Model

In the 1989 EPRI study **(EPRI NP-6395-D 1989)**, the six EPRI ESTs used an exponential magnitude distribution to represent earthquake sizes for their Charleston sources. Parameters of the exponential magnitude distribution were estimated from historical seismicity in the respective source areas. This resulted in recurrence intervals for M_{max} earthquakes (at the upper end of the exponential distribution) of several thousand years.

The current model for earthquake recurrence is a composite model consisting of two distributions. The first is an exponential magnitude distribution used to estimate recurrence between the lower-bound magnitude used for hazard calculations and m_b 6.7. The parameters of this distribution are estimated from the earthquake catalog, as they were for the 1989 EPRI study. This is the standard procedure for smaller magnitudes and is the model used, for example, by the USGS 2002 national hazard maps **(Frankel et al. 2002)**. In the second distribution, M_{max} earthquakes (**M** $\geq$ 6.7) are treated according to a characteristic model, with discrete magnitudes and mean recurrence intervals estimated through analysis of geologic data, including paleoliquefaction studies. In this document, M_{max} is used to describe the range of largest earthquakes in both the characteristic portion of the UCSS recurrence model and the EPRI exponential recurrence model.

This composite model achieves consistency between the occurrence of earthquakes with **M** < 6.7 and the earthquake catalog and between the occurrence of large earthquakes (**M** $\geq$ 6.7) with paleoliquefaction evidence. It is a type of “characteristic earthquake” model, in which the recurrence rate of large events is higher than what would be estimated from an exponential distribution inferred from the historical seismic record.

M_{max} Recurrence

This section describes how the UCSS model determines mean recurrence intervals for M_{max} earthquakes. The UCSS model incorporates geologic data to characterize the recurrence intervals for M_{max} earthquakes. As described earlier, identifying and dating paleoliquefaction features provides a basis for estimating the recurrence of large Charleston area earthquakes. Most of the available geologic data pertaining to the recurrence of large earthquakes in the Charleston area were published after 1990 and therefore were not available to the six EPRI ESTs. In the absence of geologic data, the six EPRI EST estimates of recurrence for large, Charleston-type earthquakes were based on a truncated exponential model using historical seismicity **(EPRI NP-4726 1986; NP-6395-D 1989)**. The truncated exponential model also provided the relative frequency of all earthquakes greater than m_b 5.0 up to M_{max} in the EPRI PSHA. The recurrence of M_{max} earthquakes in the EPRI models was on the order of several thousand years, which is significantly greater than more recently published estimates of about 500 to 600 years, based on paleoliquefaction data **(Talwani and Schaeffer 2001)**.

Paleoliquefaction Data

Strong ground shaking during the 1886 Charleston earthquake produced extensive liquefaction, and liquefaction features from the 1886 event are preserved in geologic deposits at numerous locations in the region. Documentation of older liquefaction-related features in geologic deposits provides evidence for prior strong ground motions during prehistoric large earthquakes. Estimates of the recurrence of large earthquakes in the UCSS are based on dating paleoliquefaction features. Many potential sources of ambiguity and/or error are associated with dating and interpreting paleoliquefaction features. This assessment does not reevaluate field interpretations and data; rather, it reevaluates criteria used to define individual paleoearthquakes in the published literature. In particular, the UCSS reevaluates the paleoearthquake record interpreted by Talwani and Schaeffer (2001) based on that study's compilation of sites with paleoliquefaction features.

Talwani and Schaeffer (2001) compiled radiocarbon ages from paleoliquefaction features along the coast of South Carolina. These data include ages that provide contemporary, minimum, and maximum limiting ages for liquefaction events. Radiocarbon ages were corrected for past variability in atmospheric ^{14}C using well established calibration curves and converted to "calibrated" (approximately calendric) ages. From their compilation of calibrated radiocarbon ages from various geographic locations, Talwani and Schaeffer (2001) correlated individual earthquake episodes. They identified an individual earthquake episode based on samples with a "contemporary" age constraint that had overlapping calibrated radiocarbon ages at approximately 1-sigma confidence interval. The estimated age of each earthquake was "calculated from the weighted averages of overlapping contemporary ages" **(Talwani and Schaeffer 2001)** (p. 6,632). They defined as many as eight events (named 1886, A, B, C, D, E,

F, and G in order of increasing age) from the paleoliquefaction record, and offered two scenarios to explain the distribution and timing of paleoliquefaction features (Table 2.5.2-13).

The two scenario paleoearthquake records proposed by Talwani and Schaeffer (2001) have different interpretations for the size and location of prehistoric events (Table 2.5.2-13). In their Scenario 1, the four prehistoric events that produced widespread liquefaction features similar to the large 1886 Charleston earthquake (A, B, E, and G) are interpreted to be large, Charleston-type events. Three events, C, D, and F, are defined by paleoliquefaction features that are more limited in geographic extent than other events and are interpreted to be smaller, moderate-magnitude events (approximately **M** 6). Events C and F are defined by features found north of Charleston in the Georgetown region, and Event D is defined by sites south of Charleston in the Bluffton area. In their Scenario 2, all events are interpreted as large, Charleston-type events. Furthermore, Events C and D are combined into a large Event C'. Talwani and Schaeffer (2001) justify the grouping of the two events based on the observation that the calibrated radiocarbon ages that constrain the timing of Events C and D are indistinguishable at the 95 percent (2-sigma) confidence interval.

The length and completeness of the paleoearthquake record based on paleoliquefaction features is a source of epistemic uncertainty in the UCSS. The paleoliquefaction record along the South Carolina coast extends from 1886 to the mid-Holocene **(Talwani and Schaeffer 2001)**. The consensus of the scientists who have evaluated these data **(Talwani and Schaeffer 2001; Talwani 2005; Obermeier 2005)** is that the paleoliquefaction record of earthquakes is complete only for the most recent about 2,000 years and that it is possible that liquefaction events are missing from the older portions of the record. The suggested incompleteness of the paleoseismic record is based on the argument that past fluctuations in sea level have produced time intervals of low water table conditions (and thus low liquefaction susceptibility), during which large earthquake events may not have been recorded in the paleoliquefaction record **(Talwani and Schaeffer 2001)**. While this assertion may be true, it cannot be ruled out that the paleoliquefaction record may be complete back to the mid-Holocene.

2-Sigma Analysis of Event Ages

Analysis of the coastal South Carolina paleoliquefaction record performed for the VEGP ESP application is based on the Talwani and Schaeffer (2001) data compilation. As described above, Talwani and Schaeffer (2001) use calibrated radiocarbon ages with 1-sigma error bands to define the timing of past liquefaction episodes in coastal South Carolina. The standard in paleoseismology, however, is to use calibrated ages with 2-sigma (95.4 percent confidence interval) error bands [e.g., **(Sieh et al. 1989; Grant and Sieh 1994)**]. Likewise, in paleoliquefaction studies, to more accurately reflect the uncertainties in radiocarbon dating, the use of calibrated radiocarbon dates with 2-sigma error bands (as opposed to narrower 1-sigma error bands) is advisable **(Tuttle 2001)**. The Talwani and Schaeffer (2001) use of 1-sigma error bands may lead to over-interpretation of the paleoliquefaction record such that more episodes

are interpreted than actually occurred. In recognition of this possibility, the conventional radiocarbon ages presented in Talwani and Schaeffer (2001) have been recalibrated and reported with 2-sigma error bands. The recalibration of individual radiocarbon samples and estimation of age ranges for paleoliquefaction events show broader age ranges with 2-sigma error bands which are used to obtain broader age ranges for paleoliquefaction events in the Charleston area.

Event ages based on overlapping 2-sigma ages of paleoliquefaction features are presented in Table 2.5.2-13. Paleoearthquakes have been distinguished based on grouping paleoliquefaction features that have contemporary radiocarbon samples with overlapping calibrated ages. Event ages have then been defined by selecting the age range common to each of the samples. For example, an event defined by overlapping 2-sigma sample ages of 100 to 200 cal yr BP and 50 to 150 cal yr BP would have an event age of 100 to 150 cal yr BP. The UCSS study considers the “trimmed” ages to represent the approximately 95 percent confidence interval, with a “best estimate” event age as the midpoint of the approximately 95 percent age range.

The 2-sigma analysis identified six distinct paleoearthquakes in the data presented by Talwani and Schaeffer (2001). As noted by that study, Events C and D are indistinguishable at the 95 percent confidence interval, and in the UCSS, those samples define Event C' (Table 2.5.2-13). Additionally, the UCSS 2-sigma analysis suggests that Talwani and Schaeffer (2001) Events F and G may have been a single, large event, defined in the UCSS as F’. One important difference between the UCSS result and that of Talwani and Schaeffer (2001) is that the three Events C, D, and F in their Scenario 1, which are inferred to be smaller, moderate-magnitude events, are grouped into more regionally extensive Events C’ and F’ (Table 2.5.2-13). Therefore, in the UCSS, all earthquakes in the 2-sigma analysis have been interpreted to represent large, Charleston-type events. The incorporation of large Events C’ and F’ into the UCSS model is, in effect, a conservative approach. In the effort to estimate the recurrence of M_{max} events (**M** 6.7 to 7.5), moderate-magnitude (about **M** 6) earthquakes C and D would be eliminated from the record of large (M_{max}) earthquakes in the UCSS model, thereby increasing the calculated M_{max} recurrence interval and lowering the hazard without sufficient justification. For these reasons the UCSS model uses a single, large Event C’ (instead of separate, smaller Events C and D) and a single, large Event F’ (instead of separate, smaller Events F and G). Analysis suggests that there have been four large earthquakes in the most-recent, about 2,000-year portion of the record (1886 and Events A, B, and C’). In the entire about 5,000-year paleoliquefaction record, there is evidence for six large, Charleston-type earthquakes (1886, A, B, C’, E, F’; Table 2.5.2-13). Figure 2.5.2-12a shows the geographic distribution of liquefaction features associated with each event in the UCSS model. The distributions of paleoliquefaction sites for Events A, B, C’, E, and F’ are all very similar to the coastal extent of the liquefaction features from the 1886 earthquake.

Recurrence intervals developed from the earthquakes recorded by paleoliquefaction features assume that these features were produced by large M_{max} events and that both the about 2,000-

year and about 5,000-year records are complete. However, the UCSS mentions at least two concerns regarding the use of the paleoliquefaction record to characterize the recurrence of past M_{max} events. First, it is possible that the paleoliquefaction features associated with one or more of these pre-1886 events were produced by multiple moderate-sized events closely spaced in time. If this were the case, then the calculated recurrence interval would yield artificially short recurrence for M_{max}, since it was calculated using repeat times of both large (M_{max}) events and smaller earthquakes. Limitations of radiocarbon dating and limitations in the stratigraphic record often preclude identifying individual events in the paleoseismologic record that are closely spaced in time (i.e., separated by only a few years to a few decades). Several seismic sources have demonstrated tightly clustered earthquake activity in space and time that are indistinguishable in the radiocarbon and paleoseismic record:

- New Madrid (1811, 1811, 1812)
- North Anatolian Fault (1999 and 1999)
- San Andreas Fault (1812 and 1857)

Therefore the UCSS acknowledges the distinct possibility that M_{max} occurs less frequently than what is calculated from the paleoliquefaction record.

A second concern is that the recurrence behavior of the M_{max} event may be highly variable through time. For example, the UCSS considers it unlikely that **M** 6.7 to **M** 7.5 events have occurred on a Charleston source at an average repeat time of about 500 to 600 years **(Talwani and Schaeffer 2001)** throughout the Holocene Epoch. Such a moment release rate would likely produce tectonic landforms with clear geomorphic expression, such as are present in regions of the world with comparably high rates of moderate to large earthquakes (for example, faults in the Eastern California shear zone with sub-millimeter per year slip rates and recurrence intervals on the order of about 5,000 years have clear geomorphic expression **(Rockwell et al. 2000)**). Perhaps it is more likely that the Charleston source has a recurrence behavior that is highly variable through time, such that a sequence of events spaced about 500 years apart is followed by quiescent intervals of thousands of years or longer. This sort of variability in inter-event time may be represented by the entire mid-Holocene record, in which both short inter-event times (e.g., about 400 years between Events A and B) are included in a record with long inter-event times (e.g., about 1,900 years between Events C' and E).

Recurrence Rates

The UCSS model calculates two average recurrence intervals covering two different time intervals, which are used as two recurrence branches on the logic tree (Figure 2.5.2-11). The first average recurrence interval is based on the four events that occurred within the past about 2,000 years. This time period is considered to represent a complete portion of the paleoseismic record based on published literature [e.g., (**Talwani and Schaeffer 2001**)] and feedback from those researchers questioned **(Talwani 2005; Obermeier 2005)**. These events include 1886, A, B, and C' (Table 2.5.2-13). The average recurrence interval calculated for the most recent

portion of the paleoliquefaction record (four events over the past about 2,000 years) is given 0.80 weight on the logic tree (Figure 2.5.2-11).

The second average recurrence interval is based on events that occurred within the past about 5,000 years. This time period represents the entire paleoseismic record based on paleoliquefaction data **(Talwani and Schaeffer 2001)**. These events include 1886, A, B, C', E, and F' as listed in Table 2.5.2-13. As mentioned previously, published papers and researchers questioned suggest that the older part of the record (older than about 2,000 years ago) may be incomplete. Whereas this assertion may be true, it is also possible that the older record, which exhibits longer inter-event times, is complete. The average recurrence interval calculated for the 5,000-year record (six events) is given 0.20 weight on the logic tree (Figure 2.5.2-11). The 0.80 and 0.20 weighting of the 2,000-year and 5,000-year paleoliquefaction records, respectively, reflect incomplete knowledge of both the current short-term recurrence behavior and the long-term recurrence behavior of the Charleston source.

The mean recurrence intervals for the most-recent 2,000-year and past 5,000-year records represent the average time interval between earthquakes attributed to the Charleston seismic source. The mean recurrence intervals and their parametric uncertainties were calculated according to the methods outlined by Savage (1991) and Cramer (2001). The methods provide a description of mean recurrence interval, with a best estimate mean T_{ave} and an uncertainty described as a lognormal distribution with median $T_{0.5}$ and parametric lognormal shape factor $\sigma_{0.5}$.

The lognormal distribution is one of several distributions, including the Weibull, Double Exponential, and Gaussian, among others, used to characterize earthquake recurrence **(Ellsworth et al. 1999a)**. Ellsworth et al. (1999a) and Matthews et al. (2002) propose a Brownian-passage time model to represent earthquake recurrence, arguing that it more closely simulates the physical process of strain build-up and release. This Brownian-passage time model is currently used to calculate earthquake probabilities in the greater San Francisco Bay region **(WGCEP 2003)**. Analyses show that the lognormal distribution is very similar to the Brownian-passage time model of earthquake recurrence for cases where the time elapsed since the most recent earthquake is less than the mean recurrence interval **(Cornell and Winterstein 1988; Ellsworth et al. 1999a)**. This is the case for Charleston, where 120 years have elapsed since the 1886 earthquake and the mean recurrence interval determined over the past 2,000 years is about 548 years. The UCSS study has chosen to calculate average recurrence interval using a lognormal distribution because its statistics are well known **(NIST/SEMATECH 2006)** and it has been used in numerous studies [e.g.,**(Savage 1991; WGCEP 1995; Cramer 2001)**].

The average interval between earthquakes is expressed as two continuous lognormal distributions. The average recurrence interval for the 2,000-year record, based on the three most recent inter-event times (1886-A, A-B, B-C'), has a best estimate mean value of 548 years and an uncertainty distribution described by a median value of 531 years and a lognormal shape

factor of 0.25. The average recurrence interval for the 5,000-year record, based on five inter-event times (1886-A, A-B, B-C', C'-E, E-F'), has a best estimate mean value of 958 years and an uncertainty distribution described by a median value of 841 years and a lognormal shape factor of 0.51. At one standard deviation, the average recurrence interval for the 2,000-year record is between 409 and 690 years; for the 5,000-year record, it is between 452 and 1,564 years. Combining these mean values of 548 and 958 years with their respective logic tree weights of 0.8 and 0.2 results in a weighted mean of 630 years for Charleston M_{max} recurrence.

The mean recurrence interval values used in the UCSS model are similar to those determined by earlier studies. Talwani and Schaeffer (2001) consider two possible scenarios to explain the distribution in time and space of paleoliquefaction features. In their Scenario 1, large earthquakes have occurred with an average recurrence of 454 ±21 years over about the past 2,000 years; in their Scenario 2, large earthquakes have occurred with an average recurrence of 523 ±100 years over the past 2,000 years. Talwani and Schaeffer (2001) state that, "In anticipation of additional data we suggest a recurrence rate between 500 and 600 years for **M** 7+ earthquakes at Charleston". For the 2,000-year record, the 1-standard-deviation range of 409 to 690 years completely encompasses the range of average recurrence interval reported by Talwani and Schaeffer (2001). The best-estimate mean recurrence interval value of 548 years is comarable to the midpoint of the Talwani and Schaeffer (2001) best-estimate range of 500 to 600 years. The best estimate mean recurrence interval value from the 5,000-year paleoseismic record of 958 years is outside the age ranges reported by Talwani and Schaeffer (2001), although they did not determine an average recurrence interval based on the longer record.

In the updated seismic hazard maps for the conterminous United States, Frankel et al. (2002) use a mean recurrence value of 550 years for characteristic earthquakes in the Charleston region. This value is based on the above-quoted 500 to 600 year estimate from Talwani and Schaeffer (2001). Frankel et al. (2002) do not incorporate uncertainty in mean recurrence interval in their calculations.

For computation of seismic hazard, discrete values of activity rate (inverse of recurrence interval) are required as input to the PSHA code (Cornell 1968). To evaluate PSHA based on mean hazard, the mean recurrence interval and its uncertainty distribution should be converted to mean activity rate with associated uncertainty. The final discretized activity rates used to model the UCSS in the PSHA reflect a mean recurrence of 548 years and 958 years for the 2,000-year and 5,000-year branches of the logic tree, respectively. Lognormal uncertainty distributions in activity rate are obtained by the following steps: (1) invert the mean recurrence intervals to get mean activity rates; (2) calculate median activity rates using the mean rates and lognormal shape factors of 0.25 and 0.51 established for the 2,000-year and 5,000-year records, respectively; and (3) determine the lognormal distributions based on the calculated median rate and shape factors. The lognormal distributions of activity rate can then be discretized to obtain individual activity rates with corresponding weights.

2.5.2.2.2.5 Eastern Tennessee Seismic Zone

The Eastern Tennessee Seismic Zone (ETSZ) is one of the most active seismic zones in Eastern North America. This region of seismicity in the southern Appalachians is described in Section 2.5.1.1.4.6. Despite its high rate of activity, the largest known earthquake was magnitude 4.6 **(Chapman et al 2002)**. No evidence for larger prehistoric earthquakes, such as paleoliquefaction features, has been discovered **(Chapman et al 2002; Wheeler 2005)**. While the lack of large earthquakes in the relatively short historical record cannot preclude the future occurrence of large events, there is a much higher degree of uncertainty associated with the assignment of Mmax for the ETSZ than other CEUS seismic source zones, such as New Madrid and Charleston, where large historical earthquakes are known to have occurred.

The EPRI source model **(EPRI NP-4726 1986)** includes various source geometries and parameters to represent the seismicity of the ETSZ. All but one of the EPRI Earth Science Teams (ESTs) modeled local source zones to capture this area of seismicity and some ESTs included more than one zone. The Law team did not include a specific, local source for the ETSZ, however the ETSZ and Giles County seismic zones were included in a larger seismic source zone called the Eastern Basement (17). A wide range of Mmax values and associated probabilities were assigned to these sources to reflect the uncertainty of multiple experts from each EST. The moment magnitude (**M**) equivalents of body-wave magnitude (m_b) Mmax values assigned by the ESTs range from **M** 4.8 to 7.5. The Dames & Moore sources for the ETSZ included the largest upper-bound Mmax value of **M** 7.5. Sources from the Woodward-Clyde and Rondout teams were also assigned large upper-bound Mmax values of **M** 7.2.

Subsequent hazard studies have used Mmax values within the range of maximum magnitudes used by the six EPRI models. Collectively, upper-bound maximum values of Mmax used by the EPRI teams ranged from **M** 6.3 to 7.5. Using three different methods specific to the Eastern Tennessee seismic source, Bollinger (1992) estimated an M_{max} of **M** 6.3. The Bollinger (1992) model also included the possibility that the ETSZ was capable of generating a larger magnitude event and included an **M** 7.8 (m_b 7.37) with a low probability of 5% in the M_{max} distribution. The 5% weighted **M** 7.8 by Bollinger (1992) slightly exceeds the ERPI range, but the **M** 6.3 value was given nearly the entire weight (95%) in his characterization of the ETSZ. This smaller magnitude is much closer to the mean magnitude (about **M** 6.2) of the EPRI study. The Trial Implementation Project (TIP) **(Savy et al. 2002)** also provided a broad M_{max} distribution for the ETSZ. This study developed magnitude distributions for all ETSZ source zone representations that ranged from as low as **M** 4.5 to as high as **M** 7.5, with a mode of about **M** 6.5 for almost each distribution **(Savy et al. 2002**, pages F-12 to F-19 of Appendix F**)**. The broad distribution of the TIP study magnitude distribution for the ETSZ source zones is very similar to the EPRI distribution of **M** 4.8 to **M** 7.5. The USGS source model assigns a single M_{max} value of **M** 7.5 for the ETSZ **(Frankel et al 2002)**. The most recent characterizations of the ETSZ M_{max} by the USGS and TIP study consider **M** 7.5 as the largest magnitude in the distribution, and this magnitude is captured by the

range of M_{max} values used in EPRI (NP-4726 1986). Therefore, it is concluded that no new information has been developed since 1986 that would require a significant revision to the EPRI seismic source model.

For the VEGP ESP site, the contribution to hazard from the ETSZ sources in the EPRI study was minimal. With the exception of the Law source 17 (Eastern Basement), none of the ETSZ sources contributed more than one percent of the site hazard, and thus were excluded from the final hazard calculations **(EPRI NP-6452-D 1989)**. The ground motion hazard at the VEGP ESP site is dominated by the Charleston seismic source, and the inclusion of new recurrence values for Charleston based on paleoliquefaction serves to increase the relative contribution of Charleston with respect to any distant source, such as the ETSZ. No modifications to the EPRI parameters for ETSZ source zones were made as part of this ESP study.

2.5.2.3 Correlation of Seismicity with Geologic Structures and EPRI Sources

The final part of the review and update of the 1989 EPRI seismic source model was a correlation of updated seismicity with the 1989 model source. The EPRI seismicity catalog covers earthquakes in the CEUS through 1984, as described in Section 2.5.2.1. Figures 2.5.2-1 through 2.5.2-6 shows the distribution of earthquake epicenters from both the EPRI (pre-1985) and updated (post-1984 through April 2005) earthquake catalogs in comparison to the seismic sources identified by each of the EPRI ESTs.

Comparison of the additional events of the updated earthquake catalog to the EPRI earthquake catalog shows:

- There are no new earthquakes within the site region that can be associated with a known geologic structure.
- There are no unique clusters of seismicity that would suggest a new seismic source not captured by the EPRI seismic source model.
- The updated catalog does not show a pattern of seismicity that would require significant revision to the geometry of any of the EPRI seismic sources.
- The updated catalog neither shows nor suggests any increase in M_{max} for any of the EPRI seismic sources.
- The updated catalog does not imply a significant change in seismicity parameters (rate of activity, b-value) for any of the EPRI seismic sources (see also Section 2.5.2.4.2).

2.5.2.4 Probabilistic Seismic Hazard Analysis and Controlling Earthquakes

PSHA is an accepted method for determining seismic design levels (RG 1.165). The PSHA developed here relies on seismic source inputs from the EPRI-SOG study **(EPRI NP-6395-D 1989a)**, which is accepted by the NRC (RG 1.165), on updates to those sources as described in

Section 2.5.2.2, and on ground motion models **(EPRI 1009684 2004)** that have been accepted under other ESP applications.

The final GMRS ground motion for the VEGP ESP site is developed using a performance-based approach, which has as its foundation a well-justified PSHA for the VEGP ESP site. Ground motion levels corresponding to mean annual frequencies of exceedance (MAFEs) of 10^{-4} to 10^{-6} are developed, because this range encompasses the range of motions necessary to establish the GMRS ground motion under several criteria.

The seismic hazard at the VEGP ESP was first calculated using the assumptions of the EPRI (NP-6395-D 1989) study. This was to confirm that the 1989 results could be replicated. Then the seismic sources were updated with the UCSS models, including sources surrounding the Charleston source for each team, as described in Section 2.5.2.2.2. Also, the EPRI (1009684 2004) ground motion model was adopted for calculations of seismic hazard at seven structural frequencies. Sensitivity studies were conducted to determine the effects of these changes.

The seismic hazard was calculated for hard rock conditions for a range of ground motions corresponding to a range of annual frequencies of exceedance. This hard rock hazard formed the basis with which to integrate the effects of surficial materials on ground motion, to calculate the seismic hazard at a horizon appropriate for seismic design. The ASCE 43-05 2005 procedure was used to recommend an appropriate GMRS seismic spectrum. This procedure requires ground motion amplitudes and slopes of seismic hazard curves in the range of 10^{-4} to 10^{-5} mean annual frequency of exceedance. To obtain a full design spectrum from structural frequencies of 0.1 to 100 Hz, a smooth site-specific spectral shape was fit to the seven structural frequencies for which specific seismic hazard calculations were made.

2.5.2.4.1 Replication of 1989 EPRI Probabilistic Seismic Hazard Results

PSHA calculations were initially made using the original 1989 EPRI-SOG seismic sources and ground motion assumptions **(EPRI NP-6395-D 1989)**. The purpose of these calculations was to validate Risk Engineering Inc.'s (REI) proprietary FRISK88 seismic hazard code, the EPRI-SOG seismic sources, the EPRI-SOG source combinations, and the EPRI-SOG attenuation equations, as modeled by the FRISK88 code. The results used in this replication were the peak ground acceleration (PGA) results available for VEGP site (see Appendix E, Table 3-103 of **(EPRI NP-6395-D 1989)**).

Seismic sources used to represent the seismic hazard for each of the six teams in the EPRI-SOG study are shown in Table 2.5.2-14. These are the primary sources used for the VEGP site in the original EPRI-SOG study, as documented in the EQHAZARD input files transmitted by EPRI.

The ground motion attenuation relations and their relative weights used in this analysis are those specified in the EPRI-SOG study (see Table 4-1 of **(EPRI NP-6395-D 1989)**). Following Table 4-1 of EPRI NP-6395-D, a standard deviation of (log) amplitude of 0.5 was assumed for each ground motion equation. These equations were used to calculate hard rock hazard.

The VEGP site is classified in EPRI NP-6395-D 1989 as a "Soil V" site (see Table 2-2 of **(EPRI NP-6395-D 1989)**). The site amplification factor versus PGA for this site class is shown in Figure 2-6 of EPRI NP-6395-D. To avoid having to apply site amplification factors to the rock curves, the results calculated here were compared to original EPRI-SOG hard rock results received from EPRI.

Results of this seismic hazard calculation are compared to the EPRI-SOG results in Table 2.5.2-15.

Agreement is excellent, generally within 5.1 percent in hazard for amplitudes up to 1g. For the 85 percent, replication is slightly less accurate, with a difference of -11.5 percent and -11.7 percent at 0.05g and 0.1g, respectively. This slight difference is of less concern, because the mean hazard curve is used to develop the GMRS ground motions. Comparison plots of the mean, median, and 85 percent PGA hazard curves are shown in Figures 2.5.2-13 through 2.5.2-15.

This comparison validates the FRISK88 code, the EPRI-SOG seismic sources, the EPRI-SOG source combinations, and the EPRI-SOG attenuation equations.

2.5.2.4.2 Effects of New Regional Earthquake Catalog

The effects of the new regional earthquake catalog were examined by comparing seismicity rates in two regions critical to seismic hazard at the VEGP ESP site: the Charleston, South Carolina, region and the local region in South Carolina and into Georgia around the VEGP ESP site. The importance of these regions to seismic hazard is addressed in Section 2.5.2.4.6. The effects of two seismicity catalogs were compared: (1) the EPRI-SOG **(EPRI NP-4726-A 1988)** earthquake catalog (through 1984) and (2) the EPRI-SOG catalog updated to include more recent seismicity (Section 2.5.2.1). The fundamental question to be addressed is whether or not the seismicity recorded since 1984 indicates that the seismic activity rates used in the EPRI-SOG study **(EPRI NP-6395-D 1989)** are inadequate or insufficiently conservative for assessment of the seismic hazard at the VEGP ESP site.

Seismicity rates were assessed for two sources in the site region, as follows: (1) a small rectangular source around the Charleston seismicity and (2) a triangular-shaped source representing seismicity in South Carolina and a strip of Georgia incorporating the VEGP ESP site. Figure 2.5.2-16 shows a map of these two sources, along with the earthquakes from the EPRI-SOG catalog and from the updated catalog.

The seismicity in these two sources was investigated by running program EQPARAM (from the EPRI EQHAZARD package), first for the original EPRI catalog and then using the updated EPRI catalog (through April 2005). Full smoothing of a- and b-values was selected for the comparison because this was a common choice of many of the ESTs in the EPRI-SOG study. Further, if comparisons were made on an individual degree-cell basis, the rates in some cells might increase and in others might decrease; furthermore, for a source such as the triangular South

Carolina source, a composite rate would have to be used to compare seismic rates using the earthquake catalog through 1984 to those using the earthquake catalog through April 2005. The choice of full smoothing achieves this composite rate directly and automatically, since it is a composite rate for the entire source.

From the a- and b-values calculated with EQPARAM, recurrence rates were calculated for different magnitudes. Figures 2.5.2-17 and 2.5.2-18 compare the annual recurrence rates for the Charleston source and for the triangular South Carolina source, respectively. For the rectangular Charleston source, the updated catalog indicates that seismicity rates are about the same. For the triangular South Carolina source, the updated catalog indicates that seismicity rates have decreased when the seismicity from 1985 to April 2005 is added.

The conclusion is that the seismicity recorded since 1984 does not indicate that seismic activity rates have increased in those sources contributing most to the hazard at the VEGP ESP site under the assumptions of the EPRI-SOG study. Therefore, for original sources of the EPRI-SOG teams and the original seismicity rates from the EPRI-SOG **(EPRI NP-4726-A 1988)** earthquake catalog (through 1984) were used here for calculations of seismic hazard. These rates give an accurate estimate of seismicity for Charleston sources, and are slightly conservative for local sources, when compared to rates from the updated (through April 2005) catalog. Where the geometries of EPRI-SOG sources were modified to account for new information on the Charleston earthquake source (see Section 2.5.2.4.4 below), new seismicity rates were calculated using the updated earthquake catalog (through April 2005) in order to use the most recent information available.

2.5.2.4.3 New Maximum Magnitude Information

Geological and seismological data published since the 1986 EPRI seismic source model are presented in Section 2.5.1. Based on a review of these data, there are no significant changes in the EPRI M_{max} parameters, with the exception of the Charleston seismic source. A summary of M_{max} values for each EPRI EST is provided in Tables 2.5.2-2 through 2.5.2-7.

Changes to M_{max} for the Charleston seismic source are discussed in Section 2.5.2.2.2 and in a separate Engineering Study Report **(Bechtel 2006d)**.

2.5.2.4.4 New Seismic Source Characterizations

The effect of new geoscience information is to modify the interpretations for the Charleston seismic source. The EPRI-SOG teams used an exponential model to represent earthquakes for sources in the Charleston area, and some teams adopted interpretations that included (with a low weight) the possibility that a specific Charleston source did not exist (i.e., that large earthquakes could occur in a large region in the eastern US). The new interpretation of the Charleston source (see Section 2.5.2.2.2) indicates that a unique source of large earthquakes exists with weight 1.0 and that large magnitudes occur with a rate of occurrence unrelated to the

rate of smaller magnitudes. Typical recurrence intervals for large Charleston earthquakes for the EPRI-SOG teams were on the order of 2,000 years, whereas the new information indicates recurrence intervals of 500 to 1,000 years.

In addition, the geometry of the Charleston sources has changed. Some EPRI-SOG teams drew relatively broad zones within which a Charleston-size earthquake could occur or specified (under some interpretations) that Charleston-size earthquakes were not restricted to southeast South Carolina but could occur over broad areas. The new geologic and tectonic information presented in Section 2.5.2.2.2 describes a relatively restricted zone within which Charleston-size earthquakes are modeled.

These changes in rate of occurrence and location of Charleston sources generally have the effect of increasing seismic hazard at the VEGP ESP site, compared to the EPRI-SOG study. It is not possible to determine the specific effect of one change, because (for example) changing the geometry of the Charleston source affects the geometries and seismicity rates of local sources and background sources for each EPRI-SOG team. The total effect of the new geoscience information is taken into account in the revised PSHA results presented in Section 2.5.2.4.6.

Figure 2.5.2-19 (reproducing Figure 2.5.2-9 content relevant to this discussion) shows the geometry of the four sources used to characterize the Charleston seismic source (Section 2.5.2.2.2).

To update the EPRI-SOG model, these four geometries of the Charleston source were overlaid onto each of the six EPRI-SOG team sources, and new geometries were created for all EPRI-SOG team sources surrounding the Charleston source. Figure 2.5.2-20a shows an example of the original geometry, and Figures 2.5.2-20b through 2.5.2-20e show the new geometries created for the Rondout team, source 26. The purpose in creating the new geometries was to ensure that, in incorporating the new Charleston sources, no area was left without seismicity. Seismicity parameters for the new EPRI-SOG team source geometries were calculated using the same methodology and same smoothing assumptions as in the EPRI-SOG project and using the updated seismicity catalog (through April 2005). This procedure ensured that the principles underlying the seismicity representations for each EPRI-SOG team source surrounding Charleston were maintained.

The four geometries used to represent the Charleston source were modeled, for seismic hazard calculations, with parallel faults striking northeast-southwest and spaced at 10 km intervals. This spacing was narrow enough not to affect the calculated hazard (i.e., a spacing of 5 km would not have produced significantly different results). Activity rates for the faults were equally divided among the faults, and they were represented as vertical faults from the surface to a depth of 20 km. A rupture length equation (given magnitude) was used to represent a finite rupture length, and an aspect ratio (width-to-length) of 0.5 was assumed. The specific equation selected was for surface rupture length for all rupture types from Wells and Coppersmith (1994).

A characteristic earthquake was modeled for the new Charleston source geometries, with the following magnitudes and weights (Figure 2.5.2-11):

M	Weight
6.7	0.1
6.9	0.25
7.1	0.3
7.3	0.25
7.5	0.1

The magnitudes and weights were discussed in Section 2.5.2.2.2.4.2 The rate of occurrence of the characteristic earthquake was modeled with two 5-point discrete distributions representing (respectively) the 2,000-year and 5,000-year paleoliquefaction intervals described in Section 2.5.2.2.2.4.3. These distributions are as follows:

2,000-Year Interval		5,000-Year Interval	
Activity Rate	Weight	Activity Rate	Weight
1.22×10^{-3}	0.101	3.65×10^{-4}	0.101
1.45×10^{-3}	0.244	6.12×10^{-4}	0.244
1.77×10^{-3}	0.310	9.20×10^{-4}	0.310
2.16×10^{-3}	0.244	1.38×10^{-3}	0.244
2.78×10^{-3}	0.101	2.32×10^{-3}	0.101

These distributions give mean activity rates of 1.823×10^{-3} and 1.044×10^{-3}, respectively, which correspond to recurrence intervals of 548 years and 958 years, and have logarithmic shape factors of 0.25 and 0.51, as described in Section 2.5.2.2.2.4.3.

In addition to the characteristic earthquake, smaller earthquakes were modeled for each of the four source geometries for magnitudes between the lower-bound magnitude (m_b = 5.0) and M_{max} value of m_b = 6.7, with an exponential magnitude distribution. The activity rate and b-value for this distribution were determined using the EPRI-SOG catalog, EQPARAM software, and full smoothing of seismicity parameters across the source. For this exponential model, the rectangular geometries of the Charleston sources were assumed (see Figure 2.5.2-19), with earthquakes uniformly distributed within the source.

The source combinations of the EPRI-SOG teams were reviewed and modified to accurately incorporate the four new Charleston seismic sources into each team's model. This generally resulted in four times as many source combinations, because a single Charleston source was

being replaced by four alternative Charleston sources. As an example, the Rondout team originally had one source combination applicable to the VEGP ESP site:

Source Combination	Weight	Sources
1	1.0	26, 24

The revised model for the Rondout team had four source combinations applicable to the VEGP ESP site:

Source Combination	Weight	Sources
1	0.7	Charleston-A, 26-A
2	0.1	Charleston-B, 26-B
3	0.1	Charleston-B´, 26-B´
4	0.1	Charleston-C, 26-C

where, for example, “26-A” indicates Rondout source 26 with new Charleston source geometry A removed. See Figures 2.5.2-20b through 2.5.2-20e for maps of these source geometries.

Incorporating this new geoscience information into the PSHA for the VEGP ESP site ensures that the PSHA results reflect the most recent information and interpretations of seismicity in the southeastern US. This provides a strong basis for the GMRS ground motions.

2.5.2.4.5 New Ground Motion Models

The ground motion models developed by the 2004 EPRI-sponsored study **(EPRI 1009684 2004)** were used to examine the effects on seismic hazard of current estimates of seismic shaking as a function of earthquake magnitude and distance. For general area sources, nine estimates of median ground motion are combined with four estimates of aleatory uncertainty, giving 36 combinations. For fault sources in rifted regions, which applies to the ECFS fault segments, 12 estimates of median ground motion are combined with four estimates of aleatory uncertainty, giving 48 combinations. When both area sources and faults are active, a specific correlation of area source models and fault source models is used to represent ground motion models that might apply together. These families of models (36 for area sources, 48 for fault sources) represent the epistemic uncertainty in ground motion, and contribute to the epistemic uncertainty in seismic hazard.

Conclusions regarding a comparison of the EPRI NP-6395-D (1989) ground motion models with the EPRI 1009684 (2004) ground motion models depend on the specific magnitude, distance, and structural frequency being compared. Some comparison plots are shown in EPRI 1009684. In general, median ground motion amplitudes are similar at high frequencies. At low frequencies,

the EPRI 1009684 models show lower median ground motions, because these models incorporate the possibility of a two-corner seismic source. Seismic hazard is affected by the median ground motion and also by the standard deviation. The EPRI 1009684 standard deviations are universally higher than those of EPRI NP-6395-D, which leads to higher seismic hazards.

2.5.2.4.6 Updated EPRI Probabilistic Seismic Hazard Analysis, Deaggregation, and 1 Hz, 2.5 Hz, 5 Hz, and 10 Hz Spectral Accelerations Incorporating Significant Increases Based on the Above Sensitivity Studies

Sensitivity studies were conducted to determine which magnitudes and distances contribute most to the seismic hazard at the VEGP ESP site. This was done following the guidelines of RG 1.165, modified for use in calculating GMRS spectra using a performance-based procedure. Specifically, the seismic hazard was deaggregated at mean annual frequencies of exceedance (MAFEs) of 10^{-4}, 10^{-5}, and 10^{-6}. Deaggregations were conducted for two sets of spectral frequencies: a "high-frequency" (HF) set consisting of 10 Hz and 5 Hz and a "low-frequency" (LF) set consisting of 2.5 Hz and 1 Hz. Figure 2.5.2-21 shows a mean uniform hazard spectrum (UHS) for hard rock conditions at the VEGP ESP site for several MAFEs from 10^{-4} to 10^{-6}, and Table 2.5.2-16 lists the values of the mean UHS for hard rock conditions for these MAFEs for frequencies of 100 Hz (PGA), 25 Hz, 10 Hz, 5 Hz, 2.5 Hz, 1 Hz, and 0.5 Hz.

Figures 2.5.2-22 through 2.5.2-27 show the hard rock magnitude-distance deaggregations for three MAFEs and for the high- and low-frequency sets. For the low frequencies, earthquakes from the Charleston sources dominate the hazard at all MAFEs considered. For the high frequencies, local earthquakes contribute substantially to the hazard at 10^{-5} and dominate the contribution to hazard at the 10^{-6} MAFE level.

Figure 2.5.2-28 and 2.5.2-29 show marginal magnitude distributions for hard rock PSHA from the deaggregations for high- and low-frequencies, respectively, for the three MAFEs. For the low frequencies, the large earthquakes from the Charleston dominate the hazard at all three MAFEs. For the high frequencies, large earthquakes dominate 10^{-4} but the smaller earthquakes dominate 10^{-6}.

Figures 2.5.2-30 and 2.5.2-31 show marginal distance distributions for hard rock PSHA from the deaggregations for high- and low-frequencies, respectively, for the three MAFEs. These deaggregations are consistent with those for magnitude, in terms of the contribution of large earthquakes from the Charleston sources.

The contribution of the Charleston sources to hazard can be understood by plotting and comparing hazard curves from individual sources. Figure 2.5.2-32 shows such a comparison, using as an example the sources from the Rondout team (which is the simplest interpretation). Figure 2.5.2-32, for 10 Hz spectral acceleration, shows that the main Charleston source (geometry A, marked "C-A" in Figure 2.5.2-32, with a weight of 0.7) dominates for MAFEs of 10^{-3}

to 10^{-4} but that the local source "RND-26-A" dominates for lower MAFEs (below about 3 x 10^{-5}). At the 10^{-6} MAFE, most of the contribution to total hazard is from the local source. Figure 2.5.2-33, showing hazard curves for the Rondout team for 1 Hz spectral acceleration, indicates that the Charleston sources dominate the total hazard at all MAFEs (at least above 10^{-7}). Note that in both Figures 2.5.2-32 and 2.5.2-33, the mean hazard curve for each source includes the probability that source is active. Thus, the hazard curves for Charleston sources B, B´, and C (labeled C-B, C-B´, and C-C) are lower than the hazard curve for Charleston source A (labeled C-A), primarily because the former three have much lower probabilities of activity than does source A.

These results indicate that seismic sources representing earthquakes in the Charleston region have a large contribution to seismic hazard for hard rock conditions at the VEGP ESP site. The local seismic source representing seismicity in South Carolina also can have an important contribution to hazard for high frequency ground motion, particularly for MAFEs around 10^{-5} and lower.

2.5.2.5 Seismic Wave Transmission Characteristics of the Site

The uniform hazard spectra described in the preceding section are defined on hard rock (shear-wave velocity of 9,200 ft/sec), which is located more than 1,000 ft below the current ground surface at the VEGP ESP site. The subsurface materials at the VEGP ESP site are described in detail in Section 2.5.4. The material characterization is summarized in the following groups:

I. Upper Sand Stratum (Barnwell Group) – predominantly sands, silty sands, and clayey sands, with occasional clay seams. A Shelly Limestone (Utley Limestone) layer was encountered at the base of the Upper Sand Stratum or the top of the Blue Bluff Marl. The limestone contains solution channels, cracks, and discontinuities, and was the cause of severe fluid loss observed during drilling for the VEGP ESP site subsurface investigation.

II. Marl Bearing Stratum (Blue Bluff Marl or Lisbon Formation) – slightly sandy, cemented, calcareous clay.

III. Lower Sand Stratum (comprises several formations from the Still Branch just beneath the Blue Bluff Marl to the Cape Fear just above the Dunbarton Triassic Basin rock) – fine to coarse sand with interbedded silty clay and clayey silt.

IV. Dunbarton Triassic Basin Rock – red sandstone, breccia, and mudstone, weathered along the upper 120 ft.

V. Paleozoic Crystalline Rock – a competent rock with high shear-wave velocity that underlies the Triassic Basin rock. The non-capable Pen Branch fault forms the boundary between the Triassic Basin and Paleozoic basement rocks (see Section 2.5.1.2.4 for a detailed discussion of the Pen Branch fault).

The Upper Sand Stratum (Barnwell Group) will be removed because it is not considered competent material. It is susceptible to liquefaction (Section 2.5.4.8) and dissolution-related ground deformation (Section 2.5.3.8.2); also the shear-wave velocity of the Upper Sand Stratum is generally below 1000 ft/sec, see Table 2.5.4-6.

All safety-related structures will be founded on structural backfill that will be placed on top of the Blue Bluff Marl after complete removal of the Upper Sand Stratum. The structural fill will be a sandy or silty sand material following the guidelines used during construction of VEGP Units 1 and 2. The properties of this structural backfill are described in Section 2.5.4.2.

The GMRS is defined at the free ground surface of this site-specific rock, soil, fill column. The FIRS is defined as hypothetical outcrop motion at the 40-ft depth horizon within this column. The highest in situ competent material for the VEGP ESP site is the Blue Bluff marl at 86-ft depth.

To determine the GMRS, FIRS, and 86-ft depth horizon ground motions, it is necessary to adjust the uniform hazard hard rock spectra (presented in Section 2.5.2.4) for amplification or deamplification as vibratory ground motion is propagated through the subsurface materials above the 9,200 ft/s shear-wave velocity horizon. This section describes the analyses performed to develop site amplification functions associated with the different hard rock ground motions presented in Section 2.5.2.4. These site amplification factors are used in Sections 2.5.2.6 (GMRS, FIRS, and top of Blue Bluff Marl) along with the hard rock ground motions to develop site-specific ground motions at these three horizons.

2.5.2.5.1 Development of Site Amplification Factors

2.5.2.5.1.1 Methodology

The method adopted here to account for the effects of surficial soils on seismic hazard follows the procedure in NUREG/CR-6728 and NUREG/CR-6769 (**McGuire et al. 2001, 2002**), described as “Approach 2A.” This procedure requires 6 steps:

1. The seismic hazard is calculated for hard rock conditions for the seven structural frequencies, over a range of ground motion amplitudes, resulting in a range of annual frequencies of exceedance.
2. For ground motion amplitudes corresponding to annual frequencies of 10^{-4}, 10^{-5}, and 10^{-6}, the seismic hazard is deaggregated for high frequencies (HF) and low frequencies (LF), as described in Section 2.5.2.4.6, to determine the dominant magnitudes and distances for those amplitudes and frequencies.
3. HF hard rock spectra are developed to represent earthquakes dominating the 5-10 Hz ground motions, and LF hard rock spectra are developed to represent earthquakes dominating the 1-2.5 Hz ground motions. These hard rock spectra represent the mean

magnitude and distance of earthquakes that dominate the seismic hazard for those structural frequencies.

4. The rock and soil column is modeled, and soil amplitudes are calculated for input hard rock motions corresponding to frequencies of exceedance of 10^{-4}, 10^{-5}, and 10^{-6}. These calculations are made separately for ground motions dominating the HF hard rock motion and the LF hard rock motion, and the input motions have a spectrum determined by the HF or LF hard rock spectral shape, as appropriate. Multiple hard rock motions are used, and multiple soil column properties are used, so that the mean soil amplitudes can be determined accurately.

5. The soil amplification factors (AFs) are developed at 300 frequencies using analyses described in this section based on the HF and LF hard rock spectral shapes. The AFs for a given horizon represent the mean spectral acceleration (SA) at that horizon, divided by input SA at hard rock, at each frequency. At each frequency, the envelope motion is determined. This is the motion (HF or LF) that gives the higher mean soil motion, for that structural frequency and MAFE. At frequencies above 8 Hz, this is always the HF motion. At frequencies below 2 Hz, this is always the LF motion. At intermediate frequencies, the envelope motion depends on the frequency and the MAFE.

6. The uniform hazard response spectra at MAFEs of 10^{-4} and 10^{-5} at each horizon are calculated as follows. Starting from the 10^{-4} and 10^{-5} SA hard rock values (from the hazard calculations described in 2.5.2.4) at the seven structural frequencies, interpolation is performed between those SA values to obtain 10^{-4} and 10^{-5} SA values at the 300 structural frequencies using the HF and LF spectral shapes for hard rock. The choice of HF or LF is based on the envelope motion determined in the previous step. The UHS for 10^{-4} at each horizon is calculated by multiplying the hard rock 10^{-4} SA values at the 300 frequencies by the mean AFs for 10^{-4} from step 5, again using the HF or LF mean AF corresponding to the envelope motion. (At some intermediate frequencies between 2 and 8 Hz, the HF and LF AFs are weighted in order to achieve a smooth transition between HF and LF spectra.) The UHS for 10^{-5} is calculated in a similar way, using the 10^{-5} rock SA values and the 10^{-5} AFs.

This gives an accurate calculation of the soil hazard at each horizon. In step 3, it is sufficiently accurate to use the mean magnitude to generate spectral shapes for the HF and LF spectra (Approach 2A of NUREG/CR-6728 and NUREG/CR-6769 **(McGuire et al. 2001, 2002)**). Using multiple magnitudes (Approach 2B of NUREG/CR-6728 and NUREG/CR-6769) does not materially affect the calculated soil spectra, as documented in NUREG/CR-6769 **(McGuire et al. 2002)**.

From the 10^{-4} and 10^{-5} SA values at each horizon, spectra are calculated using the procedure recommended by ASCE 43-05 2005. This procedure is used to establish the spectral amplitudes at the 300 structural frequencies. To obtain final horizontal spectra smoothing of the raw spectral shape is performed as described in 2.5.2.6.3.

2.5.2.5.1.2 Base Case Soil/Rock/Fill Column and Uncertainties

Development of a base case rock/soil/fill column, is described in Section 2.5.4. Summaries of the low strain shear wave velocity, material damping, and strain-dependency properties of the base case materials, as these parameters are used in the site response analyses, are provided below in Section 2.5.2.5.1.2.1. Section 2.5.2.5.1.2.2 describes the methodology and results of randomization to address the uncertainties in rock/soil/fill column parameters. Additional subsurface data in the power block has been collected for the COL site investigation. These data are presented in Section 2.5.4. The COL information includes RCTS testing and measurements of dynamic properties of the proposed backfill. Section 2.5.2.9.3 presents an evaluation of the effects of the combined COL and ESP geotechnical data on site response to determine its significance on site response.

2.5.2.5.1.2.1 Base Case Rock/Soil/Fill Column

2.5.2.5.1.2.1.1 Soil Column

The base case shear-wave velocity model for the soil column is provided in Figure 2.5.4-7, and the corresponding values are listed in Table 2.5.4-11. Additional shear-wave velocity data have been collected for the COL site investigation of the in-situ material. Figure 2.5.4-7a shows the base case shear-wave velocity model for the combined COL and ESP data. The COL plus ESP data shear-wave velocity model is not used to develop the ESP site amplification factors. This is discussed further below. The base case assumes that the uppermost 86 feet of native material will be excavated and replaced with structural fill. Shear-wave velocity was not measured for the compacted backfill during the ESP subsurface investigation (APPENDIX 2.5A). Interpolated values based on measurements made on fill for existing Units 1 and 2 **(Bechtel 1984)** are used instead. The backfill shear-wave velocity values are summarized in Table 2.5.4-10 (these values are also included in Table 2.5.4-11).

The variation with strain of shear modulus and damping of the soil were developed for two sets of degradation relationships:

- Based on relationships developed for EPRI **(EPRI TR-102293 1993)** and
- Based on relationships developed for SRS **(Lee 1996)**.

Site-specific soil degradation and damping ratio curves were developed as part of the COL site investigation. These curves are presented in Figures 2.5.4-9a and 2.5.4-11a respectively.

The EPRI relationships are widely used and accepted in the industry and, while the SRS curves were developed for the adjacent SRS site, the Blue Bluff Marl soil unit at the ESP site has higher velocities than the corresponding soil unit at the SRS site. Analyses are performed for both sets of degradation curves and equally weighted in developing the final spectral amplification factors.

Details of the derivation and extension of the degradation curves are presented in Section 2.5.4.7.2.

The base case degradation curves for shear modulus and damping for the EPRI-based assumption are presented in Figures 2.5.4-9 and 2.5.4-11, respectively. The base case degradation curves for shear modulus and damping for the SRS-based assumption are presented in Figures 2.5.4-10 and 2.5.4-12, respectively. The corresponding tables of values are presented in Table 2.5.4-12 and 2.5.4-13, for the EPRI-based and SRS-based relationships, respectively.

Unit weights, derived from the ESP laboratory testing program (APPENDIX 2.5A) for the shallow soils and calculation **(WSRC 1998)** for the deep sands, are provided in Table 2.5.4-4.

2.5.2.5.1.2.1.2 Rock Column

Due to the geometry of the Pen Branch fault, the shear-wave velocity character of the Triassic Basin and Paleozoic crystalline rocks below the Coastal Plain sediments, and the possible presence of a low velocity zone between the Triassic Basin and the Paleozoic crystalline rocks, a set of six (6) rock column models were used in combination with the base case soil column, described above, to adequately model uncertainty in the rock/soil column for site response analysis.

As discussed in Section 2.5.4.2.5, a rock density of 2.75 gm/cc (172 pcf) is used for the crystalline rock, and 2.53 gm/cc (158 pcf) for the Triassic rock. Based on inspection of Figures 2.5.4-11 and 2.5.4-12, the low strain damping of soils is on the order of 0.5 percent, which generally increases to 0.6 percent to 2 percent for strain compatible conditions. Rock, which would be expected to have lower damping than soil, was therefore assumed to behave as a linearly elastic material with one percent damping for all rock types.

The above-described shear-wave velocity profile, degradation relationships, and material densities were then used to develop randomized soil/rock profiles described in the following section.

2.5.2.5.1.2.2 Randomization of Site Profiles

To account for variations in shear-wave velocity across the site, sixty artificial profiles were generated using the stochastic model described in EPRI **(EPRI TR-102293 1993)** and extended in Toro (1996), with some modifications to account for the conditions at the VEGP ESP site. These artificial profiles represent the soil/rock/fill column from the top of the Paleozoic crystalline rock (with a shear-wave velocity of 9,200 feet/s) to the ground surface. This model uses as inputs the following quantities: (1) the median shear-wave velocity profile, which is equal to the base-case soil and rock profiles defined in Sections 2.5.2.5.1.2.1.1 and 2.5.2.5.1.2.1.2; (2) the logarithmic standard deviation of shear-wave velocity as a function of depth, which is set to 10 percent for the structural backfill, is set to values obtained from soil-randomization studies

performed at the SRS site **(Toro 1997; Toro 2005)** for the soil strata, and is set to values consistent with the six rock-column models described in Section 2.5.2.5.1.2.1.2; (3) the correlation coefficient between velocities in adjacent layers, which is taken from the second SRS soil-randomization study referenced above; (4) the probabilistic characterization of layer thickness as a function of depth, which is taken from the second SRS soil-randomization study referenced above, modified to allow for sharp changes in the base-case velocity profile; and (5) the depth to bedrock, which is randomized to account for the range of depths associated with the Pen Branch fault described in Section 2.5.2.5.1.2.1.2.

Figure 2.5.2-34 depicts the summary statistics for the 60 shear-wave velocity profiles. It is worth noting that the depth to the Blue Bluff Marl and to the Triassic Basin rock vary little between the profiles, and that the logarithmic standard deviation in shear-wave velocity is lower than typical values (e.g., **(Toro 1996)**). These features are a consequence of the availability of shear-wave velocity data from the VEGP ESP site and from the nearby SRS, and of the uniformity exhibited by these data. As a consequence of this uniformity, the average amplification factors computed from site-response calculations using these profiles may not be as smooth as those obtained using artificial profiles with more variability.

Figure 2.5.2-34a shows the upper part of the soil column shear wave velocity profile. The ESP base case shear-wave model is shown in red, each of the 60 individual randomizations used in the site amplification factor analysis are shown in light gray lines, and the statistical characterization of the randomization is shown in black lines. In addition, the COL plus ESP shear-wave velocity base case model is shown in turquoise. The COL plus ESP shear-wave velocity model falls well within the range of randomized ESP base case velocity models. Pending additional COL data on site-specific soil degradation and damping ratio curves and measured dynamic properties for the proposed backfill, the differences in the ESP to ESP plus COL soil column shear wave velocity do not warrant at this time recalculation of site amplification factors and the GMRS.

The degradation curves for shear modulus and damping were also randomized to account for the epistemic and aleatory uncertainty in these properties. These randomizations used as input the following quantities: (1) the median degradation curves, which are equal to the base-case degradation curves in Sections 2.5.2.5.1.2.1.1 and 2.5.2.5.1.2.1.2; (2) the uncertainties in the degradation properties of soil, which are taken from Costantino (1996), except for the engineered backfill, for which they are reduced by 1/3; and (3) the uncertainty in the damping ratio for the Triassic Basin rock, which is represented by a 5-95 percentile range of 0.7-1.5, which corresponds to a logarithmic standard deviation of 0.41. For each randomized velocity profile, one set of randomized degradation curves was generated for the EPRI curves and another set was generated for the SRS curves.

2.5.2.5.1.3 Development of Low-Frequency and High-Frequency Hard Rock Target Spectra

Hard rock target spectra were developed for the two different frequency ranges: HF (5-10 Hz) and LF (1-2.5 Hz), as defined in Reg. Guide 1.165, at each of three annual probability levels (10^{-4}, 10^{-5}, and 10^{-6}). The target spectra are based on the computed mean magnitude (Mbar) and distance (Dbar) values from the deaggregation of the hazard curves. For the HF cases (5-10 Hz), only those sources less than 105 km were used to compute the Mbar and Dbar values. For the LF cases (1-2.5 Hz), only those sources at distances greater than 105 km from the site were used to compute the Mbar and Dbar values. This distinction was made based on the noted dominance of the Charleston source for low frequencies and long return periods. The computed Mbar and Dbar results were based on the average of the 5 – 10 Hz values for the HF cases and the average of the 1 – 2.5 Hz for the LF cases. These computed values are given in Table 2.5.2-17. Based on the similar Mbar and Dbar values for each of the three probability levels for the HF and LF cases, a single recommended Mbar and Dbar pair was selected to represent the computed values for each of the HF and LF cases. For the LF case, the recommended distance was set at 130 km to model the Charleston source. For the HF case, the recommended distance is approximately equal to the log-average of the three computed values rounded to the nearest km. The recommended magnitude value is approximately equal to the linear average of the three computed magnitude values. The recommended magnitude values for both the high- and low-frequency cases are equal to the linear average of the three magnitude values rounded to the nearest tenth of a magnitude unit.

Given the Mbar and Dbar values, the Central and Eastern United States spectral shape (log-average of the single and double corner source models) from NUREG/CR-6728 **(McGuire et al. 2001)** were computed for both the HF and LF cases. These spectral shapes were scaled to the corresponding uniform hazard spectral (UHS) values (see Table 2.5.2-16) at 7.5 Hz and 1.75 Hz for the HF and LF cases, respectively. An additional requirement that the envelop spectrum of the scaled target spectra for a given annual probability level be no less than 90 percent of the UHS was applied. In any case for which this requirement was not met, either the scaled HF or LF target spectrum was increased to meet this requirement at the seven frequencies at which the hard rock UHS is computed. For the HF case, this requirement caused an increase of the 25 Hz spectral acceleration value at the 10^{-6} probability level. For the LF case at all three probability levels, the scaled LF spectra fall below the 90 percent UHS limit at 1 and 0.5 Hz. Thus, the scaled LF spectra were increased to 90 percent of the UHS value for the 1 and 0.5 Hz values, and for frequencies less than 0.5 Hz, the spectral shape of the LF spectrum scaled to the 90 percent of the 0.5 Hz UHS value was used.

The scaled hard rock target spectra were interpolated (log-log) to the recommended sampling rate of 100 equally log spaced values per frequency decade. The HF and LF target spectra for the three annual probability levels used to develop the spectrum-compatible time histories are shown in Figures 2.5.2-35a and b.

2.5.2.5.1.4 Selection of Seed Time Histories

The selection of the seed input time histories used in the spectral matching procedure was guided by the deaggregation results described in the previous section. For the HF case, the recommended Mbar and Dbar values are 5.6 and 12 km. For the low frequency case, the recommended Mbar and Dbar values are 7.2 and 130 km. These values were considered appropriate for all three MAFEs. Based on these recommended magnitude and distance values, a total of 30 seed time histories were selected for both the HF and LF cases.

Because of the limited number of strong ground motion acceleration time histories from stations located in the Eastern North America, 58 of the 60 selected seed input time histories were recorded at stations located in other regions than the Eastern North America. The additional two seed time histories that are used for the HF case were recorded in Eastern Canada. Time histories were selected based on the database of recorded strong ground motion records, recommended magnitude and distance values, and shear-wave velocities in the top 30 meters at recording sites of greater than 600 m/sec (about 1,970 ft/sec). The selected seed time histories are listed in Table 2.5.2-18a and Table 2.5.2-18b, for the HF and LF cases, respectively.

The spectral matching was performed based on a given horizontal target spectra with a spectral damping of 5 percent. The spectral matching procedure is a time domain spectral matching procedure and emphasis was placed on maintaining the phasing characteristics of the initial time history in the final modified spectrum-compatible time history. In addition, emphasis was placed on maintaining the characteristic of the normalized Arias intensities (the integral of the square of the acceleration-time history, a ground motion parameter that captures the potential destructiveness of an earthquake) of the initial and final modified spectrum-compatible time histories. The spectral matching criteria given in NUREG/CR-6728 **(McGuire et al. 2001)** that are applicable with the use of multiple time histories were used to check the average spectrum from the 30 time histories for a given frequency range (high- or low-frequency) and annual probability level. This is the recommended procedure in NUREG/CR-6728 **(McGuire et al. 2001)** when multiple time histories are being generated and used.

The selected 60 seed time histories were first matched to their respective 10^{-6} high and low frequency target spectra. As an example, the acceleration, velocity, and displacement time histories for one of the thirty 10-6 HF target spectrum seed time histories are shown in Figure 2.5.2-45a. The final modified spectrum-compatible acceleration, velocity, and displacement time histories (matched to the 10-6 HF target spectrum) are plotted in Figure 2.5.2-45b. Figure 2.5.2-46 shows the 10-6 HF target spectrum (thick grey line), the response spectrum from the initial acceleration time history scaled to the target PGA value (thin blue line), and the response spectrum from the final modified spectrum-compatible time history (thin red line). The initial and final modified spectrum-compatible normalized Arias intensities for this example are plotted in Figure 2.5.2-47. These results are representative of the goodness of fit for all spectrum-compatible time histories. For the 10^{-5} probability level, the final modified spectrum-compatible

time histories from the 10^{-6} probability level were used as the input time histories for the spectral matching. In a similar fashion, the final modified spectrum-compatible time histories for the 10^{-5} probability level were used as the input time histories for the spectral matching at the 10^{-4} probability level. The results of the spectral matching for the high and low frequency cases at each of the three annual probability levels are shown in Figures 2.5.2-36a through f. These spectrum-compatible time histories were used in the site response analysis presented in the next section.

2.5.2.5.1.5 Site Response Analyses

The site response analyses were conducted using the randomized shear-wave velocity profiles and soil modulus and damping relationships discussed in Section 2.5.2.5.1.2.1.1 to account for variation in the dynamic soil properties across the VEGP ESP Site. Two separate sets of degradation relationships for shear modulus and damping were applied in the site response analyses: EPRI-based curves and SRS-based curves (see Section 2.5.2.5.1.2). The depth to hard rock (V_s > 9200 fps) was also randomized to reflect its uncertainty. All site response analyses assumed that the sedimentary rock below 1049 ft (depth to bottom of Coastal Plain sediments) remains linear during earthquake shaking with one percent damping for all rock types. This randomization process resulted in 60 randomized rock/soil/fill profiles (that included combinations of depths to hard rock and degradation relationships) for each family of degradation curves (i.e., EPRI or SRS). Additional details about the generation of profiles for the site response analyses are included in Section 2.5.2.5.1.2.

Each of the 60 randomized soil profiles was paired with 30 seed time histories (each time history was applied to two of the randomized soil profiles) for each of the hard rock input motions (i.e., 30 time histories for the HF spectra and 30 time histories for the low frequency spectra). Three different mean annual frequency of exceedance events (10^{-4}, 10^{-5}, and 10^{-6}, see Section 2.5.2.5.1.3) were analyzed for each profile—seed time history pairing in order to calculate the amplification factors, defined as the ratios of five percent damped spectral accelerations for rock input motion at the 9,200 ft/s shear-wave velocity horizon to the five percent damped spectral accelerations motions computed at a hypothetical outcrop at the top of the Blue Bluff Marl (86-ft depth) at a hypothetical outcrop at the 40-ft depth horizon, and at the ground surface.

The computer program SHAKE **(Bechtel 2000)** was used to perform these analyses and amplification factors were extracted from each analysis resulting in 720 spectral amplifications (see Table 2.5.2-19) for each horizon.

The mean of the site amplification functions based on the suite of multiple input spectrum-compatible time histories for each group of 60 randomized soil profiles was used to develop site amplification factors for the VEGP ESP Site, as described in NUREG/ CR-6728 **(McGuire et al. 2001)**.

Figure 2.5.2-37b depicts the mean spectral amplification results of a typical analysis for HF content of a 10^{-4} MAFE seismic event using EPRI degradation curves for the ground surface. Similar plots of the computed amplification results for the 40-ft and 86-ft horizons are shown in Figures 2.5.2-37a and 2.5.2-37, respectively. The curves shown were determined by averaging the logarithms of amplification values for each frequency. As described in Section 2.5.2.5.1.2.1.1, analyses are performed for both sets of degradation curves and equally weighted in the subsequent development of the final spectral amplification factors.

In order to implement site response analysis Approach 2A, as discussed in Section 2.5.2.5.1.1, the amplification factors are prepared as a function of hard rock input motion. Tables 2.5.2-20e and 2.5.2-20f present the amplification factors at the ground surface for input hard rock motions corresponding to 10^{-4}, 10^{-5}, and 10^{-6} HF and LF MAFE target spectra, respectively (see Figures 2.5.2-35a and b). Similar results for the 40-ft horizon outcrop motion and the top of the Blue Bluff Marl are given in Tables 2.5.2-20c and 2.5.2-20d and Tables 2.5.2-20a and 2.5.2-20b, respectively. These results are presented for 30 structural frequencies, including the seven structural frequencies at which seismic hazards were calculated.

2.5.2.6 Horrizontal Ground Motion

2.5.2.6.1 Criterion for GMRS

The criterion used to calculate the recommended design spectrum comes from ASCE 43-05 **(ASCE 2005).** This criterion is based on the mean seismic hazard curves for multiple structural frequencies at the ground surface, taking into account the effect of rock, soil, and fill above the hard rock horizon. The spectral amplitudes at this horizon corresponding to a mean annual frequency of exceedance (MAFE) of 10^{-4} are scaled so that structures and components designed to the scaled spectral amplitudes will achieve a target performance goal corresponding to a mean annual frequency of onset of significant inelastic deformation (FOSID) of 10^{-5} per year. The soil hazard values that form the basis for this calculation were developed following Approach 2A as described in Section 2.5.2.5.1.1.

2.5.2.6.2 Discrete Frequency Horizontal GMRS Amplitudes

Table 2.5.2-21b shows ground motion amplitudes corresponding to MAFEs of 10^{-4}, 10^{-5}, and (for information purposes only) 10^{-6} for hard rock conditions. Thirty structural frequencies are tabulated, including the seven frequencies developed in Section 2.5.2.4 and an additional twenty three frequencies from the 300 frequency values per step 6 of 2.5.2.5.1.1. Table 2.5.2-21b also shows ground motion amplitudes for the free ground surface of the site-specific rock/soil/fill column that were calculated from the hard rock motions and the amplification factors of Section 2.5.2.5.

The horizontal GMRS (the design response spectrum (DRS) in the nomenclature of the ASCE 43-05 **(ASCE 2005)**) is derived from the amplitudes for MAFEs of 10^{-4} and 10^{-5} in Table 2.5.2-21b. That is, the Amplitude Ratio, AR, of 10-5 to 10-4 amplitudes is determined for spectral accelerations (SA) at each structural frequency:

$A_R = SA(10^{-5})/SA(10^{-4})$ (Equation 2.5.2-4)

and the horizontal GMRS is calculated as:

$GMRS = SA(10^{-4}) \times \max(1.0, 0.6\ A_R^{0.8})$ (Equation 2.5.2-5)

Table 2.5.2-22b shows thirty of the GMRS values calculated from Equation 2.5.2-5, at the free ground surface. In Table 2.5.2-22b, the last term in Equation 2.5.2-5, $0.6\ A_R^{0.8}$, is indicated as "DF2" in the table.

2.5.2.6.3 Full GMRS Horizontal Spectrum

The horizontal GMRS values at the 300 structural frequencies, thirty of which are provided in Table 2.5.2-22b, are used to define the raw horizontal GMRS. This spectrum is then smoothed by a running average filter for the 100-points-per-decade spectral amplitudes above 1 Hz, but is constrained to go through the seven structural frequencies at which hazard calculations were made. (An exception was made for 5 Hz, where the site amplification analysis indicated a trough, so the 5 Hz GMRS value was smoothed based on amplitudes at adjacent frequencies, which raised the 5 Hz GMRS value slightly and improved the shape of the spectrum.) This step smooths out the spectral peaks and troughs above 1 Hz, which are not statistically significant, but maintains the low-frequency peaks and troughs representing lower-mode soil column response for this site.

Figure 2.5.2-38b shows the raw spectrum and the smoothed VEGP ESP horizontal GMRS.

2.5.2.6.4 Foundation Input Response Spectrum (FIRS) and Top of In Situ Competent Material (top of Blue Bluff Marl) Ground Motions

2.5.2.6.4.1 Development of FIRS and Top of In Situ Competent Material Spectra

The criterion used to calculate the recommended outcrop FIRS and top of Blue Bluff Marl spectra (at the 40-ft and 86-ft depth horizons, respectively) are the same as was used to develop the ground surface GMRS motion. That is, as described above the methodology of ASCE 43-05 **(ASCE 2005)** was used**.** And, as for the GMRS, the soil hazard values that form the basis for this calculation were developed following Approach 2A and the characterization of subsurface materials as described in Section 2.5.2.5.1.1.

Table 2.5.2-21a shows ground motion amplitudes corresponding to MAFEs of 10^{-4}, 10^{-5}, and (for information purposes only) 10-6 for hard rock conditions (thirty structural frequencies are tabulated including, the seven frequencies developed in Section 2.5.2.4 and an additional twenty

three frequencies from the 300 frequency values per step 6 of 2.5.2.5.1.1). Table 2.5.2-21a also shows ground motion amplitudes for an outcrop at the 40-ft depth horizon; these were calculated from the hard rock motions and the amplification factors of Section 2.5.2.5.

Table 2.5.2-21 shows similar values for the top of Blue Bluff Marl horizon.

The FIRS and top of Blue Bluff Marl horizons outcrop spectra are derived from the amplitudes for MAFEs of 10^{-4} and 10^{-5} in Tables 2.5.2-21a and 2.4.2-21, respectively. That is, the Amplitude Ratio, AR, of 10^{-5} to 10^{-4} amplitudes are determined for spectral accelerations (SA) at each structural frequency using the ASCE 43-05 formula given above in the development of the GMRS spectra.

Tables 2.5.2-22a and 2.5.2-22 shows thirty of the FIRS and top of Blue Bluff Marl values calculated at the hypothetical outcrops at the 40-ft and 86-ft horizons, respectively.

The FIRS and top of Blue Bluff Marl values at the 300 structural frequencies, thirty of which are provided in Tables 2.5.2-22a and 2.5.2-22, are used to define the raw ground motion response spectra. These spectra are then smoothed, as were the GMRS spectra, by a running average filter for the 100-points-per-decade spectral amplitudes above 1 Hz, but is constrained to go through the seven structural frequencies at which hazard calculations were made.

Figures 2.5.2-38a and 2.5.2-38 show the raw and smoothed spectrum.

The vertical FIRS and top of Blue Bluff Marl spectra were computed by applying the V/H spectral ratio presented in Section 2.5.2.7.1.3 to the smoothed FIRS and top of Blue Bluff Marl horizontal spectra plotted in Figures 2.5.2-38a and 2.5.2-38. The resulting VEGP ESP vertical and horizontal FIRS and top of Blue Bluff Marl spectra are plotted in Figures 2.5.2-44a and 2.5.2-44.

2.5.2.6.4.2 Selection of Time Histories and Spectral Matching to the FIRS

Time histories matching the FIRS are used in several sensitivity analyses summarized in Section 2.5.2.9. Therefore, these time histories are developed here. Given the FIRS horizontal and vertical spectra presented in Section 2.5.2.7.1 and plotted in Figure 2.5.2-44a, one set of three component time histories was developed to be spectrum compatible to the FIRS target spectra. The single three component set was selected based on the deaggregation of the low frequency (LF) results. For the low frequency case, the recommended Mbar and Dbar values are 7.2 and 130 km. These values were considered appropriate for all three MAFEs. For this analysis, the three component time histories from the 1999 Hector Mine earthquake (Mw=7.13) recorded at the Heart Bar State Park station (R=61.21 km) were selected. This was one of the 30 sets of time histories selected for the site response analysis (see Table 2.5.2-18b).

The spectral matching procedure is a time domain procedure and emphasis was placed on maintaining the phase characteristics of the initial time history in the final modified spectrum-compatible time history. In addition, emphasis was placed on maintaining the characteristic of the normalized Arias intensities (the integral of the square of the acceleration-time history, a

ground motion parameter that captures the potential destructiveness of an earthquake) of the initial and final modified spectrum-compatible time histories. The spectral matching criteria given in NUREG/CR-6728 **(McGuire et al. 2001)** that are applicable were used to check the acceptability of the modified spectrum compatible time history. In most cases, an additional scale factor which is applied after the spectral matching process is used to assure that the final modified time history satisfies the spectral matching criteria given in NUREG/CR-6728. A common scale factor of 1% (i.e., 1.01) was used for each of the three components. The modified acceleration, velocity, and displacement time history prior to the application of this 1.01 scale factor is shown in Figure 2.5.2-48a for the first horizontal component. Figure 2.5.2-48b shows target FIRS horizontal spectrum, 1.3*FIRS target spectrum, 0.9*FIRS target spectrum and the modified time history response spectrum including the 1.01 scale factor. The normalized Arias intensities for this first horizontal component are shown in Figure 2.5.2-48c. The results for the second horizontal component are shown in Figures 2.5.2-49a through 2.5.2-49c. The vertical component results are presented in Figures 2.5.2-50a through 2.5.2-50c.

2.5.2.7 Vertical GMRS Spectrum

The method to develop the vertical GMRS is to develop a vertical-to-horizontal scaling factor [V/H], which is then applied to the horizontal GMRS at the 3 horizons (GMRS, FIRS, and top of Blue Bluff Marl), presented above.

2.5.2.7.1 Development of V/H

Reg. Guide 1.60 presents acceptable standard response spectral shapes as a function of frequency that may be considered for the seismic design of nuclear power plants. These shapes are given for both horizontal and vertical ground motions as a function of damping. The shapes are independent of peak ground acceleration (PGA), which is used as a scaling factor. The ratio of the vertical to horizontal spectral shapes results in a V/H scaling function that is a value of 2/3 for frequencies less than 0.25 Hz, 1.0 for frequencies higher than 3.5 Hz, and varies between 2/3 and 1 for frequencies between 0.25 and 3.5 Hz.

A significant increase in the number of strong ground motion observations and advances in earthquake ground motion modeling since the publication of Reg. Guide 1.60 suggest that the V/H ratios implied in Reg. Guide 1.60 may not be appropriate for a given site **(EPRI TR-102293 1993; McGuire et al. 2001)**. The horizontal and vertical ground motions and the V/H ratios are observed to depend on magnitude, distance, site conditions, and regional tectonic setting (e.g. western US [WUS] vs. central and eastern US [CEUS]), which presents distinctive characteristics of earthquake source, attenuation along regional path, and shallow crust).

NUREG/CR-6728 **(McGuire et al. 2001)** presents V/H ratios for soft rock WUS sites and hard rock CEUS sites as a function of horizontal peak acceleration, as a proxy for the combined dependence on magnitude and distance. While the WUS rock V/H ratios are based on the

significant empirical database of WUS strong ground motion, there are too few CEUS recordings to develop empirically-based CEUS V/H relations. NUREG/CR-6728 follows up on a technique presented in EPRI TR-102293 of using earthquake ground motion modeling to develop CEUS rock V/H. Due to assumptions and the estimation of various required parameters, the explicit results of the CEUS modeling are not considered robust, but can be used as guidelines for the difference between V/H ratios for WUS and CEUS rock sites. For the rock CEUS V/H ratios NUREG/CR-6728 uses the WUS ratios and modifies them based on the difference in trends obtained between WUS and CEUS rock sites from their modeling studies. For example, a peak in the V/H ratio is expected to occur at higher frequencies for CEUS than for WUS sites because site kappa values in the CEUS are typically lower than in the WUS.

The VEGP ESP site, however, is a deep soil site, not a hard rock site. V/H relations for soil sites are not given in NUREG/CR-6728 **(McGuire et al. 2001)**, and, again, an insufficient number of ground motion observations have been made to develop empirical CEUS relationships for soil sites. Appendix J of NUREG/CR-6728, however, does discuss the use of modeling by which V/H ratios can be developed for CEUS soil sites. The method mirrors that used in NUREG/CR-6728 in developing the CEUS rock V/H relations, and can be represented by the following formula:

$$V/H_{CEUS,Soil} = V/H_{WUS,Soil,Empirical} * [V/H_{CEUS,Soil,Model} / V/H_{WUS,Soil,Model}] \quad \text{(Equation 2.5.2-6)}$$

The first term of Equation 2.5.2-6 can be a readily available WUS relationship, such as Abrahamson and Silva (1997), which presents both vertical and horizontal ground motion attenuation relations for deep soil sites. Magnitude and distance is specified, which allows hazard contribution-appropriate specification for a given location.

The second term is a WUS-to-CEUS "transfer function" to modify the WUS ratios from the first term to give the required $V/H_{CEUS,Soil}$. The development of this second term entails ground motion modeling of both CEUS [numerator] and WUS [denominator] ground motions appropriate for the given site (e.g., the major contributing or controlling earthquake by magnitude and distance) and considers the site-specific conditions. The model for developing $V/H_{WUS,Soil,Model}$ considers generic site soil conditions, as implicitly considered in the $V/H_{WUS,Soil,Empirical}$ term. The model for developing $V/H_{CEUS,Soil,Model}$ model can consider as site-specific soil conditions as possible.

Upon developing V/HCEUS,Soil from Eq. 2.5.2-6, the vertical GMRS response spectrum is then defined by

$$Sa_{GMRD,Vertical} = Sa_{GMRS,Horizontal} * V/H_{CEUS,Soil} \quad \text{(Equation 2.5.2-7)}$$

As discussed above, the first term on the right-hand side of Equation 2.5.2-6 can be implemented using the ground motion attenuation relationship of Abrahamson and Silva (1997). The development of the WUS-to-CEUS transfer function (the second right-had side term of Equation 2.5.2-6) needs significant analytical effort, contains potentially significant uncertainties, and

requires a number of assumptions. Two studies guide the development of a best estimate of V/$H_{CEUS,Soil}$ and, through Equation 2.5.2-7, the definition of the vertical GMRS response spectrum.

2.5.2.7.1.1 Estimate of V/H from NUREG/CR-6728

Appendix J of NUREG/CR-6728 **(McGuire et al. 2001)** discusses various characteristics of vertical strong motions and, building upon the work presented in EPRI TR-102293, presents the methodology to estimate V/H for CEUS rock and soil sites. This method is that represented by Equation 2.5.2-6, above. A generic CEUS soil column is considered in their presentation of the method. In the appendix, plots of the numerator and denominator of the WUS-to-CEUS transfer function are shown, Figures J-32 and J-31, respectively, for **M**6.5 and a suite of distances [1, 5, 10, 20, and 40km]. An estimate of the WUS-to-CEUS transfer function can be made for **M**6.5 at the given distances using these results shown in these figures.

As discussed above, the GMRS response spectrum is based on slopes of the 10-4 and 10-5 ground motion hazard curves and the scaling of the 10-4 ground motions. The resulting horizontal GMRS ground motions at the seven spectral control points are generally only slightly higher than the 10-4 ground motion levels. That is, the horizontal GMRS is dominated by the 10-4 ground motion.

In reviewing the high-frequency distance deaggregation at the 10^{-4} hazard level (Figure 2.5.2-30), about one-quarter of the hazard is coming from “near” events, or about distances less than 20 km, while about three-quarters of the hazard is coming from “far” events, or distances centered at about 130 km. In reviewing the corresponding distance deaggregation at the 10^{-5} hazard level in the same figure, the bimodal nature of the deaggregation is yet apparent, but the relative contribution of the near and far events is about the same.

In reviewing the low-frequency magnitude-distance deaggregations at both the 10^{-4} and 10^{-5} hazard levels (Figure 2.5.2-31), hazard contribution is clearly dominated by the distant event centered on about 130 km.

The magnitudes and distances that can be attributed to the near and far events are taken as those used in the development of the high-frequency and low-frequency target spectra for the site response analysis: **M**5.6 at a distance of 12 km and **M**7.2 at a distance of 130 km, respectively.

Figure 2.5.2-39 is a plot of the first term of Equation 2.5.2-6 for both near and far events using the attenuation relationship of Abrahamson and Silva (1997).

Figure 2.5.2-40 is a plot of estimates of the second term of Equation 2.5.2-6 (ratio of V/H ratios) developed as the quotient of the curves in NUREG/CR-6728 **(McGuire et al. 2001)** Figure J-32 and J-31 for highest available distances of 10, 20, and 40 km. The Appendix J figures are given only for **M**6.5. Therefore, an estimate of an equivalent ground motion proxy magnitude and distance must be made to estimate the second term of Equation 2.5.2-6. The **M**6.5, 20 km curve

may be considered a reasonable proxy for the "near" event of **M**5.6 at 12 km. The greatest distance given in the two figures of Appendix J is 40 km, so this has to be used as the proxy, along with the associated **M**6.5, for the "far" event of **M**7.2 at 130 km. Given the trend of the V/H values (decreasing with distance for a given magnitude), it is expected that the "far" event proxy may be conservative (high in value), as compared to the value expect if equivalent ratio of ratio curves had been explicitly available for **M**7.2 at 130 km. Figure 2.5.2-40 shows the recommended "near" and "far" versions of the second term of Equation 2.5.2-6. Some smoothing has been applied that may be reflecting certain aspects (peaks, valleys) of the response reflecting the generic soil models used.

Figure 2.5.2-41 is a plot of $V/H_{CEUS,Soil}$ of Equation 2.5.2-6 considering both "near" and "far" events. Given the observations made earlier with regard to the relative contributions of the deaggregation "near" and "far" events to the 10^{-4} and 10^{-5} hazards, and the relative contribution of these two hazard levels to the horizontal GMRS design response spectrum, the "near" and "far" estimates of $V/H_{CEUS,Soil}$ are weighted approximately 1:3, resulting in the final $V/H_{CEUS,Soil}$ shown in Figure 2.5.2-41, as derived from the available results in NUREG/CR-6728.

2.5.2.7.1.2 Estimate of V/H from Lee (2001)

As a second estimate of the required V/H ratio, the results of the study for the MOX Fuel Fabrication Facility [MFFF] at the Savannah River Site are considered **(Lee 2001)**. The methodology used in that study followed the same approach as presented in NUREG/CR-6728 and EPRI TR-102293, and used in the section above, with the primary exception that the function $V/H_{CEUS,Soil,Model}$ of Equation 2.5.2-6 is developed using a site-specific model of the soil conditions. Lee (2001) notes that the following vertical and horizontal modeling assumptions are made based on validations:

Vertical motions are modeled as a combination of pure SV-waves and SV-P converted waves arriving at the base of the soil/alluvium materials at inclined angles of incidence computed using ray tracing methods;

Horizontal component spectra are computed assuming pure S-waves arriving at vertical incidence;

Linear elastic analysis is assumed for computing the vertical motions;

Low strain behavior (i.e., no wave induced dynamic strain degradation) compressional and shear-wave site velocity profiles are used in computing vertical spectra;

Damping for computing vertical spectra is the low strain level damping used to compute horizontal spectra;

For computing horizontal motions, wave induced dynamic strain degradation of the shear-wave velocity and increased damping of the profile is permitted (in an equivalent linear analysis).

The consequence of these assumptions is that the model-derived V/H ratios (particularly for the MFFF site) may be conservatively high over some range of spectral frequencies and at high loading levels.

Lee (2001) directly presents final V/H ratios (i.e., the resulting $V/H_{CEUS,Soil}$ of Equation 2.5.2-6) for several magnitudes and distances. V/H ratios for **M**5.5 at 10 and 20 km and **M**6.0 at 10 and 20 km were interpolated to estimate the "near" V/H ratio for **M**5.6 at 12 km. V/H ratios for **M**7.0 at 100 km and **M**7.5 at 100 km were interpolated to estimate a "far" V/H ratio for **M**7.2 at 100 km. The distance of 100 km was the greatest considered in Lee (2001), but is considered adequate, if not slightly conservative, for a proxy of the 130 km desired for the "far" event.

Figure 2.5.2-42 is a plot of $V/H_{CEUS,Soil}$ of Equation 2.5.2-6 considering both "near" and "far" events. As before, given the observations made earlier with regard to the relative contributions of the deaggregation "near" and "far" events to the 10^{-4} and 10^{-5} hazards, and the relative contribution of these two hazard levels to the horizontal GMRS response spectrum, the "near" and "far" estimates of $V/H_{CEUS,Soil}$ are weighted approximately 1:3, resulting in the final $V/H_{CEUS,Soil}$ shown in Figure 2.5.2-42, as derived from the available results in Lee (2001).

2.5.2.7.1.3 Recommended V/H

The results of two studies have been used to guide in the development of best estimates of $V/H_{CEUS,Soil}$, as discussed above and summarized in Figure 2.5.2-43. The $V/H_{CEUS,Soil}$ developed from Lee (2001) gives a higher value V/H ratio than that developed from the available NUREG/CR-6728 results for frequencies greater than about 0.7 Hz. Both results give minimum V/H values, particularly in the lower frequencies, which appear lower than engineering judgment may suggest acceptable in the current state-of-knowledge.

Given the site specific nature of the Lee (2001) estimate, which would argue against considering an average of the two results, an approximate envelope of the results is recommended, wherein some smoothing is considered and a minimum V/H value of 0.5 is considered. The recommended final V/H ratio is shown in Figure 2.5.2-43. This V/H ratio is described as follows:

Frequencies	**V/H ratio**
≤ 1 Hz	0.5
1 to 15 Hz	log-log interpolate between 0.5 and 0.9
≥ 15 Hz	0.9

In Figure 2.5.2-43 the V/H ratio from RG 1.60 is shown for comparison. The recommended V/H ratio is marginally less than the Reg. Guide ratio at all frequencies.

2.5.2.7.1.4 Recommended Vertical GMRS Spectrum

To develop the vertical spectra, the horizontal spectra is scaled by the recommended V/H ratios provided in 2.5.2.7.1.3. Figure 2.5.2-44b, 2.5.2-44a, and 2.5.2-44 show the resulting vertical and horizontal GMRS, FIRS, and top of Blue Bluff Marl spectra, respecitively.

2.5.2.8 Operating Basis Earthquake Ground Motion

The Operating Basis Earthquake (OBE) ground motion spectra was not determined as part of the Vogtle ESP submittal. Requirements related to the OBE are provided in paragraph IV (a) (2) of Appendix S to 10 CFR Part 50, "Earthquake Engineering Criteria for Nuclear Power Plants." Under General Information in this appendix, the following statement is made: "This appendix applies to applications for the design certification or combined license pursuant to part 52 of this chapter or a construction permit…" Since OBE requirements are related to the design and performance of safety related systems, the OBE ground motion spectra will be determined during the COL stage as required under Appendix S.

2.5.2.9 Sensitivity Studies

2.5.2.9.1 Sensitivity for Backfill Vs

During the COL investigation and prior to conducting the Phase I test pad program, a study was conducted to evaluate the sensitivity of the AP1000 responses to the change in backfill shear wave velocity. The shear wave velocity used for the backfill sensitivity analysis (sensitivity study) is compared with the backfill velocity used for GMRS and FIRS computation (ESP profile) in Figure 2.5.2-51. The analyses included randomization of the entire soil column with the new backfill properties and development of the new outcrop motion at the foundation level of the AP1000 Nuclear Island. The new time history and associated strain-compatible soil properties were used in the SSI analysis of the AP1000.

The study confirmed that, even with a large variation of the backfill property, the AP1000 design is applicable to the Vogtle site with a large margin. Appendix 2.5E, Vogtle Site Specific Seismic Evaluation Report provides the results of this sensitivity analysis.

2.5.2.9.2 Study of the Effects of Backfill Geometry

Due to the large volume of excavation and the lateral extent of the backfill at the Vogtle site, the backfill layers were modeled as free-field soil layers in the modeling of the soil profile for both the soil amplification for development of the ground motion (GMRS and FIRS) and the site-specific seismic SSI analysis of the AP1000.

To verify the validity of this assumption, a two-dimensional site response analysis followed by a two-dimensional SSI analysis of the AP1000 model were used to evaluate the effect of the extent of backfill on the site response and on the SSI response of the NI. The plant layout is shown in

Figure 2.5.2-52. For the 2D analysis, the cross section shown in the East-West direction shown in Figure 2.5.2-53 was used. The analysis consists of two parts.

In part I, 2D site response analysis was performed. The 2D SASSI model of the site is based on Section A shown in Figure 2.5.2-53 that represent a "bathtub" model of the site with backfill modeled with plane strain elements. The 2D SASSI model for site response analysis is shown in Figure 2.5.2-54. An axis of symmetry was used to consider the backfill geometry for both units. The in-situ upper sand layers are modeled using the site-specific dynamic properties measured at the site. The properties of the backfill, blue bluff marl, the lower sand layers and layers extending to the rock at the base were the same as those used in the site response analysis to develop GMRS and FIRS. However, since computation of GMRS and FIRS were based a wide range of soil columns and input motions (60 randomized profiles, 30 time histories for HF and 30 time histories for LF rock motion), only a subset of the properties and input motion were considered. The analysis in part I included the upper, mean and lower bound soil profiles and only 3 time histories for each of HF and LF rock input motion. The results of the site amplification for the 2D site response analysis was compared with the site amplification factors from the1D SHAKE results for the same set of input motion and soil properties. The differences in site amplification factors are shown in Figures 2.5.2-55, 2.5.2-56, and 2.5.2-57. The results from SHAKE are represented in terms “in-column” motions to be comparable with the 2D SASSI nodal response motions at the three locations at centerline of the backfill (Figure 2.5.2-54), As shown in these figures, the differences are very small confirming that geometry of the backfill has insignificant effect on GMRS and FIRS. Additionally in Figure 2.5.2-55 the mean amplification used to develop the GMRS motion is plotted as a red dotted line; the close fit of the curves confirms the adequacy of the selection of limited number of soil columns and time histories for this study. In addition, transfer functions are obtained from the same set of calculations that provided the spectral amplifications. Transfer functions represent the harmonic amplification of the input motion used as input to soil column analysis to the “in-column” motion at the two horizons (0 ft and 40 ft depth). Transfer functions for the mean (Best Estimate) soil profile subjected to one HF input motion are compared for the 1D SHAKE and 2D SASSI analysis at two horizons, 0 ft and 40 ft depth, in Figure 2.5.2-55a and Figure 2.5.2-56a, respectively. The comparison of transfer function also confirms that 1D SHAKE analysis isadequate for the development of the ground motion given the geometry of the backfill at the site.

In part II, a new Vogtle 2D SASSI model of the NI was created to include the backfill as part of the structural model as shown in Figure 2.5.2-58. This model is similar to the "bathtub" model shown in Figure 2.5.2-54 except the AP1000 NI model is included. For this model the strain-compatible soil properties for the in-situ upper sand layer were used as part of the free-field SASSI model. The analysis in Part II was limited to the mean soil profile and for one time history from the analysis performed in Part I. The input motions for the two SSI analyses are obtained from the respective 1D SHAKE analysis in part I consistent with the free-field model used in each SASSI model. The SSI responses for the Vogtle "bathtub" 2D SASSI NI model (Bathtub Model-

d5) at key locations in the NI are compared with the SSI results of the Vogtle 2D SASSI NI model (2D-AP-d5) that assumes backfill extends to infinity in lateral directions. The results of the analysis are compared at the following key locations in the NI.

Nodes	Elevation (ft)	Description
4041	99.000	NI at Reactor Vessel Support Elevation
4061	116.5	Auxiliary Shield Building at Control Room Floor
4120	179.560	ASB Auxiliary Building Roof Area
4310	327.41	ASB Shield Building Roof Area
4412	224	Steel Containment Vessel near Polar Crane
4535	134.250	Containment Internal Structure at Operating Deck

These comparisons are shown in Figures 2.5.2-59 though 2.5.2-64. The response spectra are similar and the differences are considered negligible. For information the generic AP1000 standard design response spectra are plotted for comparison purposes which confirms significant margin between the AP1000 generic response and the Vogtle 2D results. A more detailed discussion of the Vogtle "bathtub" 2D SASSI NI model and a comparison of transfer functions are documented in Appendix A of Appendix 2.5E.

The comparison of the results confirms that the extent and geometry of the backfill has negligible effects on GMRS and FIRS and has small effects on the structural responses which are well within the range of the margin of the design.

2.5.2.9.3 Updated Site Response Analyses

As discussed in Section 2.5.4.7, additional geotechnical data was collected as part of COL investigation and the ESP data was supplemented with the new data. The completed data set is referred to as “COL” data. Section 2.5.4.7.1 presents a discussion of the shear wave velocity profile of the ESP and COL data sets and Section 2.5.4.7.2 presents a discussion of the strain-dependent soil properties of the two data sets. Site specific (COL) strain-dependant soil properties are presented in Figures 2.5.4-9a and 2.5.4-11a and in Table 2.5.4-12a. Section 2.5.4.7.5 presents the comparison of the data in terms of the shear wave velocity profile (Figure 2.5.4-7a) and strain-dependent soil properties (Figures 2.5.4-19a through 2.5.4-20c). Soil amplification analysis and development of FIRS described in Section 2.5.2.5.1 are based on the ESP data. In this section, the effect of COL data on the soil amplification at the depth of 40 ft (FIRS) is presented. The FIRS at 40 ft depth has been used as input for the site specific evaluation of the AP1000 design.

As described in Section 2.5.2.5.1, development of soil amplification using ESP data is based on 60 randomized velocity profiles and associated EPRI and SRS strain-dependent soil properties incorporating 30 time histories for the HF and LF motions at each MAFE of 10^{-4}, 10^{-5}, and 10^{-6} levels. However for the purpose of sensitivity analysis and evaluation of the effects of COL data, a limited number of soil column analysis have been performed as described below.

Using the best estimate COL velocity profile (Figure 2.5.4-7a), the upper bound and lower bound profiles were developed using a variation of the data set. The three COL velocity profiles and the associated COL strain-dependent soil properties were analyzed using three HF and three LF time histories corresponding to MAFE of 10^{-4}. All analyses were performed twice to consider the low and high PI strain-dependent soil properties for BBM (Figures 2.5.4-19b and 2.5.4-20b). Several iterations were performed in each run to converge on the soil properties. The strain-compatible velocity profiles and damping profiles obtained from the analysis are shown in Figure 2.5.2-65a and 2.5.2-65b labeled as COL. From each run, the response motion in terms of 5% acceleration response spectrum at the depth of 40 ft as SHAKE "outcrop" motion was computed. The results of HF input motion were averaged over the three time histories and over the three soil profiles as well as the low and high PI cases of the BBM. The same averaging method was used for the LF input motions. The averaged results were divided by the corresponding HF and LF input response spectrum at MAFE of 10^{-4} to compute the spectral amplification at the 40 ft horizon. The resultant two amplifications curves were enveloped. The enveloped amplification values are shown in Figure 2.5.2-65c labeled as COL.

To provide a consistent soil amplification for comparison with the results using COL data, from the ESP set of runs described in Section 2.5.2.5.1, the strain-compatible velocity and damping profiles were used to obtain the median and upper and lower bound profiles (using one standard deviation as the variation). The velocity and damping profiles are compared with the corresponding profiles from the analysis of the COL data in Figures 2.5.2-65a and 2.5.2-65b, respectively. Except for the damping profile at shallow depths, the two sets of data are consistent. The three profiles selected from the analysis of the ESP data were subsequently analyzed using the same three HF and LF time histories used in the analysis of the COL data. Since the soil properties are already compatible with shear strains, no further iteration on soil properties was performed. The results in terms of acceleration response spectrum at 5% damping at 40 ft depth as outcrop motion were obtained. The spectra for each HF and LF motions were averaged over the three time histories and over the three profiles. The averaged responses were divided by the respective HF and LF response spectra at MAFE of 10^{-4} and the resultant amplifications were enveloped. Figure 2.5.2-65c shows the amplification labeled as ESP.

To confirm the adequacy of the limited number of profiles and time histories for the purpose of this evaluation, the amplification corresponding to the analyses of the fully randomized ESP soil profiles (Section 2.5.2.) is also shown in Figure 2.5.2.65c labeled as "ESP-all". The comparison of the two sets of results based on ESP data shows the selection of limited number of profiles

and time histories are adequate for the purpose of the evaluation of the impact of the COL data. Furthermore, the comparison of the amplification between ESP and COL data is considered small and is expected to be reduced to be negligible if the fully randomized soil profiles were used in the COL set of analyses.

In addition, an assessment of the small differences in the amplification of the FIRS motion on the structural response of the AP1000 has been made. The AP1000 has significant margin when compared to Vogtle site specific seismic floor response spectra associated with the ESP and sensitivity soil profiles. Based on this evaluation, it has been determined that the AP1000 certified Design remains acceptable for the Vogtle site.

Table 2.5.2-1 Earthquakes 1985–2005, Update to the EPRI (NP-4726-A 1988) Seismicity Catalog with $Em_b \geq 3.0$, Within a 30° to 37° N, 78° to 86° W Latitude-Longitude Window, Incorporating the 200 mi (320 km) Radius Site Region

Year	Mo	Dy	Hr	Mn	Sec	Lat	Lon	Z(km)	Int	Emb	Smb	Rmb
1985	12	22	0	56	5.0	35.701	-83.720	13.4		3.25	0.30	3.35
1986	1	7	1	26	43.3	35.610	-84.761	23.1		3.06	0.30	3.17
1986	2	13	11	35	45.6	34.755	-82.943	5.0		3.50	0.10	3.51
1986	3	13	2	29	31.4	33.229	-83.226	5.0	4	3.30	0.25	3.37
1986	7	11	14	26	14.8	34.937	-84.987	13.0	6	3.80	0.10	3.81
1986	9	17	9	33	49.5	32.931	-80.159	6.7	4	3.30	0.25	3.37
1987	3	16	13	9	26.8	34.560	-80.948	3.0		3.06	0.30	3.17
1987	3	27	7	29	30.5	35.565	-84.230	18.5	6	4.20	0.10	4.21
1987	7	11	0	4	29.5	36.105	-83.816	25.1	5	3.79	0.10	3.80
1987	7	11	2	48	5.9	36.103	-83.819	23.8	4	3.43	0.10	3.44
1987	9	1	23	2	49.4	35.515	-84.396	21.1		3.06	0.30	3.17
1987	9	22	17	23	50.1	35.623	-84.312	19.4	5	3.50	0.10	3.51
1987	11	27	18	58	29.3	36.852	-83.110	26.8	5	3.50	0.10	3.51
1987	12	12	3	53	28.8	34.244	-82.628	5.0		3.00	0.10	3.01
1988	1	9	1	7	40.6	35.279	-84.199	12.2	4	3.30	0.25	3.37
1988	1	23	1	57	16.4	32.935	-80.157	7.4	5	3.50	0.25	3.57
1988	2	16	15	26	54.8	36.595	-82.274	4.0	4	3.30	0.10	3.31
1988	2	18	0	37	45.4	35.346	-83.837	2.4	4	3.50	0.10	3.51
1989	6	2	5	4	34.0	32.934	-80.166	5.8	4	3.30	0.25	3.37
1990	8	17	21	1	15.9	36.934	-83.384	0.6	5	4.00	0.10	4.01
1990	11	13	15	22	13.0	32.947	-80.136	3.4	5	3.50	0.10	3.51
1991	6	2	6	5	34.9	32.980	-80.214	5.0	5	3.50	0.25	3.57
1991	9	24	7	21	7.0	35.701	-84.117	13.3	4	3.30	0.10	3.31
1991	10	30	14	54	12.6	34.904	-84.713	8.1		3.06	0.30	3.17
1992	1	3	4	21	23.9	33.981	-82.421	3.3	5	3.50	0.25	3.57
1992	8	21	16	31	56.1	32.985	-80.163	6.5	6	4.10	0.10	4.11
1993	1	15	2	2	50.9	35.039	-85.025	8.1	4	3.30	0.10	3.31
1993	7	12	4	48	20.8	36.035	-79.823	5.0	4	3.30	0.10	3.31
1993	8	8	9	24	32.4	33.597	-81.591	8.5	5	3.50	0.10	3.51
1994	2	12	2	40	24.5	36.800	-82.000	5.0		3.42	0.41	3.61
1994	4	5	22	22	0.4	34.969	-85.491	24.3	5	3.50	0.10	3.51
1994	4	16	20	10	12.2	35.752	-83.968	1.8	5	3.50	0.25	3.57
1995	3	11	8	15	52.3	36.959	-83.133	1.0		3.80	0.10	3.81
1995	3	11	9	50	4.4	36.990	-83.180	1.0		3.30	0.10	3.31
1995	3	18	22	6	20.8	35.422	-84.941	26.0		3.25	0.30	3.35
1995	4	17	13	46	0.0	32.997	-80.171	8.4	6	3.90	0.10	3.91
1995	6	26	0	36	17.1	36.752	-81.481	1.8	5	3.40	0.10	3.41
1995	7	5	14	16	44.7	35.334	-84.163	10.0	4	3.70	0.10	3.71
1995	7	7	21	1	3.0	36.493	-81.833	10.0	4	3.06	0.10	3.08
1996	4	19	8	50	14.0	36.981	-83.018	0.0		3.90	0.10	3.91
1997	5	19	19	45	35.8	34.622	-85.353	2.7	4	3.06	0.10	3.08
1997	7	19	17	6	34.4	34.953	-84.811	2.8	4	3.61	0.10	3.62

Table 2.5.2-1 (cont.) Earthquakes 1985–2005, Update to the EPRI (NP-4726-A 1988) Seismicity Catalog with $Em_b \geq 3.0$, Within a 30° to 37° N, 78° to 86° W Latitude-Longitude Window, Incorporating the 200 mi (320 km) Radius Site Region

Year	Mo	Dy	Hr	Mn	Sec	Lat	Lon	Z(km)	Int	Emb	Smb	Rmb
1997	7	30	12	29	25.3	36.512	-83.547	23.0	5	3.80	0.10	3.81
1998	4	13	9	56	15.6	34.471	-80.603	6.6	5	3.90	0.10	3.91
1998	6	5	2	31	3.9	35.554	-80.785	9.4		3.34	0.10	3.35
1998	6	17	8	0	23.9	35.944	-84.392	11.3	5	3.60	0.10	3.61
1999	1	17	18	38	5.1	36.893	-83.799	1.0	3	3.06	0.27	3.15
2000	1	18	22	19	32.2	32.920	-83.465	19.2	5	3.50	0.10	3.51
2001	3	7	17	12	23.8	35.552	-84.850	6.8	3	3.20	0.10	3.21
2001	3	21	23	35	34.9	34.847	-85.438	0.0	3	3.16	0.27	3.24
2001	6	11	18	27	54.3	30.226	-79.885	10.0		3.33	0.41	3.53
2001	7	26	5	26	46.0	35.971	-83.552	14.3	3	3.25	0.10	3.26
2002	11	8	13	29	3.2	32.422	-79.950	3.9		3.50	0.41	3.69
2002	11	11	23	39	29.7	32.404	-79.936	2.4		4.23	0.41	4.42
2003	3	18	6	4	24.2	33.689	-82.888	5.0		3.50	0.41	3.69
2003	4	29	8	59	38.1	34.445	-85.620	9.1	6	4.70	0.10	4.71
2003	5	2	10	48	43.5	34.512	-85.604	10.0		3.01	0.41	3.20
2003	5	5	10	53	49.9	33.055	-80.190	11.4		3.06	0.30	3.17
2003	7	13	20	15	17.0	32.335	-82.144	5.0		3.58	0.41	3.77
2004	7	20	9	13	14.4	32.972	-80.248	10.3		3.17	0.41	3.37
2004	9	17	15	21	43.6	36.932	-84.006	1.2		3.66	0.41	3.85

Table 2.5.2-2 Summary of Bechtel Seismic Sources

Source	Description	Pa[1]	Mmax (m_b) and Wts.[2]	Smoothing Options and Wts.[3]	Inter-dependencies[4]	New Information to Suggest Change in Source: Geometry?[5]	Mmax?[6]	RI?[7]
Sources within 200 mi (320 km) that contribute to 99% of hazard								
H	**Charleston Area**	0.50	6.8 [0.20] 7.1 [0.40] 7.4 [0.40]	1 [0.33] 2 [0.34] 4 [0.33]	P(H|N3)=0.15	**Yes[8]**	**Yes[8]**	**Yes[8]**
N3	**Charleston Faults**	0.53	6.8 [0.20] 7.1 [0.40] 7.4 [0.40]	1 [0.33] 2 [0.34] 4 [0.33]	P(N3|H)=0.16	**Yes[8]**	**Yes[8]**	**Yes[8]**
BZ4	Atlantic Coastal Region	1.00	6.6 [0.10] 6.8 [0.40] 7.1 [0.40] 7.4 [0.10]	1 [0.33] 2 [0.34] 3 [0.33]	Background; P_B=1.00	No	No	No
BZ5	S. Appalachians	1.00	5.7 [0.10] 6.0 [0.40] 6.3 [0.40] 6.6 [0.10]	1 [0.33] 2 [0.34] 3 [0.33]	Background; P_B=1.00	No	No	No
F	S.E. Appalachians	0.35	5.4 [0.10] 5.7 [0.40] 6.0 [0.40] 6.6 [0.10]	1 [0.33] 2 [0.34] 4 [0.33]	ME with G; ME with 13, 15, 16, 17	No	No	No
G	NW South Carolina	0.35	5.4 [0.10] 5.7 [0.40] 6.0 [0.40] 6.6 [0.10]	1 [0.33] 2 [0.34] 4 [0.33]	ME with F; ME with 13, 15, 16, 17	No	No	No
Other Sources within 200 mi (320 km) that do not contribute to 99% of hazard								
13	Eastern Mesozoic Basins	0.10	5.4 [0.10] 5.7 [0.40] 6.0 [0.40] 6.6 [0.10]	1 [0.33] 2 [0.34] 4 [0.33]	no overlap with H or N3; ME with all sources in BZ5	No	No	No
24	Bristol Trends	0.25	5.7 [0.10] 6.0 [0.40] 6.3 [0.40] 6.6 [0.10]	1 [0.33] 2 [0.34] 4 [0.33]	ME with 19, 25, 25A	No	No	No
15	Rosman Fault	0.05	5.4 [0.10] 5.7 [0.40] 6.0 [0.40] 6.6 [0.10]	1 [0.33] 2 [0.34] 4 [0.33]	ME with all other sources	No	No	No

Table 2.5.2-2 Summary of Bechtel Seismic Sources

Source	Description	Pa[1]	Mmax (m_b) and Wts.[2]	Smoothing Options and Wts.[3]	Inter-dependencies[4]	New Information to Suggest Change in Source: Geometry?[5]	Mmax?[6]	RI?[7]
16	Belair Fault	0.05	5.4 [0.10] 5.7 [0.40] 6.0 [0.40] 6.6 [0.10]	1 [0.33] 2 [0.34] 4 [0.33]	ME with all other sources	No	No	No

1 Pa = probability of activity; (from EPRI NP-6452-D 1989)
2 Maximum Magnitude (Mmax) and weights (wts.); (from EPRI NP-6452-D 1989)
3 Smoothing options are defined as follows (from EPRI NP-6452-D 1989):
1 = constant a, constant b (no prior b);
2 = low smoothing on a, high smoothing on b (no prior b);
3 = low smoothing on a, low smoothing on b (no prior b);
4 = low smoothing on a, low smoothing on b (weak prior of 1.05).
Weights on magnitude intervals are [1.0, 1.0, 1.0, 1.0, 1.0, 1.0, 1.0].
4 ME = mutually exclusive; PD = perfectly dependent
5 No, unless (1) new geometry proposed in literature or (2) new seismicity pattern
6 No, unless (1) new data suggests Mmax exceeds or differs significantly from the EPRI Mmax distribution or (2) exceeded by historical seismicity.
7 RI = recurrence interval; assumed no change if no new paleoseismic data or rate of seismicity has not significantly changed
8 Replace this source with the Updated Charleston Seismic Source (UCSS) Model

Table 2.5.2-3 Summary of Dames & Moore Seismic Sources

Source	Description	Pa[1]	Mmax (m_b) and Wts.[2]	Smoothing Options and Wts.[3]	Interdependencies[4]	New Information to Suggest Change in Source: Geometry?[5]	Mmax?[6]	RI?[7]
Sources within 200 mi (320 km) that contribute to 99% of hazard								
54	**Charleston Seismic Zone**	1.00	6.6 [0.75] 7.2 [0.25]	1 [0.22] 2 [0.08] 3 [0.52] 4 [0.18]	none	**Yes[8]**	**Yes[8]**	**Yes[8]**
52	Charleston Mesozoic Rift	0.46	4.7 [0.75] 7.2 [0.25]	3 [0.75] 4 [0.25]	ME with 47 thru 50, 65; ME with 52	No	No	No
53	S. Appalachian Mobile Belt (Default Zone)	0.26	5.6 [0.80] 7.2 [0.20]	1 [0.75] 2 [0.25]	Default for 47 thru 52, 65	No	No	No
41	S. Cratonic Margin (Default Zone)	0.12	6.1 [0.80] 7.2 [0.20]	1 [0.75] 2 [0.25]	Default for 42, 43, and 46	No	No	No
20	S. Coastal Margin	1.00	5.3 [0.80] 7.2 [0.20]	1 [0.75] 2 [0.25]	none	No	No	No
Other Sources within 200 mi (320 km) that do not contribute to 99% of hazard								
4	Appalachian Fold Belts	0.35	6.0 [0.80] 7.2 [0.20]	1 [0.75] 2 [0.25]	ME with 4A, 4B, 4C, 4D	No	No	No
4A	Kink in Fold Belt	0.65	5.0 [0.75] 7.2 [0.25]	3 [0.75] 4 [0.25]	ME with 4	No	No	No
49	Jonesboro Basin	0.28	6.0 [0.75] 7.2 [0.25]	3 [0.75] 4 [0.25]	PD with 47, 48, 50, 51, 65; ME with 52	No	No	No
50	Buried Triassic Basins	0.28	6.0 [0.75] 7.2 [0.25]	3 [0.75] 4 [0.25]	PD with 47, 48, 49, 51, 65; ME with 52	No	No	No
51	Florence Basin	0.28	6.0 [0.75] 7.2 [0.25]	3 [0.75] 4 [0.25]	PD with 47 thru 50, 65; ME with 52	No	No	No

Table 2.5.2-3 (cont.) Summary of Dames & Moore Seismic Sources

Source	Description	Pa[1]	Mmax (m_b) and Wts.[2]	Smoothing Options and Wts.[3]	Interdependencies[4]	New Information to Suggest Change in Source: Geometry?[5]	Mmax?[6]	RI?[7]
65	Dunbarton Triassic Basin	0.28	5.9 [0.75] 7.2 [0.25]	3 [0.75] 4 [0.25]	PD with 47 thru 51; ME with 52	No	No	No
C01	Combination zone 4-4A-4B-4C-4D	NA	6.0 [0.80] 7.2 [0.20]	1 [0.75] 2 [0.25]	NA	No	No	No

1 Pa = probability of activity; (from EPRI NP-6452-D 1989)
2 Maximum Magnitude (Mmax) and weights (wts.); (from EPRI NP-6452-D 1989)
3 Smoothing options are defined as follows (from EPRI NP-6452-D 1989)
1 = No smoothing on a, no smoothing on b (strong prior of 1.04);
2 = No smoothing on a, no smoothing on b (weak prior of 1.04);
3 = Constant a, constant b (strong prior of 1.04);
4 = Constant a, constant b (weak prior of 1.04).
Weights on magnitude intervals are [0.1, 0.2, 0.4, 1.0, 1.0, 1.0, 1.0]
4 ME = mutually exclusive; PD = perfectly dependent
5 No, unless (1) new geometry proposed in literature or (2) new seismicity pattern
6 No, unless (1) new data suggests Mmax exceeds or differs significantly from the EPRI Mmax distribution or (2) exceeded by historical seismicity.
7 RI = recurrence interval; assumed no change if no new paleoseismic data or rate of seismicity has not significantly changed
8 Replace this source with the Updated Charleston Seismic Source (UCSS) Model

Table 2.5.2-4 Summary of Law Engineering Seismic Sources

Source	Description	Pa[1]	Mmax (m_b) and Wts.[2]	Smoothing Options and Wts.[3]	Inter-dependencies[4]	New Information to Suggest Change in Source: Geometry?[5]	Mmax?[6]	RI?[7]
Sources within 200 mi (320 km) that contribute to 99% of hazard								
35	**Charleston Seismic Zone**	0.45	6.8 [1.00]	2a [1.00]	Overlaps 8 and 22	**Yes[8]**	**Yes[8]**	**Yes[8]**
17	Eastern Basement	0.62	5.7 [0.20] 6.8 [0.80]	1b [1.00]	none	No	No	No
22	Reactivated E. Seaboard Normal	0.27	6.8 [1.00]	2a [1.00]	ME with 8 and 21; overlaps 24, 35, and 39	No	No	No
108	Brunswick, NC Background	1.00	4.9 [0.50] 5.5 [0.30] 6.8 [0.20]	2a [1.00]	Background; P_B=0.42	No	No	No
C09	Mesozoic Basins (8 - Bridged)	NA	6.8 [1.00]	2a [1.00]	NA	No	No	No
C10	8-35	NA	6.8 [1.00]	2a [1.00]	NA	No	No	No
C11	22 - 35	NA	6.8 [1.00]	2a [1.00]	NA	No	No	No
M33	Mafic Pluton	0.43	6.8 [1.00]	5 [1.00]	none	No	No	No
M36	Mafic Pluton	0.43	6.8 [1.00]	5 [1.00]	none	No	No	No
M37	Mafic Pluton	0.43	6.8 [1.00]	5 [1.00]	none	No	No	No
M38	Mafic Pluton	0.43	6.8 [1.00]	5 [1.00]	none	No	No	No
M39	Mafic Pluton	0.43	6.8 [1.00]	5 [1.00]	none	No	No	No
M40	Mafic Pluton	0.43	6.8 [1.00]	5 [1.00]	none	No	No	No
M41	Mafic Pluton	0.43	6.8 [1.00]	5 [1.00]	none	No	No	No
M42	Mafic Pluton	0.43	6.8 [1.00]	5 [1.00]	none	No	No	No
Other Sources within 200 mi (320 km) that do not contribute to 99% of hazard								
217	Eastern Basement Background	1.00	4.9 [0.50] 5.7 [0.50]	1b [1.00]	Background; P_B=0.29; same geometry as 17	No	No	No

Table 2.5.2-4 (cont.) Summary of Law Engineering Seismic Sources

Source	Description	Pa[1]	Mmax (m_b) and Wts.[2]	Smoothing Options and Wts.[3]	Inter-dependencies[4]	New Information to Suggest Change in Source: Geometry?[5]	Mmax?[6]	RI?[7]
107	Eastern Piedmont	1.00	4.9 [0.30] 5.5 [0.40] 5.7 [0.30]	1a [1.00]	Background; P_B=0.42	No	No	No
GC13	22 - 24 - 35	NA	6.8 [1.00]	2a [1.00]	NA	No	No	No
GC12	22 - 24	NA	6.8 [1.00]	2a [1.00]	NA	No	No	No
8	Mesozoic Basins	0.27	6.8 [1.00]	a and b values calculated for C09	ME with 22; overlaps with 35	No	No	No

1 Pa = probability of activity; (from EPRI NP-6452-D 1989)
2 Maximum Magnitude (Mmax) and weights (wts.); (from EPRI NP-6452-D 1989)
3 Smoothing options are defined as follows: (from EPRI NP-6452-D 1989)
1a = High smoothing on a, constant b (strong prior of 1.05);
1b = High smoothing on b, constant b (strong prior of 1.00);
1c = High smoothing on a, constant b (strong prior of 0.95);
1d = High smoothing on a, constant b (strong prior of 0.90);
1e = High smoothing on a, constant b (strong prior of 0.70);
2a = Constant a, constant b (strong prior of 1.05);
2c = Constant a, constant b (strong prior of 0.95);
2d = Constant a, constant b (strong prior of 0.90).
Weights on magnitude intervals are all 1.0 for above options.
3a = High smoothing on a, constant b (strong prior of 1.05).
Weights on magnitude intervals are [0.0, 1.0, 1.0, 1.0, 1.0, 1.0, 1.0] for option 3a.
4 ME = mutually exclusive; PD = perfectly dependent
5 No, unless (1) new geometry proposed in literature or (2) new seismicity pattern
6 No, unless (1) new data suggests Mmax exceeds or differs significantly from the EPRI Mmax distribution or (2) exceeded by historical seismicity.
7 RI = recurrence interval; assumed no change if no new paleoseismic data or rate of seismicity has not significantly changed
8 Replace this source with the Updated Charleston Seismic Source (UCSS) Model

Table 2.5.2-5 Summary of Rondout Seismic Sources

Source	Description	Pa[1]	Mmax (m_b) and Wts.[2]	Smoothing Options and Wts.[3]	Interdependencies[4]	New Information to Suggest Change in Source: Geometry?[5]	Mmax?[6]	RI?[7]
Sources within 200 mi (320 km) that contribute to 99% of hazard								
24	**Charleston**	1.00	6.6 [0.20] 6.8 [0.60] 7.0 [0.20]	1 [1.00] (a=-0.710, b=1.020)	none	**Yes[8]**	**Yes[8]**	**Yes[8]**
26	South Carolina	1.00	5.8 [0.15] 6.5 [0.60] 6.8 [0.25]	1 [1.00] (a=-1.390, b=0.970)	none	No	No	No
Other Sources within 200 mi (320 km) that do not contribute to 99% of hazard								
49	Appalachian	1.00	4.8 [0.20] 5.5 [0.60] 5.8 [0.20]	2 [1.00]	Background; P_B=1.00	No	No	No
C01	Background 49	NA	4.8 [0.20] 5.5 [0.60] 5.8 [0.20]	3 [1.00]	none	No	No	No
C09	49+32	NA	4.8 [0.20] 5.5 [0.60] 5.8 [0.20]	3 [1.00]	none	No	No	No
50	Grenville	1.00	4.8 [0.20] 5.5 [0.60] 5.8 [0.20]	2 [1.00]	Background; P_B=1.00	No	No	No
C02	Background 50	NA	4.8 [0.20] 5.5 [0.60] 5.8 [0.20]	3 [1.00]	does not contain 12 or 13	No	No	No
C07	50 (02) + 12	NA	4.8 [0.20] 5.5 [0.60] 5.8 [0.20]	3 [1.00]	none	No	No	No
25	Southern Appalachians	0.99	6.6 [0.30] 6.8 [0.60] 7.0 [0.10]	1 [1.00] (a=-0.630, b=1.150)	none	No	No	No

Table 2.5.2-5 (cont.) Summary of Rondout Seismic Sources

Source	Description	Pa[1]	Mmax (m_b) and Wts.[2]	Smoothing Options and Wts.[3]	Interdependencies[4]	New Information to Suggest Change in Source: Geometry?[5]	Mmax?[6]	RI?[7]
27	Tennessee-VA Border Zone	0.99	5.2 [0.30] 6.3 [0.55] 6.5 [0.15]	1 [1.00] (a=-1.120, b=0.930)	none	No	No	No

1 Pa = probability of activity; (from EPRI NP-6452-D 1989)
2 Maximum Magnitude (Mmax) and weights (wts.); (from EPRI NP-6452-D 1989)
3 Smoothing options are defined as follows: (from EPRI NP-6452-D 1989)
1, 6, 7, 8 = a, b values as listed above, with weights shown;
3 = Low smoothing on a, constant b (strong prior of 1.0);
5 = a, b values as listed above, with weights shown.
4 ME = mutually exclusive; PD = perfectly dependent
5 No, unless (1) new geometry proposed in literature or (2) new seismicity pattern
6 No, unless (1) new data suggests Mmax exceeds or differs significantly from the EPRI Mmax distribution or (2) exceeded by historical seismicity.
7 RI = recurrence interval; assumed no change if no new paleoseismic data or rate of seismicity has not significantly changed
8 Replace this source with the Updated Charleston Seismic Source (UCSS) Model

Table 2.5.2-6 Summary of Weston Seismic Sources

Source	Description	Pa[1]	Mmax (m_b) and Wts.[2]	Smoothing Options and Wts.[3]	Interdependencies[4]	New Information to Suggest Change in Source: Geometry?[5]	Mmax?[6]	RI?[7]
Sources within 200 mi (320 km) that contribute to 99% of hazard								
25	**Charleston Seismic Zone**	0.99	6.6 [0.90] 7.2 [0.10]	1b [1.00]	none	**Yes[8]**	**Yes[8]**	**Yes[8]**
26	South Carolina	0.86	6.0 [0.67] 6.6 [0.27] 7.2 [0.06]	1b [1.00]	none	No	No	No
104	Southern Coastal Plain	1.00	5.4 [0.24] 6.0 [0.61] 6.6 [0.15]	1a [0.20] 2a [0.80]	Background; P_B=1.00	No	No	No
C19	103-23-24	NA	5.4 [0.26] 6.0 [0.58] 6.6 [0.16]	1a [1.00]	NA	No	No	No
C20	104-22	NA	6.0 [0.85] 6.6 [0.15]	1a [0.30] 2a [0.70]	NA	No	No	No
C21	104-25	NA	5.4 [0.24] 6.0 [0.61] 6.6 [0.15]	1a [0.30] 2a [0.70]	NA	No	No	No
C23	104-22-26	NA	5.4 [0.80] 6.0 [0.14] 6.6 [0.06]	1a [0.50] 2a [0.50]	NA	No	No	No
C24	104-22-25	NA	5.4 [0.80] 6.0 [0.14] 6.6 [0.06]	1a [0.50] 2a [0.50]	NA	No	No	No
C26	104-28BCDE-22	NA	5.4 [0.24] 6.0 [0.61] 6.6 [0.15]	1a [0.30] 2a [0.70]	NA	No	No	No
C27	104-28BCDE-22-25	NA	5.4 [0.30] 6.0 [0.70]	1a [0.70] 2a [0.30]	NA	No	No	No

Table 2.5.2-6 (cont.) Summary of Weston Seismic Sources

Source	Description	Pa[1]	Mmax (m_b) and Wts.[2]	Smoothing Options and Wts.[3]	Interdependencies[4]	New Information to Suggest Change in Source: Geometry?[5]	Mmax?[6]	RI?[7]
C33	26-25		6.6 [0.90] 7.2 [0.10]	1b [1.00]	NA	No	No	No
C35	104-28BE-25	NA	5.4 [0.24] 6.0 [0.61] 6.6 [0.15]	1a [0.20] 1b [0.80]	NA	No	No	No
Other Sources within 200 mi (320 km) that do not contribute to 99% of hazard								
C22	104-26	NA	5.4 [0.24] 6.0 [0.61] 6.6 [0.15]	1a [0.30] 1b [0.70]	NA	No	No	No
C34	104-28BE-26	NA	5.4 [0.24] 6.0 [0.61] 6.6 [0.15]	1a [0.20] 1b [0.80]	NA	No	No	No
C25	104-28BCDE	NA	5.4 [0.24] 6.6 [0.61] 6.6 [0.15]	1a [0.30] 2a [0.70]	NA	No	No	No
C28	104-28BCDE-22-26	NA	5.4 [0.30] 6.0 [0.70]	1a [0.70] 2a [0.30]	NA	No	No	No
28B	Zone of Mesozoic Basin	0.26	5.4 [0.65] 6.0 [0.25] 6.6 [0.10]	1b [1.00]	PD with 28C, 28D, and 28E	No	No	No
C01	28A thru E	NA	5.4 [0.65] 6.0 [0.25] 6.6 [0.10]	1b [1.00]	NA	No	No	No
103	Southern Appalachians	1.00	5.4 [0.26] 6.0 [0.58] 6.6 [0.16]	1a [0.20] 2a [0.80]	Background; P_B=1.00	No	No	No
C17	103-23	NA	5.4 [0.26] 6.0 [0.58] 6.6 [0.16]	1a [0.70] 2a [0.30]	NA	No	No	No
C18	103-24	NA	5.4 [0.26] 6.0 [0.58] 6.6 [0.16]	1a [0.70] 1b [0.30]	NA	No	No	No

Table 2.5.2-6 (cont.) Summary of Weston Seismic Sources

Source	Description	Pa[1]	Mmax (m_b) and Wts.[2]	Smoothing Options and Wts.[3]	Interdependencies[4]	New Information to Suggest Change in Source: Geometry?[5]	Mmax?[6]	RI?[7]
28D	Zone of Mesozoic Basin	0.26	5.4 [0.65] 6.0 [0.25] 6.6 [0.10]	1b [1.00]	PD with 28B, 28C, and 28E	No	No	No
28E	Zone of Mesozoic Basin	0.26	5.4 [0.65] 6.0 [0.25] 6.6 [0.10]	1b [1.00]	PD with 28B, 28C, and 28D	No	No	No
102	Appalachian Plateau	1.00	5.4 [0.62] 6.0 [0.29] 6.6 [0.09]	1a [0.20] 2a [0.80]	Background; P_B=1.00	No	No	No
24	New York-Alabama-Clingman	0.90	5.4 [0.26] 6.0 [0.58] 6.6 [0.16]	1b [1.00]	Contained in 103	No	No	No

1 Pa = probability of activity; (from EPRI NP-6452-D 1989)
2 Maximum Magnitude (Mmax) and weights (wts.); (from EPRI NP-6452-D 1989)
3 Smoothing options are defined as follows: (from EPRI NP-6452-D 1989)
1a = Constant a, constant b (medium prior of 1.0);
1b = Constant a, constant b (medium prior of 0.9);
1c = Constant a, constant b (medium prior of 0.7);
2a = Medium smoothing on a, medium smoothing on b (medium prior of 1.0);
2b = Medium smoothing on a, medium smoothing on b (medium prior of 0.9);
2c = Medium smoothing on a, medium smoothing on b (medium prior of 0.7).
4 ME = mutually exclusive; PD = perfectly dependent
5 No, unless (1) new geometry proposed in literature or (2) new seismicity pattern
6 No, unless (1) new data suggests Mmax exceeds or differs significantly from the EPRI Mmax distribution or (2) exceeded by historical seismicity.
7 RI = recurrence interval; assumed no change if no new paleoseismic data or rate of seismicity has not significantly changed
8 Replace this source with the Updated Charleston Seismic Source (UCSS) Model

Table 2.5.2-7 Summary of Woodward-Clyde Seismic Sources

Source	Description	Pa[1]	Mmax (m_b) and Wts.[2]	Smoothing Options and Wts.[3]	Interdependencies[4]	New Information to Suggest Change in Source: Geometry?[5]	Mmax?[6]	RI?[7]
Sources within 200 mi (320 km) that contribute to 99% of hazard								
30	**Charleston (includes NOTA)**	0.573	6.8 [0.33] 7.3 [0.34] 7.5 [0.33]	2 [0.10] 3 [0.10] 4 [0.10] 5 [0.10] 9 [0.60] (a = -1.005, b = 0.852)	ME with 29, 29A	**Yes[8]**	**Yes[8]**	**Yes[8]**
29	**S. Carolina Gravity Saddle (Extended)**	0.122	6.7 [0.33] 7.0 [0.34] 7.4 [0.33]	2 [0.25] 3 [0.25] 4 [0.25] 5 [0.25]	ME with 29A, 29B, and 30	**Yes[8]**	**Yes[8]**	**Yes[8]**
29A	**SC Gravity Saddle No. 2 (Combo C3)**	0.305	6.7 [0.33] 7.0 [0.34] 7.4 [0.33]	2 [0.25] 3 [0.25] 4 [0.25] 5 [0.25]	ME with 29, 29B, and 30	**Yes[8]**	**Yes[8]**	**Yes[8]**
29B	SC Gravity Saddle No. 3 (NW Portion)	0.183	5.4 [0.33] 6.0 [0.34] 7.0 [0.33]	2 [0.25] 3 [0.25] 4 [0.25] 5 [0.25]	ME with 29, 29A	No	No	No
	Vogtle Background		5.8 [0.33] 6.0 [0.34] 6.6 [0.33]		None	No	No	No
Other Sources within 200 mi (320 km) that do not contribute to 99% of hazard								
31	Blue Ridge Combo	0.024	5.9 [0.33] 6.3 [0.34] 7.0 [0.33]	2 [0.25] 3 [0.25] 4 [0.25] 5 [0.25]	ME with 31A	No	No	No

Table 2.5.2-7 (cont.) Summary of Woodward-Clyde Seismic Sources

Source	Description	Pa[1]	Mmax (m_b) and Wts.[2]	Smoothing Options and Wts.[3]	Interdependencies[4]	New Information to Suggest Change in Source: Geometry?[5]	Mmax?[6]	RI?[7]
31A	Blue Ridge	0.211	5.9 [0.33]	2 [0.25]	ME with 31	No	No	No
	Combination -		6.3 [0.34]	3 [0.25]				
	Alternate		7.0 [0.33]	4 [0.25]				
	Configuration			5 [0.25]				

1 Pa = probability of activity; (from EPRI NP-6452-D 1989)
2 Maximum Magnitude (Mmax) and weights (wts.); (from EPRI NP-6452-D 1989)
3 Smoothing options are defined as follows: (from EPRI NP-6452-D 1989)
1 = Low smoothing on a, high smoothing on b (no prior);
2 = High smoothing on a, high smoothing on b (no prior);
3 = High smoothing on a, high smoothing on b (moderate prior of 1.0);
4 = High smoothing on a, high smoothing on b (moderate prior of 0.9);
5 = High smoothing on a, high smoothing on b (moderate prior of 0.8);
6 = Low smoothing on a, high smoothing on b (moderate prior of 1.0);
7 = Low smoothing on a, high smoothing on b (moderate prior of 0.9);
8 = Low smoothing on a, high smoothing on b (moderate prior of0.8).
Weights on magnitude intervals are all 1.0.
9 = a and b values as listed.
4 ME = mutually exclusive; PD = perfectly dependent
5 No, unless (1) new geometry proposed in literature or (2) new seismicity pattern
6 No, unless (1) new data suggests Mmax exceeds or differs significantly from the EPRI Mmax distribution or (2) exceeded by historical seismicity.
7 RI = recurrence interval; assumed no change if no new paleoseismic data or rate of seismicity has not significantly changed
8 Replace this source with the Updated Charleston Seismic Source (UCSS) Model

Table 2.5.2-8 Summary of USGS Seismic Sources (Frankel et al. 2002)

Source	Mmax (Mw) and Wts.	Largest Mmax Value Considered by USGS	
		Mw	mb[1]
Sources within 200 mi (320 km)			
Extended Margin Background	7.5 [1.00]	7.5	7.2
Charleston	**6.8 [0.20]** **7.1 [0.20]** **7.3 [0.45]** **7.5 [0.15]**	7.5	7.2
Eastern Tennessee	7.5 [1.00]	7.5	7.2
Selected Sources Beyond 200 mi (320km)			
New Madrid	7.3 [0.15] 7.5 [0.20] 7.7 [0.50] 8.0 [0.15]	8.0	7.5
Stable Craton Background	7.0 [1.00]	7.0	6.9

1 m_b converted from Mw using average of Atkinson and Boore (1995), Frankel et al (1996), and EPRI (TR-102293 1993) relations

Table 2.5.2-9 Chapman and Talwani (2002) Seismic Source Zone Parameters

				Mmax[2]	
Charleston Characteristic Sources		**Mean Recurrence**		**m_{blg}**	**M**
Charleston Area Source		550 years		nr	7.1 [.2]
					7.3 [.6]
					7.5 [.2]
ZRA Fault Source (Zone of River Anomalies)		550 years		nr	7.1 [.2]
					7.3 [.6]
					7.5 [.2]
Ashley River-Woodstock Fault Source (modeled as 3 parallel faults)		550 years		nr	7.1 [.2]
					7.3 [.6]
					7.5 [.2]
Non-Characteristic Background Sources		**a[1]**	**b[1]**	**m_{blg}**	**M**
1.	Zone1	0.242	0.84	6.84	7.00
2.	Zone2	-0.270	0.84	6.84	7.00
3.	Central Virginia	1.184	0.64	6.84	7.00
4.	Zone4	0.319	0.84	6.84	7.00
5.	Zone5	0.596	0.84	6.84	7.00
6.	Piedmont and Coastal Plain	1.537	0.84	6.84	7.00
6a.	Pied&CP NE	0.604	0.84	6.84	7.00
6b.	Pied&CP SW	1.312	0.84	6.84	7.00
7.	South Carolina Piedmont	2.220	0.84	6.84	7.00
8.	Middleton Place	1.690	0.77	6.84	7.00
9.	Florida and continental margin	1.371	0.84	6.84	7.00
10.	Alabama	1.800	0.84	6.84	7.00
11.	Eastern Tennessee	2.720	0.90	6.84	7.00
12.	Southern Appalachian	2.420	0.84	6.84	7.00
12a.	Southern Appalachian North	2.185	0.84	6.84	7.00
13.	Giles County, VA	1.070	0.84	6.84	7.00
14.	Central Appalachians	1.630	0.84	6.84	7.00
15.	Western Tennessee	2.431	1.00	6.84	7.00
16.	Central Tennessee	2.273	1.00	6.84	7.00
17.	Ohio-Kentucky	2.726	1.00	6.84	7.00
18.	West VA-Pennsylvania	2.491	1.00	6.84	7.00
19.	USGS (1996) gridded seismicity rates and b value	nr[3]	0.95	6.84	7.00

1 a and b values in terms of mblg magnitude, reported in Chapman and Talwani (2002).

2 Mmax range for characteristic events was designed to "represent the range of magnitude estimates of the 1886 Charleston shock proposed by Johnston (1996)" (Chapman and Talwani, 2002, p. 12). Square brackets indicate weights assigned to characteristic magnitudes. For non-characteristic background events, a truncated form of the exponential probability density function was used (Chapman and Talwani, 2002, p. 6-7).

3 nr = not reported

Table 2.5.2-10 Local Charleston-Area Tectonic Features

Name of Feature	Evidence	Key References
Adams Run fault	**subsurface stratigraphy**	**Weems and Lewis (2002)**
Ashley River fault	microseismicity	Talwani (1982, 2000) Weems and Lewis (2002)
Appalachian detachment (decollement)	gravity & magnetic data seismic reflection & refraction	Cook *et al.* (1979, 1981) Behrendt *et al.* (1981, 1983) Seeber and Armbruster (1981)
Blake Spur fracture zone	oceanic transform postulated to extend westward to Charleston area	Fletcher *et al.* (1978) Sykes (1978) Seeber and Armbruster (1981)
Bowman seismic zone	microseismicity	Smith and Talwani (1985)
Charleston fault	subsurface stratigraphy	Colquhoun *et al*. (1983) Lennon (1986) Talwani (2000) Weems and Lewis (2002)
Cooke fault	seismic reflection	Behrendt *et al.* (1981, 1983) Hamilton *et al.* (1983) Wentworth and Mergner-Keefer (1983) Behrendt and Yuan (1987)
Drayton fault	seismic reflection	Hamilton *et al.* (1983) Behrendt *et al*. (1983) Behrendt and Yuan (1987)
East Coast fault system/ Zone of river anomalies (ZRA)	**geomorphology** **seismic reflection** **microseismicity**	**Marple and Talwani (1993)** **Marple and Talwani (2000, 2004)**
Gants fault	seismic reflection	Hamilton *et al*. (1983) Behrendt and Yuan (1987)
Garner-Edisto fault	subsurface stratigraphy	Colquhoun *et al.* (1983)
Helena Banks fault zone	seismic reflection	Behrendt *et al.* (1981, 1983) Behrendt and Yuan (1987)
Middleton Place-Summerville seismic zone	microseismicity	Tarr *et al.* (1981) Madabhushi and Talwani (1993)
Sawmill Branch fault	**microseismicity**	**Talwani and Katuna (2004)**
Summerville fault	**microseismicity**	**Weems *et al.* (1997)**
Woodstock fault	geomorphology microseismicity	Talwani (1982, 1999, 2000) Marple and Talwani (1990, 2000)

Note: Those tectonic features identified following publication of the EPRI teams' reports (post-1986) are highlighted by **bold-face** type.

Table 2.5.2-11 Geographic Coordinates (Latitude and Longitude) of Corner Points of Updated Charleston Seismic Source (UCSS) Geometries

Source Geometry	Longitude (decimal degrees)	Latitude (decimal degrees)
A	-80.707	32.811
A	-79.840	33.354
A	-79.527	32.997
A	-80.392	32.455
B	-81.216	32.485
B	-78.965	33.891
B	-78.3432	33.168
B	-80.587	31.775
B'	-78.965	33.891
B'	-78.654	33.531
B'	-80.900	32.131
B'	-81.216	32.485
C	-80.397	32.687
C	-79.776	34.425
C	-79.483	34.351
C	-80.109	32.614

Table 2.5.2-12 Comparison of Post-EPRI NP-6395-D 1989 Magnitude Estimates for the 1886 Charleston Earthquake

Study	Magnitude Estimation Method	Reported Magnitude Estimate	Assigned Weights	Mean Magnitude (M)
Johnston *et al.* (1994)	worldwide survey of passive-margin, extended-crust earthquakes	**M**7.56 ± 0.35 [a]	--	7.56
Martin and Clough (1994)	geotechnical assessment of 1886 liquefaction data	**M**7 - 7.5	--	7.25
Johnston (1996)	isoseismal area regression, accounting for eastern North America anelastic attenuation	**M**7.3 ± 0.26	--	7.3
Chapman and Talwani (2002) (South Carolina Department of Transportation)	consideration of available magnitude estimates	**M**7.1 **M**7.3 **M**7.5	0.2 0.6 0.2	7.3
Frankel *et al.* (2002) (USGS National seismic hazard mapping project)	consideration of available magnitude estimates	**M**6.8 **M**7.1 **M**7.3 **M**7.5	0.20 0.20 0.45 0.15	7.2
Bakun and Hopper (2004)	isoseismal area regression, including empirical site corrections	M_I 6.4 - 7.2 [b]	--	6.9 [c]

Notes:

[a] Estimate from Johnston *et al*. (1994) Chapter 3.

[b] 95% confidence interval estimate; M_I (intensity magnitude) is considered equivalent to **M** (Bakun and Hopper, 2004).

[c] Bakun and Hopper's (2004) *preferred* estimate.

Table 2.5.2-13 Comparison of Talwani and Schaeffer (2001) and UCSS Age Constraints on Charleston-Area Paleoliquefaction Events

		Talwani and Schaeffer (2001) [a]				
		scenario 1		*scenario 2*		(this study)
Liquefaction Event	**Event Age** (YBP) [b]	**Source**	**M**	**Source**	**M**	**Event Age** (YBP) [b, c, d]
1886 A.D.	64	Charleston	7.3	Charleston	7.3	64
A	546 ± 17	Charleston	7+	Charleston	7+	600 ± 70
B	1,021 ± 30	Charleston	7+	Charleston	7+	1,025 ± 25
C	1,648 ± 74	*Northern*	6+	--	--	--
C'	1,683 ± 70	--		Charleston	7+	1,695 ± 175
D	1,966 ± 212	*Southern*	6+	--	--	--
E	3,548 ± 66	Charleston	7+	Charleston	7+	3,585 ± 115
F	5,038 ± 166	*Northern*	6+	Charleston	7+	--
F'	--	--	--	--	--	5,075 ± 215
G	5,800 ± 500	Charleston	7+	Charleston	7+	--

Notes:

[a] Modified after Talwani and Schaeffer's (2001) Table 2.

[b] Years before present, relative to 1950 A.D.

[c] Event ages based upon our recalibration of radiocarbon (to 2-sigma using OxCal 3.8 (Bronk Ramsey, 1995; 2001) data presented in Talwani and Schaeffer's (2001) Table 2.

[d] See Table B-1 for recalibrated 2-sigma sample ages and Table B-2 for 2-sigma age constraints on paleoliquefaction events.

Table 2.5.2-14 Seismic Sources Used for Each 1986 EPRI Team

Earth Science Team	Sources used
Bechtel	F, G, H, ,N3,BZ4, BZ5
Dames & Moore	20, 41, 52, 53, 54
Law Engineering	17, 22, 35, 108, C09, C10, C11, M33, M36, M37, M38, M39, M40, M41, M42
Rondout Associates	24, 26
Woodward-Clyde Cons.	29, 29A, 29B, 30, 32
Weston Geophysical Corp.	25, 26, 104, C19, C20, C21, C23, C24, C26, C27, C33, C35

Table 2.5.2-15 Comparison of Seismic Hazard at VEGP ESP

Mean Hazard Comparison

PGA	EPRI-SOG	REI 2005	
cm/s^2	hazard	hazard	% diff
50	8.15E-04	8.23E-04	0.97%
100	2.23E-04	2.26E-04	1.48%
250	2.84E-05	2.91E-05	2.29%
500	4.04E-06	4.21E-06	4.11%
700	1.36E-06	1.42E-06	4.71%
1000	3.82E-07	4.02E-07	5.10%

Median Hazard Comparison

PGA	EPRI-SOG	REI 2005	
cm/s^2	hazard	hazard	% diff
50	5.65E-04	5.75E-04	1.84%
100	1.43E-04	1.45E-04	1.05%
250	1.99E-05	2.16E-05	8.69%
500	2.53E-06	2.63E-06	3.95%
700	7.86E-07	8.13E-07	3.41%
1000	2.05E-07	2.19E-07	6.73%

85% Hazard Comparison

PGA	EPRI-SOG	REI 2005	
cm/s^2	hazard	hazard	% diff
50	1.49E-03	1.32E-03	-11.54%
100	4.16E-04	3.67E-04	-11.71%
250	4.96E-05	4.79E-05	-3.51%
500	7.01E-06	7.16E-06	2.15%
700	2.44E-06	2.46E-06	0.61%
1000	6.98E-07	7.08E-07	1.42%

Table 2.5.2-16 Hard Rock Mean UHS Results (in g) for VEGP ESP

Mean annual frequency of exceedance	Spectral frequency						
	PGA	25 Hz	10 Hz	5 Hz	2.5 Hz	1 Hz	0.5 Hz
10^{-4}	0.214	0.551	0.399	0.317	0.223	0.101	0.0653
$5x10^{-5}$	0.288	0.762	0.532	0.412	0.294	0.134	0.0924
10^{-5}	0.559	1.54	0.983	0.728	0.512	0.235	0.185
$5x10^{-6}$	0.747	2.06	1.28	0.914	0.635	0.294	0.241
10^{-6}	1.48	4.09	2.33	1.54	1.02	0.465	0.423

Table 2.5.2-17 Computed and Recommended Mbar and Dbar Values Used for Development of High and Low Frequency Target Spectra

High Frequency (5-10 Hz)				
	10^{-4}	**10^{-5}**	**10^{-6}**	**Recommended Values**
Mbar (Mw)	5.5	5.6	5.6	5.6
Dbar (km)	17.7	11.5	9.1	12
Low Frequency (1-2.5 Hz)				
	10^{-4}	**10^{-5}**	**10^{-6}**	**Recommended Values**
Mbar (Mw)	7.2	7.2	7.2	7.2
Dbar (km)	136.5	134.3	132.9	130

Table 2.5.2-18a Candidate High-Frequency (M5.6, R = 12km) Time Histories for Spectral Matching

Earthquake	Date	Mw	Station	Distance (km)	Vs30m (m/s)
Saguenay	11/25/88	5.9	GSC Site 16	51.9	"???"
San Francisco	03/22/57	5.28	Golden Gate Park	11.13	874.0
Coyote Lake	08/06/79	5.74	Gilroy Array #1	10.67	1428.0
Mammoth Lakes-09	06/11/80	4.85	USC McGee Creek	7.49	684.9
Coalinga-04	07/09/83	5.18	Sulphur Baths (temp)	14.47	617.4
Coalinga-05	07/22/83	5.77	Sulphur Baths (temp)	13.40	617.4
Morgan Hill	04/24/84	6.19	Gilroy - Gavilan Coll.	14.84	729.7
Morgan Hill	04/24/84	6.19	Gilroy Array #1	14.91	1428.0
N. Palm Springs	07/08/86	6.06	Silent Valley - Poppet Flat	17.03	684.9
Whittier Narrows-01	10/01/87	5.99	Mt Wilson - CIT Seis Sta	22.73	821.7
Whittier Narrows-02	10/04/87	5.27	Mt Wilson - CIT Seis Sta	18.74	821.7
Anza-02	10/31/01	4.92	Anza - Pinyon Flat	12.37	724.9
Anza-02	10/31/01	4.92	Anza - Tripp Flats Training	24.73	684.9
Anza-02	10/31/01	4.92	Idyllwild - Keenwild Fire Sta.	29.07	845.4
Gilroy	05/14/02	4.90	Gilroy - Gavilan Coll.	2.82	729.7

Table 2.5.2-18b Candidate Low-Frequency (M7.2, R = 130 km) Time Histories for Spectral Matching

Earthquake	Date	Mw	Station	Distance (km)	Vs30m (m/s)
San Fernando	02/09/1971	6.61	Isabella Dam (Aux Abut)	130.98	684.9
Loma Prieta	10/18/1989	6.93	SF-Rincon Hill	74.14	873.1
Loma Prieta	10/18/1989	6.93	So. San Francisco, Sierra Pt.	63.15	1020.6
Loma Prieta	10/18/1989	6.93	Yerba Buena Island	75.17	659.8
Northridge	01/17/1994	6.69	Rancho Cucamonga-Deer Canyon	79.99	821.7
Northridge	01/17/1994	6.69	Wrightwood-Jackson Flat	64.66	821.7
Kobe	01/16/1995	6.90	OKA	86.94	609.0
Kocaeli	08/17/1999	7.51	Bursa Sivil	65.53	659.6
Chi-Chi	09/20/1999	7.62	ILA031	83.31	649.3
Kobe	01/16/1995	6.90	MZH	70.26	609.0
Hector Mine	10/16/1999	7.13	Anza-Pinyon Flat	89.98	724.9
Hector Mine	10/16/1999	7.13	Anza-Tripp Flats Training	102.40	684.9
Hector Mine	10/16/1999	7.13	Banning-Twin Pines Road	83.43	684.9
Hector Mine	10/16/1999	7.13	Heart Bar State Park	61.21	684.9
Hector Mine	10/16/1999	7.13	Seven Oaks Dam Project Office	87.20	659.6

Table 2.5.2-19 Site Response Analyses Performed

Probability (per year) ->	10^{-4}		10^{-5}		10^{-6}				Total No. Analyses
Time Histories Analyzed ->	30 High Freq.	30 Low Freq.	30 High Freq.	30 Low Freq.	30 High Freq.	30 Low Freq.			
Randomized Soil Columns (EPRI) ->	60	60	60	60	60	60			360
Randomized Soil Columns (SRS) ->	60	60	60	60	60	60			360
									720

Table 2.5.2-20a Amplification Factors as a Function of Input Hard Rock Motion at Top of Blue Bluff Marl (depth 86 feet), as Developed from Site Response Analysis using SRS and EPRI Soil Degradation Models, for High-frequency Rock Motions

-		10^{-4}			10^{-5}			10^{-6}	
-	Hard rock input motion	mean amp. factors		Hard rock input motion	mean amp. factors		Hard rock input motion	mean amp. factors	
Freq, Hz		EPRI	SRS		EPRI	SRS		EPRI	SRS
100	0.294	1.18	1.20	0.703	0.979	0.920	1.60	0.766	0.620
76	0.400	0.903	0.930	0.957	0.740	0.695	2.17	0.571	0.462
60	0.499	0.769	0.799	1.19	0.606	0.573	2.71	0.456	0.369
50	0.595	0.697	0.722	1.42	0.531	0.500	3.23	0.386	0.313
40	0.631	0.775	0.819	1.51	0.553	0.523	3.43	0.379	0.306
30	0.655	0.961	1.02	1.57	0.664	0.626	3.63	0.398	0.319
25	0.647	1.14	1.21	1.55	0.812	0.768	3.71	0.446	0.354
20	0.615	1.33	1.39	1.47	0.991	0.937	3.34	0.579	0.453
16.5	0.575	1.47	1.52	1.38	1.133	1.07	3.13	0.705	0.560
13.4	0.521	1.67	1.69	1.25	1.312	1.23	2.83	0.875	0.685
12.2	0.494	1.78	1.81	1.18	1.417	1.33	2.69	0.953	0.754
10	0.438	1.81	1.82	1.05	1.600	1.50	2.38	1.15	0.928
8.1	0.377	2.19	2.18	0.902	1.747	1.65	2.05	1.34	1.09
7	0.339	2.30	2.26	0.811	1.984	1.87	1.84	1.47	1.21
6	0.298	2.05	2.03	0.713	2.096	1.93	1.62	1.68	1.38
5	0.257	2.11	2.08	0.615	2.022	1.88	1.40	1.90	1.56
4	0.212	2.56	2.54	0.507	2.300	2.16	1.15	2.09	1.70
3.3	0.175	2.88	2.81	0.419	2.687	2.51	0.952	2.42	2.00
2.5	0.131	3.16	3.05	0.314	3.089	2.83	0.713	2.78	2.33
2	0.101	2.49	2.38	0.242	2.651	2.38	0.549	2.96	2.39
1.5	0.064	3.22	3.12	0.154	3.193	2.86	0.350	3.28	2.48
1	0.035	2.34	2.30	0.0828	2.542	2.41	0.188	3.00	2.55
0.8	0.024	2.63	2.59	0.0563	2.695	2.55	0.128	2.95	2.54
0.7	0.0187	3.15	3.10	0.0447	3.141	2.97	0.101	3.31	2.86
0.61	0.0148	3.80	3.78	0.0354	3.842	3.69	0.0804	4.02	3.52
0.5	0.0109	3.40	3.43	0.0260	3.597	3.59	0.0590	4.00	3.81
0.33	0.00525	2.19	2.19	0.0126	2.269	2.25	0.0286	2.52	2.40
0.25	0.00314	1.98	1.97	0.00751	2.059	2.00	0.0171	2.24	2.07
0.15	0.00106	2.06	2.04	0.00254	2.149	2.05	0.00577	2.37	2.06
0.1	0.000370	2.27	2.23	0.000890	2.341	2.18	0.00201	2.43	2.06

Table 2.5.2-20b Amplification Factors as a Function of Input Hard Rock Motion at Top of Blue Bluff Marl (depth 86 feet), as Developed from Site Response Analysis using SRS and EPRI Soil Degradation Models, for Low-frequency Rock Motions

	10^{-4}			10^{-5}			10^{-6}		
	Hard rock input motion	mean amp. factors		Hard rock input motion	mean amp. factors		Hard rock input motion	mean amp. factors	
Freq, Hz		EPRI	SRS		EPRI	SRS		EPRI	SRS
100	0.224	1.31	1.25	0.517	1.111	0.896	1.03	0.931	0.591
76	0.305	0.987	0.942	0.704	0.828	0.667	1.40	0.692	0.439
60	0.380	0.802	0.765	0.878	0.660	0.532	1.74	0.550	0.349
50	0.453	0.695	0.662	1.047	0.557	0.449	2.08	0.462	0.293
40	0.483	0.677	0.644	1.115	0.532	0.428	2.22	0.437	0.277
30	0.506	0.764	0.73	1.168	0.529	0.417	2.32	0.417	0.264
25	0.505	0.90	0.86	1.167	0.570	0.440	2.32	0.422	0.266
20	0.493	1.07	1.02	1.139	0.653	0.492	2.26	0.445	0.276
16.5	0.476	1.21	1.16	1.101	0.762	0.57	2.19	0.481	0.293
13.4	0.453	1.41	1.34	1.046	0.877	0.66	2.08	0.536	0.316
12.2	0.440	1.49	1.42	1.017	0.943	0.71	2.02	0.571	0.335
10	0.413	1.61	1.54	0.954	1.151	0.87	1.90	0.68	0.389
8.1	0.381	1.91	1.82	0.880	1.343	1.05	1.75	0.83	0.46
7	0.359	2.09	1.96	0.830	1.534	1.23	1.65	0.97	0.55
6	0.334	1.99	1.88	0.771	1.734	1.35	1.53	1.12	0.66
5	0.307	1.97	1.89	0.709	1.804	1.38	1.41	1.36	0.78
4	0.275	2.46	2.37	0.635	1.967	1.62	1.26	1.57	0.93
3.3	0.246	2.90	2.78	0.569	2.443	2.05	1.13	1.94	1.21
2.5	0.209	3.29	3.05	0.483	2.813	2.29	0.960	2.43	1.61
2	0.181	2.34	2.16	0.418	2.817	2.24	0.831	2.82	1.82
1.5	0.137	3.30	3.07	0.318	3.124	2.29	0.632	3.19	1.70
1	0.0917	2.27	2.21	0.214	2.697	2.42	0.423	3.70	2.32
0.8	0.0768	2.67	2.56	0.193	2.754	2.41	0.405	3.26	2.42
0.7	0.0703	3.25	3.10	0.184	3.233	2.80	0.397	3.50	2.48
0.61	0.0652	4.00	3.90	0.177	3.933	3.43	0.390	3.94	2.71
0.5	0.0590	3.66	3.72	0.167	4.107	4.01	0.382	4.75	3.46
0.33	0.0317	1.97	2.00	0.0901	2.219	2.30	0.206	2.85	2.96
0.25	0.0209	1.64	1.65	0.0592	1.726	1.75	0.136	2.05	2.06
0.15	0.0095	1.36	1.36	0.0270	1.395	1.39	0.0617	1.55	1.54
0.1	0.0047	1.30	1.29	0.0134	1.321	1.31	0.0307	1.45	1.40

Table 2.5.2-20c Amplification Factors as a Function of Input Hard Rock Motion at 40-ft Depth Horizon (FIRS), as Developed from Site Response Analysis using SRS and EPRI Soil Degradation Models, for High-Frequency Rock Motions

	10-4			10-5			10-6		
	Hard rock input motion	mean amp. factors		Hard rock input motion	mean amp. factors		Hard rock input motion	mean amp. factors	
Freq, Hz		EPRI	SRS		EPRI	SRS		EPRI	SRS
100	0.294	1.13	1.17	0.703	0.874	0.874	1.60	0.608	0.568
76	0.400	0.851	0.885	0.957	0.655	0.655	2.17	0.452	0.422
60	0.499	0.706	0.739	1.19	0.527	0.528	2.71	0.361	0.336
50	0.595	0.627	0.660	1.42	0.451	0.453	3.23	0.304	0.283
40	0.631	0.687	0.733	1.51	0.457	0.458	3.43	0.292	0.272
30	0.655	0.826	0.89	1.57	0.516	0.516	3.63	0.291	0.269
25	0.647	0.99	1.07	1.55	0.621	0.626	3.71	0.310	0.284
20	0.615	1.19	1.27	1.47	0.776	0.778	3.34	0.390	0.358
16.5	0.575	1.34	1.42	1.38	0.919	0.92	3.13	0.480	0.444
13.4	0.521	1.56	1.63	1.25	1.102	1.10	2.83	0.609	0.554
12.2	0.494	1.71	1.78	1.18	1.216	1.22	2.69	0.675	0.617
10	0.438	1.76	1.82	1.05	1.430	1.43	2.38	0.85	0.795
8.1	0.377	2.08	2.15	0.902	1.575	1.59	2.05	1.03	0.96
7	0.339	2.19	2.23	0.811	1.780	1.80	1.84	1.15	1.09
6	0.298	2.05	2.08	0.713	1.916	1.89	1.62	1.34	1.27
5	0.257	2.22	2.24	0.615	1.966	1.94	1.40	1.57	1.49
4	0.212	2.76	2.82	0.507	2.335	2.33	1.15	1.79	1.68
3.3	0.175	3.09	3.16	0.419	2.777	2.79	0.952	2.12	2.03
2.5	0.131	3.30	3.34	0.314	3.160	3.16	0.713	2.52	2.47
2	0.101	2.56	2.56	0.242	2.702	2.65	0.549	2.68	2.57
1.5	0.064	3.26	3.26	0.154	3.162	3.04	0.350	2.96	2.61
1	0.035	2.35	2.37	0.0828	2.510	2.50	0.188	2.72	2.61
0.8	0.024	2.64	2.64	0.0563	2.655	2.62	0.128	2.71	2.57
0.7	0.0187	3.15	3.14	0.0447	3.097	3.03	0.101	3.03	2.86
0.61	0.0148	3.79	3.82	0.0354	3.773	3.72	0.0804	3.72	3.51
0.5	0.0109	3.40	3.46	0.0260	3.556	3.63	0.0590	3.76	3.81
0.33	0.00525	2.18	2.21	0.0126	2.237	2.28	0.0286	2.35	2.40
0.25	0.00314	1.98	2.00	0.00751	2.015	2.03	0.0171	2.06	2.06
0.15	0.00106	2.08	2.10	0.00254	2.102	2.10	0.00577	2.15	2.07
0.1	0.000370	2.31	2.33	0.000890	2.295	2.27	0.00201	2.18	2.08

Table 2.5.2-20d Amplification Factors as a Function of Input Hard Rock Motion at 40-ft Depth Horizon (FIRS), as Developed from Site Response Analysis Using SRS and EPRI Soil Degradation Models, for Low-Frequency Rock Motions

	10^{-4}			10^{-5}			10^{-6}		
	Hard rock input motion	mean amp. factors		Hard rock input motion	mean amp. factors		Hard rock input motion	mean amp. factors	
Freq, Hz		EPRI	SRS		EPRI	SRS		EPRI	SRS
100	0.224	1.26	1.25	0.517	0.978	0.888	1.03	0.715	0.549
76	0.305	0.947	0.942	0.704	0.728	0.661	1.40	0.531	0.408
60	0.380	0.762	0.759	0.878	0.581	0.527	1.74	0.422	0.324
50	0.453	0.653	0.647	1.047	0.489	0.443	2.08	0.354	0.272
40	0.483	0.629	0.623	1.115	0.462	0.418	2.22	0.333	0.255
30	0.506	0.682	0.67	1.168	0.450	0.405	2.32	0.319	0.244
25	0.505	0.78	0.77	1.167	0.467	0.415	2.32	0.321	0.246
20	0.493	0.93	0.92	1.139	0.520	0.453	2.26	0.334	0.254
16.5	0.476	1.08	1.07	1.101	0.600	0.52	2.19	0.355	0.267
13.4	0.453	1.28	1.27	1.046	0.701	0.59	2.08	0.388	0.286
12.2	0.440	1.38	1.37	1.017	0.758	0.65	2.02	0.411	0.301
10	0.413	1.51	1.50	0.954	0.943	0.80	1.90	0.48	0.344
8.1	0.381	1.77	1.76	0.880	1.101	0.96	1.75	0.56	0.40
7	0.359	1.96	1.92	0.830	1.271	1.14	1.65	0.66	0.48
6	0.334	1.94	1.91	0.771	1.464	1.28	1.53	0.78	0.57
5	0.307	2.02	2.01	0.709	1.594	1.37	1.41	0.96	0.69
4	0.275	2.59	2.60	0.635	1.835	1.67	1.26	1.15	0.84
3.3	0.246	3.06	3.09	0.569	2.292	2.16	1.13	1.45	1.10
2.5	0.209	3.37	3.33	0.483	2.617	2.44	0.960	1.83	1.51
2	0.181	2.38	2.35	0.418	2.661	2.43	0.831	2.11	1.69
1.5	0.137	3.29	3.19	0.318	2.871	2.35	0.632	2.46	1.61
1	0.0917	2.26	2.26	0.214	2.517	2.45	0.423	3.00	2.21
0.8	0.0768	2.65	2.59	0.193	2.605	2.42	0.405	2.75	2.30
0.7	0.0703	3.23	3.13	0.184	3.075	2.80	0.397	2.98	2.35
0.61	0.0652	3.97	3.92	0.177	3.766	3.43	0.390	3.40	2.59
0.5	0.0590	3.64	3.74	0.167	3.953	4.01	0.382	4.18	3.32
0.33	0.0317	1.96	2.00	0.0901	2.158	2.29	0.206	2.59	2.87
0.25	0.0209	1.63	1.65	0.0592	1.688	1.75	0.136	1.88	2.01
0.15	0.0095	1.35	1.36	0.0270	1.372	1.39	0.0617	1.46	1.51
0.1	0.0047	1.29	1.30	0.0134	1.295	1.31	0.0307	1.36	1.38

Table 2.5.2-20e Amplification Factors as a Function of Input Hard Rock Motion at Ground Surface (GMRS), as Developed from Site Response Analysis Using SRS and EPRI Soil Degradation Models, for High-Frequency Rock Motions

-	10-4			10-5			10-6		
-	Hard rock input motion	mean amp. factors		Hard rock input motion	mean amp. factors		Hard rock input motion	mean amp. factors	
Freq, Hz		EPRI	SRS		EPRI	SRS		EPRI	SRS
100	0.294	1.22	1.26	0.703	0.849	0.847	1.60	0.540	0.510
76	0.400	0.915	0.945	0.957	0.634	0.632	2.17	0.401	0.379
60	0.499	0.743	0.768	1.19	0.508	0.506	2.71	0.319	0.301
50	0.595	0.640	0.665	1.42	0.428	0.427	3.23	0.268	0.253
40	0.631	0.664	0.694	1.51	0.415	0.414	3.43	0.254	0.240
30	0.655	0.775	0.82	1.57	0.434	0.434	3.63	0.244	0.230
25	0.647	0.96	1.02	1.55	0.495	0.495	3.71	0.245	0.232
20	0.615	1.25	1.33	1.47	0.627	0.629	3.34	0.289	0.274
16.5	0.575	1.42	1.50	1.38	0.777	0.78	3.13	0.344	0.326
13.4	0.521	1.68	1.75	1.25	0.950	0.96	2.83	0.420	0.397
12.2	0.494	1.86	1.93	1.18	1.071	1.08	2.69	0.469	0.444
10	0.438	1.95	2.02	1.05	1.307	1.31	2.38	0.61	0.585
8.1	0.377	2.38	2.46	0.902	1.517	1.53	2.05	0.76	0.72
7	0.339	2.55	2.60	0.811	1.793	1.81	1.84	0.88	0.85
6	0.298	2.40	2.44	0.713	2.013	1.98	1.62	1.09	1.06
5	0.257	2.55	2.57	0.615	2.136	2.10	1.40	1.39	1.33
4	0.212	3.09	3.17	0.507	2.554	2.55	1.15	1.71	1.62
3.3	0.175	3.37	3.45	0.419	3.010	3.03	0.952	2.16	2.07
2.5	0.131	3.49	3.53	0.314	3.336	3.33	0.713	2.72	2.67
2	0.101	2.66	2.66	0.242	2.804	2.75	0.549	2.93	2.79
1.5	0.064	3.32	3.32	0.154	3.208	3.08	0.350	3.20	2.79
1	0.035	2.37	2.40	0.0828	2.528	2.52	0.188	2.83	2.69
0.8	0.024	2.65	2.66	0.0563	2.656	2.62	0.128	2.75	2.59
0.7	0.0187	3.17	3.16	0.0447	3.088	3.02	0.101	3.06	2.88
0.61	0.0148	3.80	3.82	0.0354	3.761	3.71	0.0804	3.74	3.51
0.5	0.0109	3.40	3.46	0.0260	3.538	3.61	0.0590	3.77	3.80
0.33	0.00525	2.20	2.23	0.0126	2.236	2.27	0.0286	2.37	2.40
0.25	0.00314	2.01	2.02	0.00751	2.027	2.04	0.0171	2.09	2.07
0.15	0.00106	2.14	2.17	0.00254	2.130	2.13	0.00577	2.21	2.13
0.1	0.000370	2.41	2.44	0.000890	2.339	2.32	0.00201	2.26	2.15

Table 2.5.2-20f Amplification Factors as a Function of Input Hard Rock Motion at Ground Surface (GMRS), as Developed from Site Response Analysis Using SRS and EPRI Soil Degradation Models, for Low-Frequency Rock Motions

-		10-4			10-5			10-6	
-	Hard rock input motion	mean amp. factors		Hard rock input motion	mean amp. factors		Hard rock input motion	mean amp. factors	
Freq, Hz		EPRI	SRS		EPRI	SRS		EPRI	SRS
100	0.224	1.33	1.33	0.517	0.957	0.871	1.03	0.662	0.527
76	0.305	1.002	0.997	0.704	0.713	0.648	1.40	0.492	0.392
60	0.380	0.803	0.799	0.878	0.568	0.516	1.74	0.391	0.311
50	0.453	0.680	0.676	1.047	0.478	0.434	2.08	0.328	0.261
40	0.483	0.654	0.648	1.115	0.450	0.409	2.22	0.308	0.245
30	0.506	0.687	0.68	1.168	0.434	0.395	2.32	0.294	0.234
25	0.505	0.77	0.76	1.167	0.442	0.401	2.32	0.296	0.235
20	0.493	0.95	0.94	1.139	0.478	0.429	2.26	0.305	0.242
16.5	0.476	1.12	1.11	1.101	0.541	0.48	2.19	0.320	0.253
13.4	0.453	1.33	1.32	1.046	0.625	0.55	2.08	0.343	0.270
12.2	0.440	1.44	1.42	1.017	0.676	0.60	2.02	0.359	0.281
10	0.413	1.62	1.60	0.954	0.838	0.74	1.90	0.40	0.315
8.1	0.381	1.95	1.94	0.880	1.008	0.91	1.75	0.47	0.36
7	0.359	2.18	2.14	0.830	1.205	1.10	1.65	0.55	0.42
6	0.334	2.17	2.13	0.771	1.434	1.28	1.53	0.65	0.51
5	0.307	2.25	2.23	0.709	1.600	1.39	1.41	0.81	0.62
4	0.275	2.82	2.84	0.635	1.883	1.72	1.26	1.00	0.77
3.3	0.246	3.26	3.30	0.569	2.360	2.23	1.13	1.28	1.05
2.5	0.209	3.50	3.45	0.483	2.658	2.48	0.960	1.72	1.47
2	0.181	2.43	2.39	0.418	2.662	2.43	0.831	2.06	1.66
1.5	0.137	3.30	3.20	0.318	2.845	2.33	0.632	2.43	1.58
1	0.0917	2.26	2.25	0.214	2.481	2.42	0.423	2.92	2.16
0.8	0.0768	2.64	2.58	0.193	2.564	2.39	0.405	2.66	2.24
0.7	0.0703	3.21	3.11	0.184	3.031	2.77	0.397	2.90	2.30
0.61	0.0652	3.96	3.90	0.177	3.716	3.39	0.390	3.30	2.53
0.5	0.0590	3.62	3.73	0.167	3.903	3.96	0.382	4.08	3.26
0.33	0.0317	1.95	1.99	0.0901	2.136	2.27	0.206	2.53	2.83
0.25	0.0209	1.63	1.65	0.0592	1.673	1.73	0.136	1.84	1.98
0.15	0.0095	1.35	1.36	0.0270	1.362	1.38	0.0617	1.43	1.49
0.1	0.0047	1.29	1.29	0.0134	1.287	1.30	0.0307	1.35	1.37

Table 2.5.2-21 Spectral Accelerations (SA, in g) for Hard Rock Conditions and for Hypothetical Outcrop of Highest Competent In Situ Layer (Top of Blue Bluff Marl)

	Hard Rock spectral accel, g			Soil spectral accel, g		
Freq	10^{-4}	10^{-5}	10^{-6}	10^{-4}	10^{-5}	10^{-6}
100	0.214	0.559	1.480	0.255	0.531	1.025
76	0.293	0.777	2.059	0.268	0.558	1.063
60	0.394	1.057	2.802	0.311	0.629	1.167
50	0.464	1.257	3.334	0.333	0.656	1.180
40	0.517	1.416	3.758	0.423	0.778	1.310
30	0.545	1.511	4.011	0.545	0.984	1.452
25	0.551	1.540	4.090	0.646	1.217	1.636
20	0.522	1.419	3.685	0.723	1.390	1.925
16.5	0.493	1.309	3.330	0.758	1.474	2.139
13.4	0.456	1.176	2.914	0.784	1.523	2.299
12.2	0.438	1.115	2.727	0.800	1.553	2.349
10	0.399	0.983	2.330	0.722	1.522	2.405
8.1	0.375	0.904	2.071	0.831	1.551	2.517
7	0.359	0.852	1.909	0.801	1.658	2.574
6	0.339	0.792	1.728	0.671	1.601	2.650
5	0.317	0.728	1.540	0.612	1.306	2.665
4	0.287	0.659	1.369	0.694	1.190	2.419
3.3	0.259	0.595	1.213	0.735	1.335	2.350
2.5	0.223	0.512	1.020	0.706	1.300	2.184
2	0.193	0.445	0.886	0.440	1.153	2.036
1.5	0.152	0.352	0.698	0.484	0.952	1.705
1	0.101	0.235	0.465	0.226	0.597	1.396
0.8	0.091	0.230	0.489	0.237	0.595	1.388
0.7	0.083	0.220	0.481	0.264	0.664	1.436
0.61	0.076	0.207	0.462	0.299	0.761	1.535
0.5	0.065	0.185	0.423	0.238	0.745	1.741
0.33	0.038	0.107	0.245	0.075	0.242	0.712
0.25	0.026	0.072	0.166	0.042	0.126	0.341
0.15	0.012	0.033	0.075	0.016	0.046	0.116
0.1	0.006	0.016	0.036	0.007	0.021	0.051

Table 2.5.2-21a Spectral Accelerations (SA, in g) for Hard Rock Conditions and for Hypothetical Outcrop at 40-ft Depth Horizon (FIRS)

	Hard Rock spectral accel, g			Soil spectral accel, g		
Freq	10^{-4}	10^{-5}	10^{-6}	10^{-4}	10^{-5}	10^{-6}
100	0.214	0.559	1.480	0.246	0.489	0.870
76	0.293	0.777	2.059	0.254	0.509	0.900
60	0.394	1.057	2.802	0.287	0.563	0.986
50	0.464	1.257	3.334	0.302	0.575	0.991
40	0.517	1.416	3.758	0.372	0.658	1.074
30	0.545	1.511	4.011	0.473	0.788	1.134
25	0.551	1.540	4.090	0.566	0.961	1.214
20	0.522	1.419	3.685	0.656	1.120	1.396
16.5	0.493	1.309	3.330	0.699	1.230	1.562
13.4	0.456	1.176	2.914	0.744	1.319	1.714
12.2	0.438	1.115	2.727	0.778	1.374	1.777
10	0.399	0.983	2.330	0.713	1.398	1.901
8.1	0.375	0.904	2.071	0.803	1.442	2.068
7	0.359	0.852	1.909	0.775	1.539	2.145
6	0.339	0.792	1.728	0.673	1.512	2.261
5	0.317	0.728	1.540	0.637	1.265	2.346
4	0.287	0.659	1.369	0.745	1.163	2.164
3.3	0.259	0.595	1.213	0.796	1.324	2.093
2.5	0.223	0.512	1.020	0.747	1.289	1.902
2	0.193	0.445	0.886	0.457	1.133	1.690
1.5	0.152	0.352	0.698	0.492	0.918	1.418
1	0.101	0.235	0.465	0.227	0.580	1.208
0.8	0.091	0.230	0.489	0.238	0.579	1.233
0.7	0.083	0.220	0.481	0.265	0.647	1.282
0.61	0.076	0.207	0.462	0.299	0.743	1.381
0.5	0.065	0.185	0.423	0.238	0.731	1.592
0.33	0.038	0.107	0.245	0.075	0.239	0.670
0.25	0.026	0.072	0.166	0.042	0.124	0.322
0.15	0.012	0.033	0.075	0.016	0.045	0.112
0.1	0.006	0.016	0.036	0.007	0.020	0.049

Table 2.5.2-21b Spectral Accelerations (SA, in g) for Hard Rock Conditions and for Ground Surface Motions (GMRS)

	Hard Rock spectral accel, g			Soil spectral accel, g		
Freq	10-4	10-5	10-6	10-4	10-5	10-6
100	0.214	0.559	1.480	0.266	0.474	0.777
76	0.293	0.777	2.059	0.272	0.492	0.803
60	0.394	1.057	2.802	0.300	0.541	0.877
50	0.464	1.257	3.334	0.306	0.545	0.879
40	0.517	1.416	3.758	0.356	0.595	0.942
30	0.545	1.511	4.011	0.440	0.662	0.959
25	0.551	1.540	4.090	0.547	0.762	0.976
20	0.522	1.419	3.685	0.686	0.905	1.050
16.5	0.493	1.309	3.330	0.739	1.042	1.132
13.4	0.456	1.176	2.914	0.802	1.140	1.205
12.2	0.438	1.115	2.727	0.846	1.213	1.256
10	0.399	0.983	2.330	0.789	1.279	1.379
8.1	0.375	0.904	2.071	0.920	1.390	1.542
7	0.359	0.852	1.909	0.892	1.551	1.662
6	0.339	0.792	1.728	0.767	1.586	1.861
5	0.317	0.728	1.540	0.709	1.335	2.076
4	0.287	0.659	1.369	0.812	1.197	2.060
3.3	0.259	0.595	1.213	0.849	1.365	2.060
2.5	0.223	0.512	1.020	0.775	1.309	1.893
2	0.193	0.445	0.886	0.466	1.134	1.654
1.5	0.152	0.352	0.698	0.494	0.910	1.397
1	0.101	0.235	0.465	0.227	0.572	1.178
0.8	0.091	0.230	0.489	0.237	0.570	1.197
0.7	0.083	0.220	0.481	0.263	0.638	1.250
0.61	0.076	0.207	0.462	0.297	0.734	1.346
0.5	0.065	0.185	0.423	0.237	0.722	1.556
0.33	0.038	0.107	0.245	0.075	0.236	0.657
0.25	0.026	0.072	0.166	0.042	0.123	0.317
0.15	0.012	0.033	0.075	0.016	0.045	0.110
0.1	0.006	0.016	0.036	0.007	0.020	0.049

Table 2.5.2-22 Amplitudes (g) for the Hypothetical Outcrop of Highest Competent In Situ Layer (Top of Blue Bluff Marl)

	Soil amplitudes				raw	smoothed
Freq	10^{-4}	10^{-5}	AR	DF2	SSE	SSE
100	0.255	0.531	2.08	1.08	0.275	0.275
76	0.268	0.558	2.08	1.08	0.289	0.295
60	0.311	0.629	2.02	1.05	0.328	0.326
50	0.333	0.656	1.97	1.03	0.344	0.366
40	0.423	0.778	1.84	0.978	0.423	0.435
30	0.545	0.984	1.80	0.962	0.545	0.551
25	0.646	1.217	1.88	0.995	0.646	0.646
20	0.723	1.390	1.92	1.01	0.732	0.725
16.5	0.758	1.474	1.95	1.02	0.774	0.764
13.4	0.784	1.523	1.94	1.02	0.800	0.795
12.2	0.800	1.553	1.94	1.02	0.816	0.803
10	0.722	1.522	2.11	1.09	0.787	0.787
8.1	0.831	1.551	1.87	0.989	0.831	0.789
7	0.801	1.658	2.07	1.07	0.860	0.773
6	0.671	1.601	2.39	1.20	0.807	0.758
5	0.612	1.306	2.13	1.10	0.673	0.748
4	0.694	1.190	1.71	0.924	0.694	0.724
3.3	0.735	1.335	1.82	0.967	0.735	0.710
2.5	0.706	1.300	1.84	0.977	0.706	0.706
2	0.440	1.153	2.62	1.30	0.571	0.580
1.5	0.484	0.952	1.96	1.03	0.499	0.480
1	0.226	0.597	2.65	1.31	0.295	0.295
0.8	0.237	0.595	2.51	1.25	0.297	0.297
0.7	0.264	0.664	2.51	1.25	0.332	0.332
0.61	0.299	0.761	2.55	1.27	0.379	0.379
0.5	0.238	0.745	3.13	1.50	0.356	0.356
0.33	0.0750	0.242	3.23	1.53	0.115	0.115
0.25	0.0420	0.126	3.00	1.44	0.0606	0.0606
0.15	0.0158	0.0458	2.90	1.41	0.0222	0.0222
0.1	0.00718	0.0207	2.88	1.40	0.0100	0.0100

Table 2.5.2-22a FIRS Amplitudes (g) for the Hypothetical Outcrop at 40-ft Depth Horizon

	Soil amplitudes				raw	smoothed
Freq	10^{-4}	10^{-5}	AR	DF2	FIRS	FIRS
100	0.246	0.489	1.99	1.04	0.255	0.255
76	0.254	0.509	2.00	1.05	0.266	0.270
60	0.287	0.563	1.96	1.03	0.295	0.293
50	0.302	0.575	1.90	1.00	0.304	0.325
40	0.372	0.658	1.77	0.946	0.372	0.381
30	0.473	0.788	1.67	0.903	0.473	0.480
25	0.566	0.961	1.70	0.916	0.566	0.566
20	0.656	1.120	1.71	0.92	0.656	0.649
16.5	0.699	1.230	1.76	0.94	0.699	0.697
13.4	0.744	1.319	1.77	0.95	0.744	0.734
12.2	0.778	1.374	1.77	0.95	0.778	0.749
10	0.713	1.398	1.96	1.03	0.733	0.733
8.1	0.803	1.442	1.80	0.958	0.803	0.749
7	0.775	1.539	1.99	1.04	0.805	0.745
6	0.673	1.512	2.25	1.15	0.771	0.745
5	0.637	1.265	1.99	1.04	0.662	0.748
4	0.745	1.163	1.56	0.857	0.745	0.737
3.3	0.796	1.324	1.66	0.902	0.796	0.753
2.5	0.747	1.289	1.72	0.928	0.747	0.747
2	0.457	1.133	2.48	1.24	0.567	0.582
1.5	0.492	0.918	1.87	0.99	0.492	0.478
1	0.227	0.580	2.55	1.27	0.288	0.288
0.8	0.238	0.579	2.44	1.22	0.291	0.291
0.7	0.265	0.647	2.45	1.23	0.325	0.325
0.61	0.299	0.743	2.49	1.24	0.372	0.372
0.5	0.238	0.731	3.07	1.47	0.350	0.350
0.33	0.075	0.239	3.18	1.52	0.114	0.114
0.25	0.042	0.124	2.96	1.43	0.060	0.060
0.15	0.016	0.045	2.88	1.40	0.022	0.022
0.1	0.007	0.020	2.85	1.39	0.010	0.010

Table 2.5.2-22b SSE Amplitudes (g) for the Ground Surface (GMRS)

-	Soil amplitudes		-	-	raw	smoothed
Freq	10^{-4}	10^{-5}	AR	DF2	SSE	SSE
100	0.266	0.474	1.78	0.95	0.266	0.266
76	0.272	0.492	1.81	0.96	0.272	0.277
60	0.300	0.541	1.80	0.96	0.300	0.297
50	0.306	0.545	1.78	0.95	0.306	0.321
40	0.356	0.595	1.67	0.905	0.356	0.365
30	0.440	0.662	1.50	0.832	0.440	0.452
25	0.547	0.762	1.39	0.783	0.547	0.547
20	0.686	0.905	1.32	0.75	0.686	0.670
16.5	0.739	1.042	1.41	0.79	0.739	0.737
13.4	0.802	1.140	1.42	0.80	0.802	0.789
12.2	0.846	1.213	1.43	0.80	0.846	0.809
10	0.789	1.279	1.62	0.88	0.789	0.789
8.1	0.920	1.390	1.51	0.835	0.920	0.818
7	0.892	1.551	1.74	0.93	0.892	0.815
6	0.767	1.586	2.07	1.07	0.823	0.814
5	0.709	1.335	1.88	1.00	0.709	0.814
4	0.812	1.197	1.47	0.818	0.812	0.787
3.3	0.849	1.365	1.61	0.877	0.849	0.802
2.5	0.775	1.309	1.69	0.912	0.775	0.775
2	0.466	1.134	2.43	1.22	0.569	0.589
1.5	0.494	0.910	1.84	0.98	0.494	0.481
1	0.227	0.572	2.52	1.26	0.285	0.285
0.8	0.237	0.570	2.41	1.21	0.287	0.287
0.7	0.263	0.638	2.42	1.22	0.321	0.321
0.61	0.297	0.734	2.47	1.24	0.367	0.367
0.5	0.237	0.722	3.05	1.46	0.347	0.347
0.33	0.0747	0.236	3.16	1.51	0.113	0.113
0.25	0.0419	0.123	2.95	1.42	0.0597	0.0597
0.15	0.0157	0.0451	2.86	1.39	0.0219	0.0219
0.1	0.00718	0.0204	2.84	1.38	0.00992	0.00992

Table 2.5.2-23 Coversion Between Body-Wave (m_b) and Moment (M) Magnitudes

Convert	To	Convert	To
m_b	M	M	m_b
4.00	3.77	4.00	4.28
4.10	3.84	4.10	4.41
4.20	3.92	4.20	4.54
4.30	4.00	4.30	4.66
4.40	4.08	4.40	4.78
4.50	4.16	4.50	4.90
4.60	4.24	4.60	5.01
4.70	4.33	4.70	5.12
4.80	4.42	4.80	5.23
4.90	4.50	4.90	5.33
5.00	4.59	5.00	5.43
5.10	4.69	5.10	5.52
5.20	4.78	5.20	5.61
5.30	4.88	5.30	5.70
5.40	4.97	5.40	5.78
5.50	5.08	5.50	5.87
5.60	5.19	5.60	5.95
5.70	5.31	5.70	6.03
5.80	5.42	5.80	6.11
5.90	5.54	5.90	6.18
6.00	5.66	6.00	6.26
6.10	5.79	6.10	6.33
6.20	5.92	6.20	6.40
6.30	6.06	6.30	6.47
6.40	6.20	6.40	6.53
6.50	6.34	6.50	6.60
6.60	6.49	6.60	6.66
6.70	6.65	6.70	6.73
6.80	6.82	6.80	6.79
6.90	6.98	6.90	6.85
7.00	7.16	7.00	6.91
7.10	7.33	7.10	6.97
7.20	7.51	7.20	7.03
7.30	7.69	7.30	7.09
7.40	7.87	7.40	7.15
7.50	8.04	7.50	7.20
		7.60	7.26
		7.70	7.32
		7.80	7.37
		7.90	7.43
		8.00	7.49

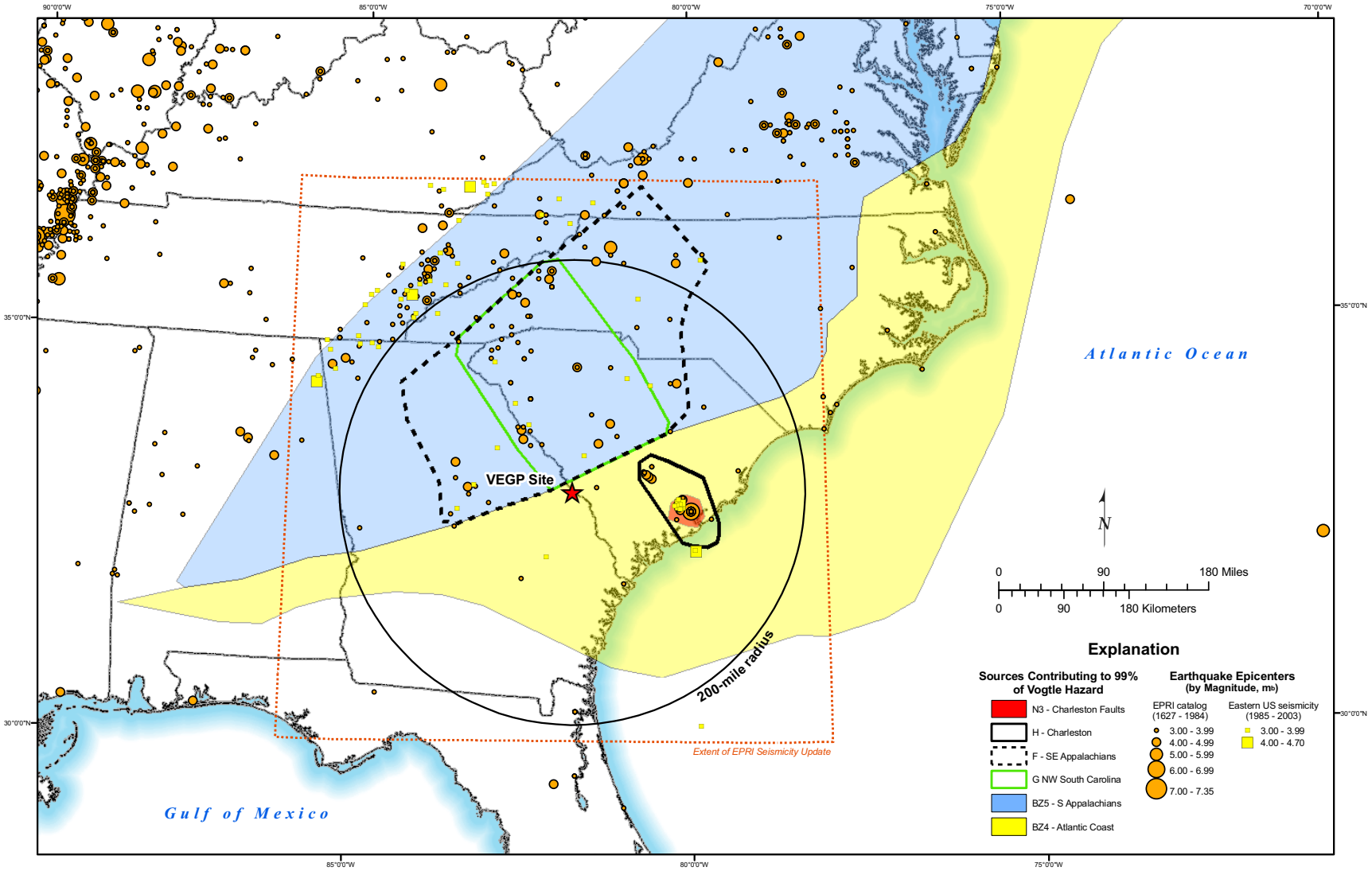

Figure 2.5.2-1 Bechtel EPRI Zones

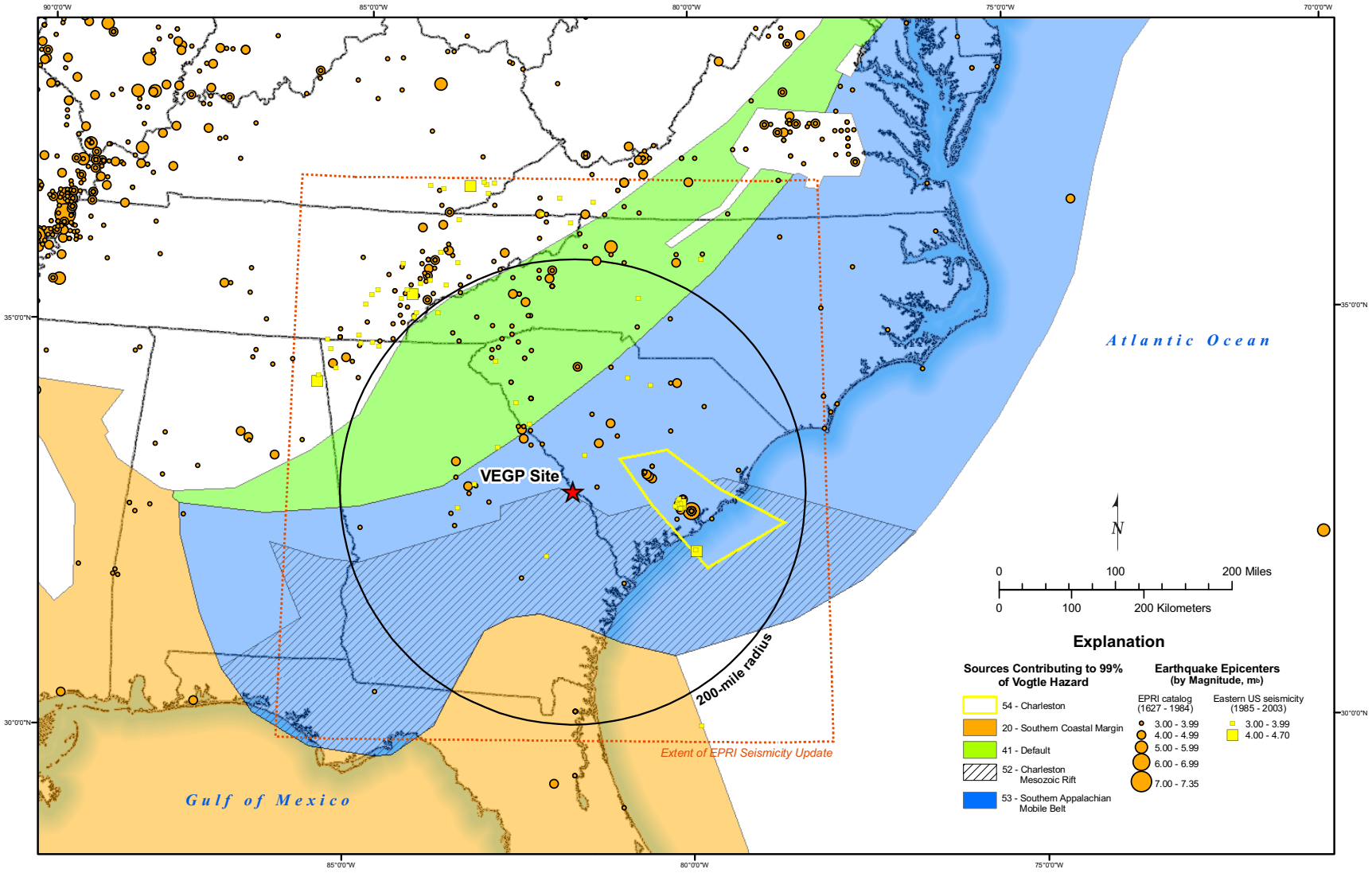

Figure 2.5.2-2 Dames and Moore EPRI Zones

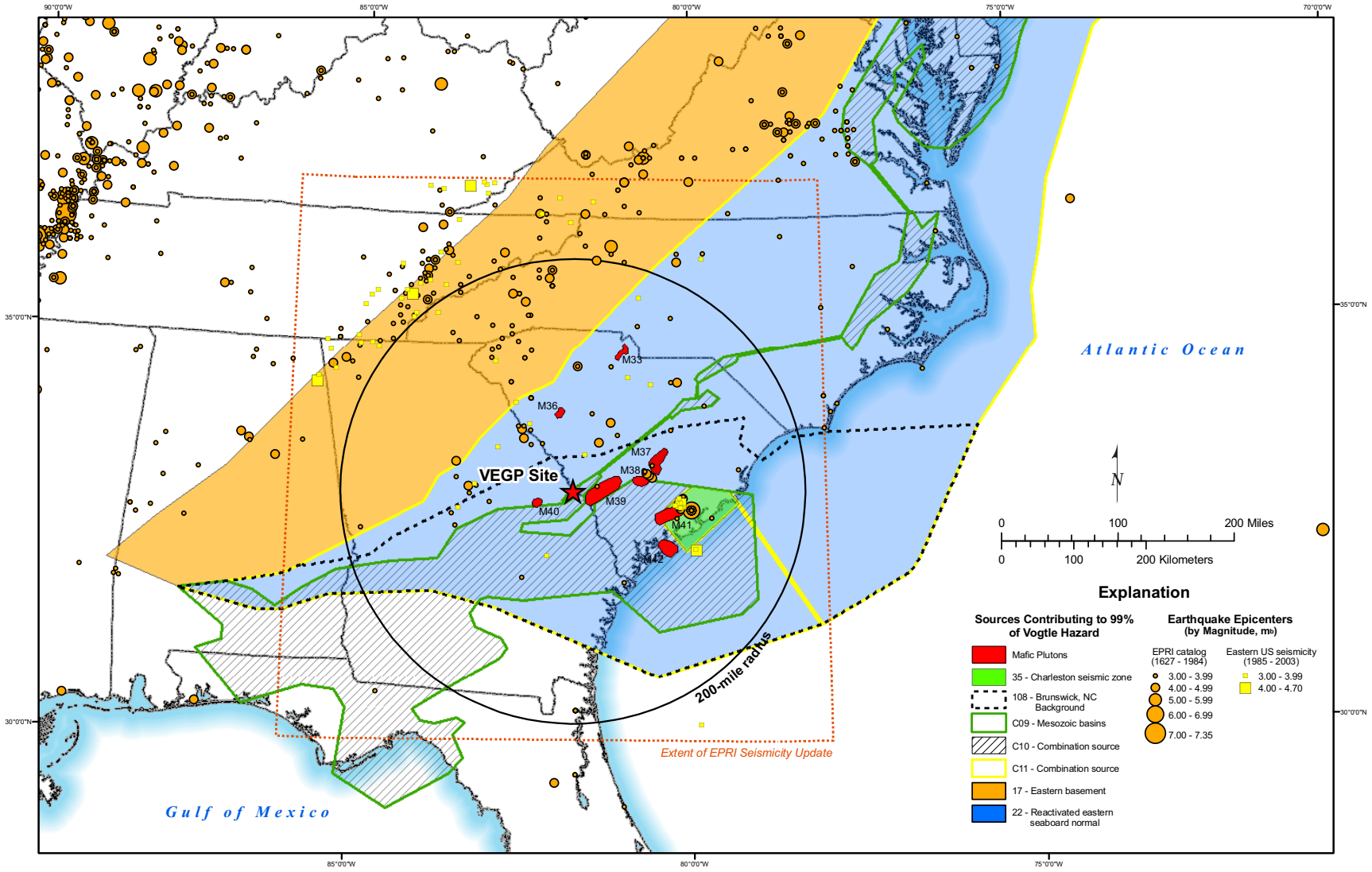

Figure 2.5.2-3 Law EPRI Zones

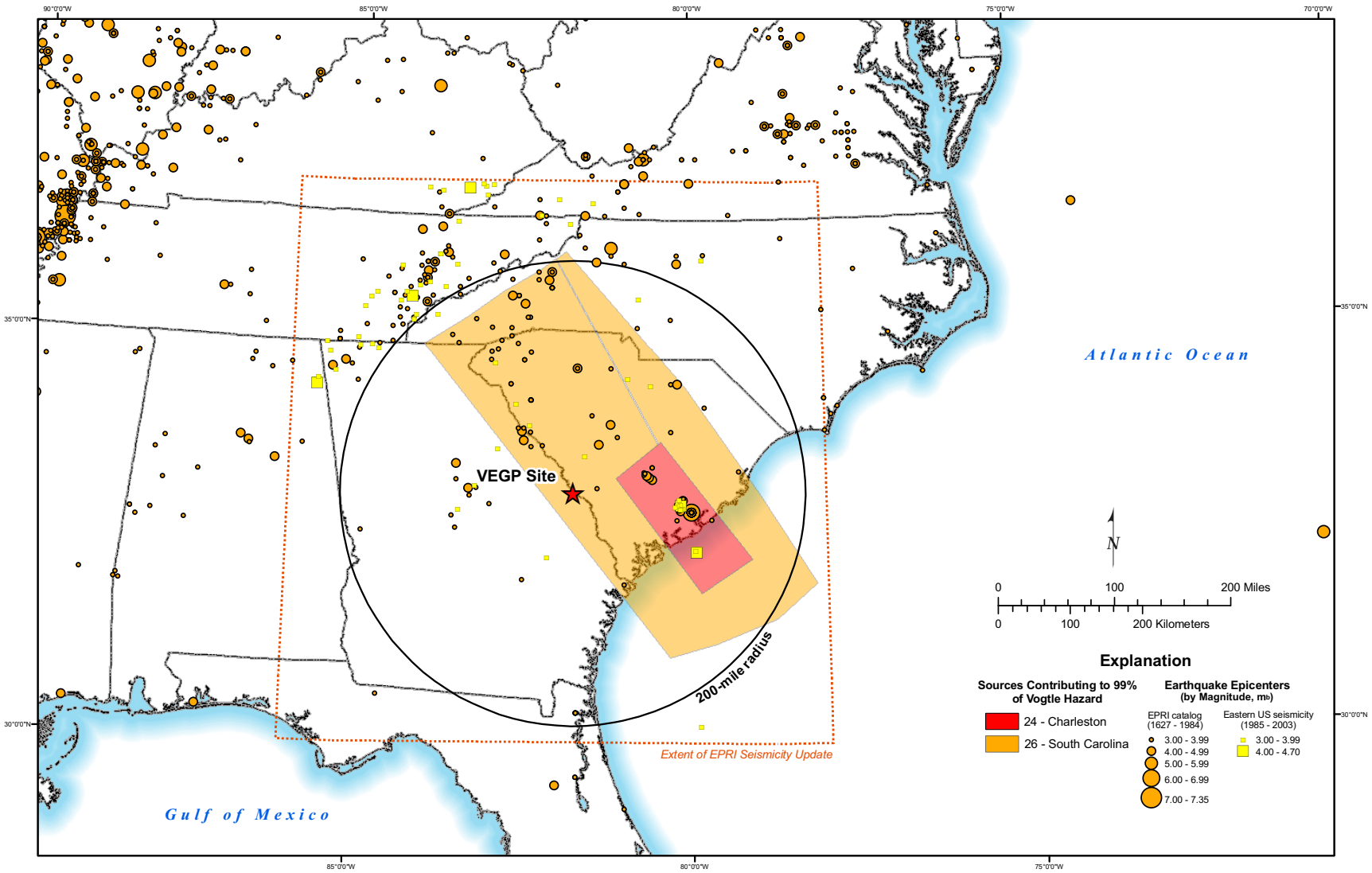

Figure 2.5.2-4 Rondout EPRI Zones

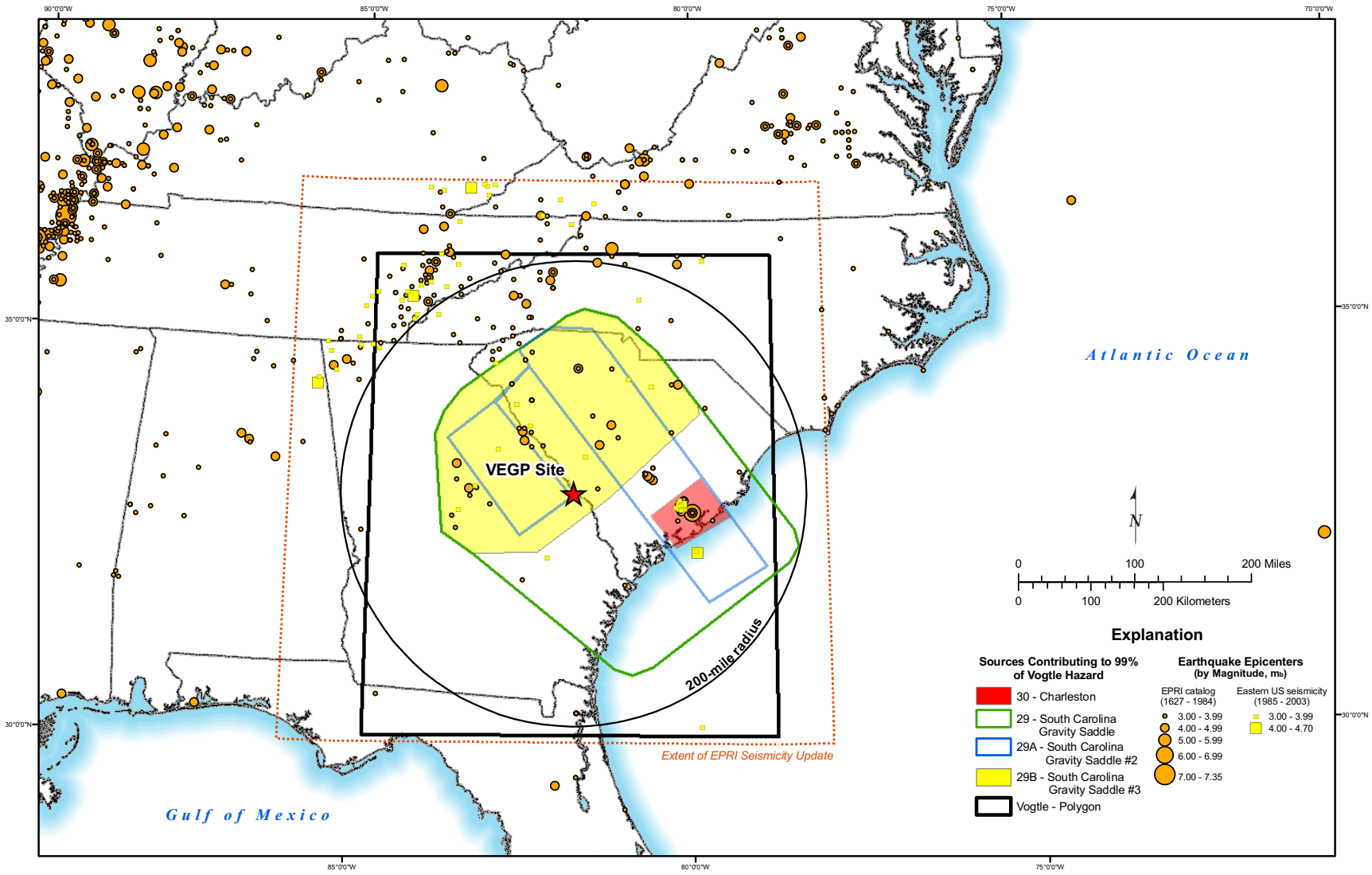

Figure 2.5.2-5 Woodward-Clyde EPRI Zones

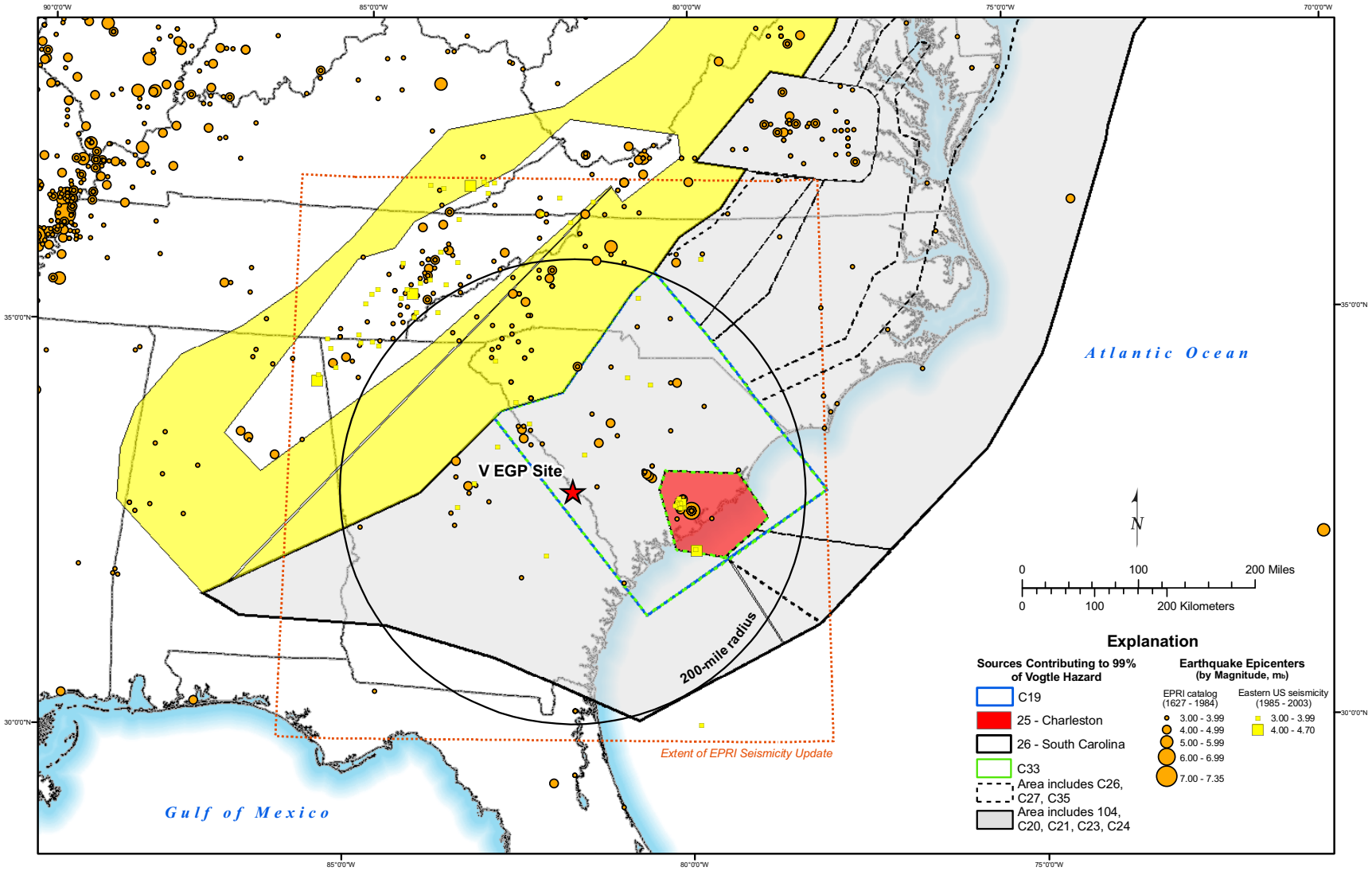

Figure 2.5.2-6 Weston EPRI Zones

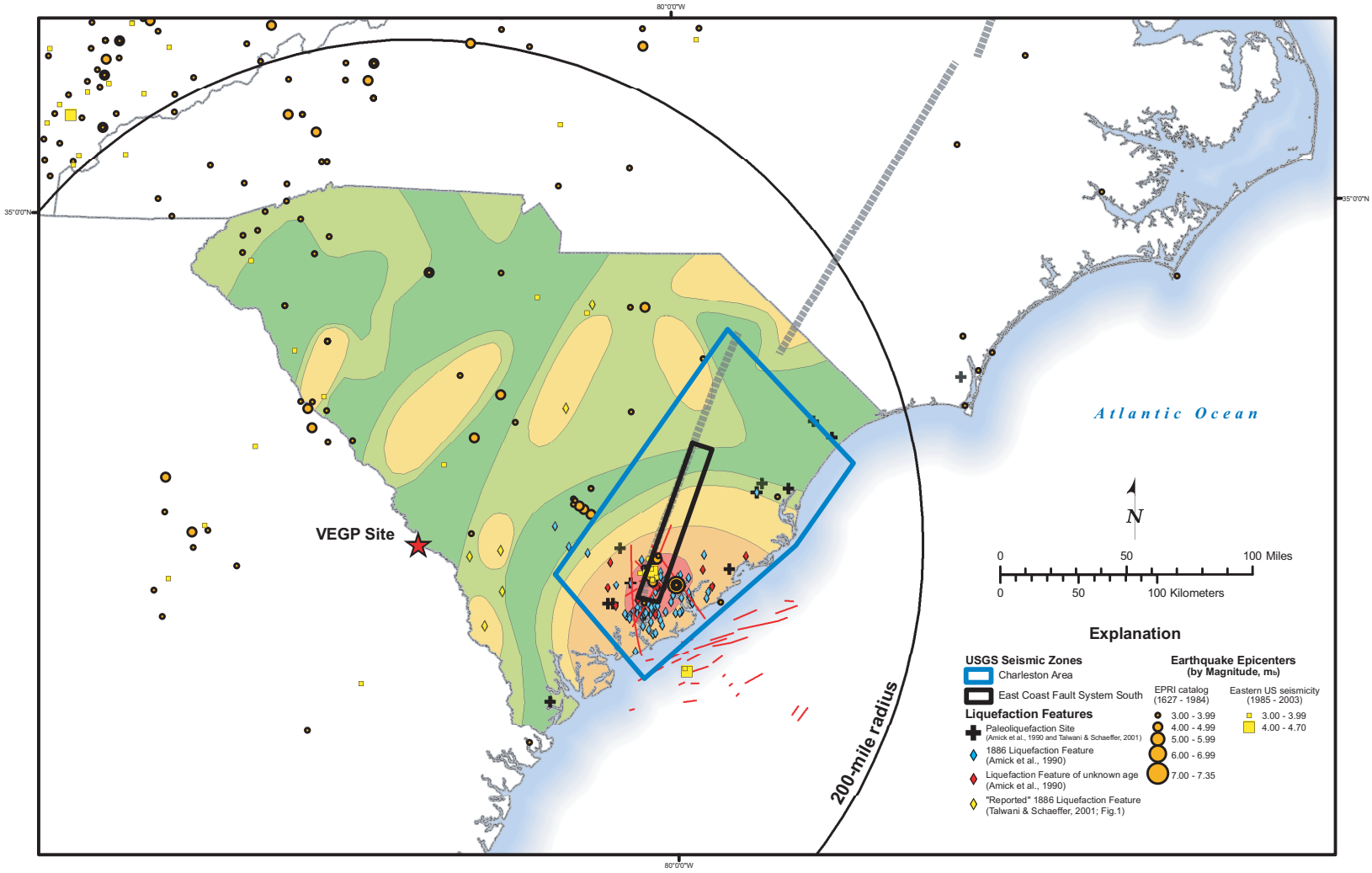

Figure 2.5.2-7 USGS Model

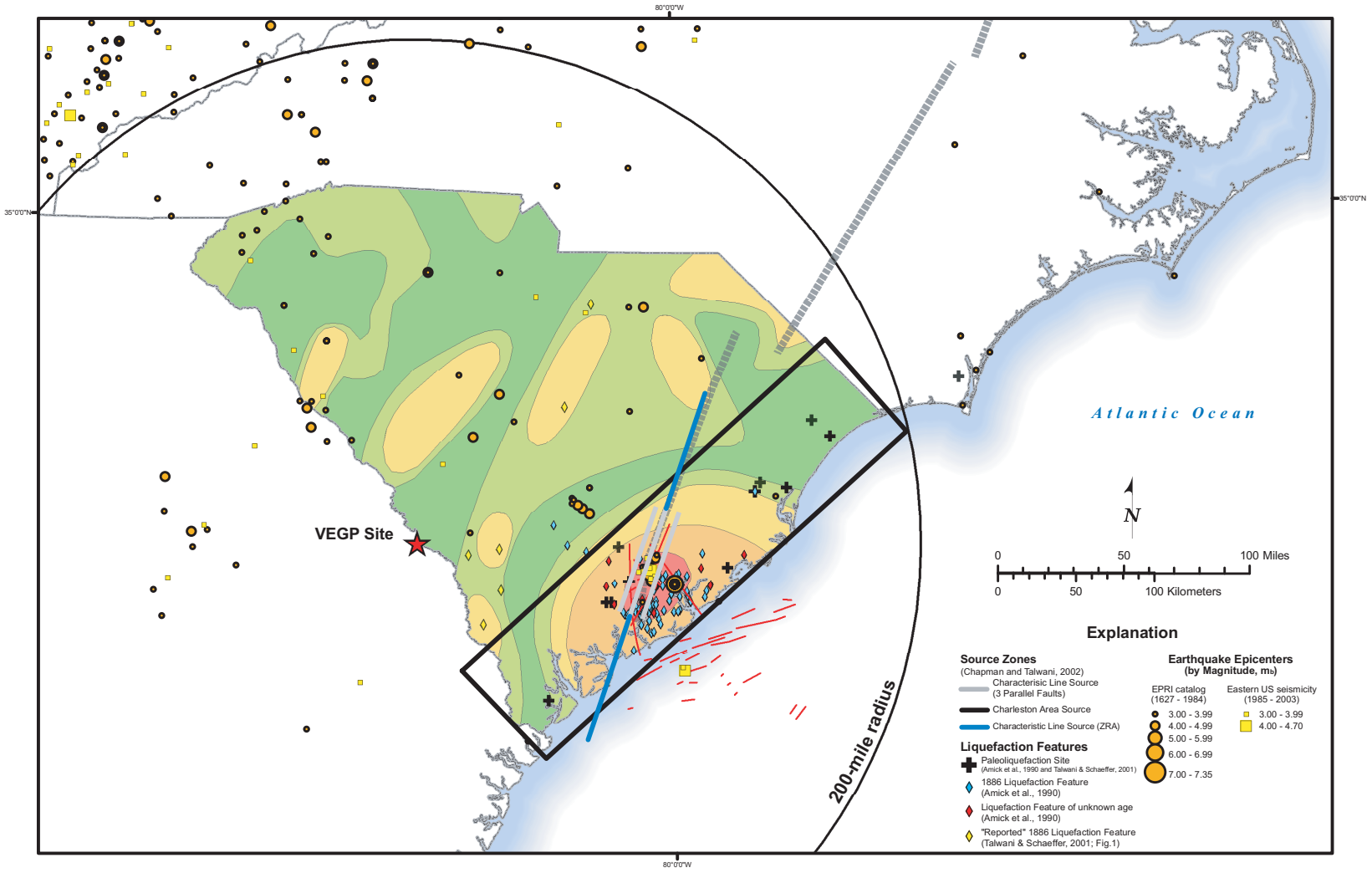

Figure 2.5.2-8 SCDOT Model

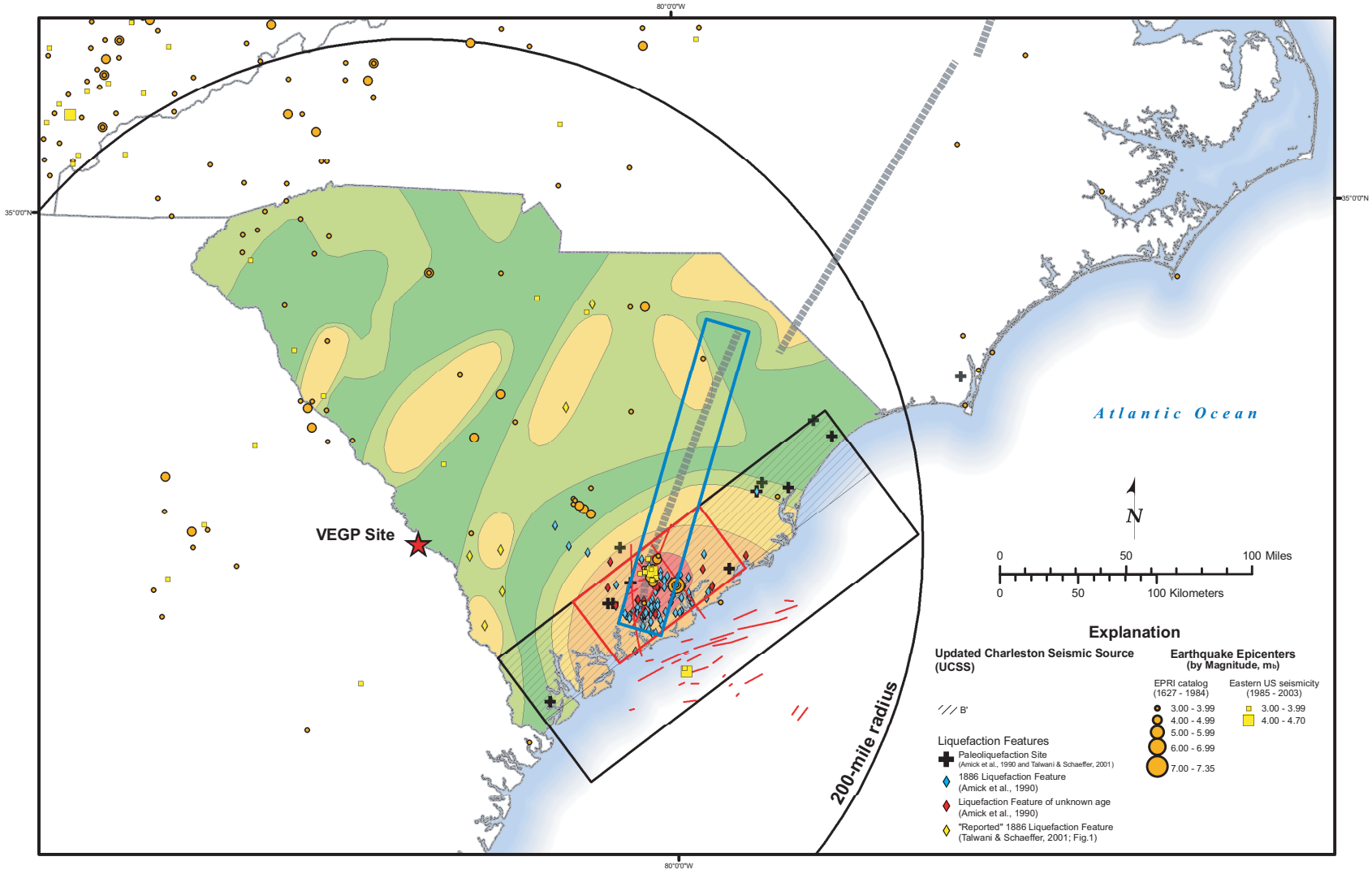

Figure 2.5.2-9 UCSS Map

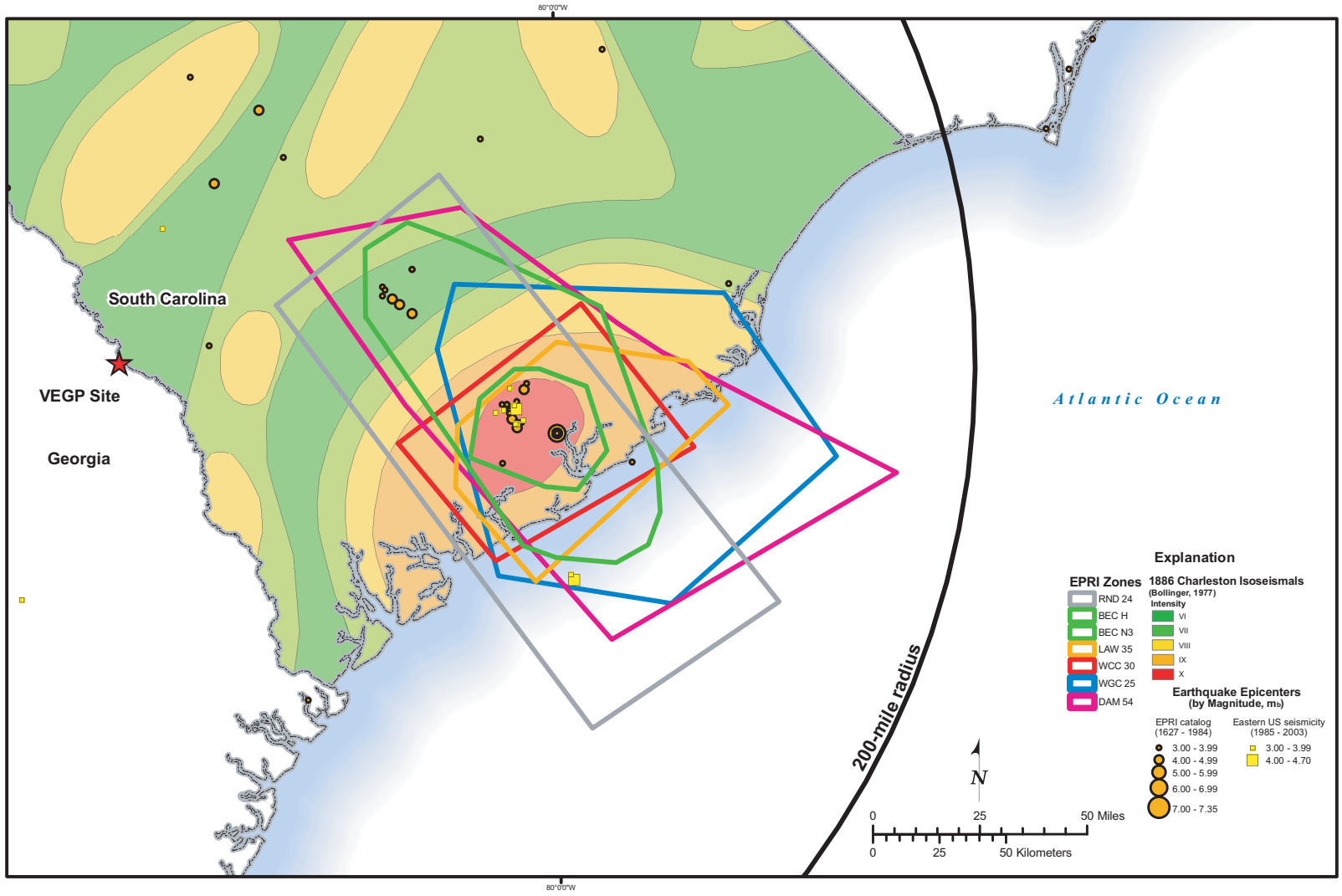

Figure 2.5.2-10 EPRI All Charleston Map

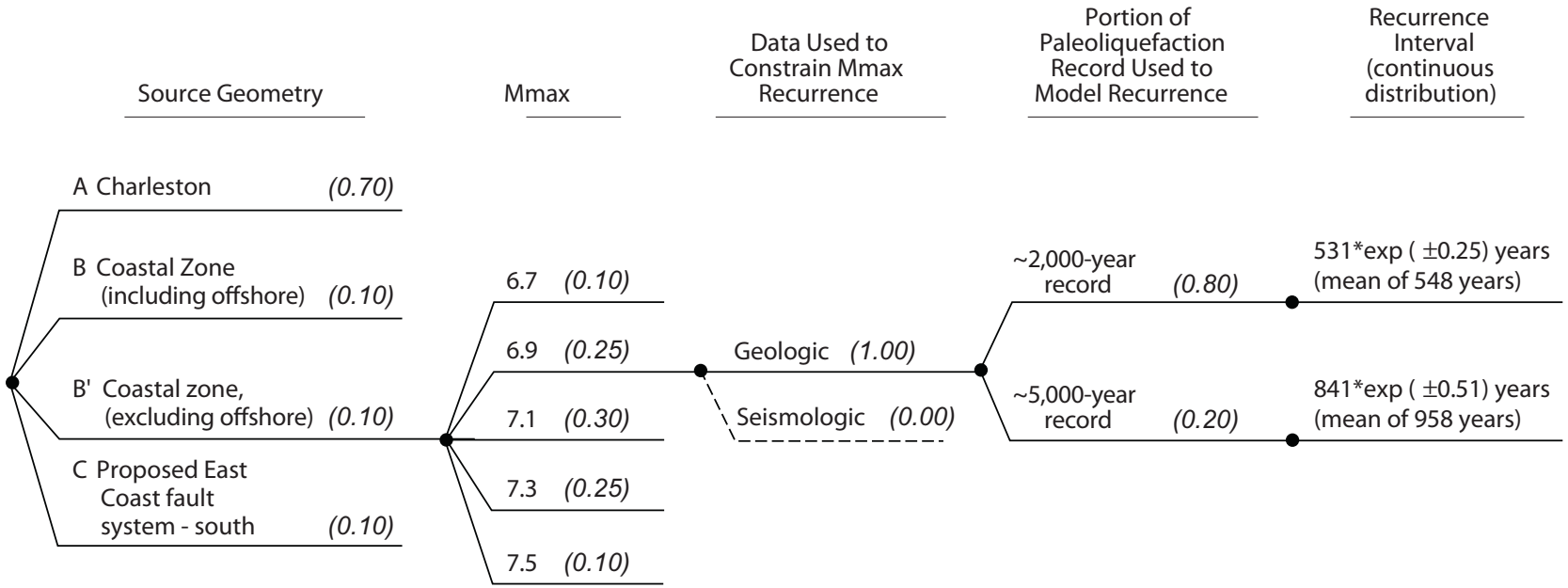

Figure 2.5.2-11 Updated Charleston Seismic Source (USGS) Logic Tree with Weights for each Branch Shown in Italics

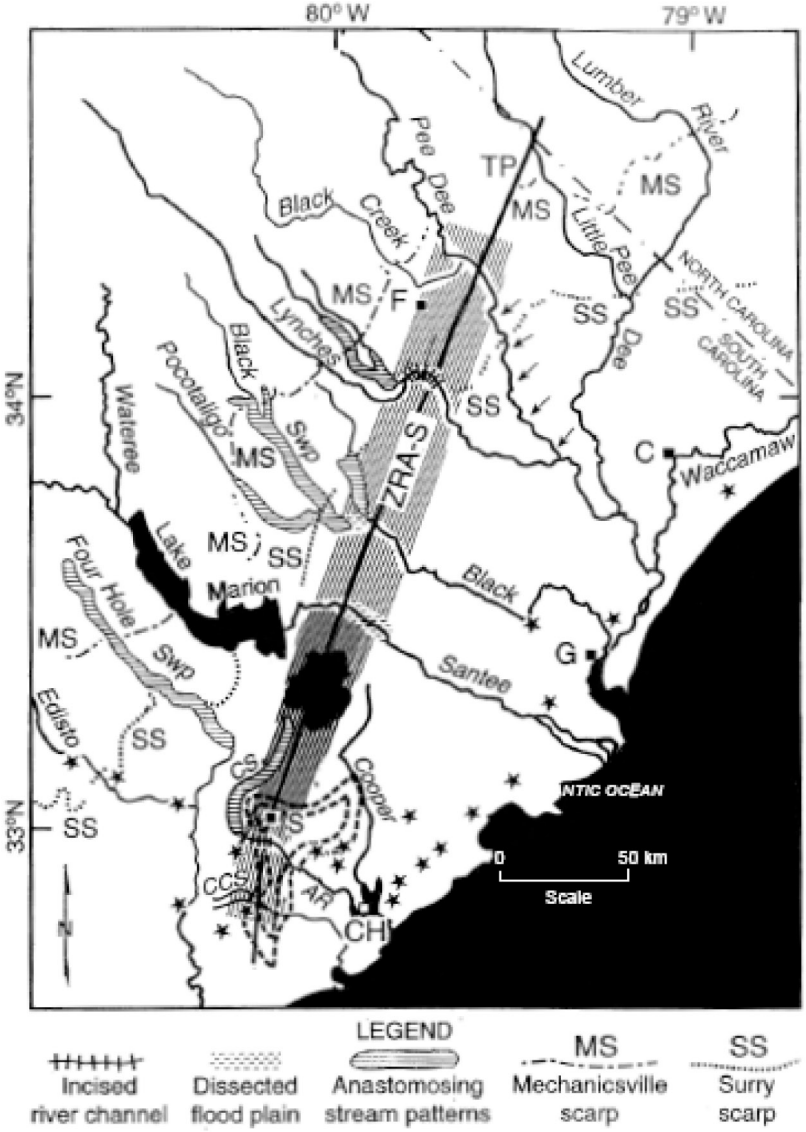

Map of ZRA-S from Marple and Talwani (2000). Figure shows southern zone of river anomalies (ZRA-S; striped area), anastomosing stream patterns, pre 1886 sandblow sites (stars), and topographic profile (TP, bold line) approximately along the ZRA-S axis. Arrows along Pee Dee River denote reach flowing against southwest valley wall. Closed dashed contours near Summerville are highest-intensity isoseismals of the 1886 Charleston, South Carolina, earthquake (from Dutton, 1889). Abbreviations are as follows: AR - Ashley River; C - Conway; CCS - Caw Caw Swamp; CH - Charleston; CS - Cypress Swamp; F - Florence; G - Georgetown; LM - Lake Moultrie; MS - Mechanicsville littoral scarp; S - Summerville; SS - Surry littoral scarp.

Figure 2.5.2-12 Map of ZRA-S from Marple and Talwani (2000)

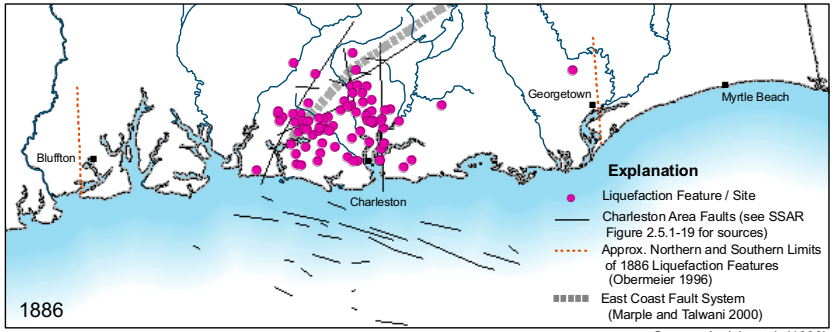

Source: Amick et al. (1990)

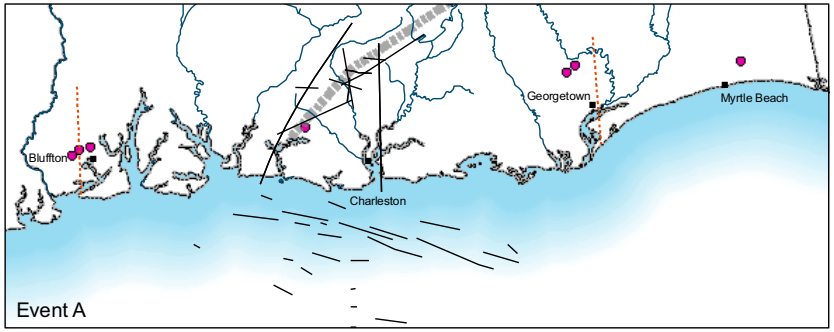

Source: Talwani and Schaeffer (2001)

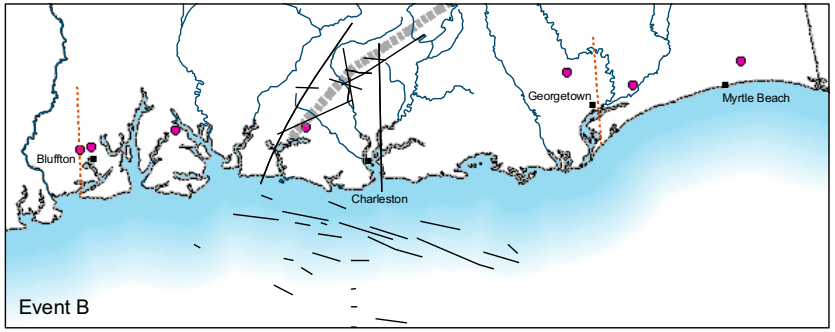

Source: Talwani and Schaeffer (2001)

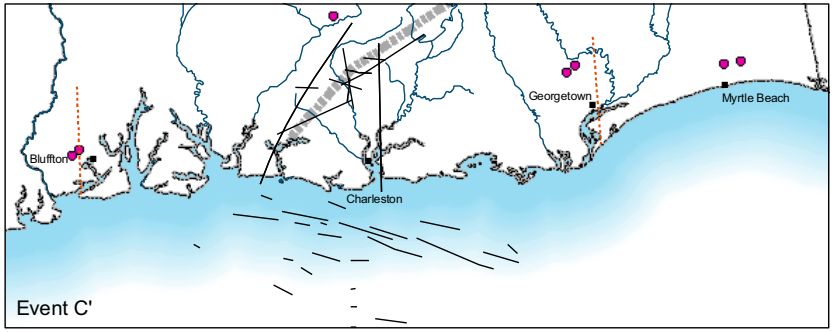

Source: modified after Talwani and Schaeffer (2001)

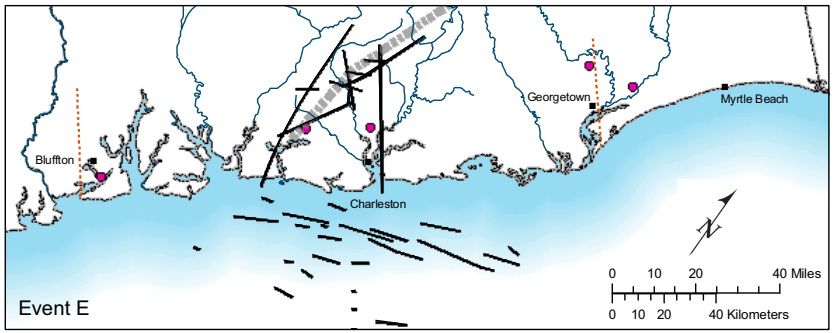

Source: Talwani and Schaeffer (2001)

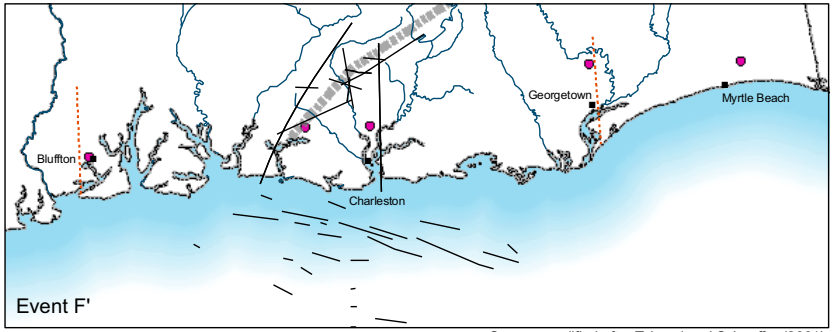

Source: modified after Talwani and Schaeffer (2001)

Figure 2.5.2-12a Geographic Distribution of Liquefaction Features Associated with Charleston Earthquakes

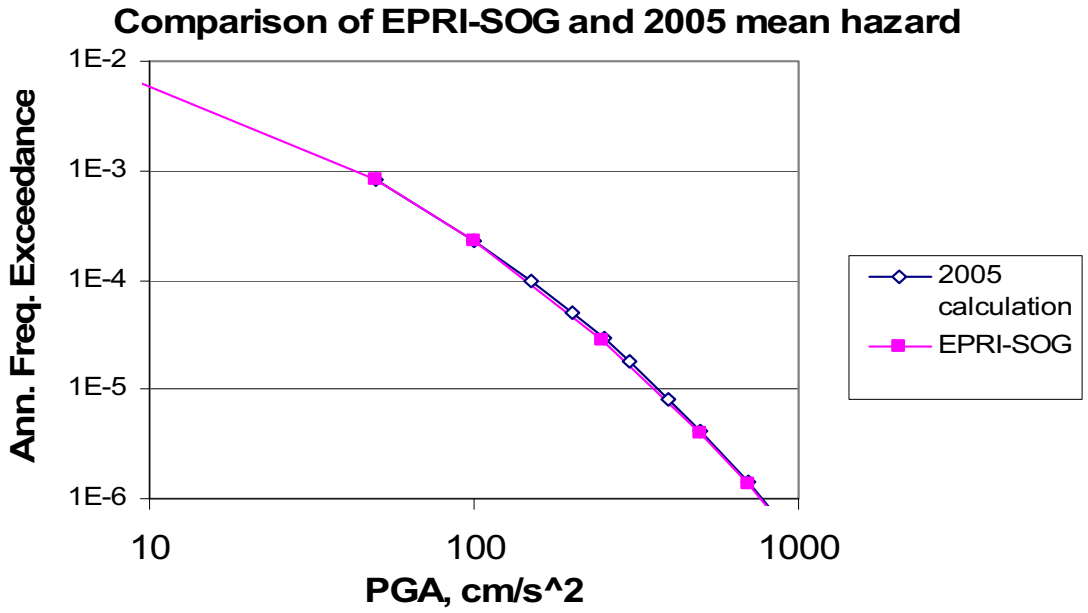

Figure 2.5.2-13 PGA Mean Seismic Hazard Curves for Current (2005) Calculation and for EPRI-SOG

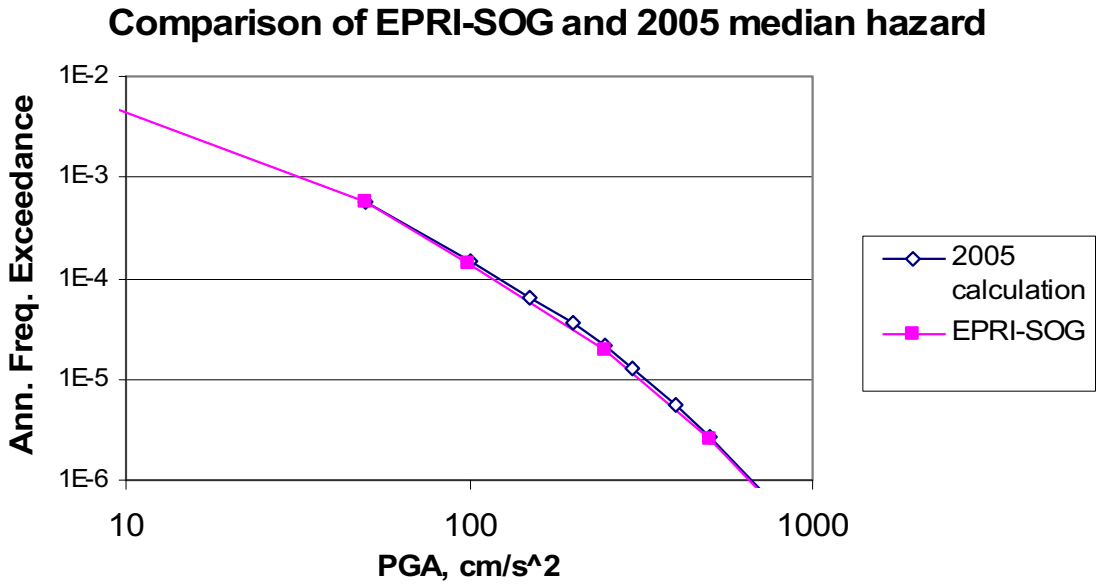

Figure 2.5.2-14 PGA Median Seismic Hazard Curves for Current (2005) Calculation and for EPRI-SOG

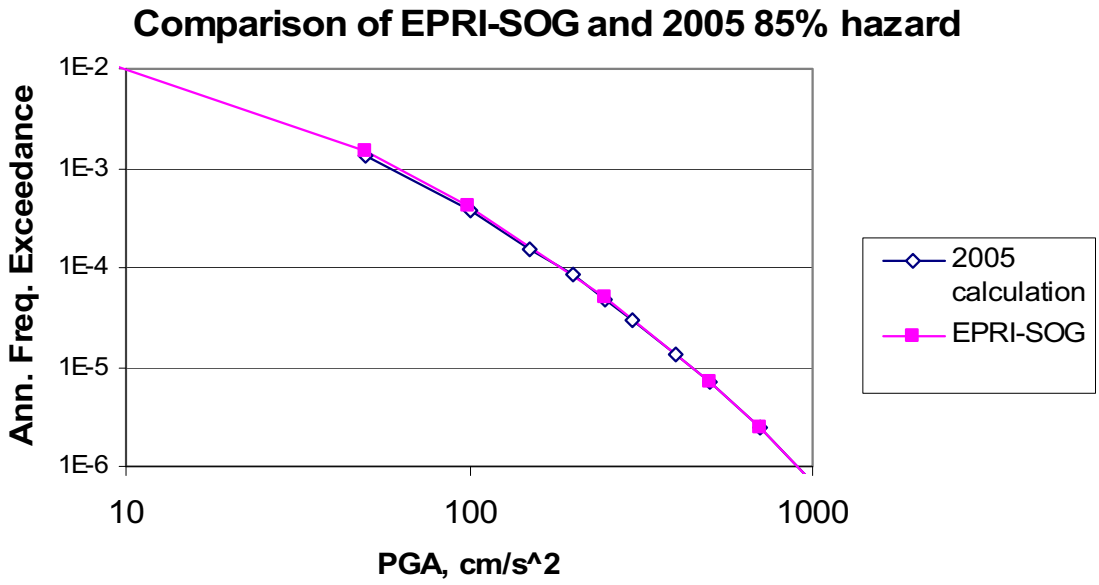

Figure 2.5.2-15 PGA 85 Percent Seismic Hazard Curves for Current (2005) Calculation and for EPRI-SOG

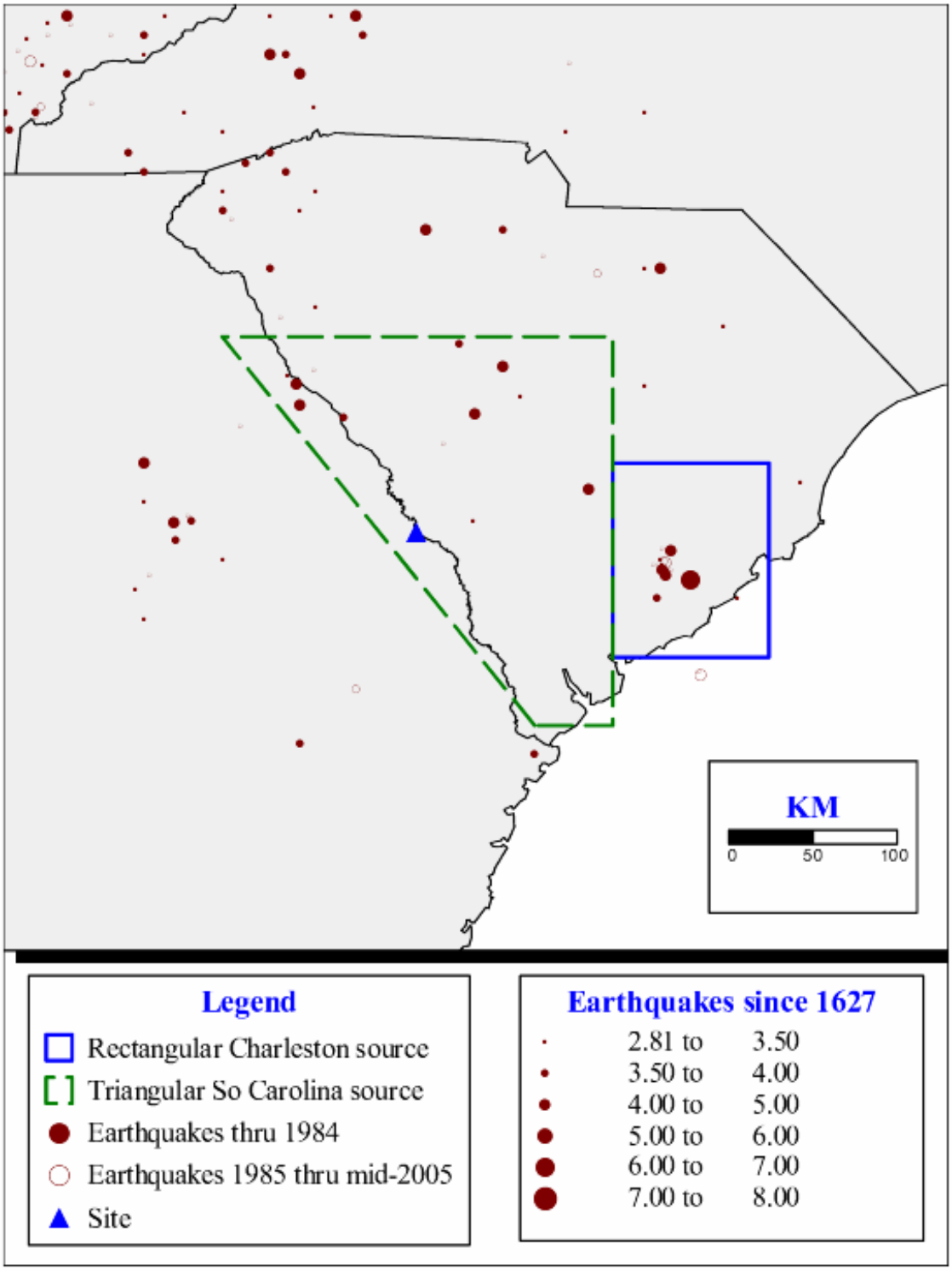

Figure 2.5.2-16 Map Showing Two Areas Used To Examine Effect of New Seismicity Information

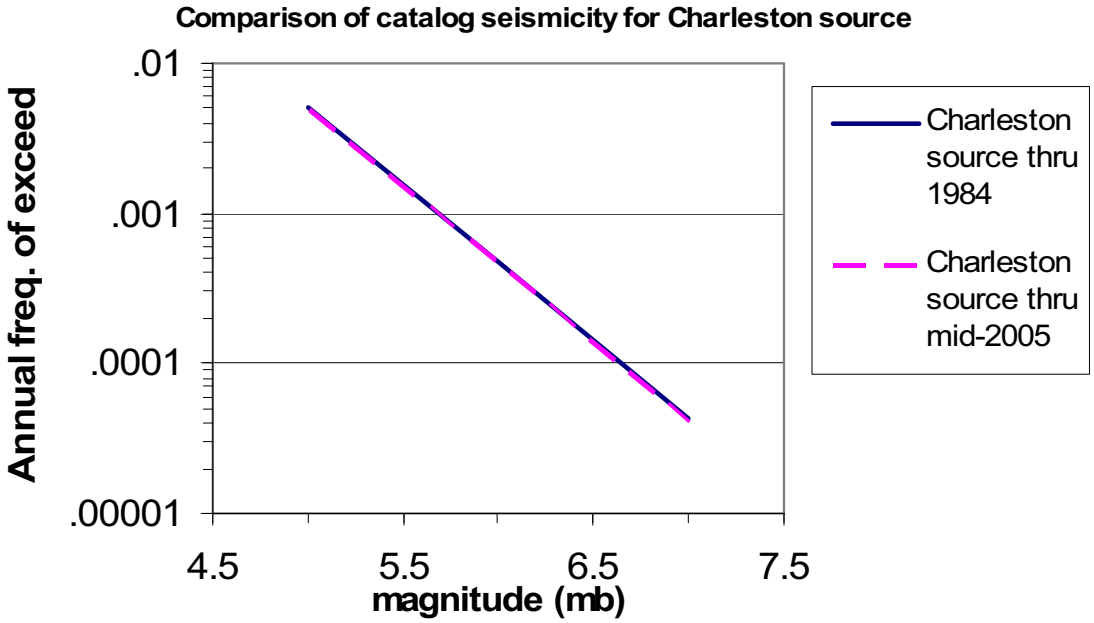

Figure 2.5.2-17 Comparison of Recurrence Rates for Rectangular Charleston Source

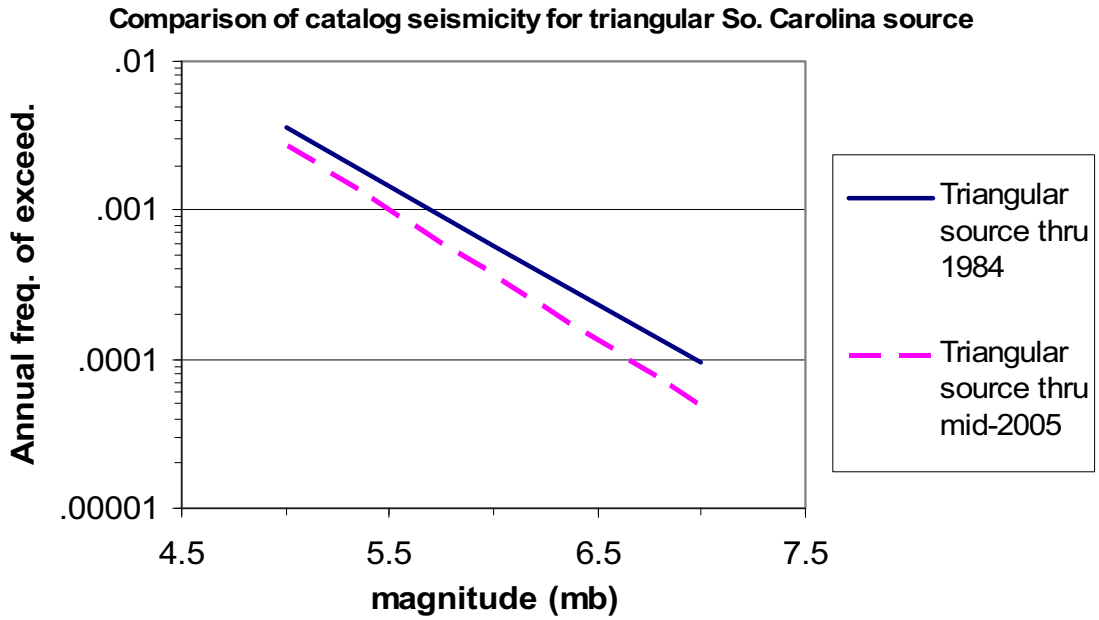

Figure 2.5.2-18 Comparison of Recurrence Rates for Triangular South Carolina Source

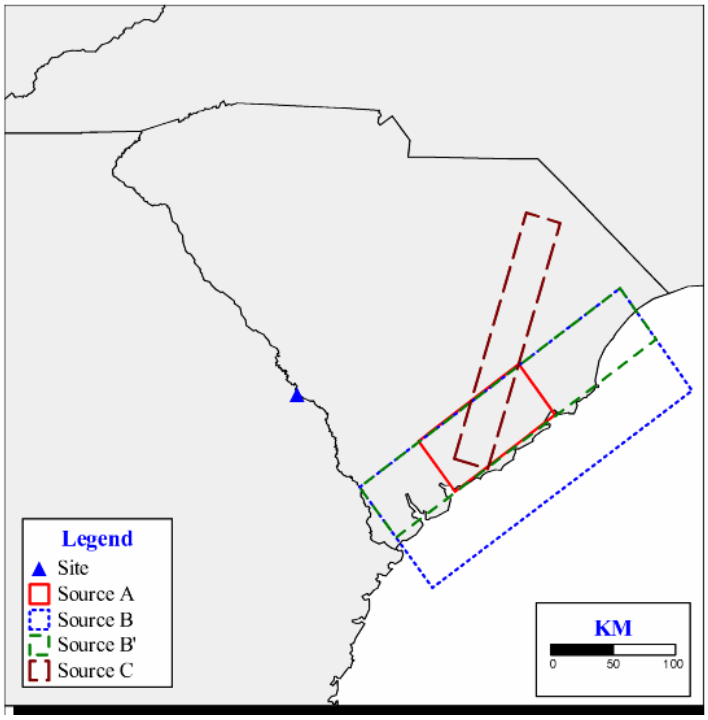

Figure 2.5.2-19 Geometry of Four New Charleston Sources

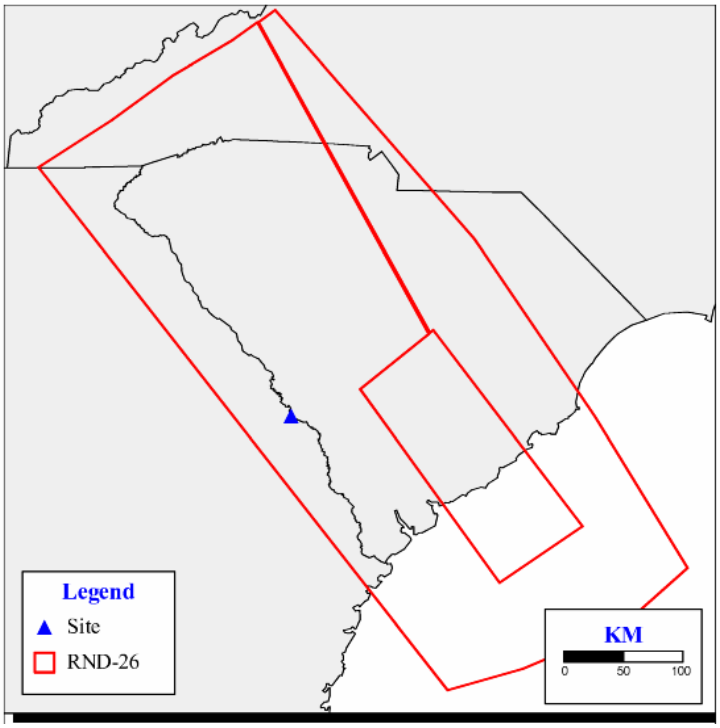

Figure 2.5.2-20a Original Rondout Source 26

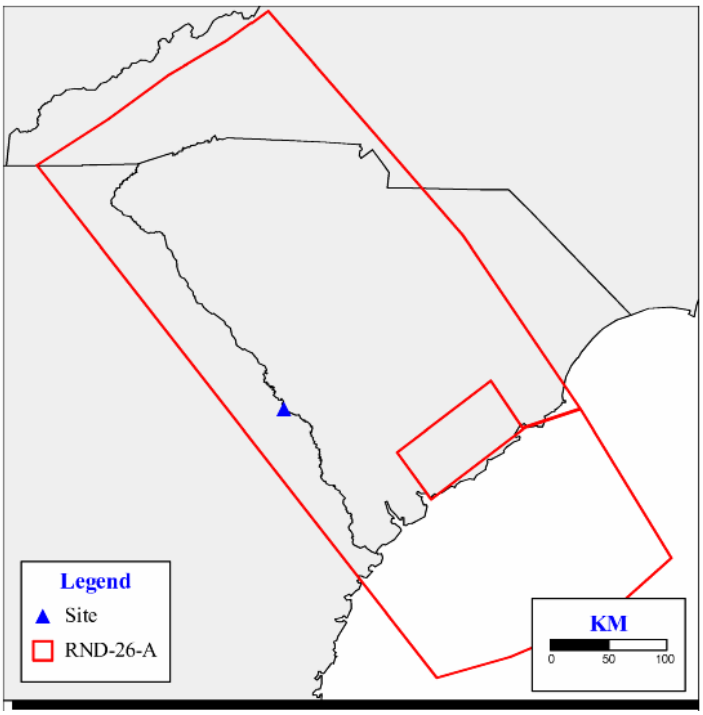

Figure 2.5.2-20b New Rondout Source 26-A that Surrounds Charleston Source A

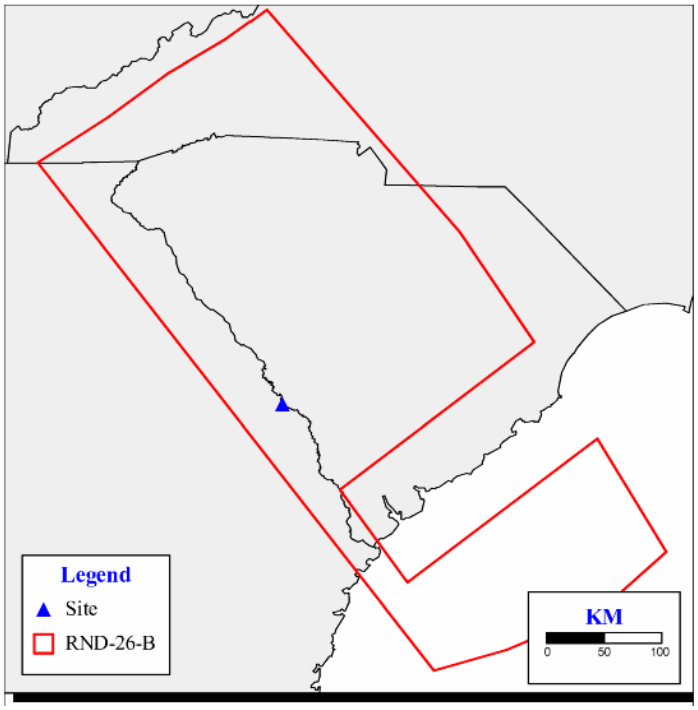

Figure 2.5.2-20c New Rondout Source 26-B that Surrounds Charleston Source B

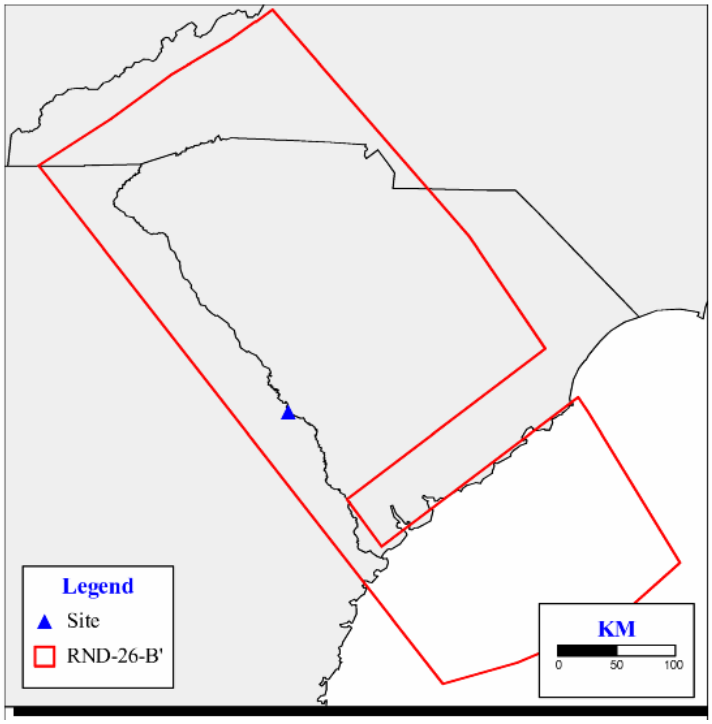

Figure 2.5.2-20d New Rondout Source 26-B´ that Surrounds Charleston Source B

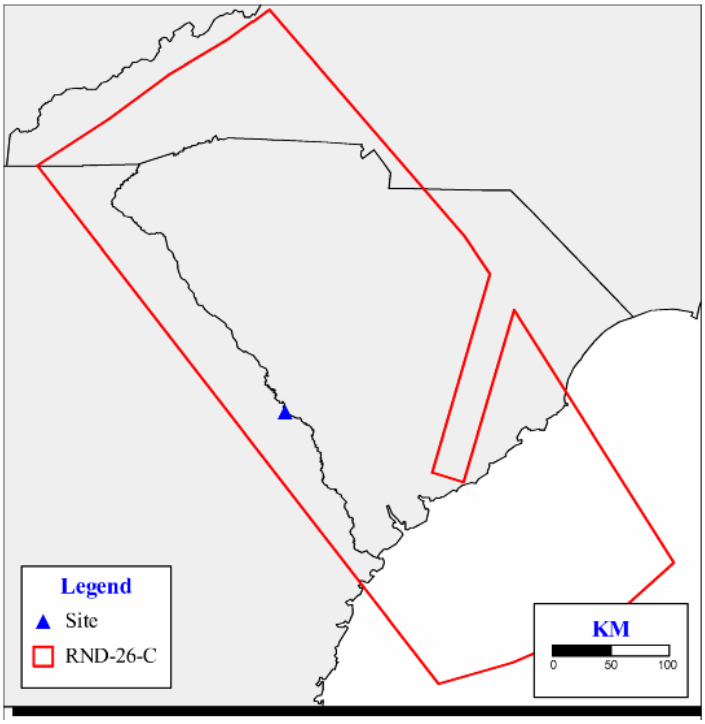

Figure 2.5.2-20e New Rondout Source 26-C that Surrounds Charleston Source C

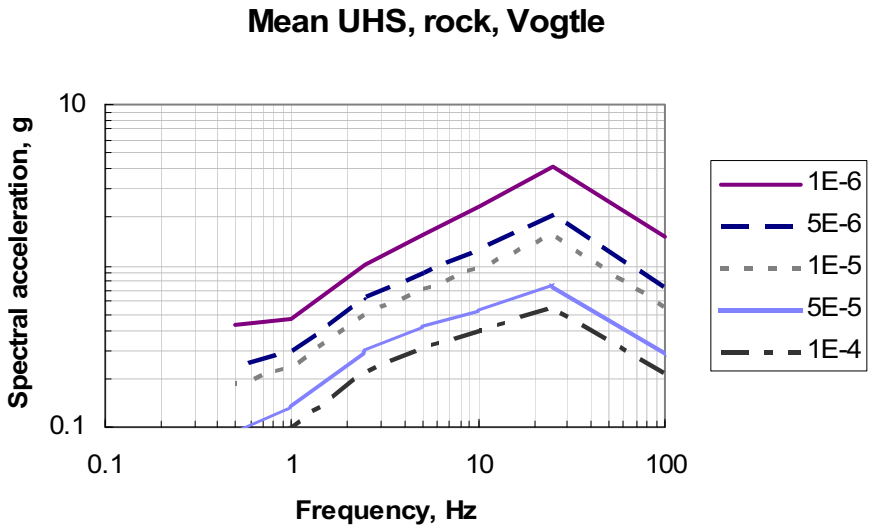

Figure 2.5.2-21 Mean Uniform Hazard Spectra, Hard Rock Conditions, for VEGP ESP

High Frequency, 1.0e-4

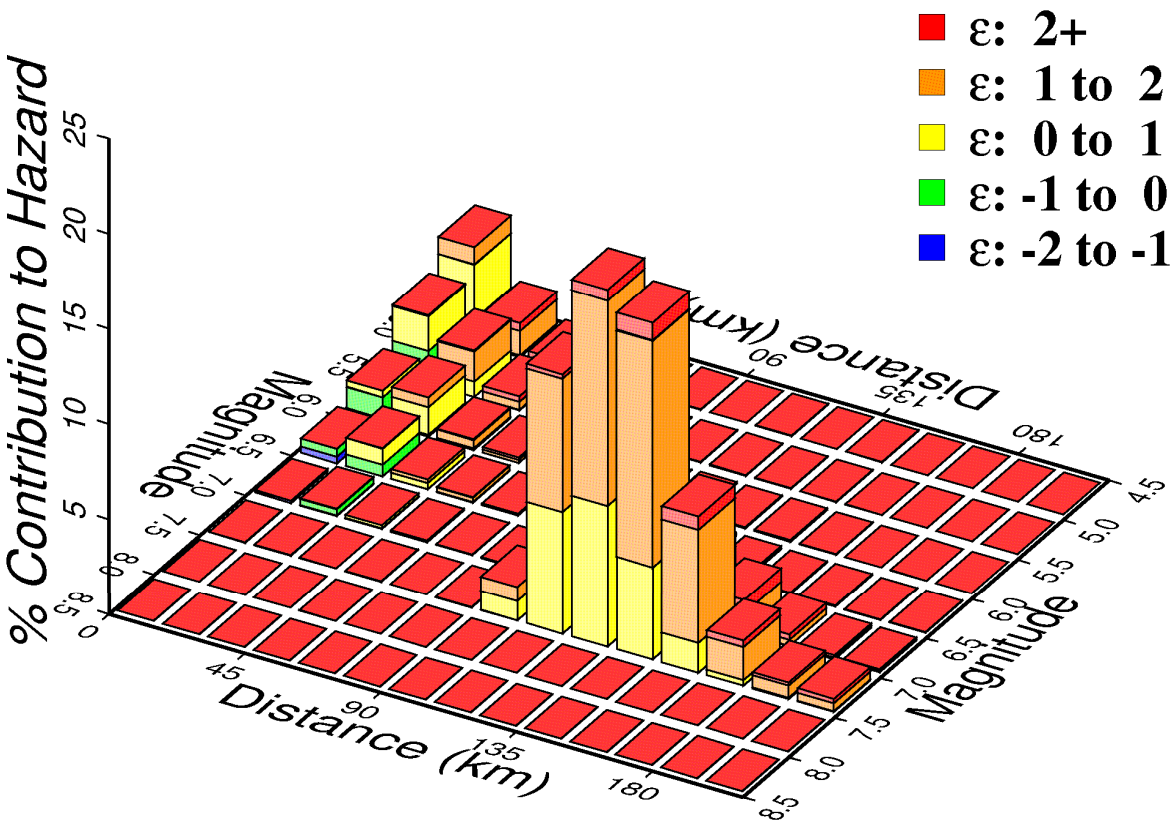

Figure 2.5.2-22 Hard Rock Magnitude-Distance Deaggregation for High Frequencies, 10^{-4} Mean Annual Frequency of Exceedance

Low Frequency, 1.0e-4

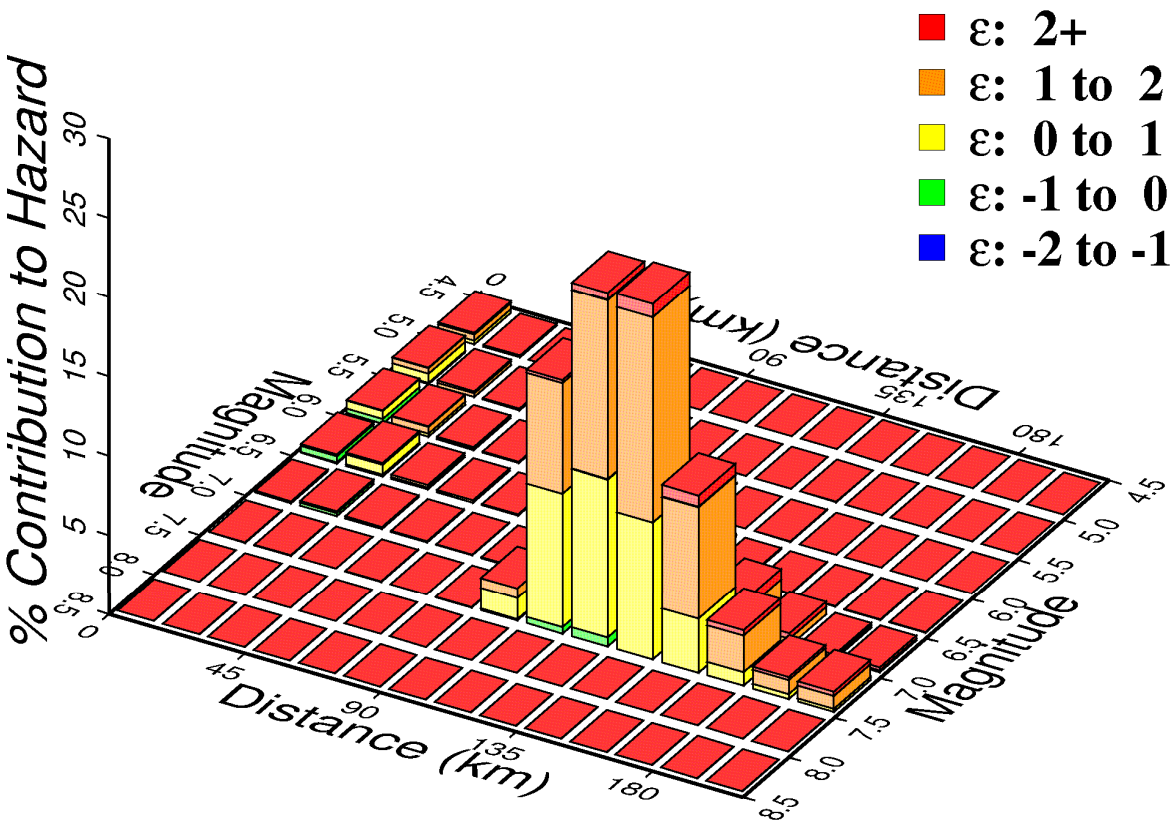

Figure 2.5.2-23 Hard Rock Magnitude-Distance Deaggregation for Low Frequencies, 10^{-4} Mean Annual Frequency of Exceedance

High Frequency, 1.0e-5

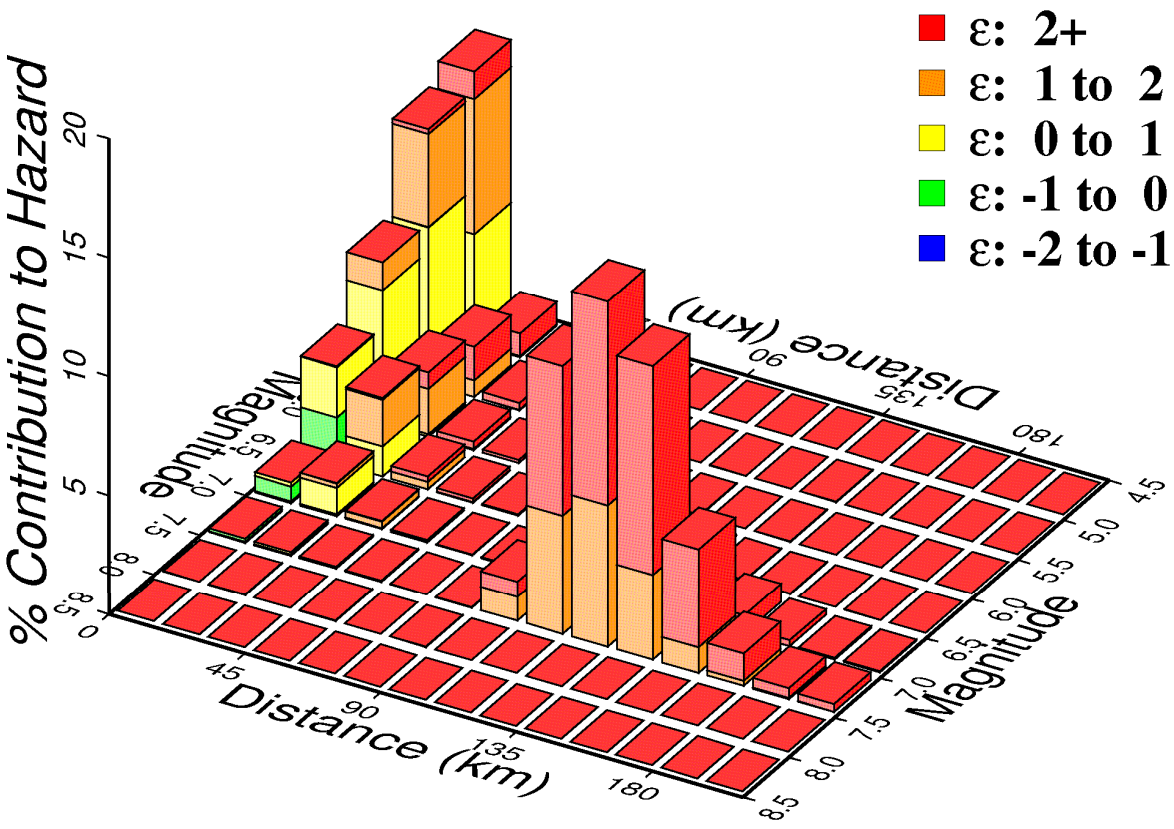

Figure 2.5.2-24 Hard Rock Magnitude-Distance Deaggregation for High Frequencies, 10^{-5} Mean Annual Frequency of Exceedance

Low Frequency, 1.0e-5

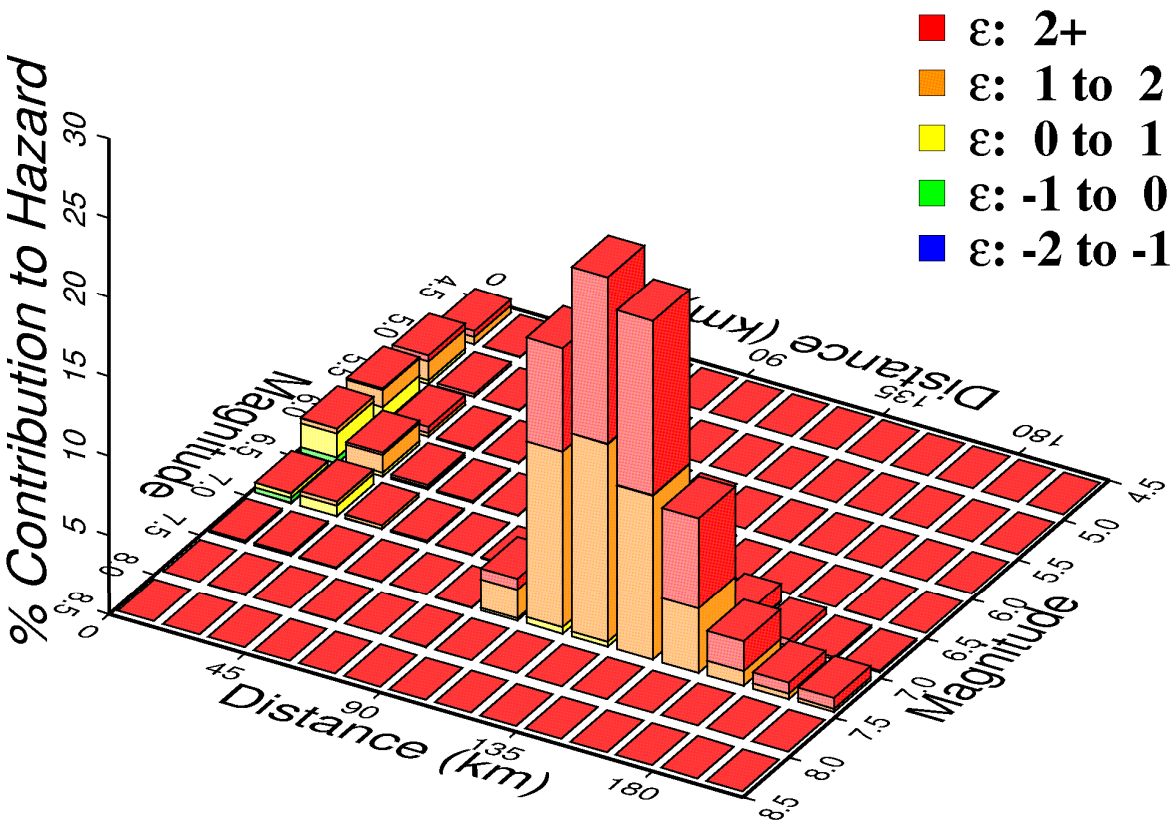

Figure 2.5.2-25 Hard Rock Magnitude-Distance Deaggregation For Low Frequencies, 10^{-5} Mean Annual Frequency of Exceedance

High Frequency, 1.0e-6

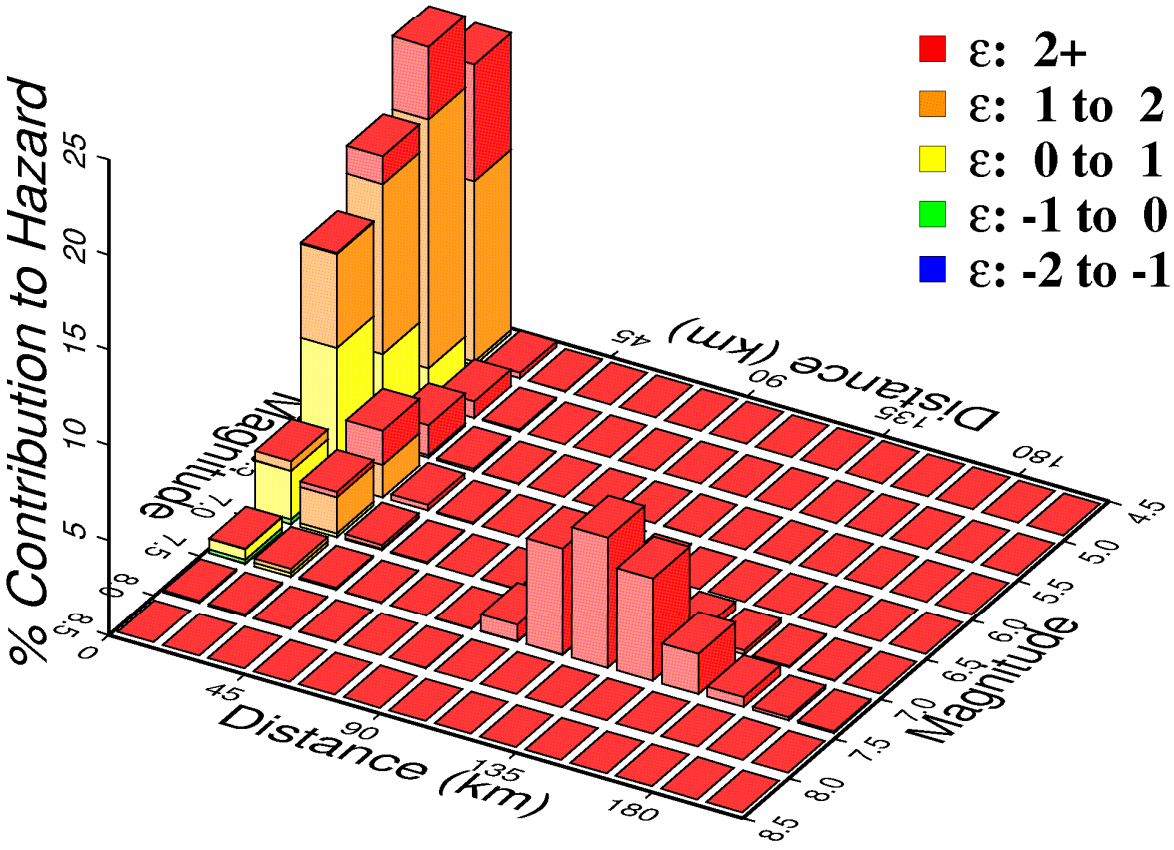

Figure 2.5.2-26 Hard Rock Magnitude-Distance Deaggregation for High Frequencies, 10^{-6} Mean Annual Frequency of Exceedance

Low Frequency, 1.0e-6

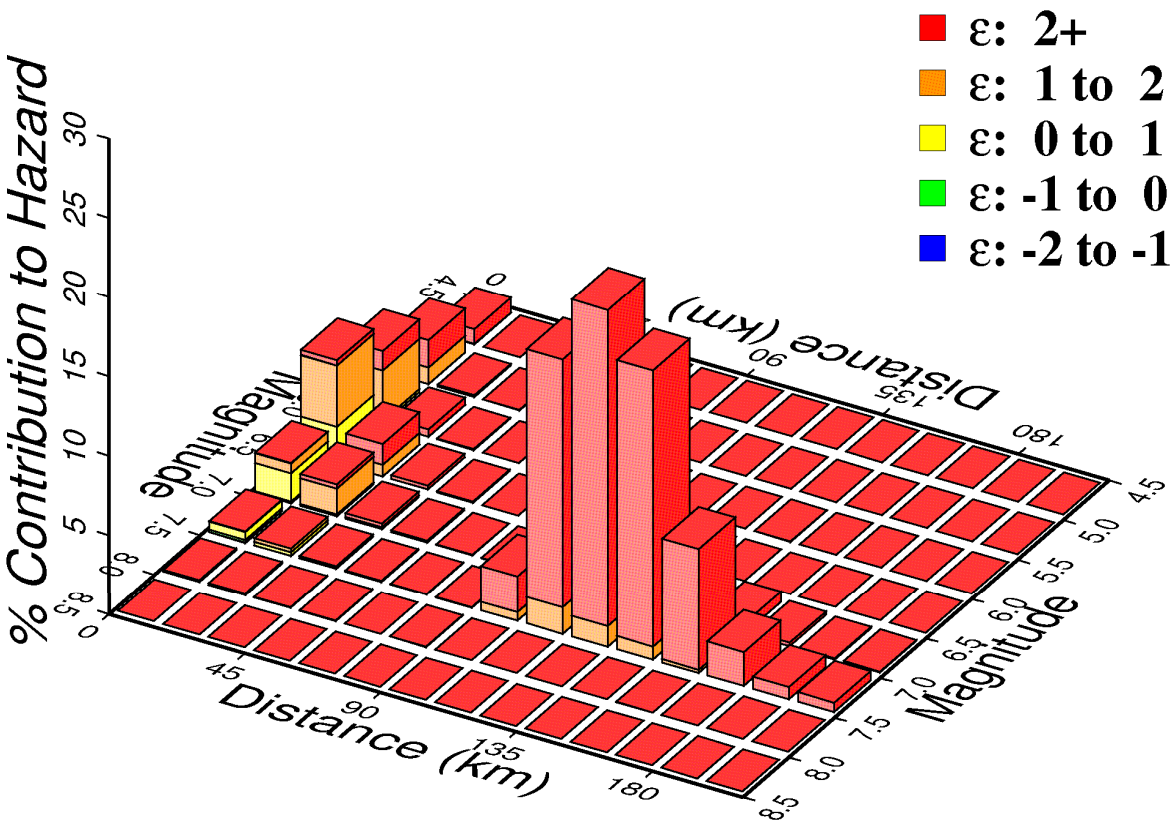

Figure 2.5.2-27 Hard Rock Magnitude-Distance Deaggregation for Low Frequencies, 10^{-6} Mean Annual Frequency of Exceedance

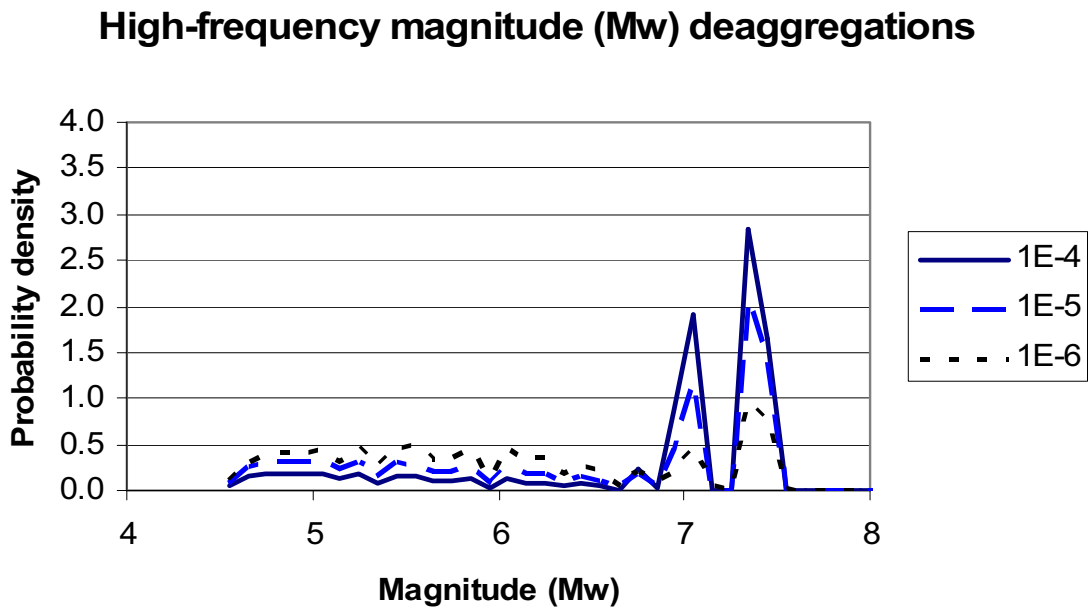

Figure 2.5.2-28 Magnitude Deaggregation for High Frequencies for Three Mean Annual Frequencies of Exceedance

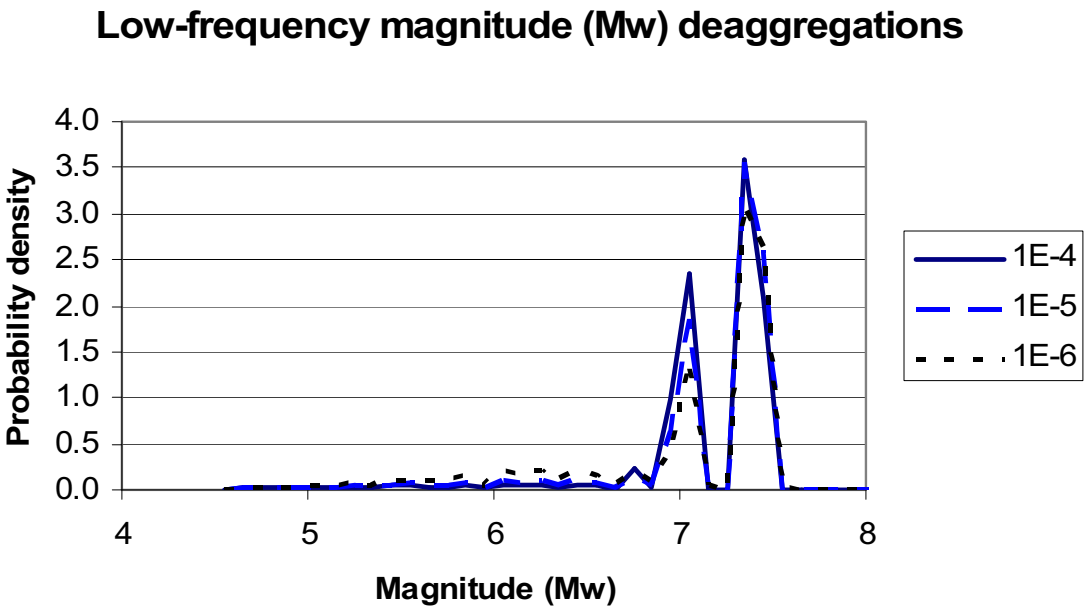

Figure 2.5.2-29 Magnitude Deaggregation for Low Frequencies for Three Mean Annual Frequencies of Exceedance

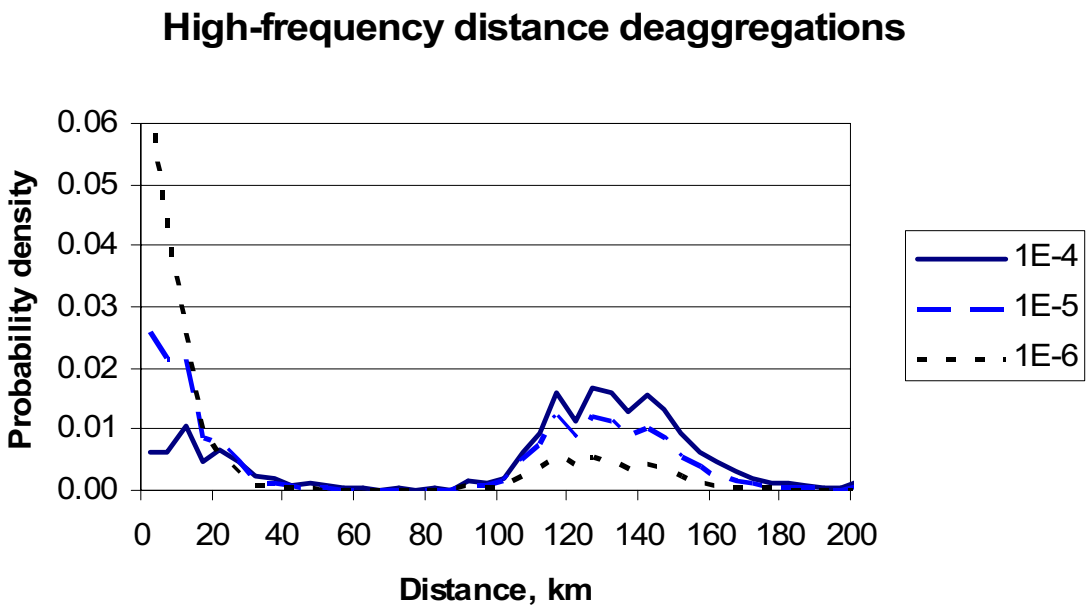

Figure 2.5.2-30 Hard Rock Distance Deaggregation for High Frequencies for Three Mean Annual Frequencies of Exceedance

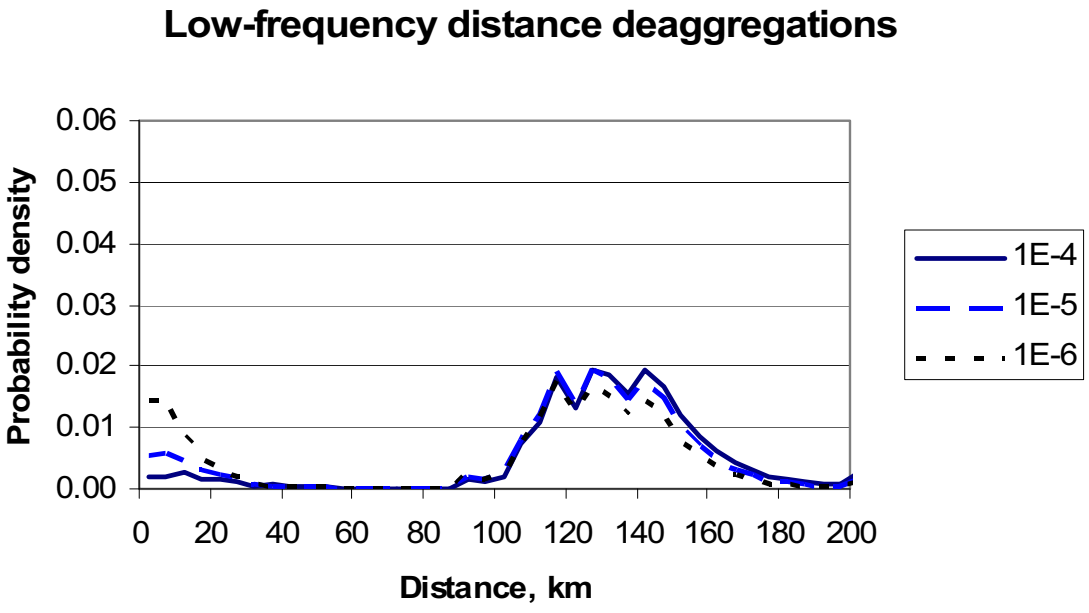

Figure 2.5.2-31 Hard Rock Magnitude Deaggregation for Low Frequencies for Three Mean Annual Frequencies of Exceedance

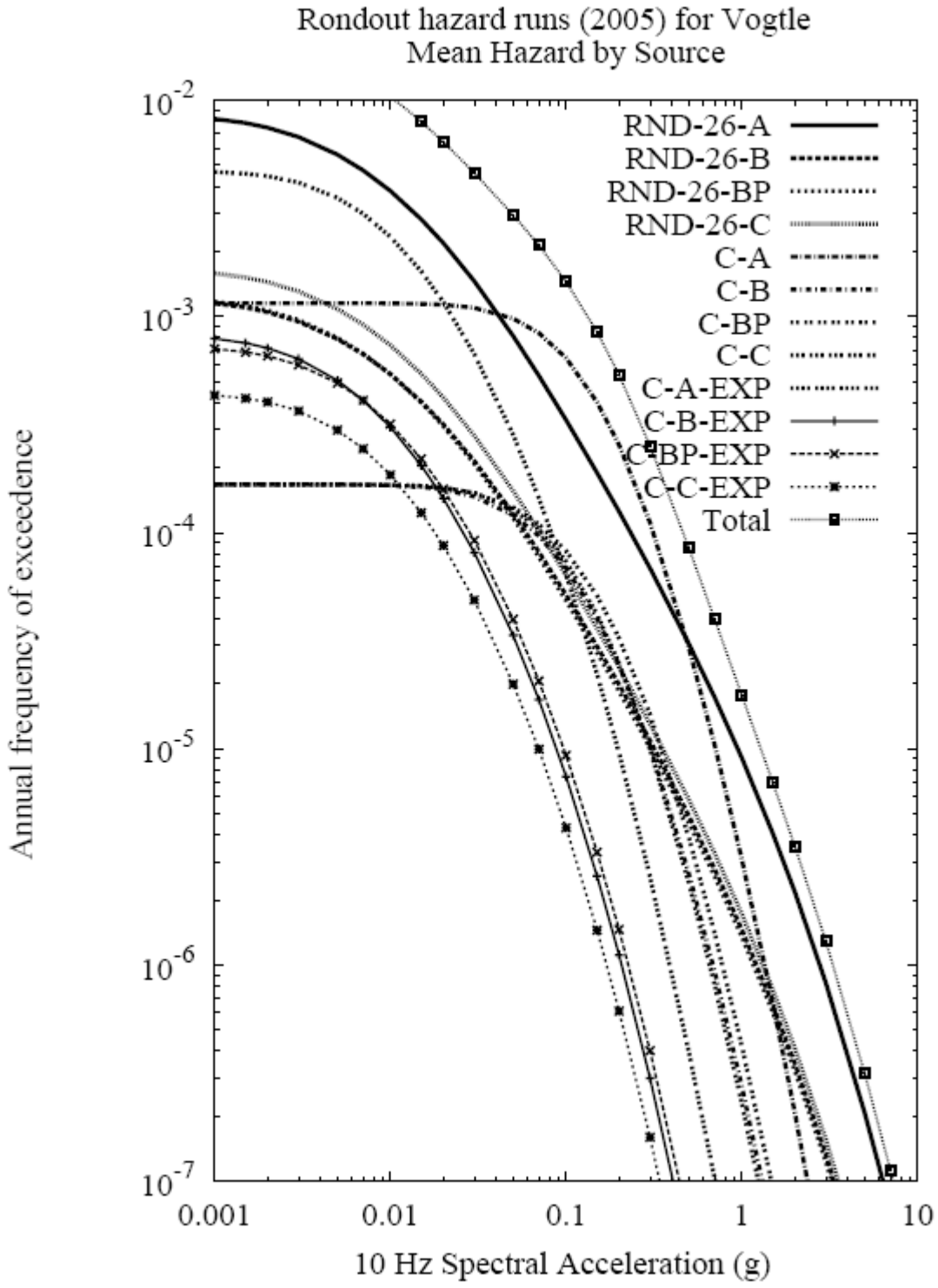

Figure 2.5.2-32 10 Hz Hard Rock Seismic Hazard Curves by Seismic Source for Rondout Team

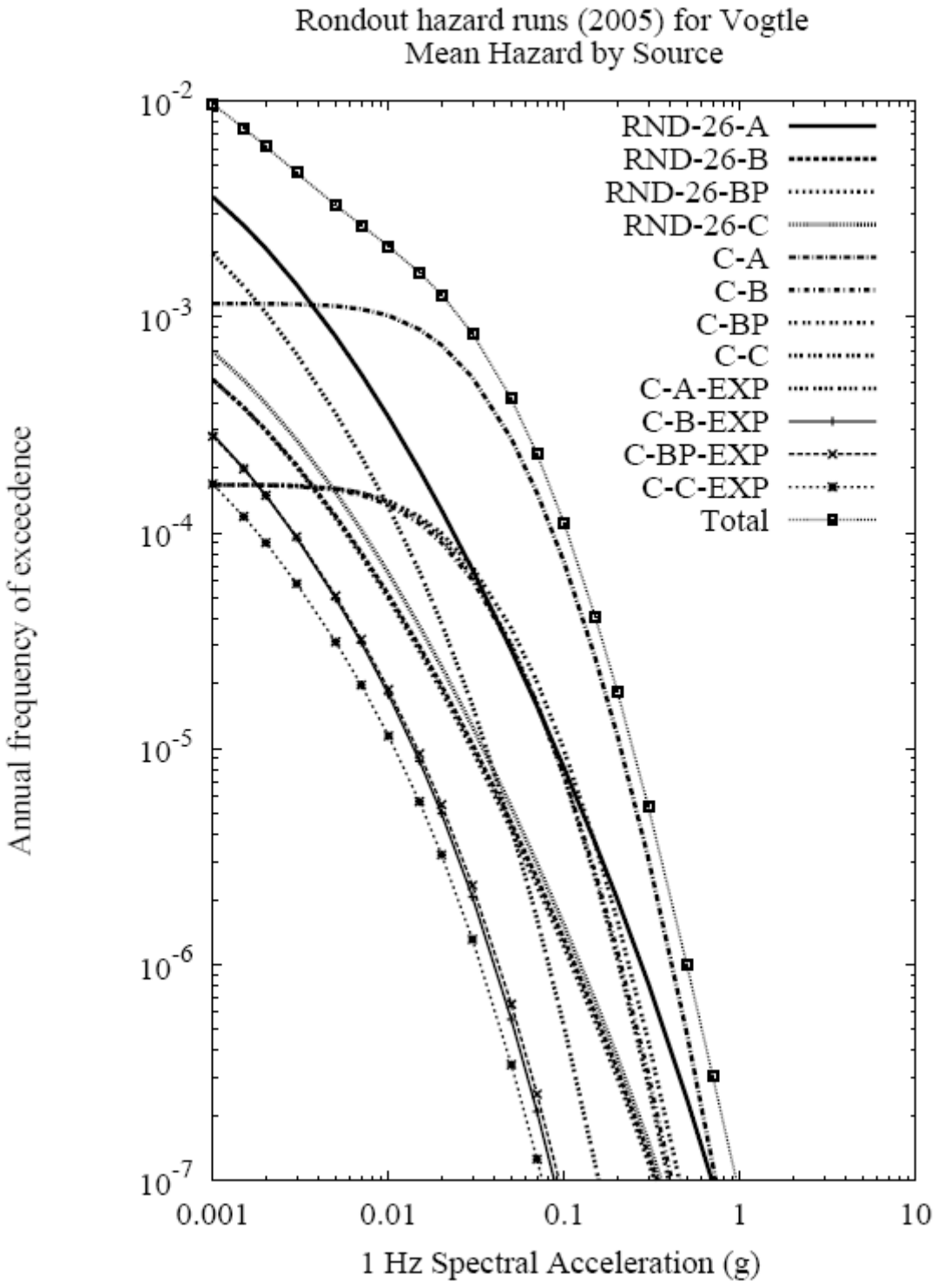

Figure 2.5.2-33 1 Hz Hard Rock Seismic Hazard Curves by Seismic Source for the Rondout Team

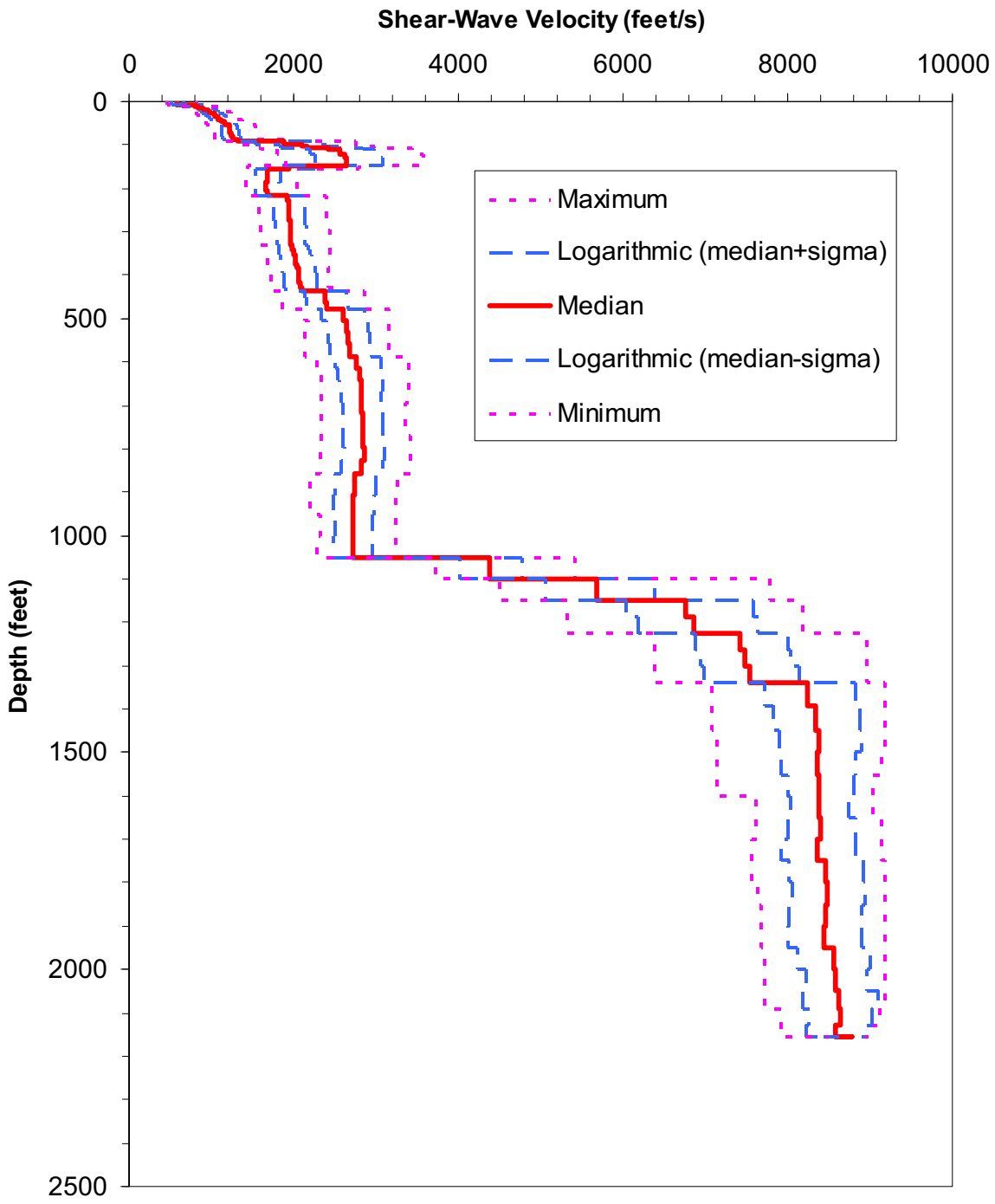

Note: Statistics do not include the velocities on the crystalline bedrock.

Figure 2.5.2-34 Summary Statistics Calculated from the 60 Shear-Wave Velocity Profiles

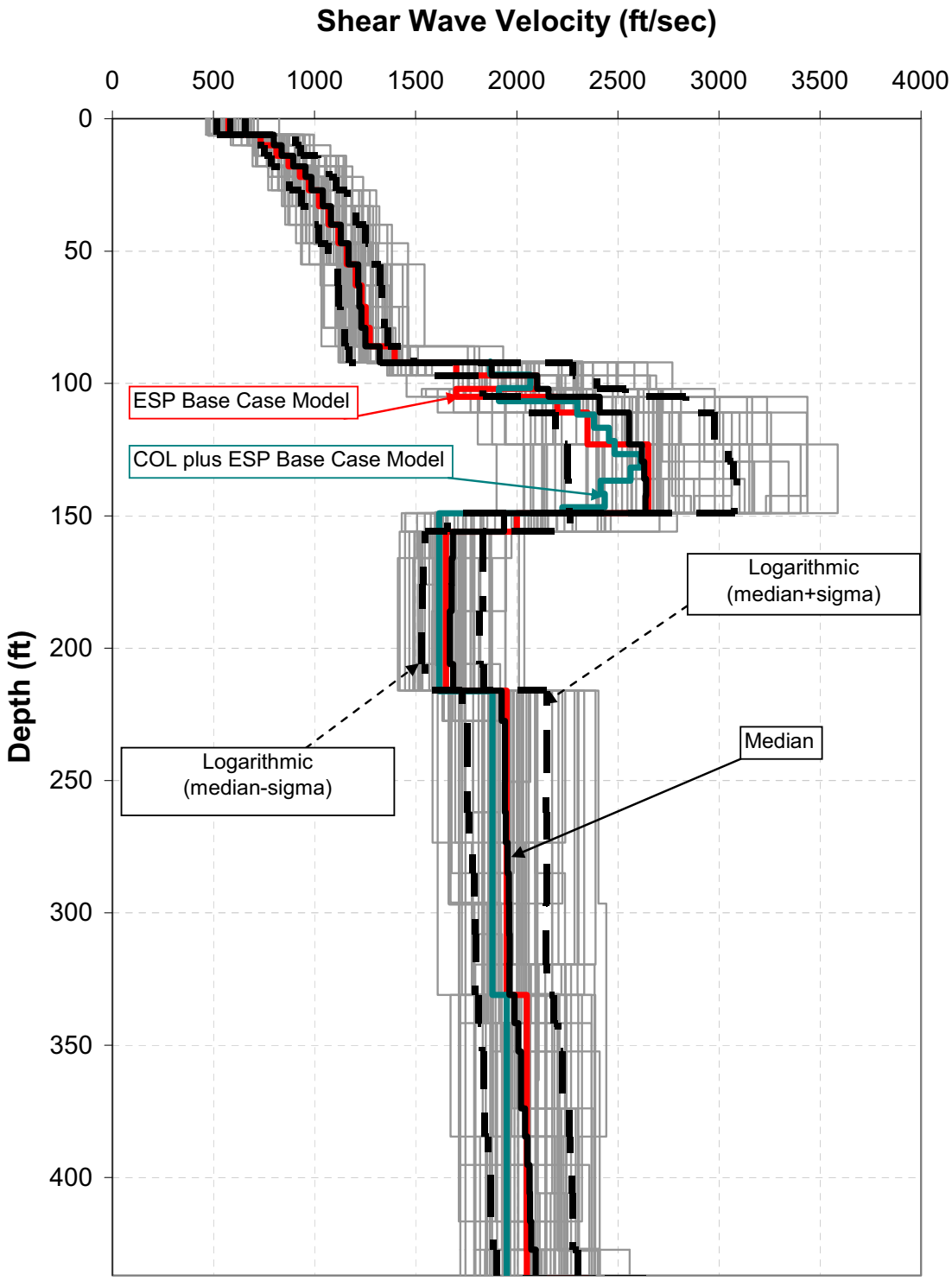

Figure 2.5.2-34a ESP and COL plus ESP Soil Models

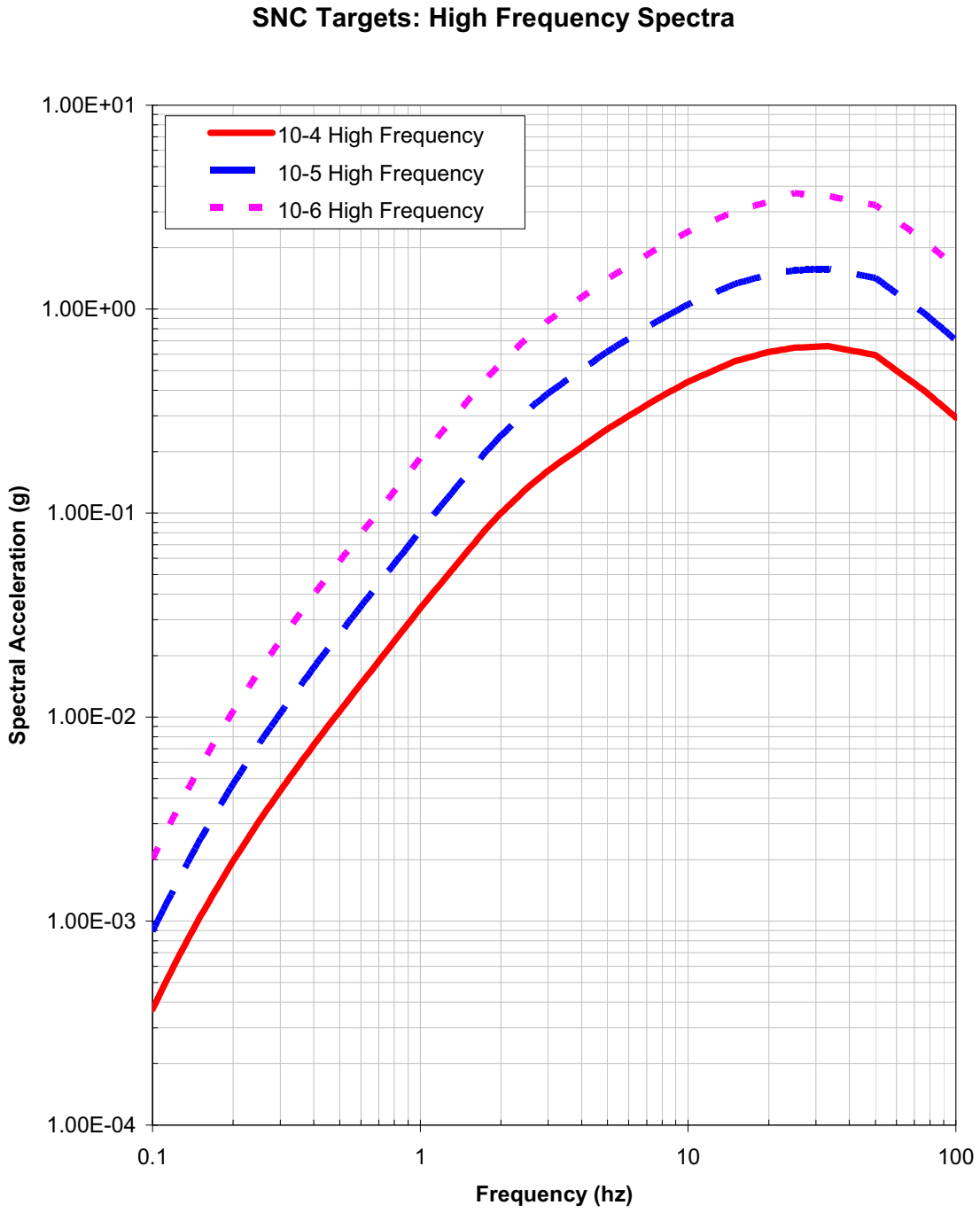

Figure 2.5.2-35a High Frequency Hard Rock Target Spectra for the Three Annual Probability Levels of 10^{-4}, 10^{-5}, and 10^{-6}

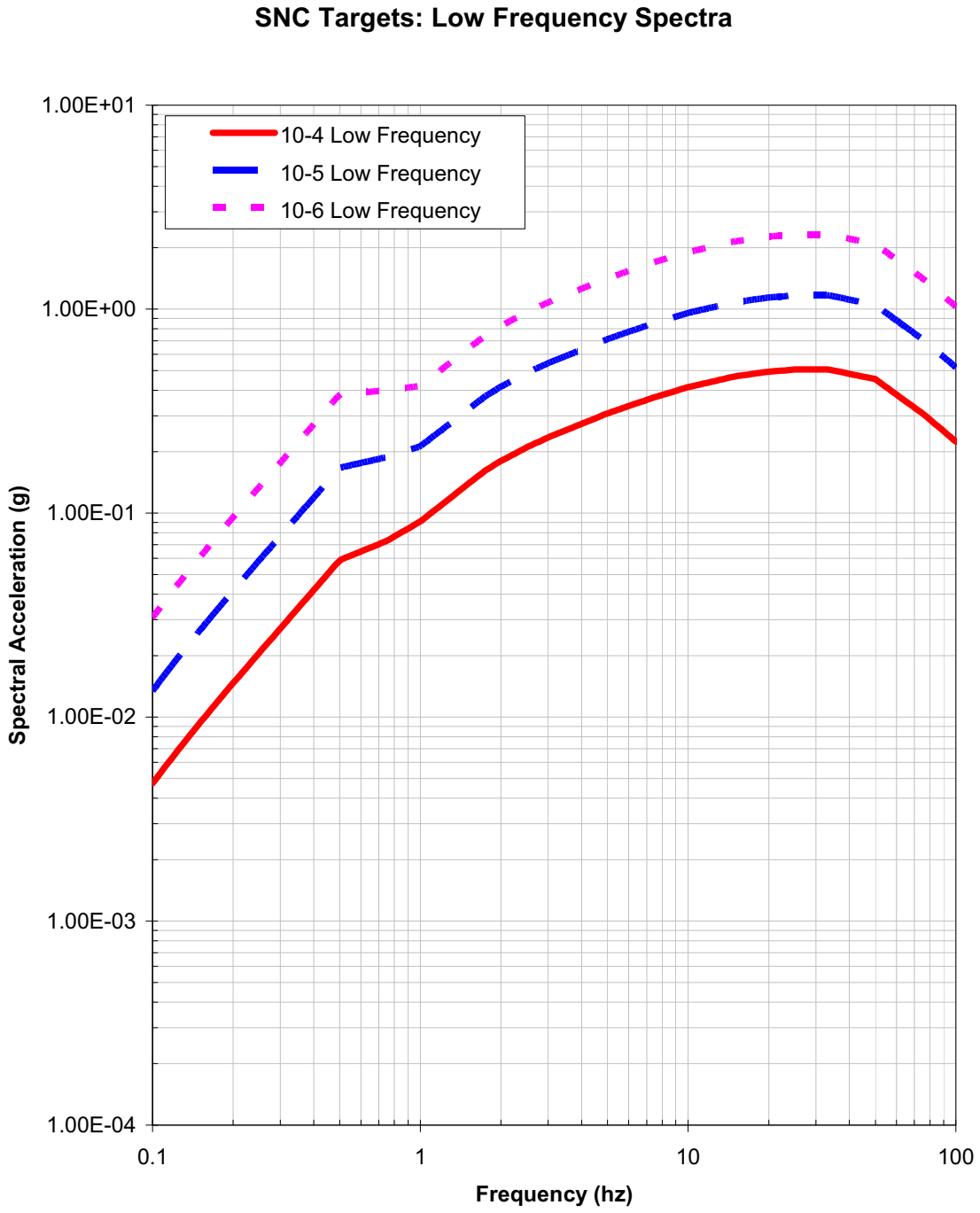

Figure 2.5.2-35b Low Frequency Hard Rock Target Spectra for the Three Annual Probability Levels of 10^{-4}, 10^{-5}, and 10^{-6}

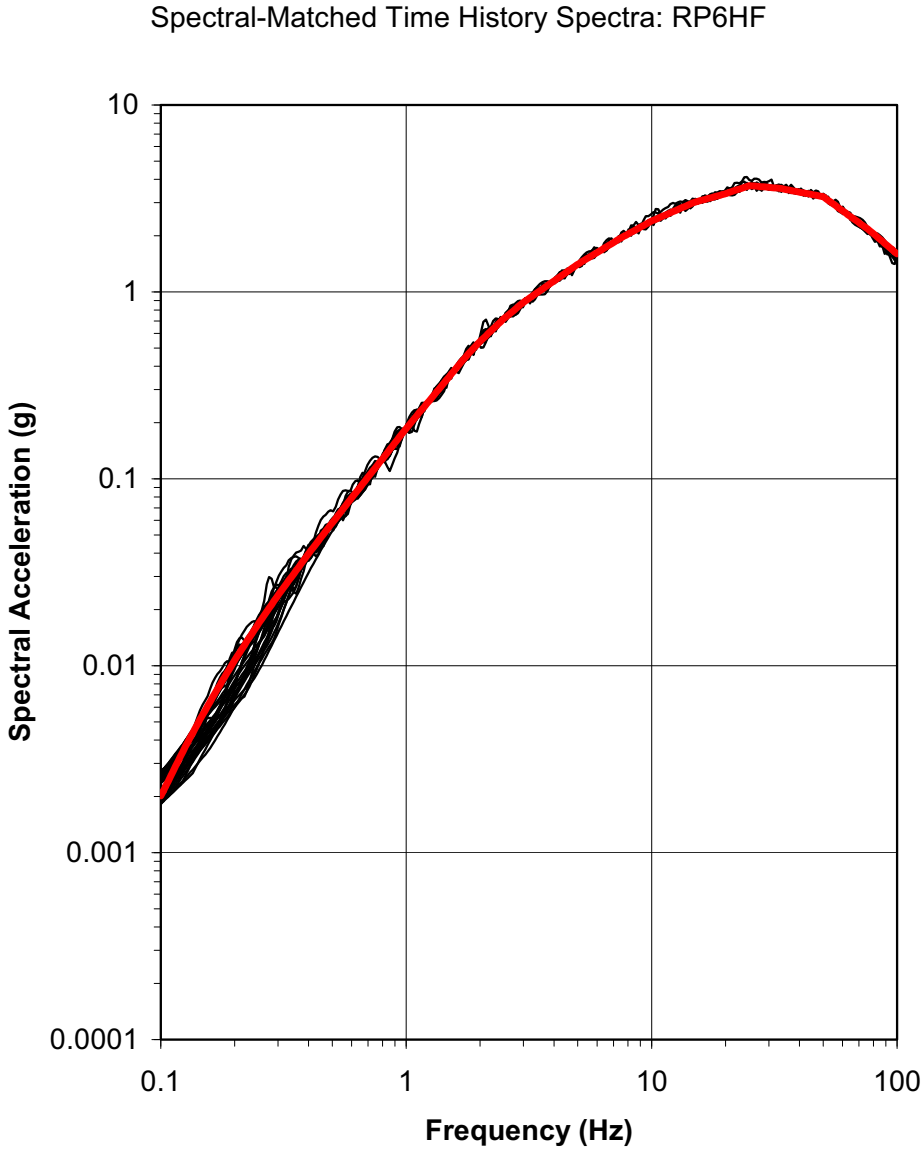

Note: Heavy red line is the target spectrum and thin black lines are the individual matches.

Figure 2.5.2-36a High Frequency (10-6) Match for the 30 Time Histories

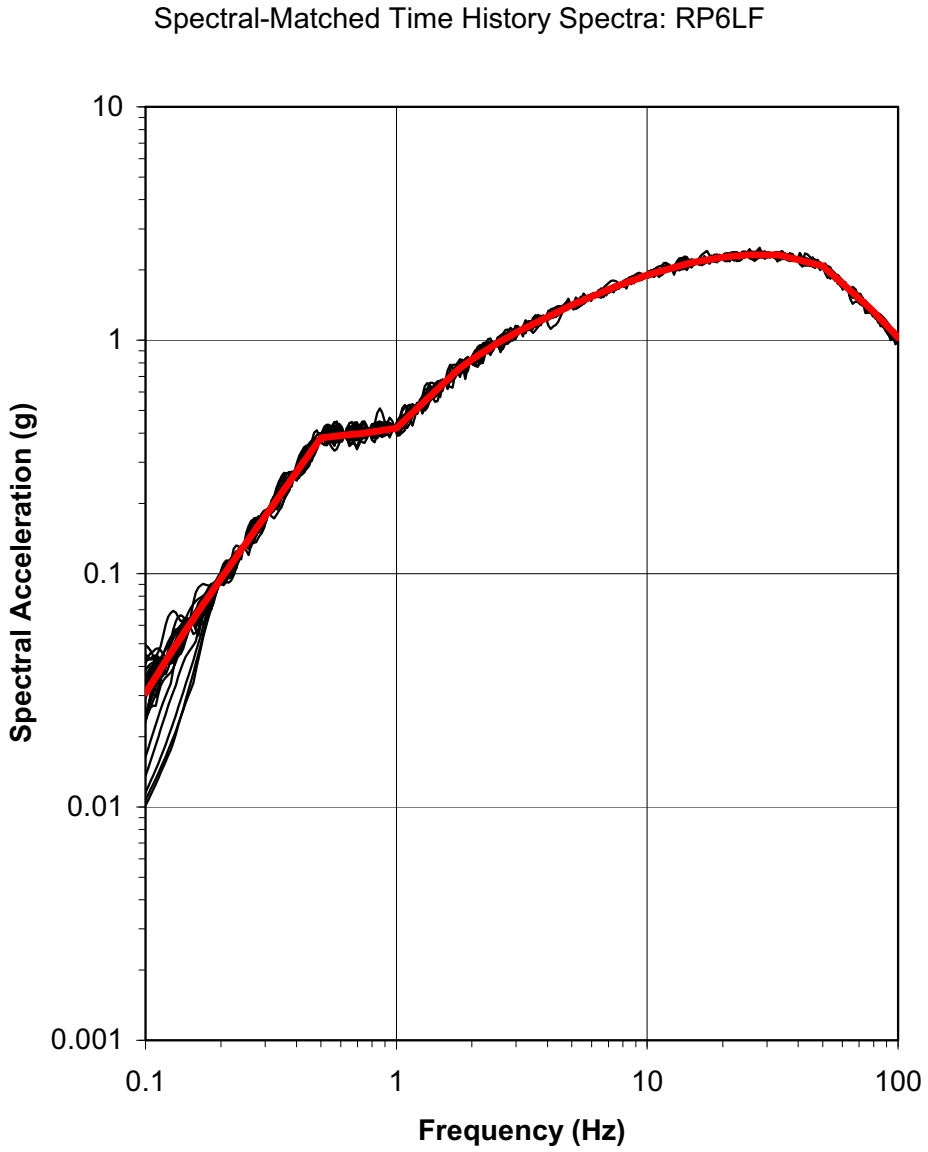

Note: Heavy red line is the target spectrum and thin black lines are the individual matches.

Figure 2.5.2-36b Low Frequency (10-6) Match for the 30 Time Histories

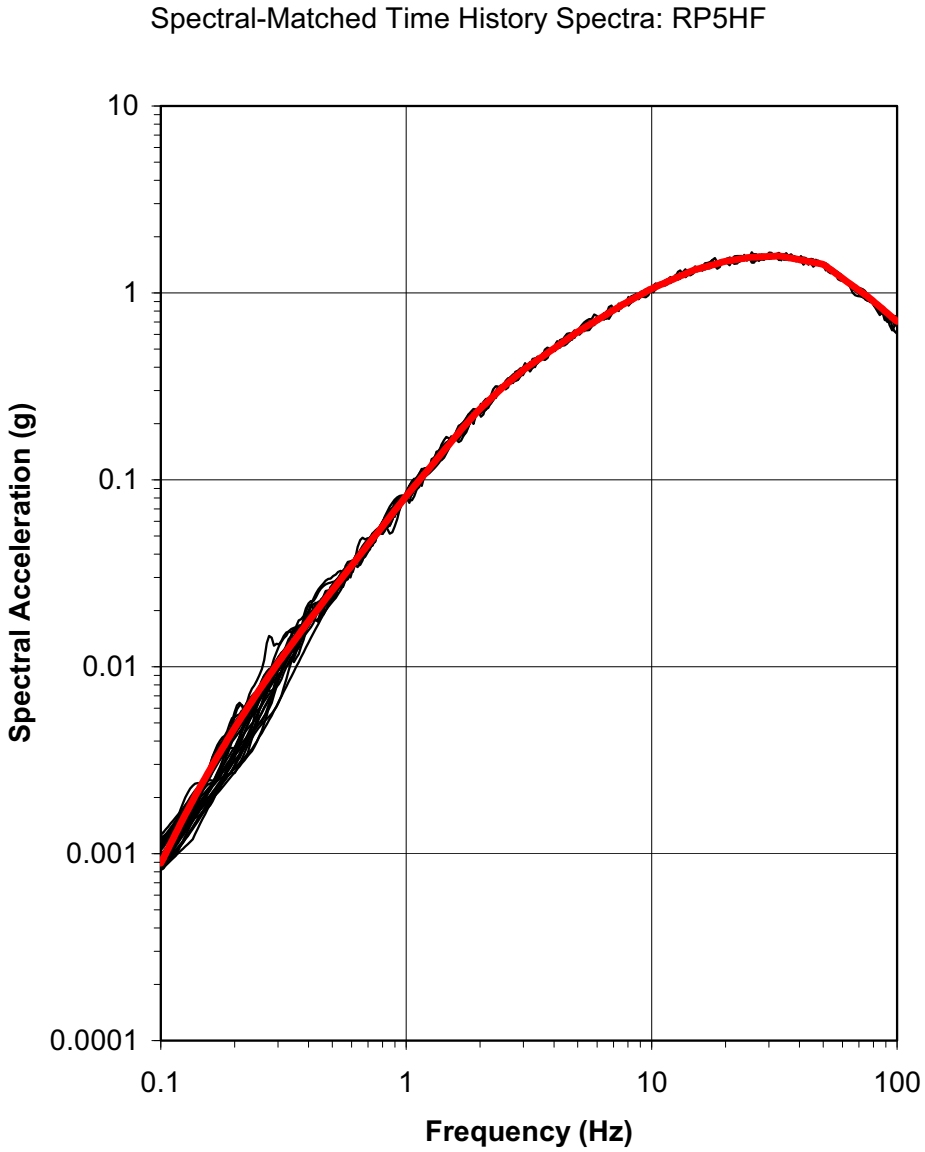

Note: Heavy red line is the target spectrum and thin black lines are the individual matches.

Figure 2.5.2-36c High Frequency (10-5) Match for the 30 Time Histories

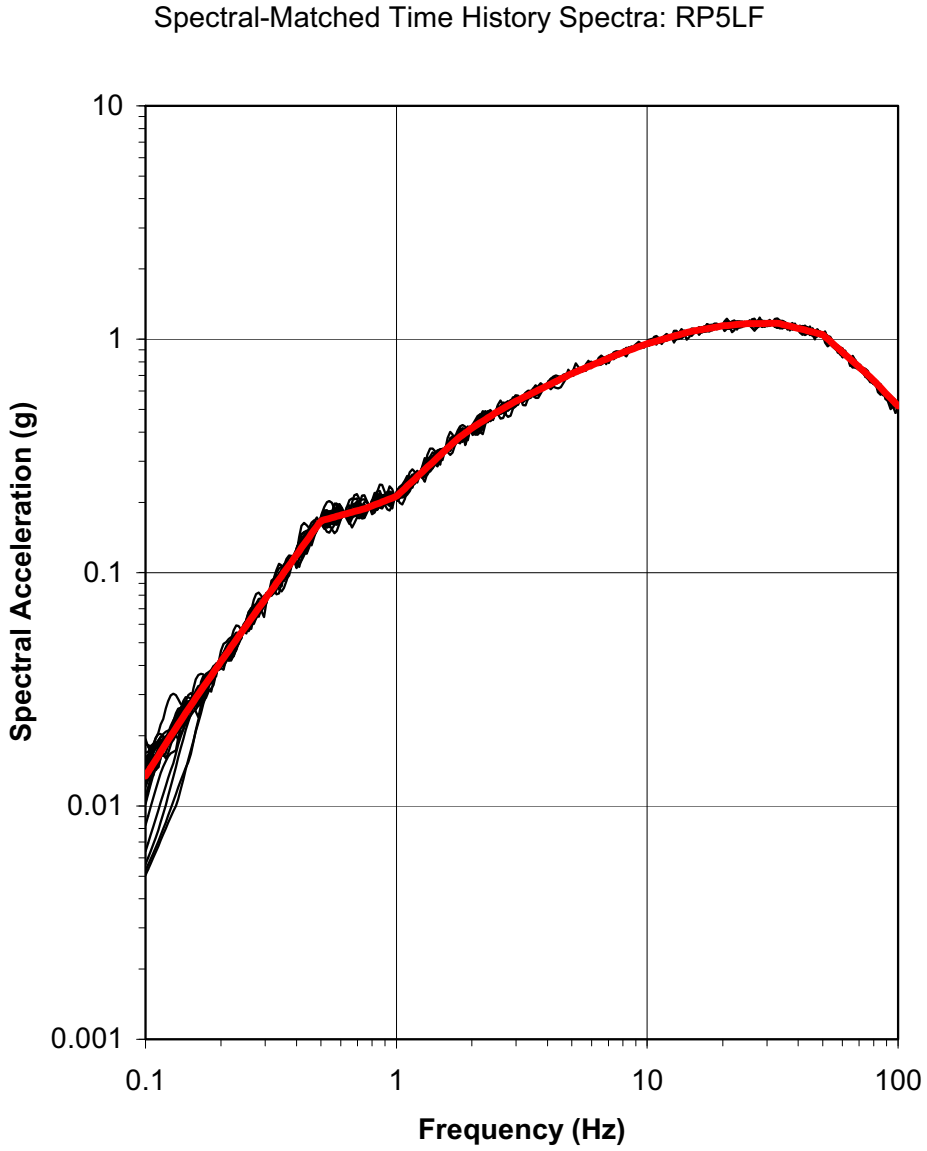

Note: Heavy red line is the target spectrum and thin black lines are the individual matches.

Figure 2.5.2-36d Low Frequency (10-5) Match for the 30 Time Histories

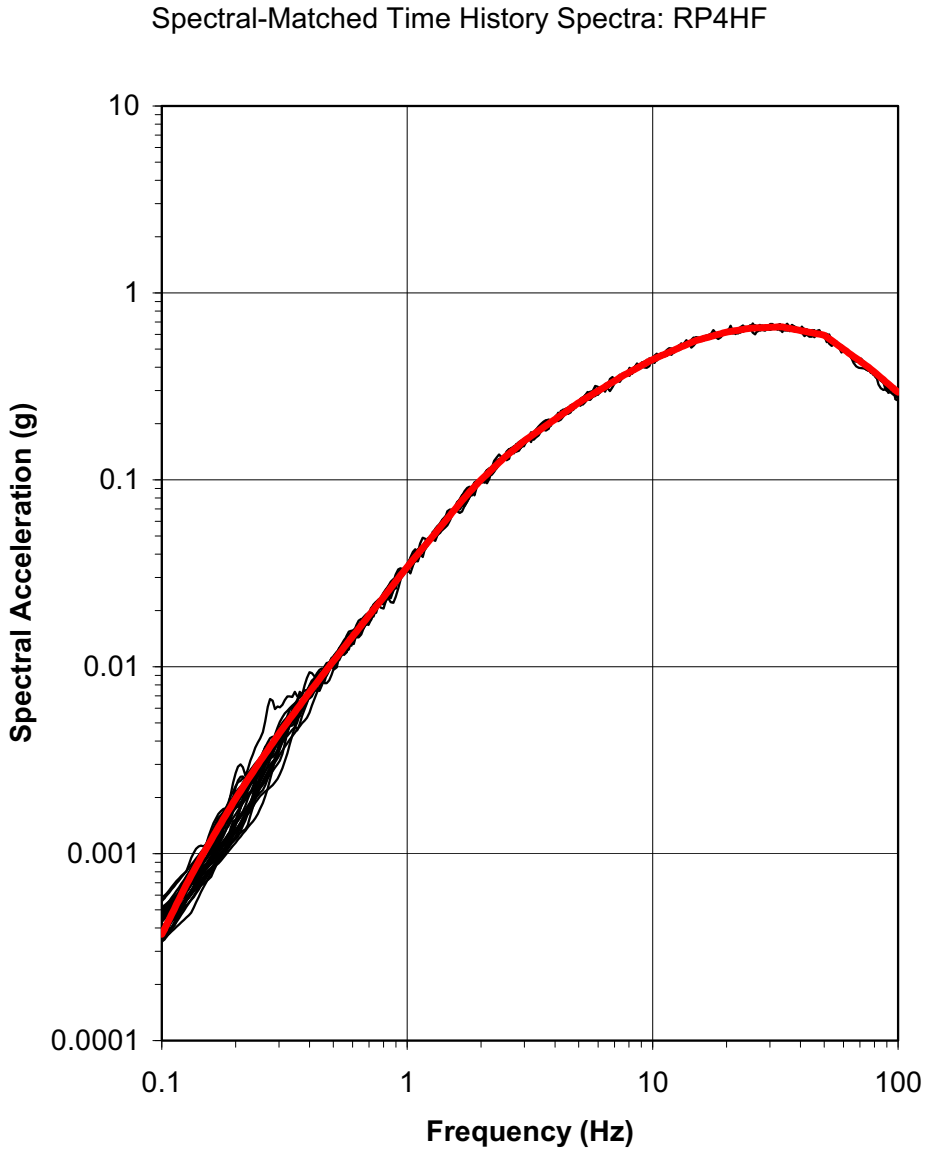

Note: Heavy red line is the target spectrum and thin black lines are the individual matches.

Figure 2.5.2-36e High Frequency (10^{-4}) Match for the 30 Time Histories

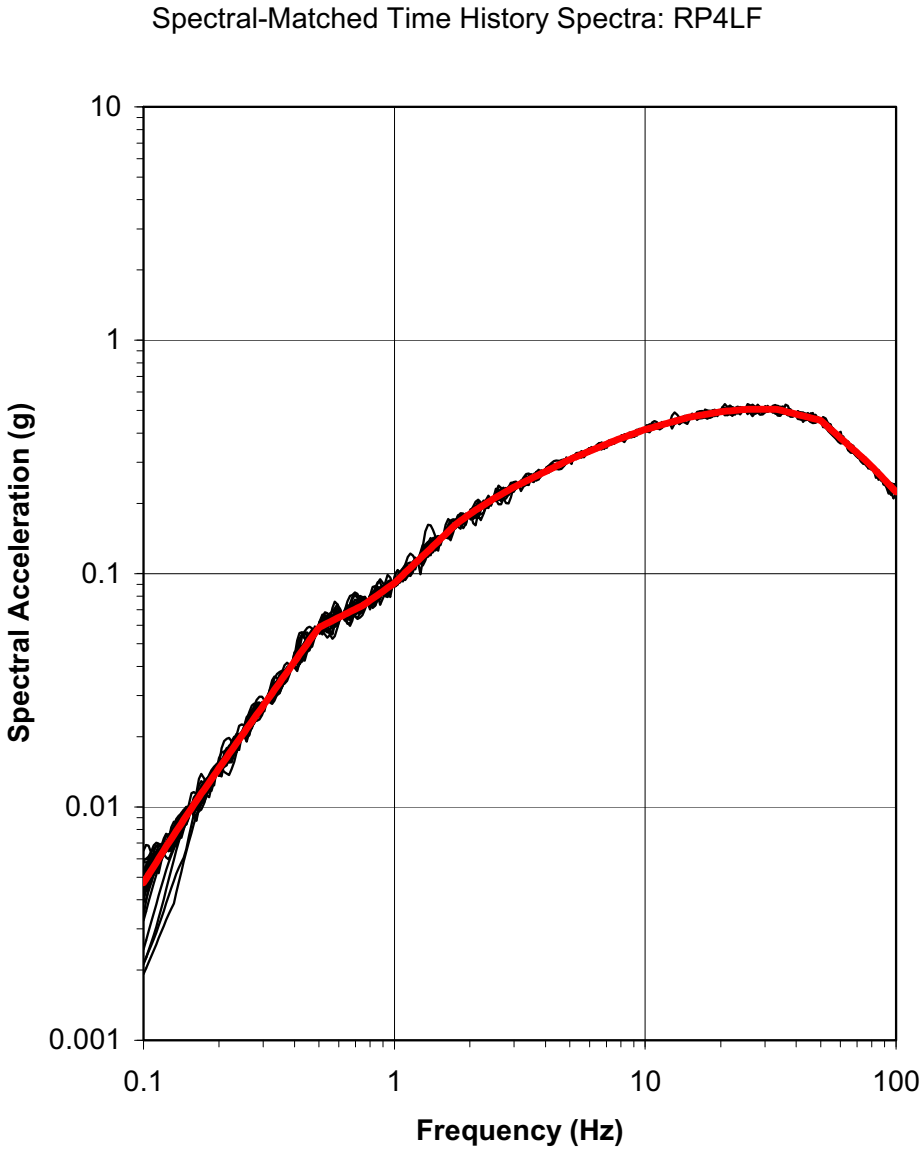

Note: Heavy red line is the target spectrum and thin black lines are the individual matches.

Figure 2.5.2-36f Low Frequency (10-4) Match for the 30 Time Histories

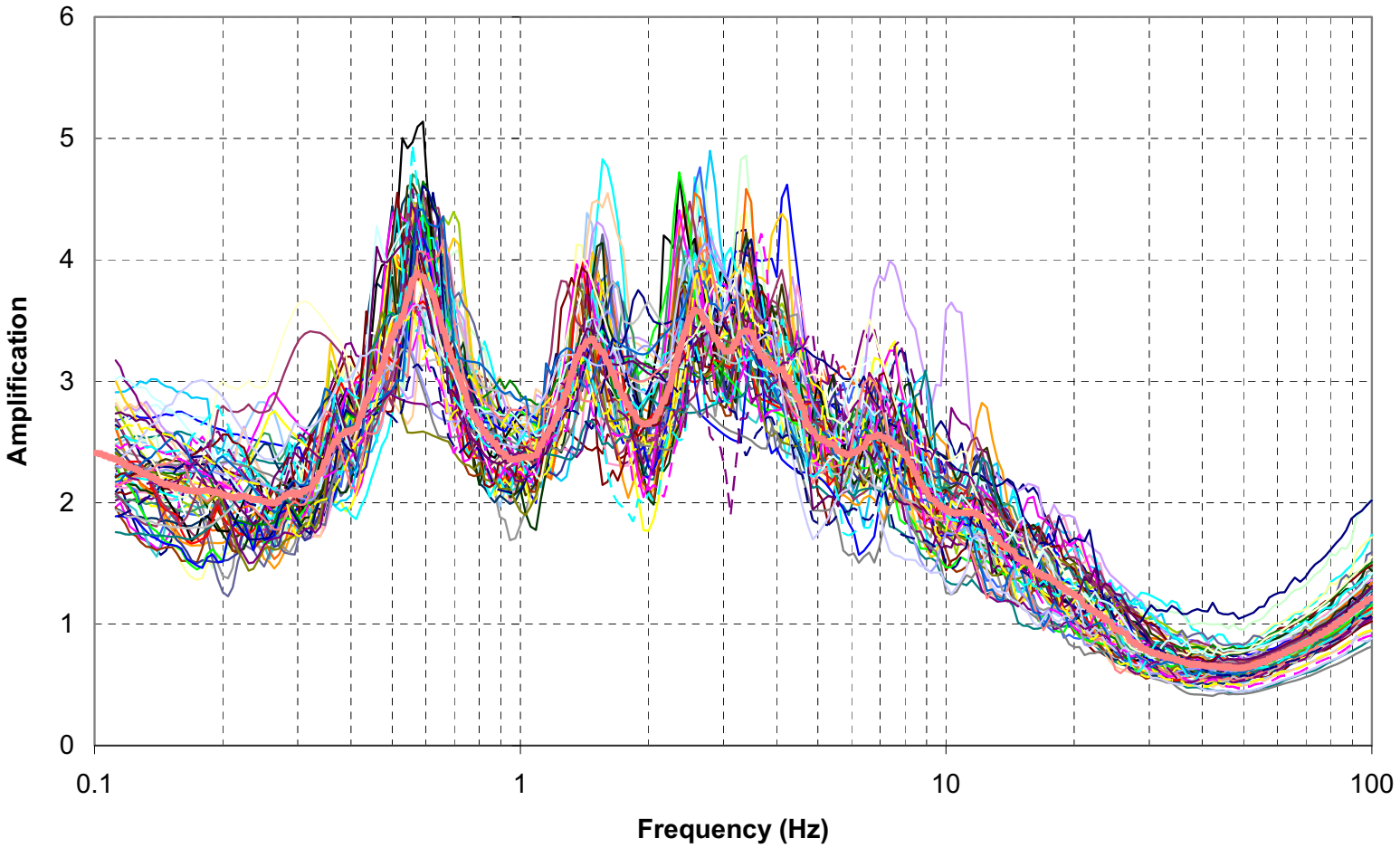

Figure 2.5.2-37 Typical Results of Spectral Amplification at 86-ft Depth (Top of Blue Bluff Marl) Using EPRI Degradation Curves for High Frequency Time Histories of 10-4 MAFE Input Motion Level

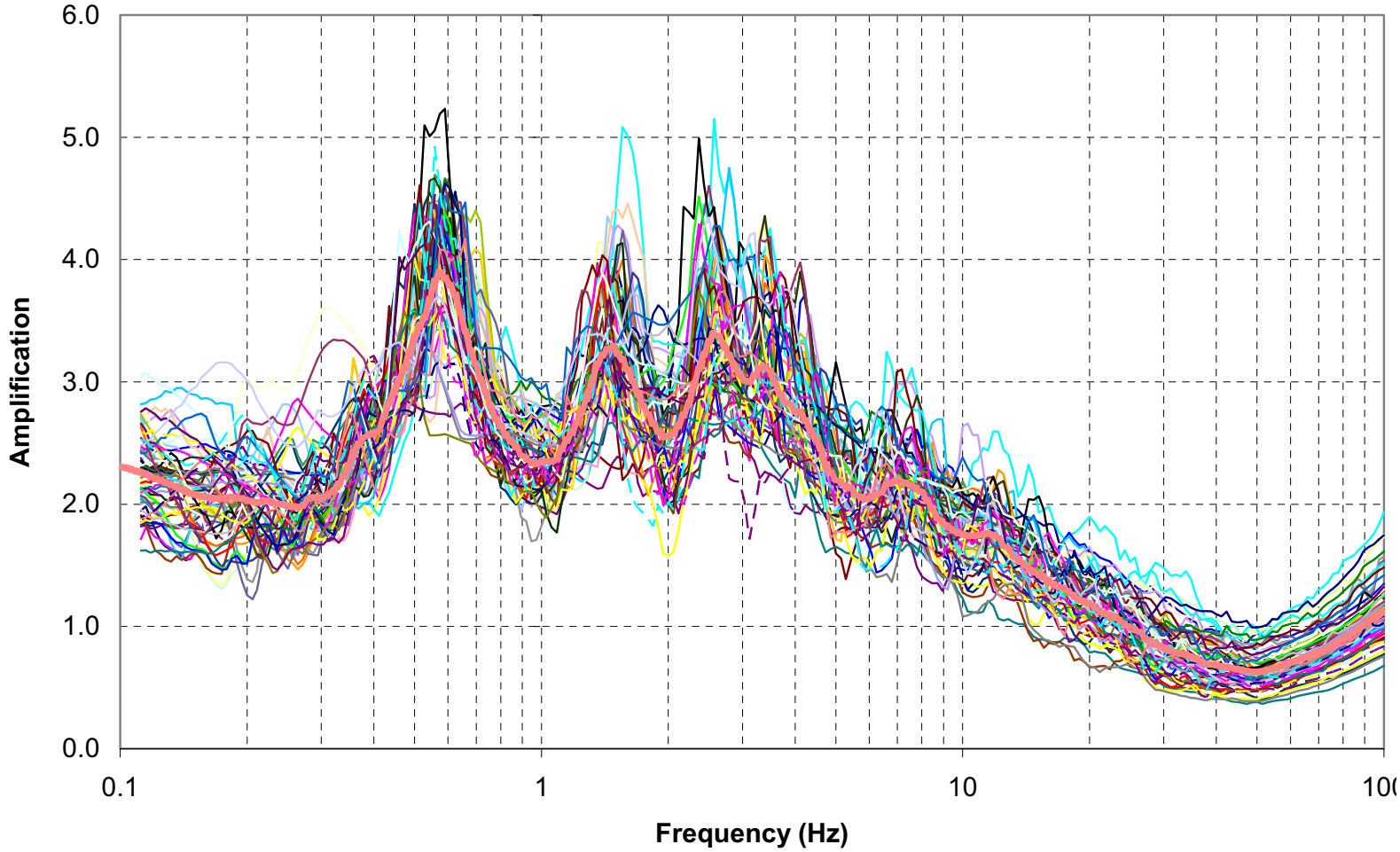

Figure 2.5.2-37a Typical Results of Spectral Amplification at 40-ft Horizon Outcrop Motion Using EPRI Degradation Curves for High-Frequency Time Histories of 10-4 MAFE Input Motion Level

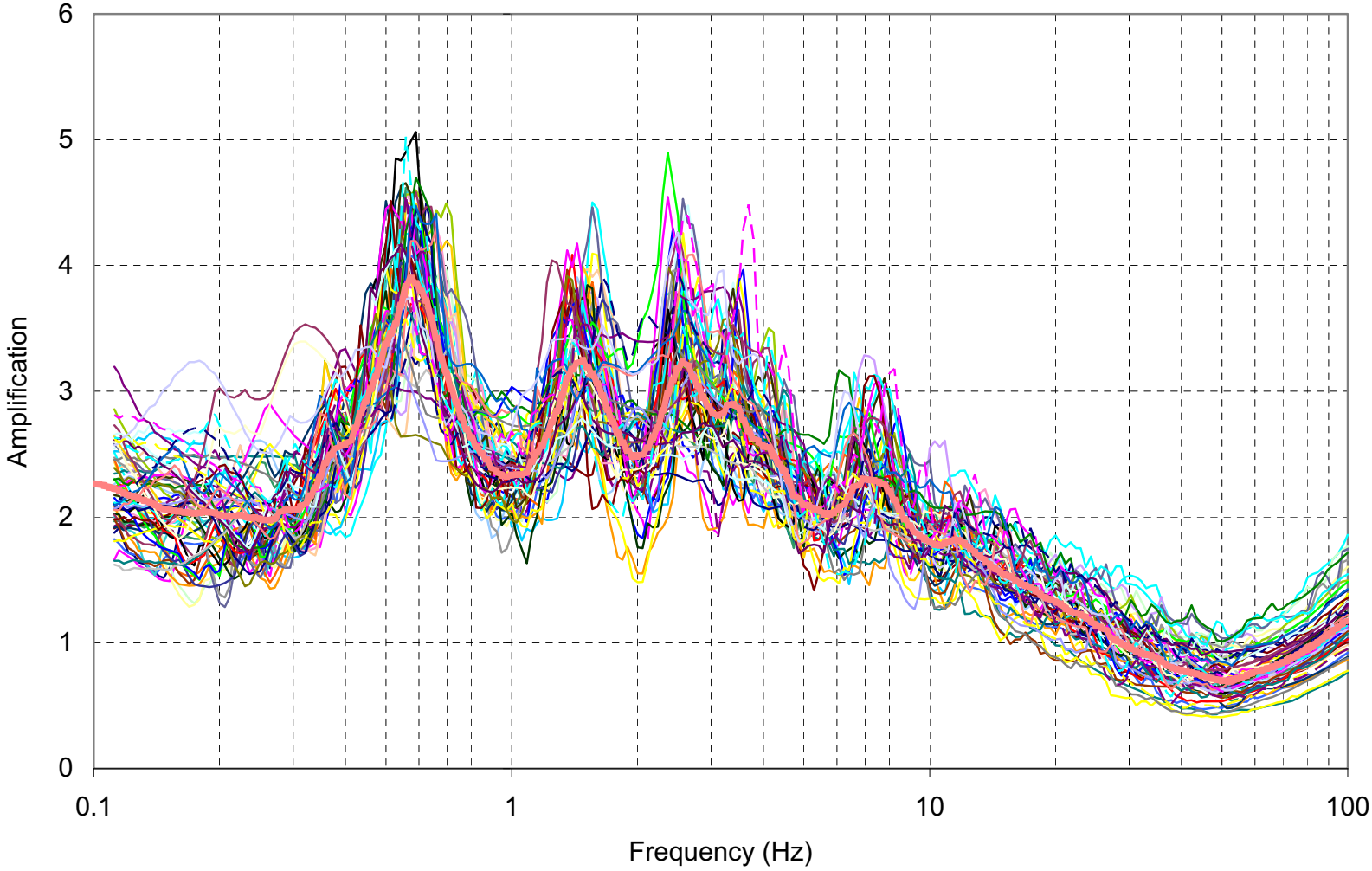

Figure 2.5.2-37b Typical Results of Spectral Amplification Ground Surface using EPRI Degradation Curves for High Frequency Time Histories of 10-4 MAFE Input Motion Level

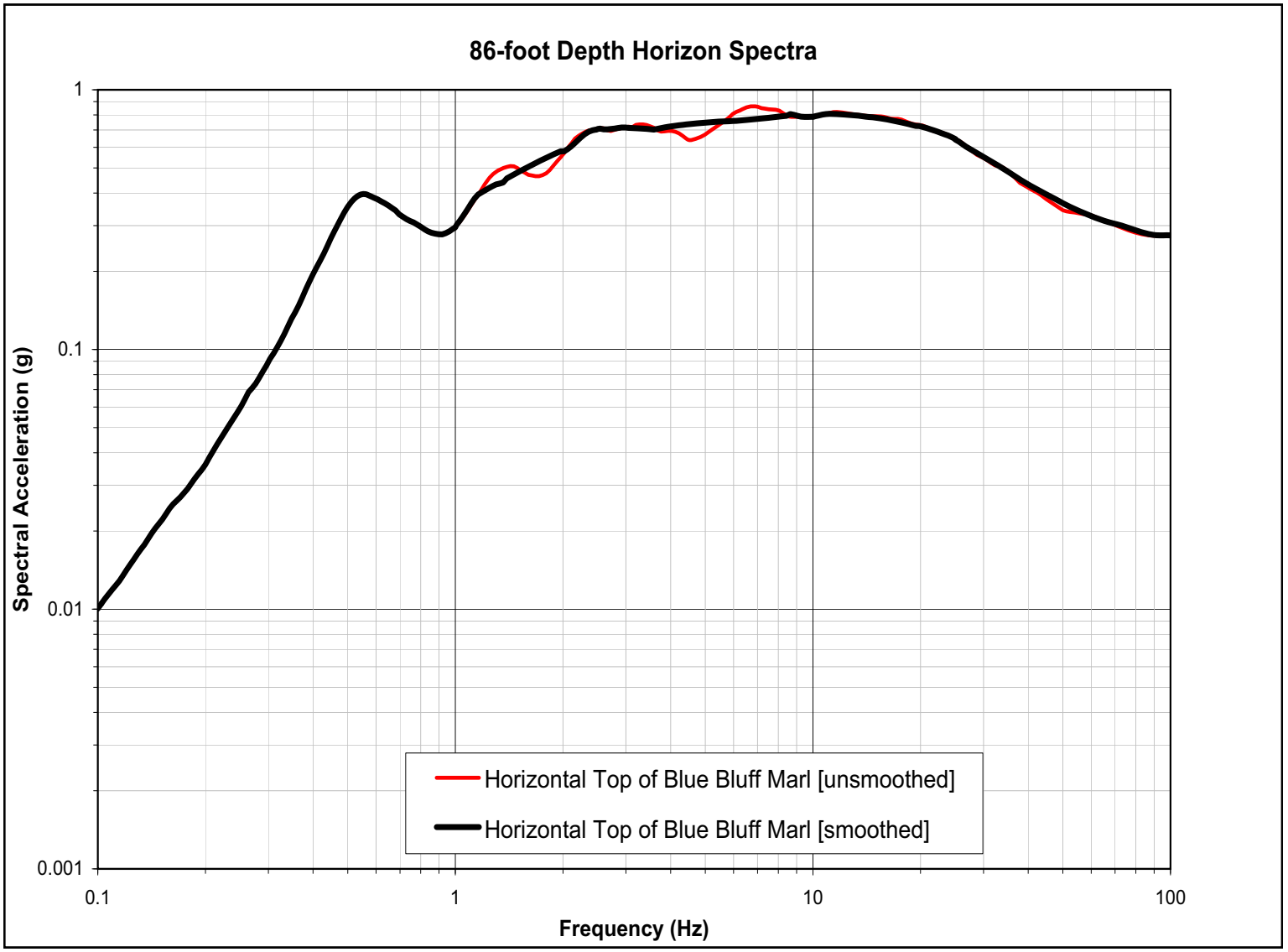

Figure 2.5.2-38 Horizontal Raw and Smoothed, Top of Blue Bluff Marl

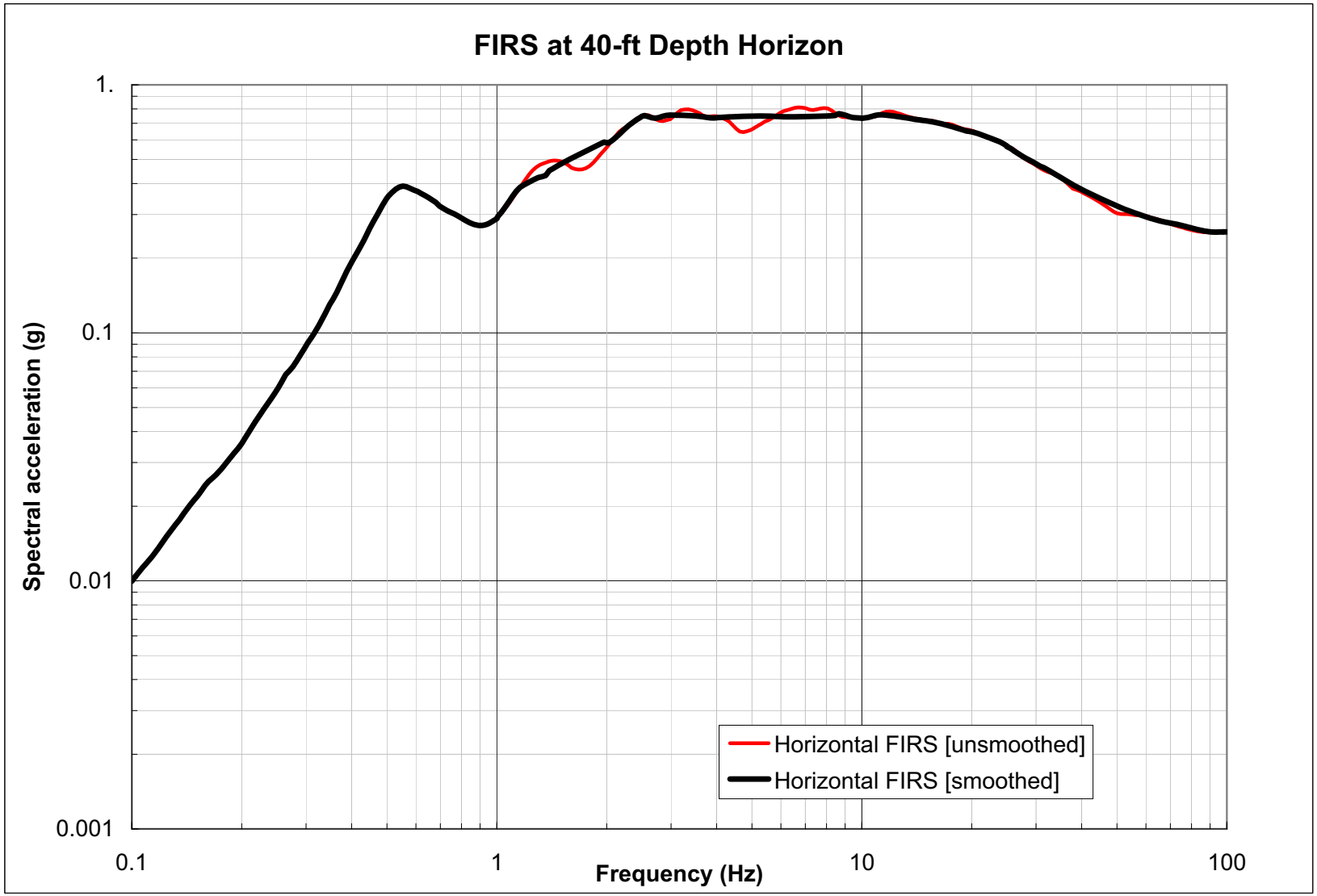

Figure 2.5.2-38a Horizontal Raw and Smoothed FIRS, 40-ft Depth Horizon

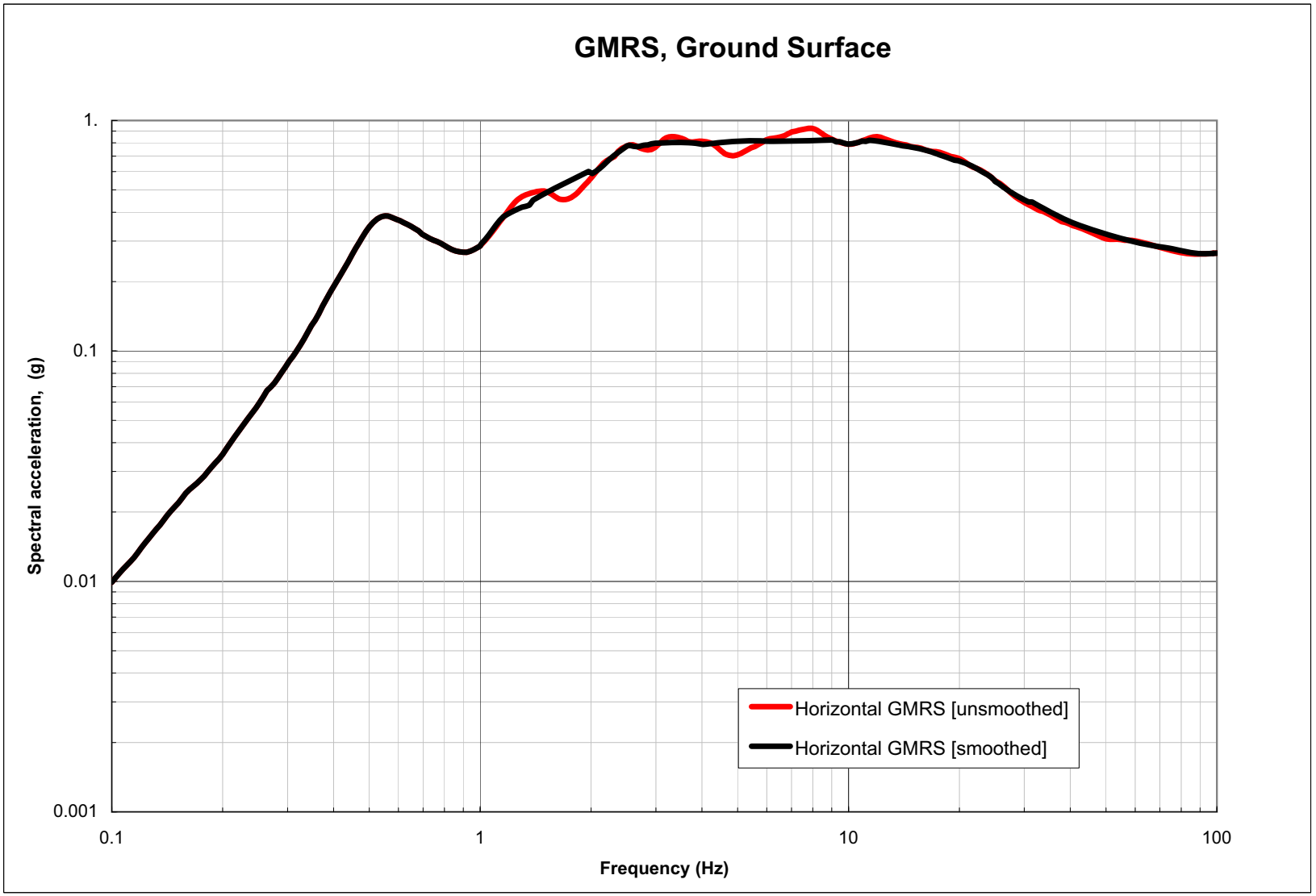

Figure 2.5.2-38b Horizontal Raw and Smoothed GMRS, Ground Surface

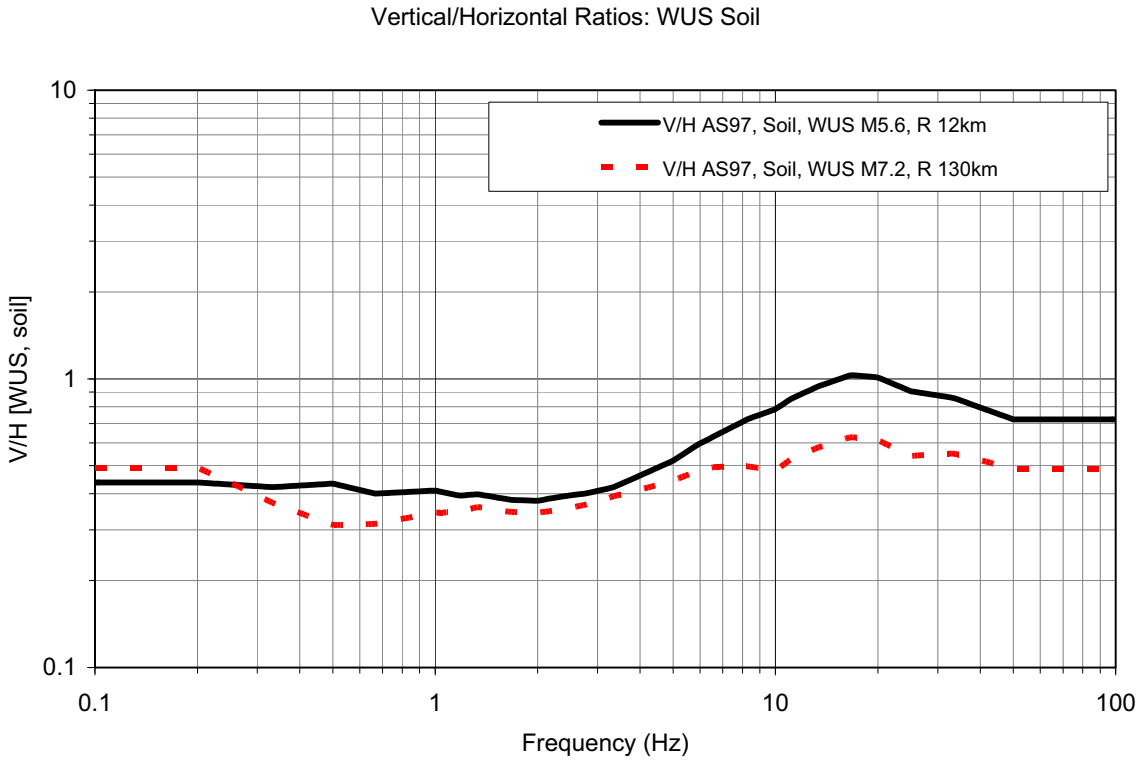

Figure 2.5.2-39 Plots of V/HWUS,Soil,Empirical Term of Equation 2.5.2-6 for "Near" [M5.6 at a Distance of 12 km] and "Far" [M7.2 at a Distance of 130 km] Events Using the Attenuation Relation of Abrahamson and Silva (1997)

NUREG/CR-6728, Figure J-31 and J-32

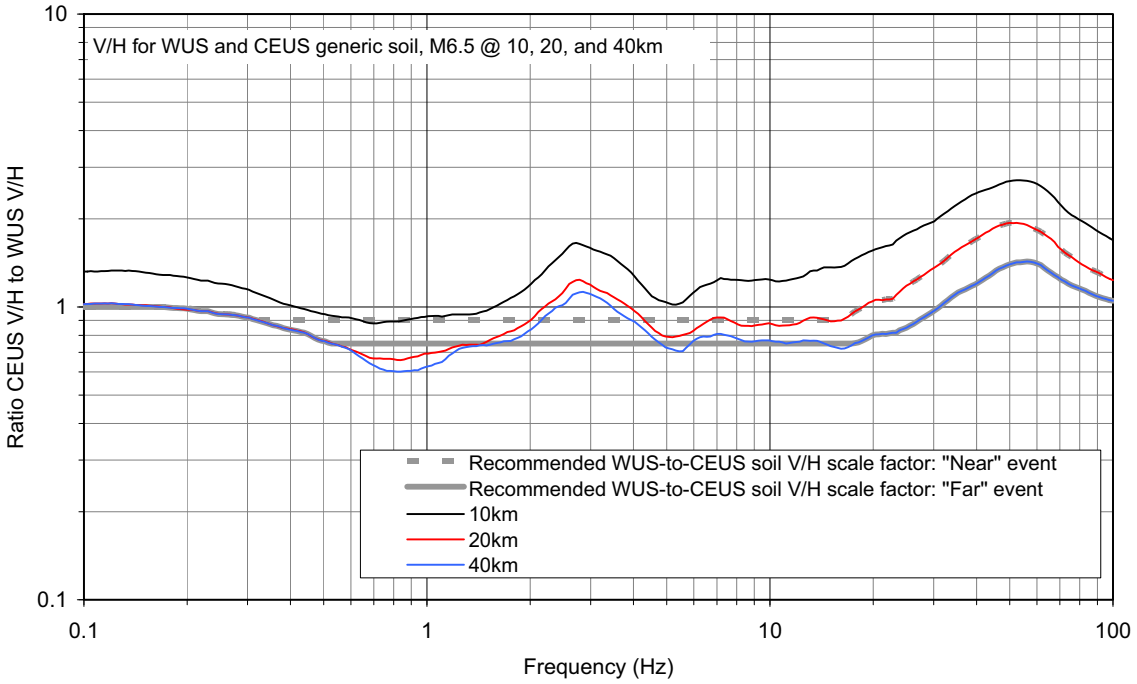

Note: The “near” and “far” ratios of V/H ratios recommended for this study are also shown.

Figure 2.5.2-40 Plots of [V/HCEUS,Soil,Model / V/HWUS,Soil,Model] Term of Equation 2.5.2-6 for M6.5 and Distances of 10, 20, and 40 km, as Available in NUREG/CR-6728 (McGuire et al 2001)

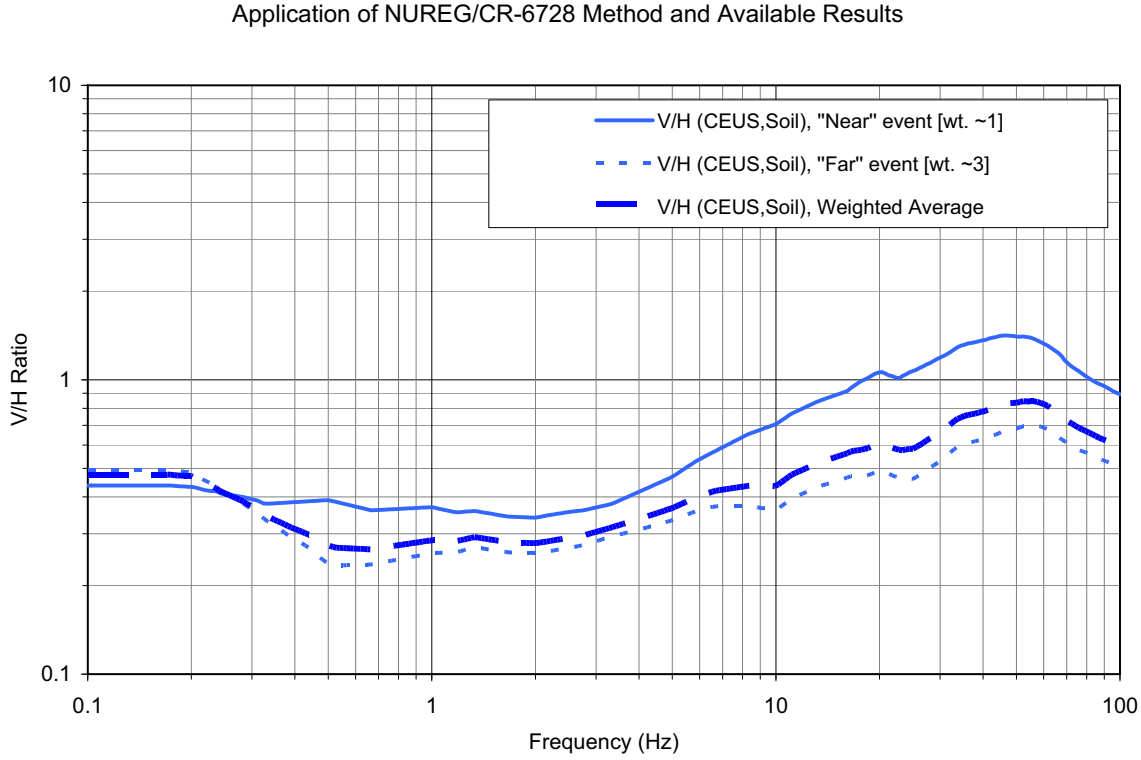

Note: Considering the relative contribution of the "near" and "far" events to the horizontal SSE design response spectrum, the approximately 1:3 weighted average is the recommended $V/H_{CEUS,Soil}$.

Figure 2.5.2-41 Plots of Recommended V/HCEUS,Soil from Equation 2.5.2-6 for "Near" and "Far" Events Using Results from NUREG/CR-6728 (McGuire et al 2001)

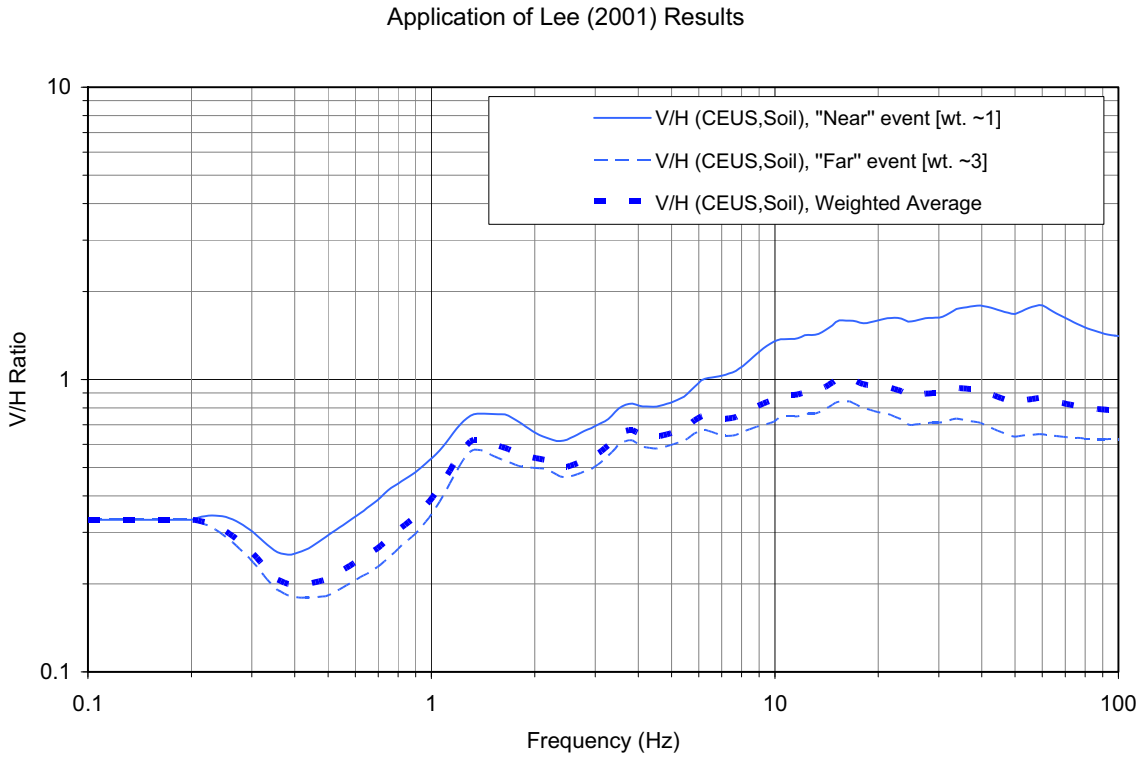

Note: Considering the relative contribution of the “near” and “far” events to the horizontal SSE design response spectrum, the approximately 1:3 weighted average is shown.

Figure 2.5.2-42 Plots of Recommended V/HCEUS,Soil from Equation 2.5.2-6 for “Near” and “Far” Events Using Results from Lee (2001)

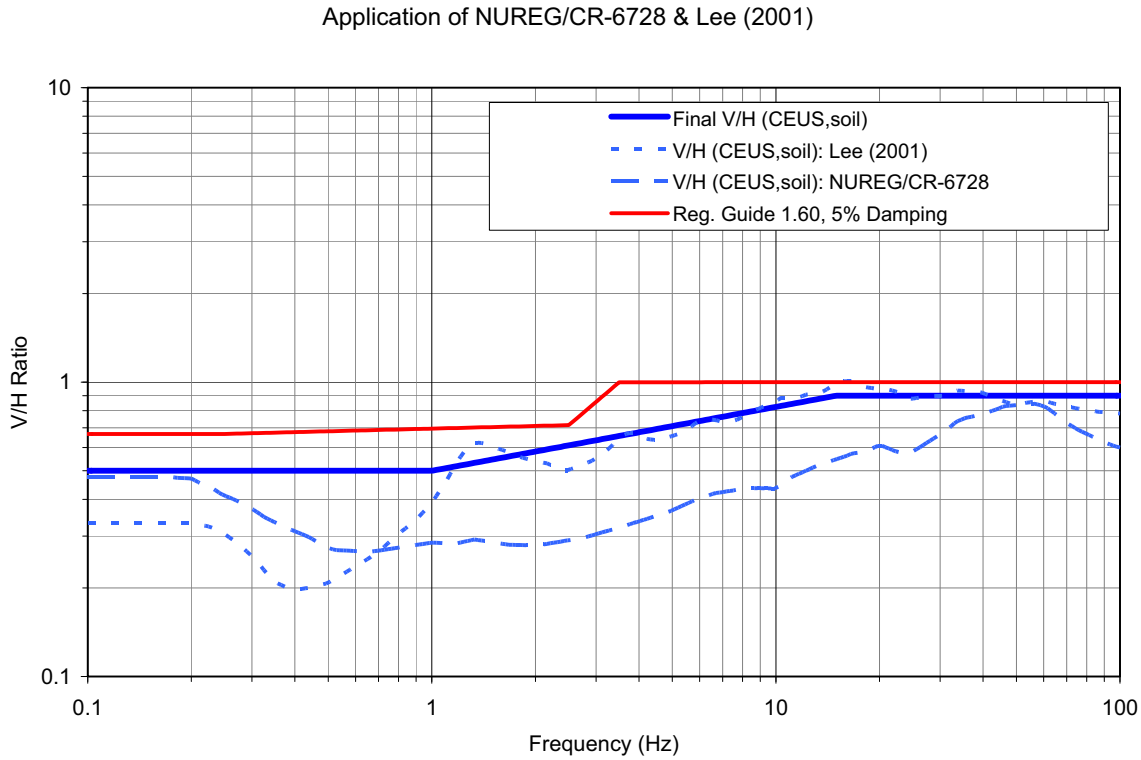

Note: Considering the site-specific aspects of the Lee (2001), it is preferred, guiding the recommended final $V/H_{CEUS,Soil}$ (blue solid). The V/H from RG 1.60 is shown (red) for comparison.

Figure 2.5.2-43 Plots of V/HCEUS,Soil (Blue Patterned) Derived from Results from NUREG/CR-6728 (McGuire et al 2001) and Lee (2001)

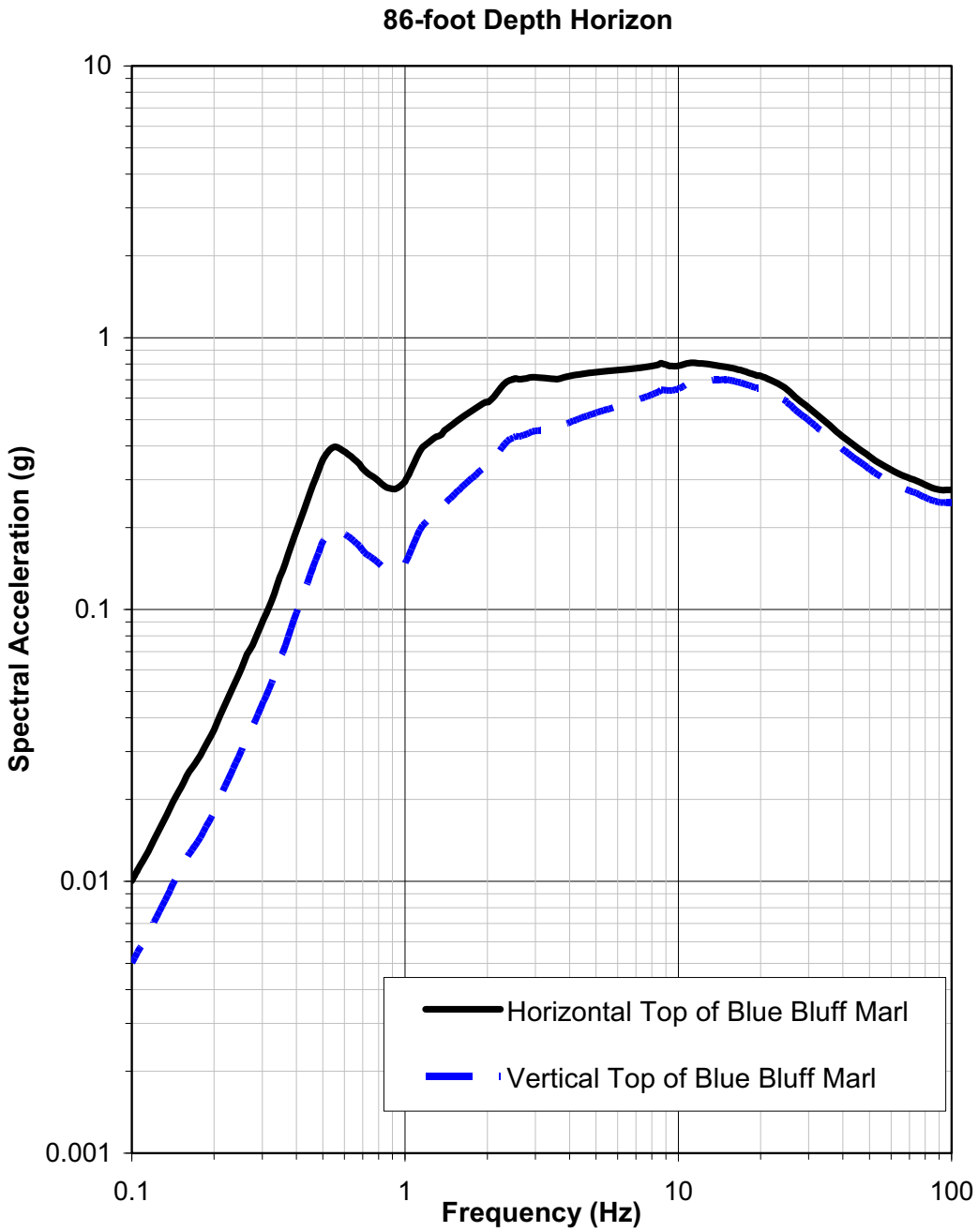

Figure 2.5.2-44 VEGP ESP Horizontal and Vertical Top of Blue Bluff Marl (5% Damping)

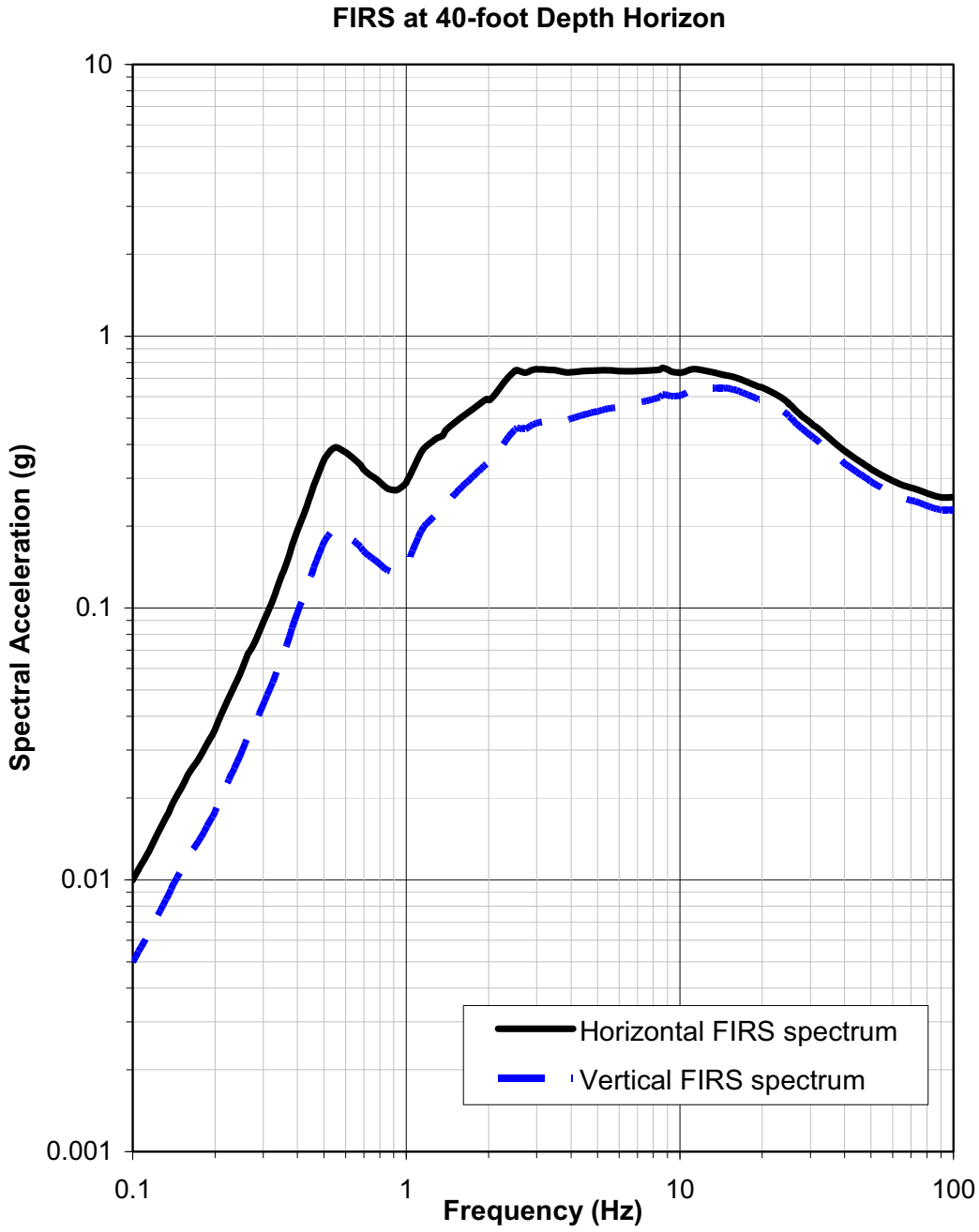

Figure 2.5.2-44a VEGP ESP Horizontal and Vertical FIRS Spectra, at the 40-ft Depth Horizon

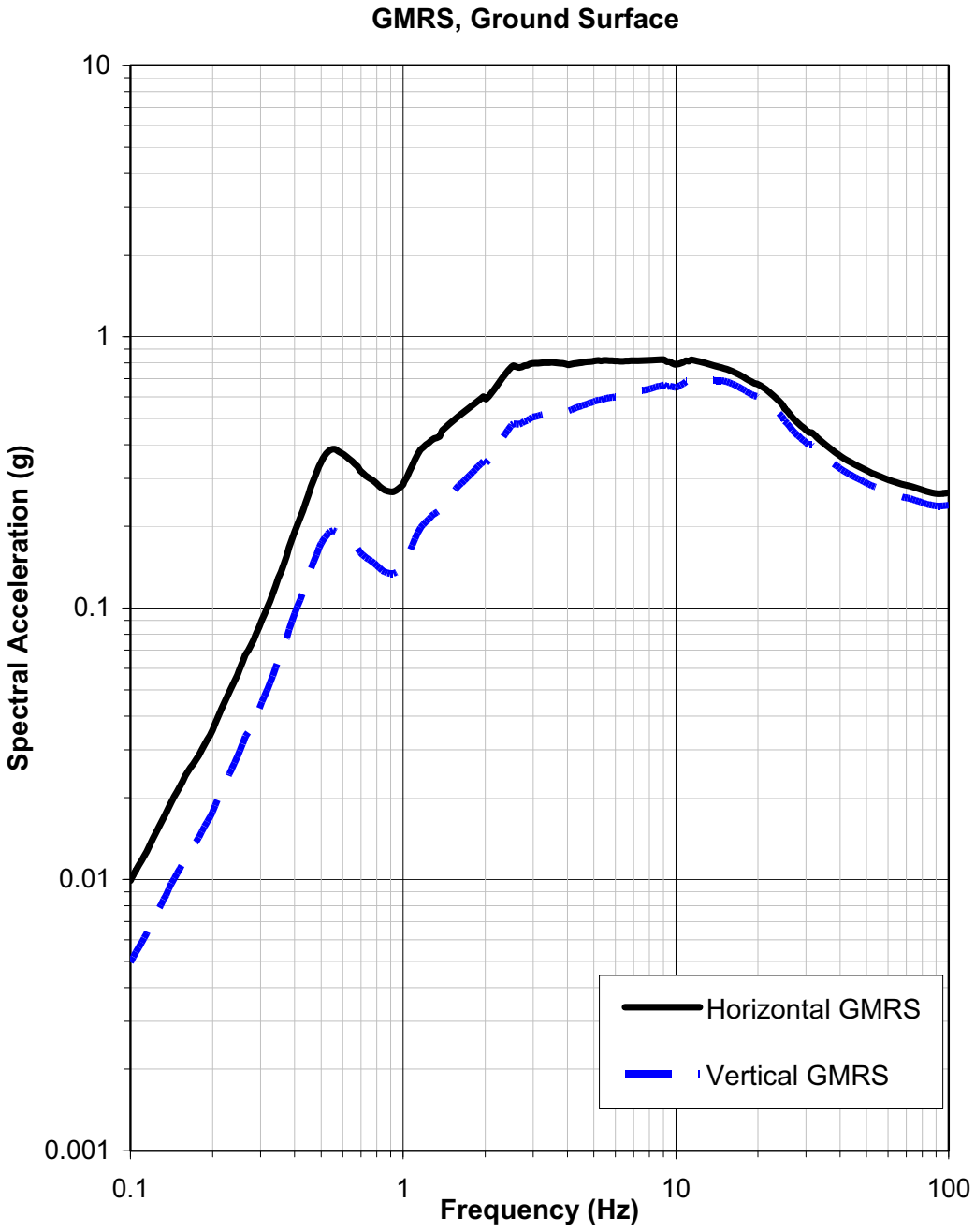

Figure 2.5.2-44b VEGP ESP Horizontal and Vertical GMRS Spectra (5% Damping)

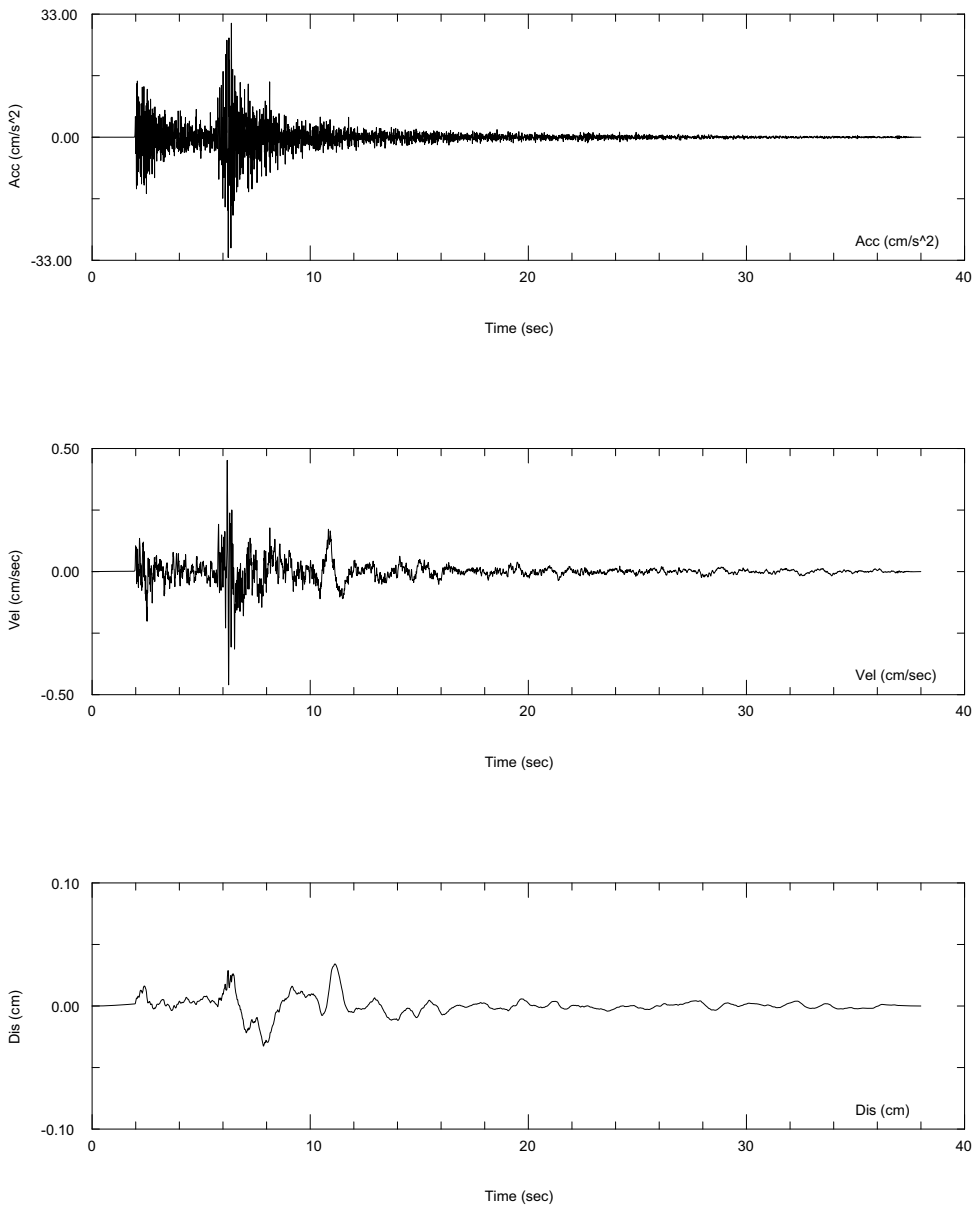

Figure 2.5.2-45a Example of Initial Seed Input Time Acceleration, Velocity, and Displacement Time Histories (One of Thirty) for High Frequency Target Spectrum

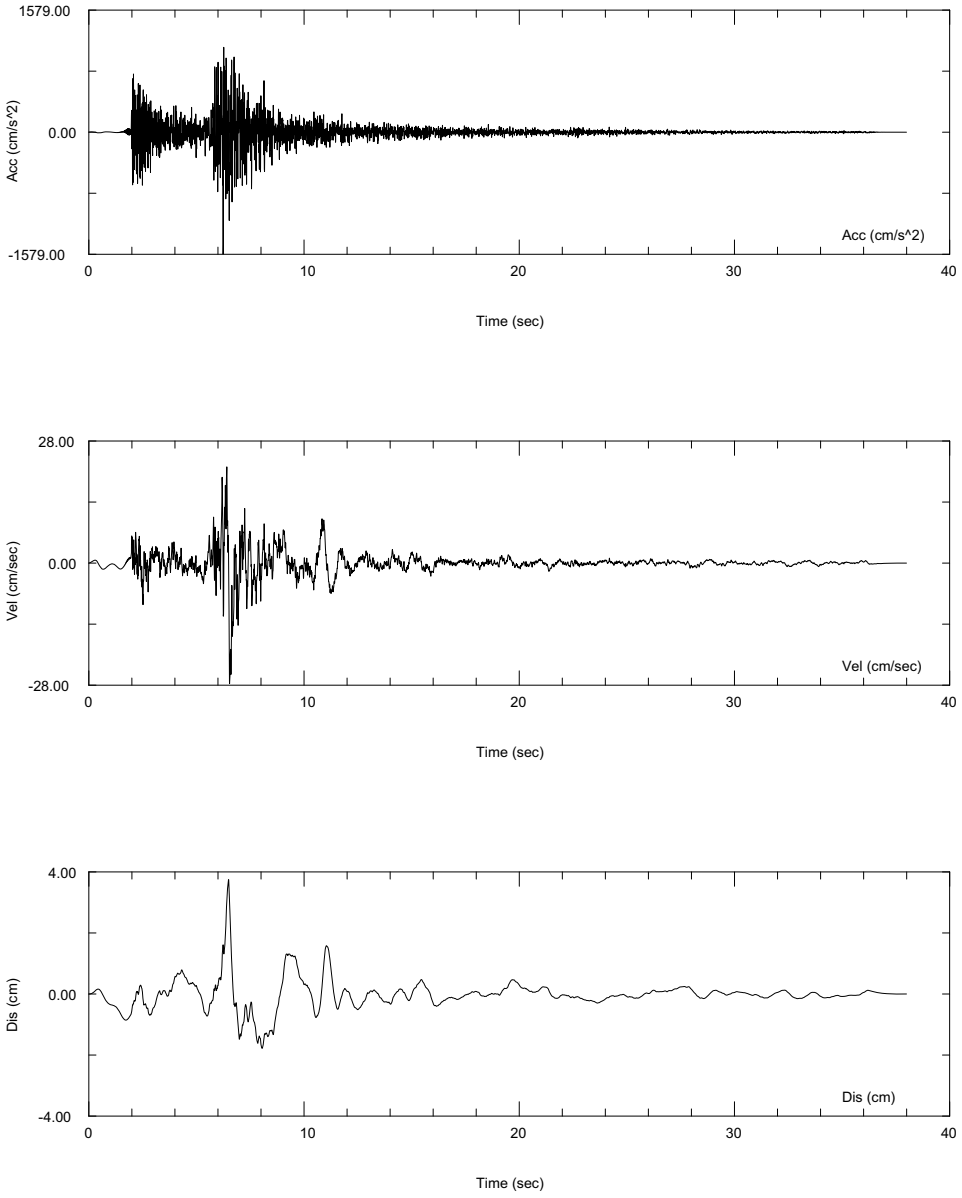

Figure 2.5.2-45b Final Modified Spectrum-Compatible Acceleration, Velocity, and Displacement Time Histories (One of Thirty) for 10^{-6} High Frequency Target Spectrum

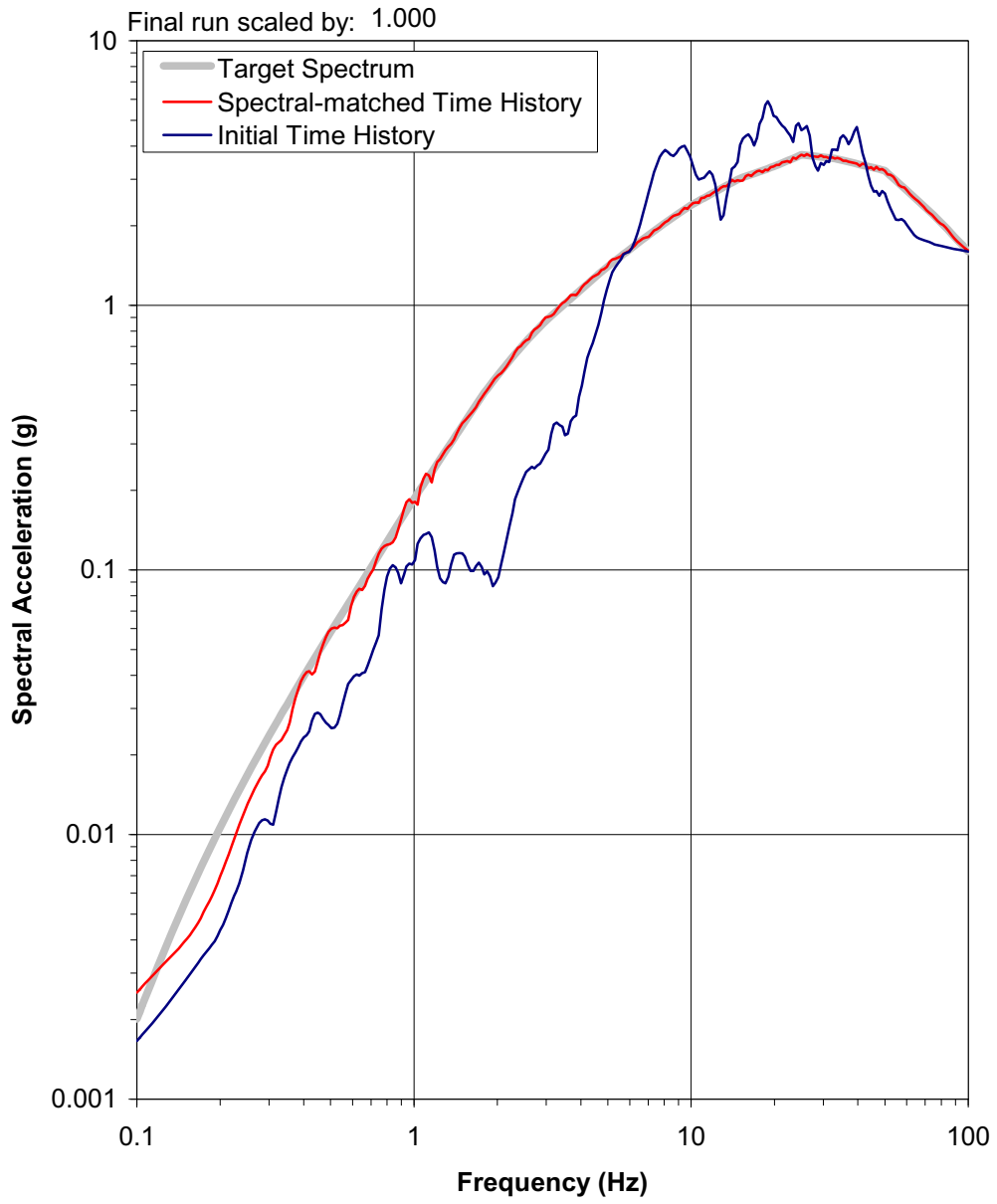

Figure 2.5.2-46 Comparison of 10^{-6} High Frequency Target Spectrum (Thick Grey Line), Response Spectrum from Initial Seed Input Acceleration Time History Scaled to Target PGA (Thin Blue Line), and Acceleration Response Spectrum for Final Modified Spectrum Compatible Time History (Thin Red Line)

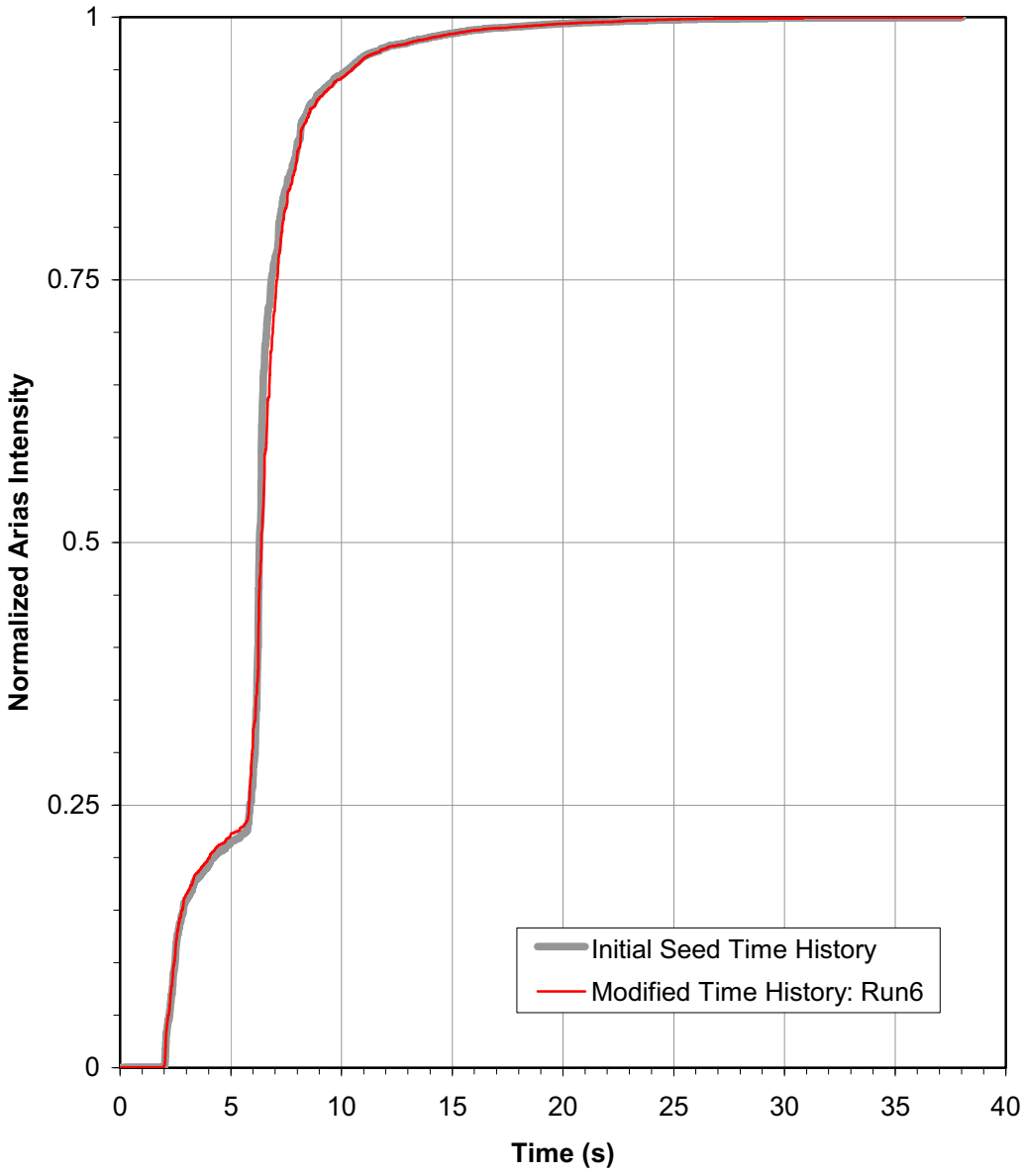

Figure 2.5.2-47 Comparison of Normalized Arias Intensity from Initial Seed Input Time History (Thick Grey Line) and Final Modified Spectrum Compatible (10^{-6} High Frequency Target Spectrum) Time History (Thin Red Line) for an Example Case

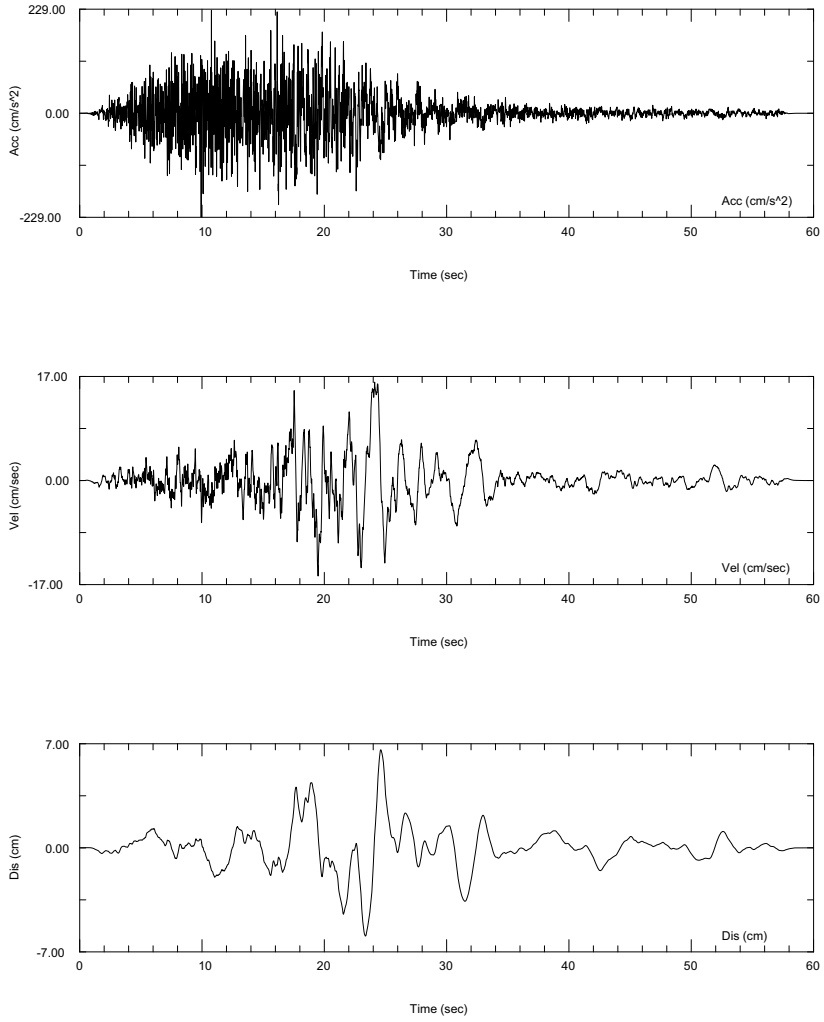

Figure 2.5.2-48a Horizontal Component 1 Modified Spectrum Compatible Time Acceleration, Velocity, and Displacement Time Histories for FIRS Horizontal Target Spectrum Prior to Application of 1.01 Scale Factor

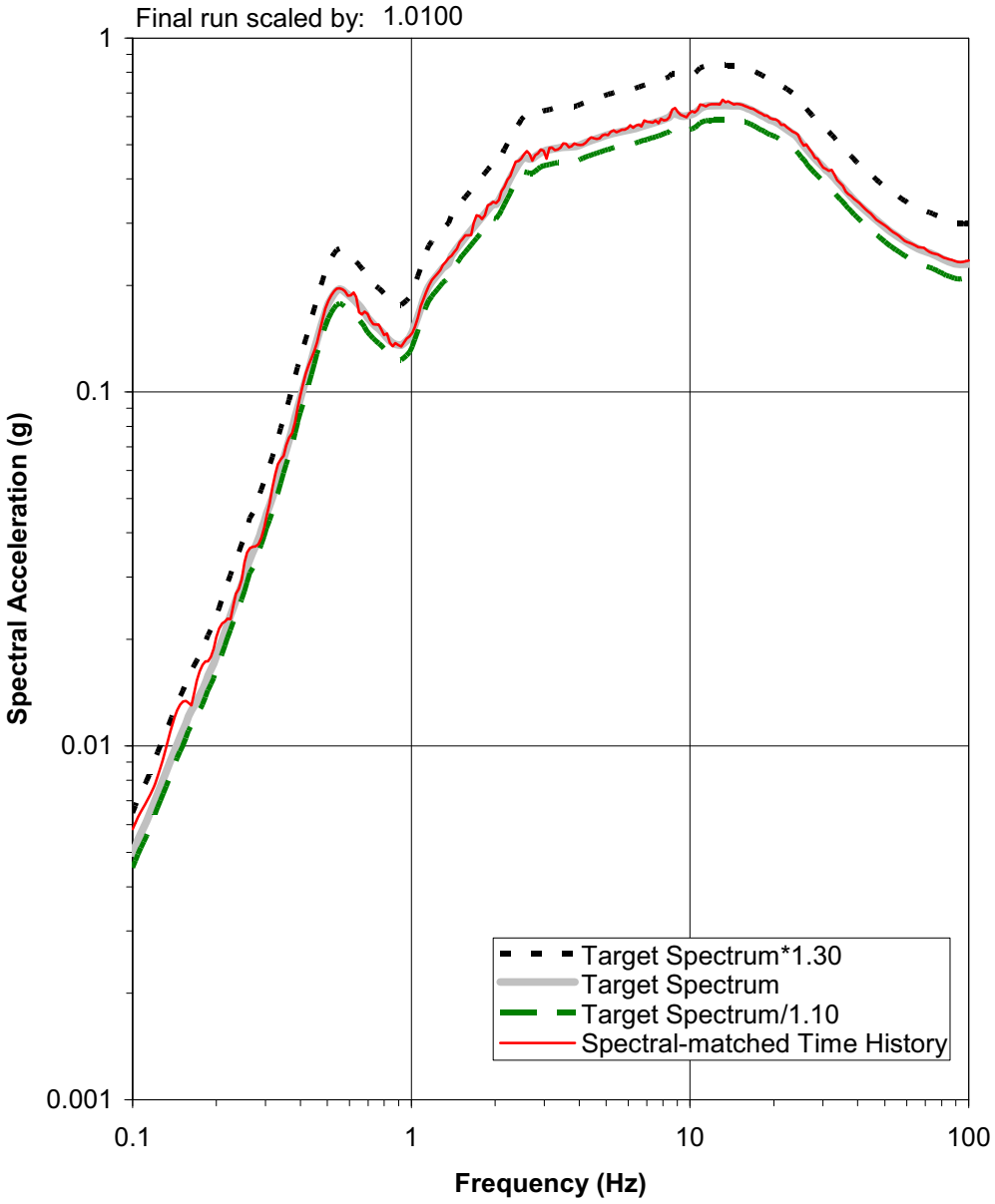

Figure 2.5.2-48b Comparison of Horizontal FIRS Target Spectrum (Thick Grey Line), 1.3*FIRS Target Spectrum (Dashed Black LIne), 0.9*FIRS Target Spectrum (Dashed Green Line), and Acceleration Response Spectrum for Final Modified Spectrum Compatible Time History (Thin Red Line) Including Application of 1.01 Scale Factor for Horizontal Component 1

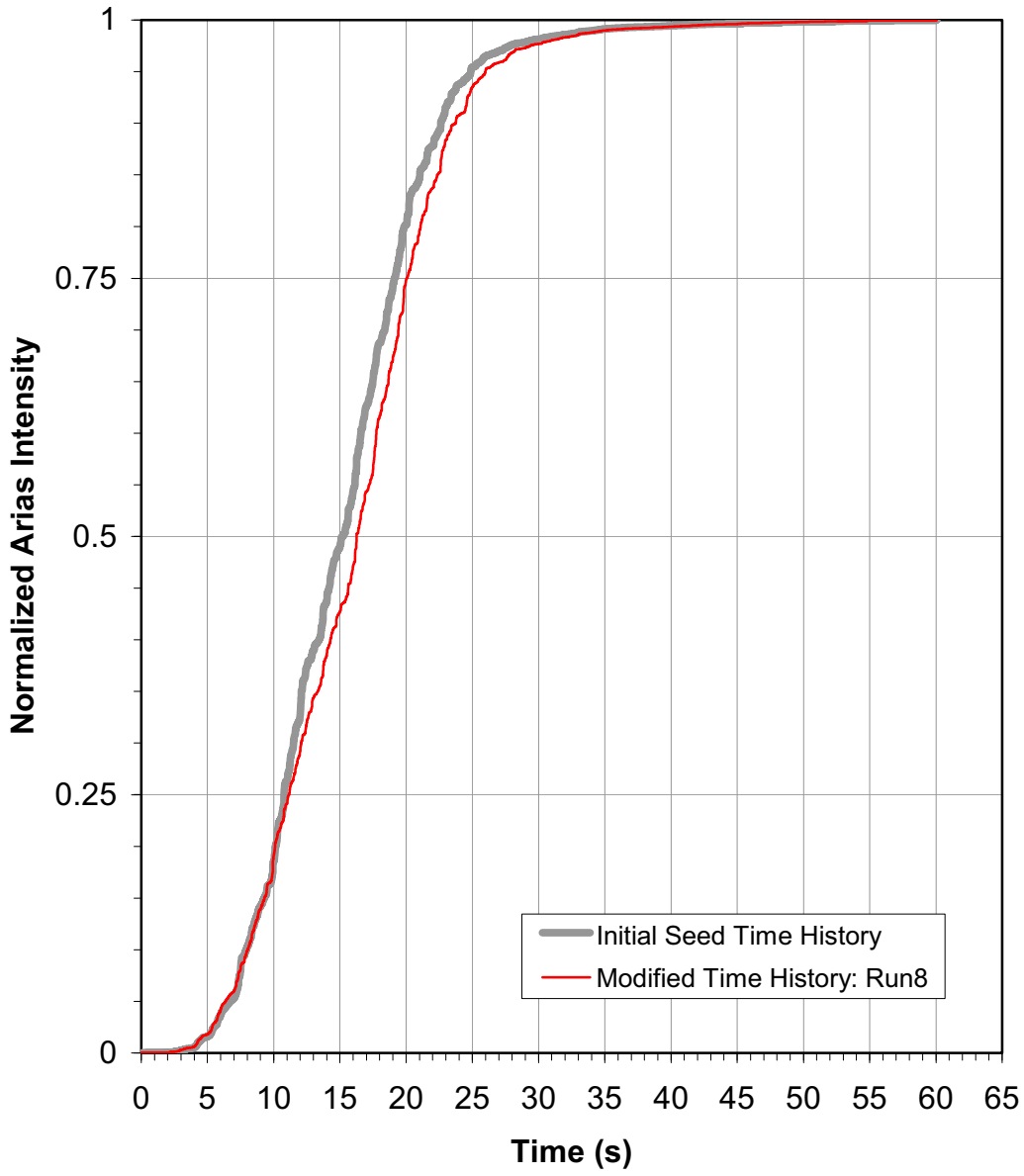

Figure 2.5.2-48c Comparison of Normalized Arias Intensity from Initial Seed Input Time History (Thick Grey Line) and Final Modified Spectrum Compatible Time History (Thin Red Line) Including Application of 1.01 Scale Factor for Horizontal Component 1

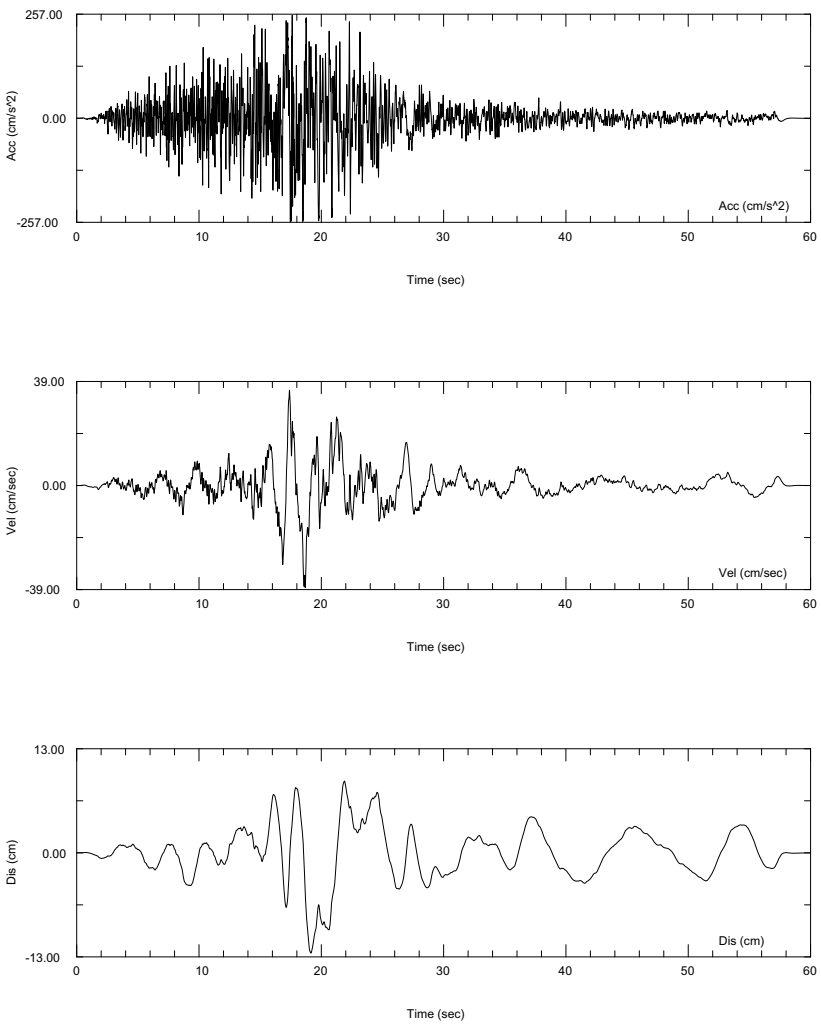

Figure 2.5.2-49a Horizontal Component 2 Modified Spectrum Compatible Time Acceleration, Velocity, and Displacement Time Histories for FIRS Horizontal Target Spectrum Prior to Application of 1.01 Scale Factor

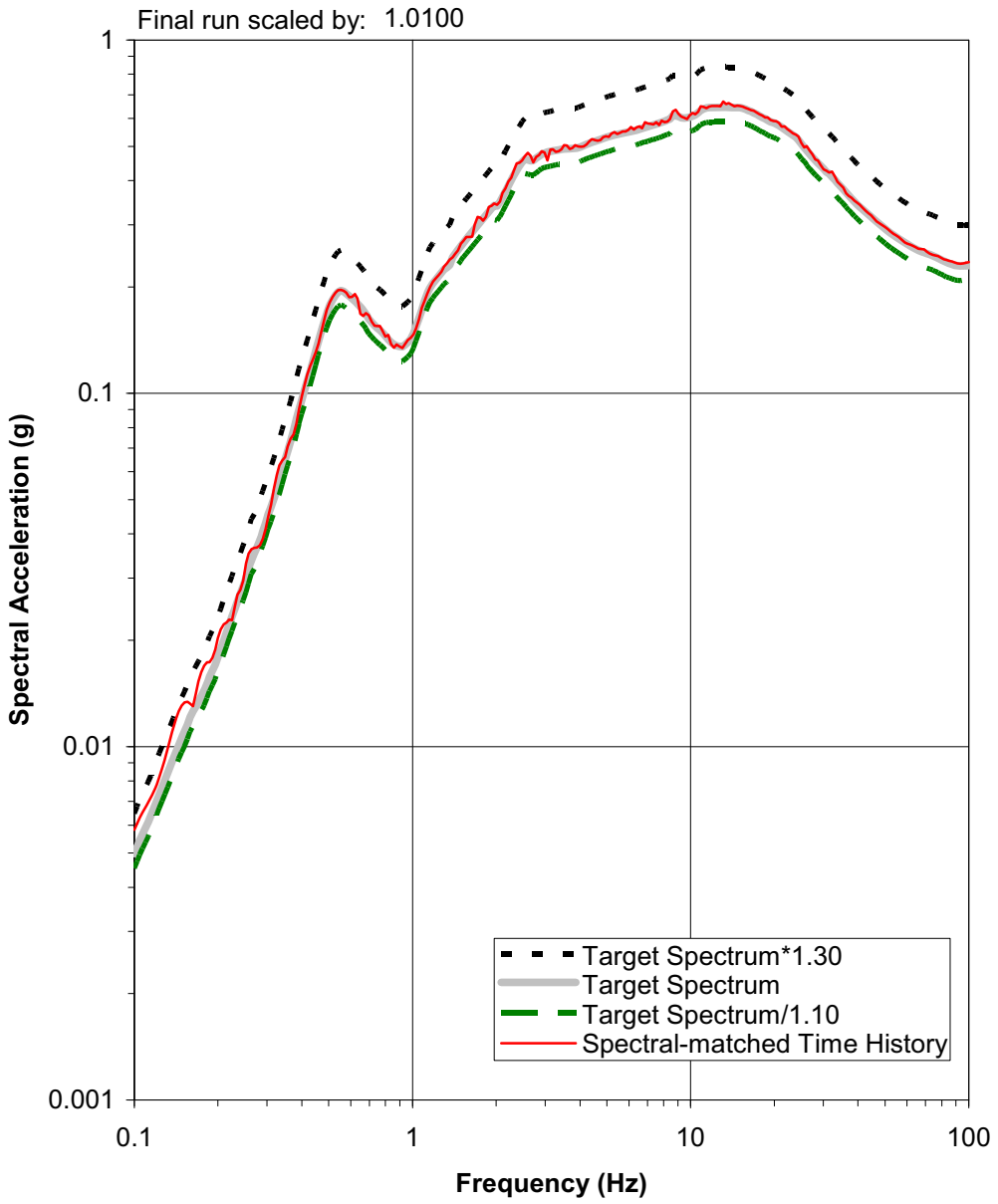

Figure 2.5.2-49b Comparison of Horizontal FIRS Target Spectrum (Thick Grey Line), 1.3*FIRS Target Spectrum (Dashed Black Line), 0.9*FIRS Target Spectrum (Dashed Green Line), and Acceleration Response Spectrum for Final Modified Spectrum Compatible Time History (Thin Red Line) Including Application of 1.01 Scale Factor for Horizontal Component 2

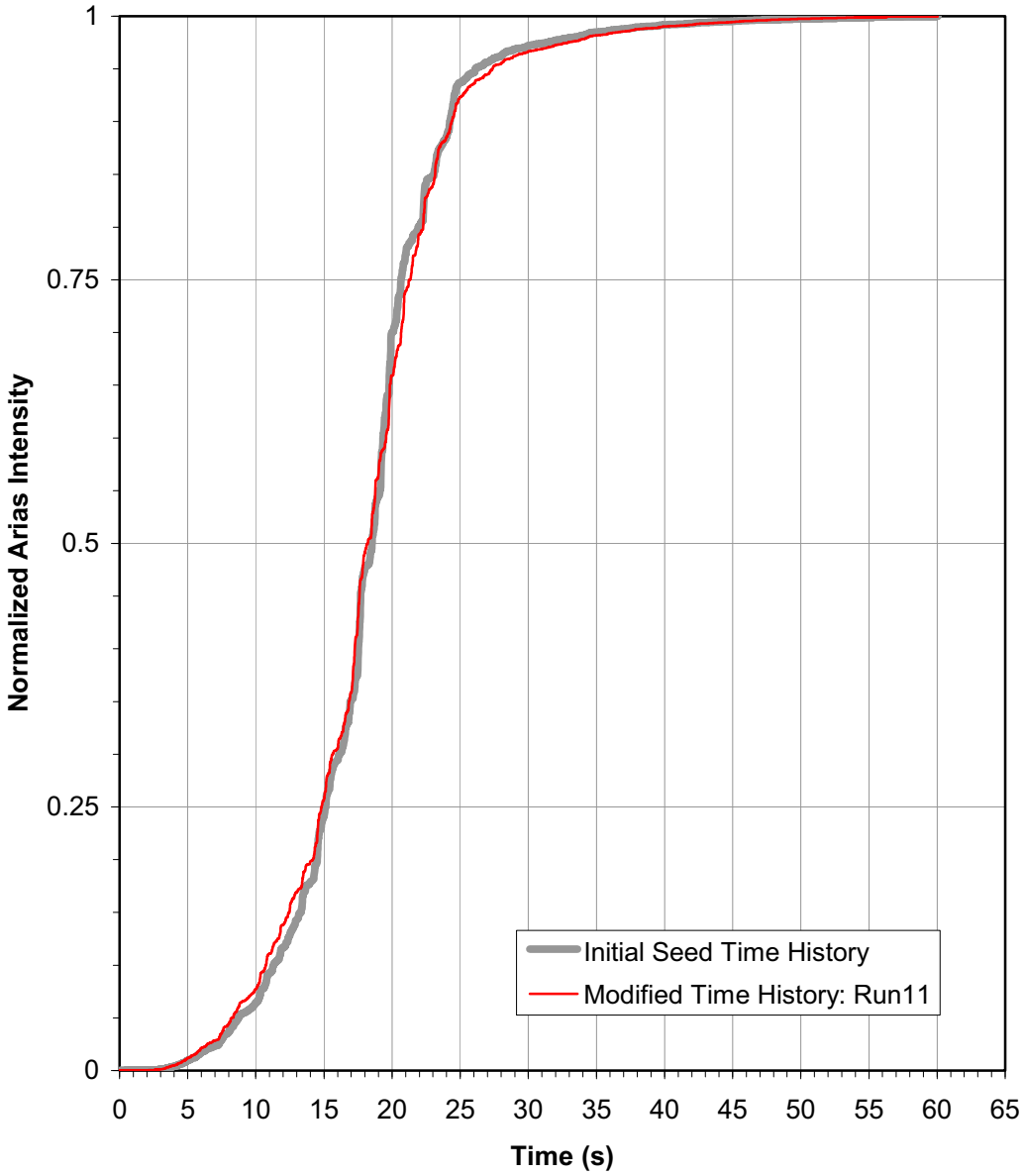

Figure 2.5.2-49c Comparison of Normalized Arias Intensity from Initial Seed Input Time History (Thick Grey Line) and Final Modified Spectrum Compatible Time History (Thin Red Line) Including Application of 1.01 Scale Factor for Horizontal Component 2

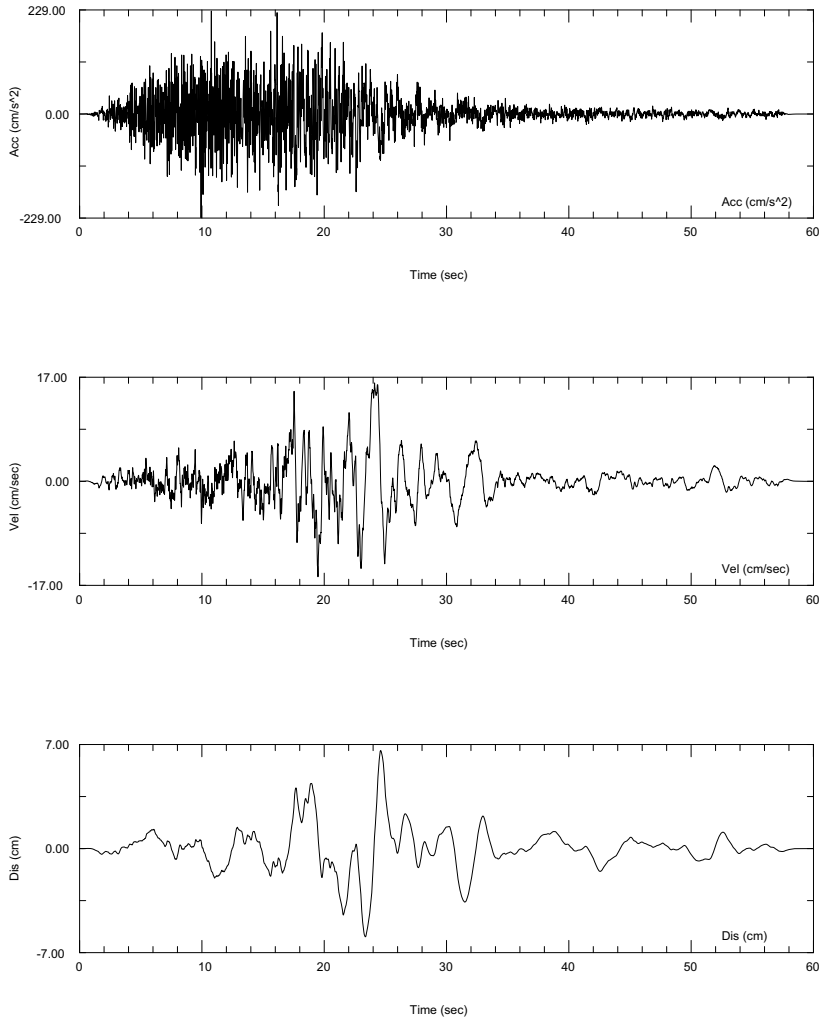

Figure 2.5.2-50a Vertical Component Modified Spectrum Compatible Time Acceleration, Velocity, and Displacement Time Histories for FIRS Vertical Target Spectrum Prior to Application of 1.01 Scale Factor

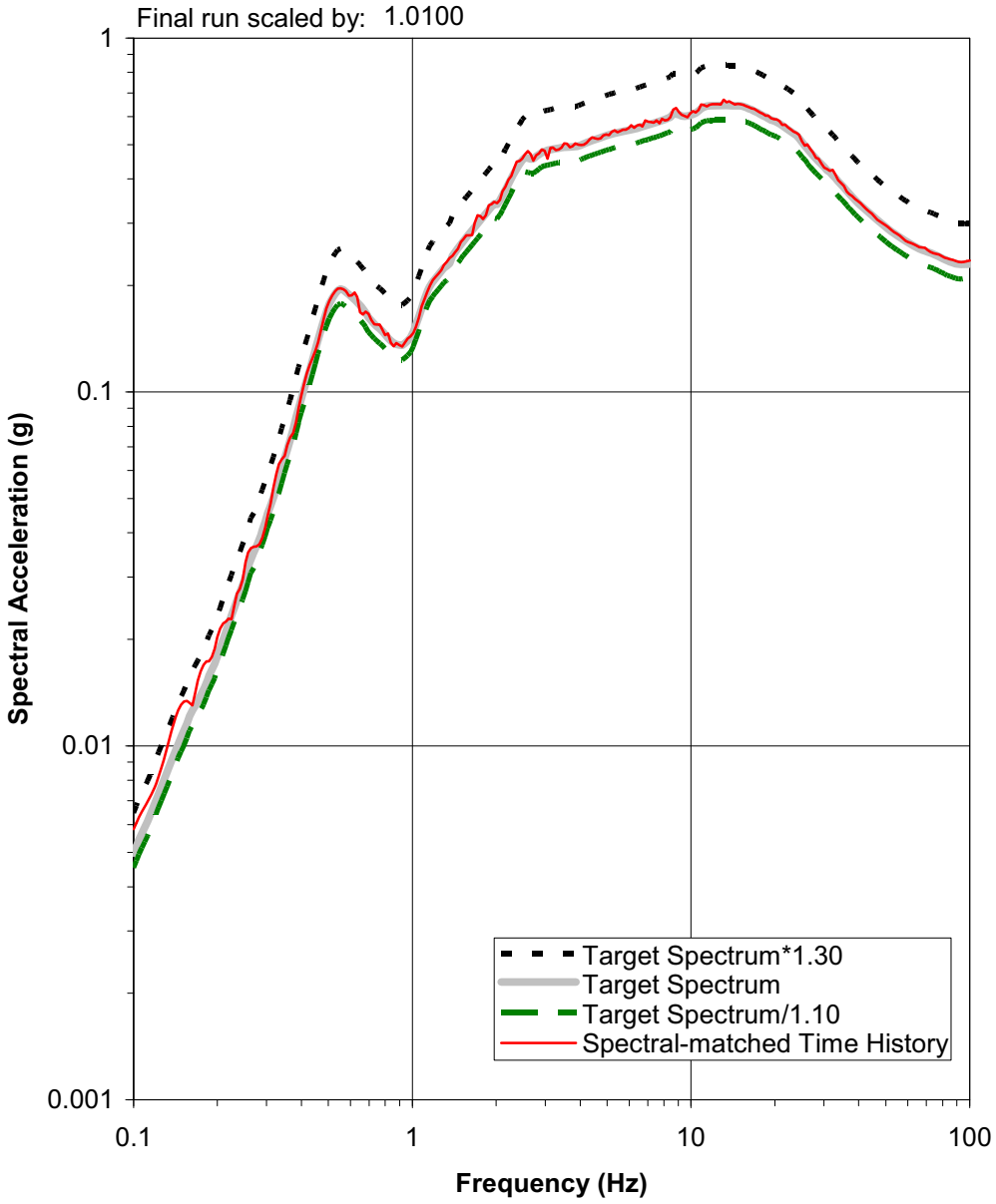

Figure 2.5.2-50b Comparison of Vertical FIRS Target Spectrum (Thick Grey Line), 1.3*FIRS Target Spectrum (Dashed Black Line), 0.9*FIRS Target Spectrum (Dashed Green Line), and Acceleration Response Spectrum for Final Modified Spectrum Compatible Time History (Thin Red Line) Including Application of 1.01 Scale Factor for Vertical Component

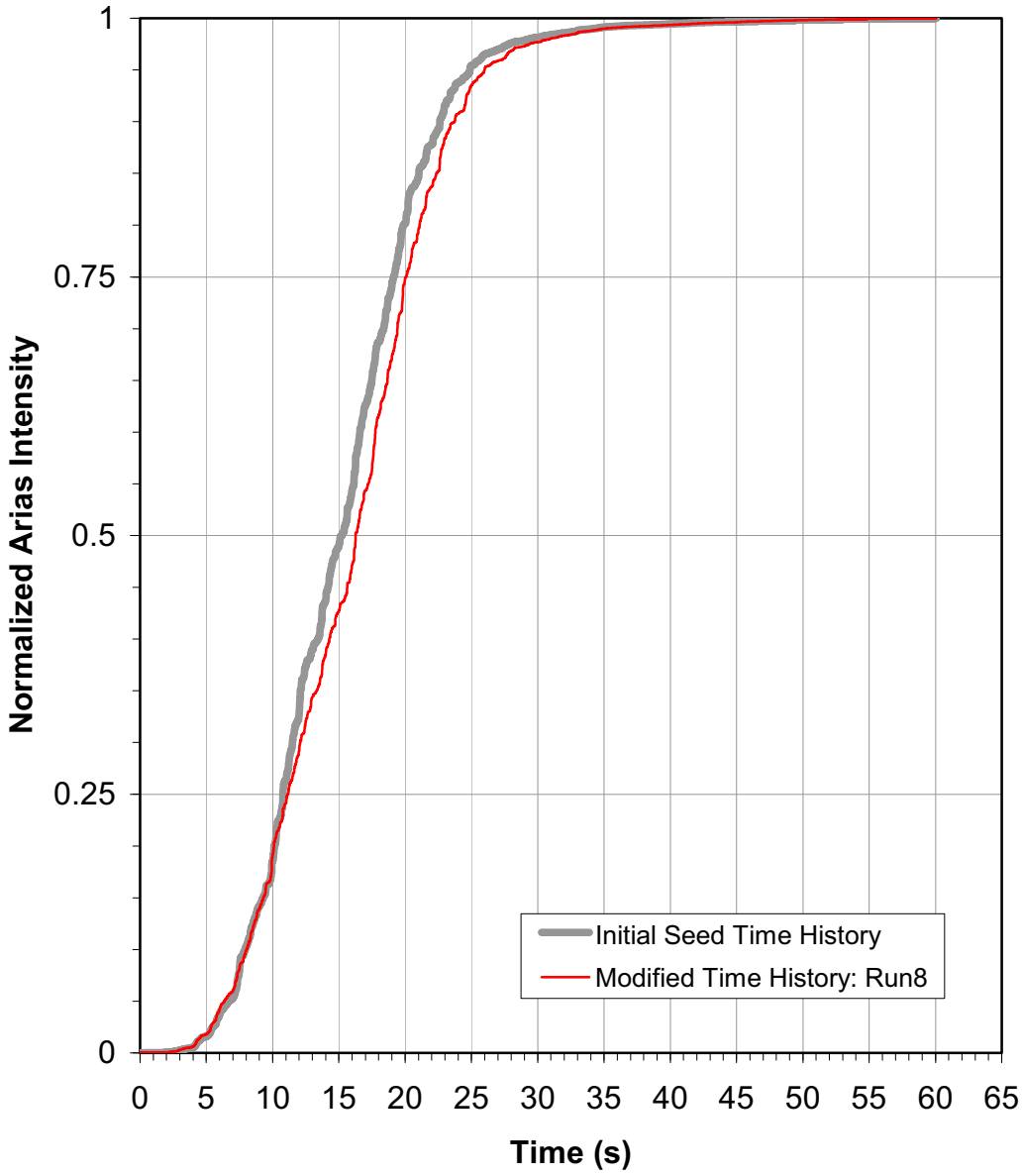

Figure 2.5.2-50c Comparison of Normalized Arias Intensity from Initial Seed Input Time History (Thick Grey Line) and Final Modified Spectrum Compatible Time History (Thin Red Line) Including Application of 1.01 Scale Factor for Vertical Component

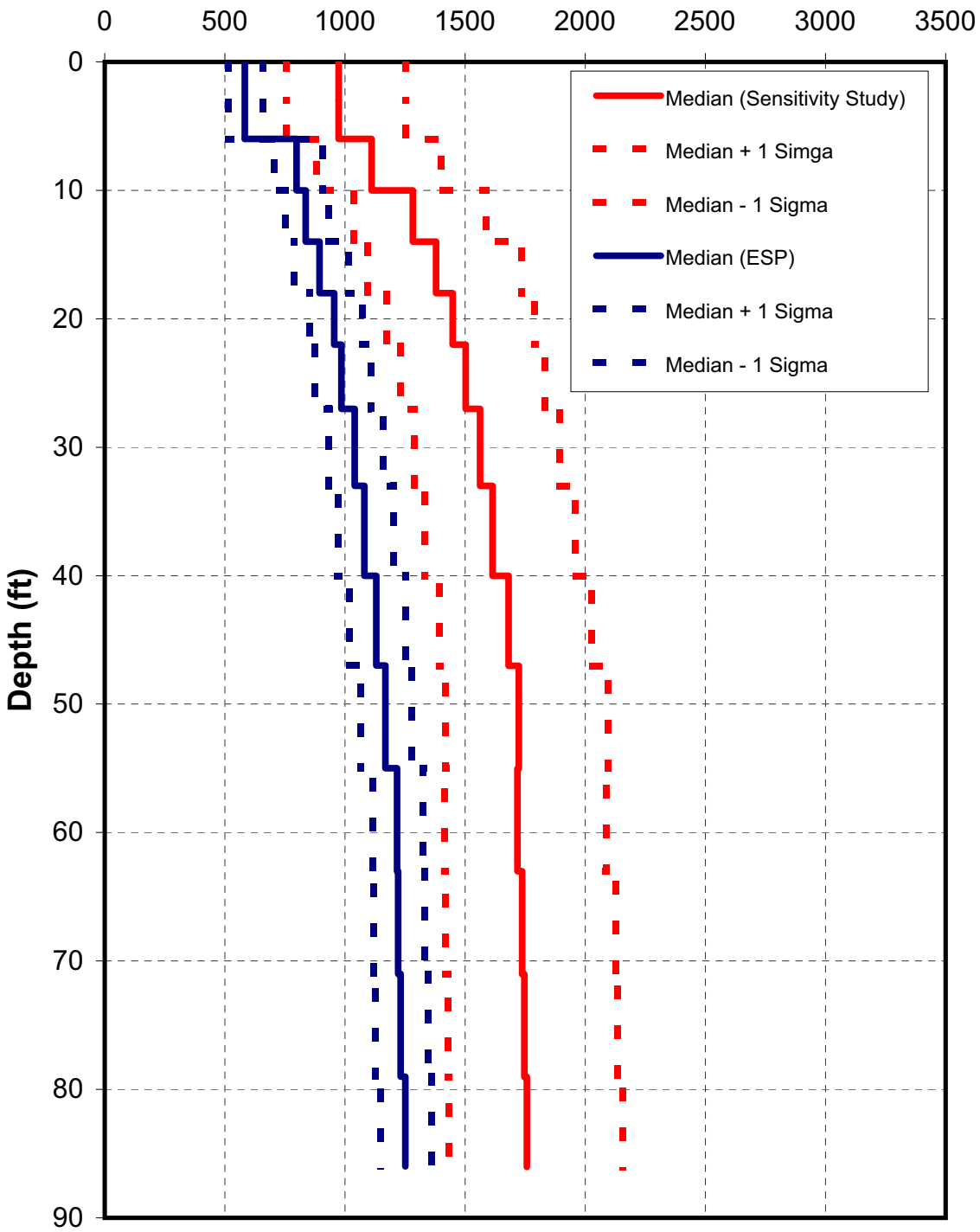

Figure 2.5.2-51 Low Strain Backfill Shear Wave Velocity (ft/sec)

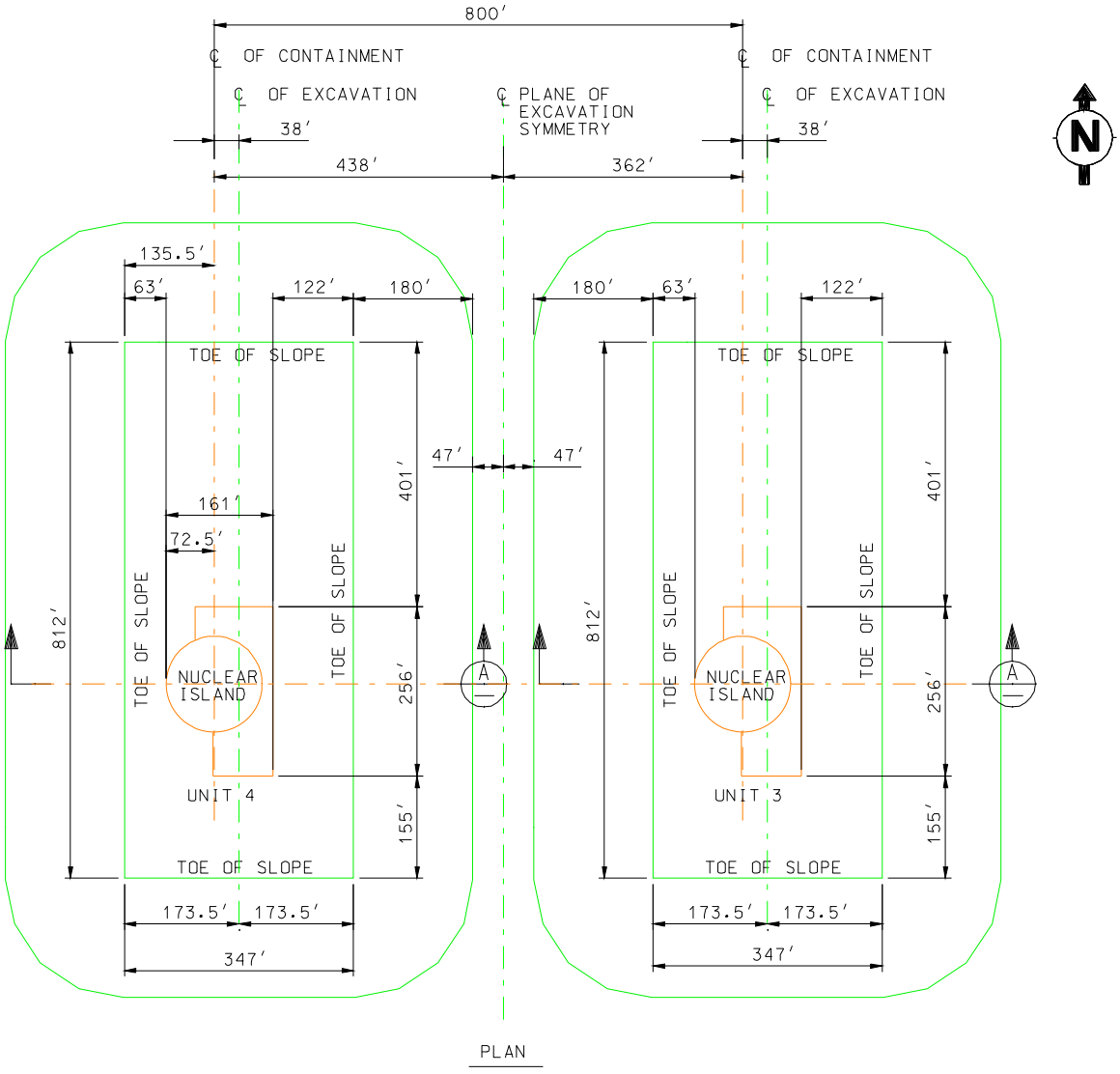

Figure 2.5.2-52 Plant Layout

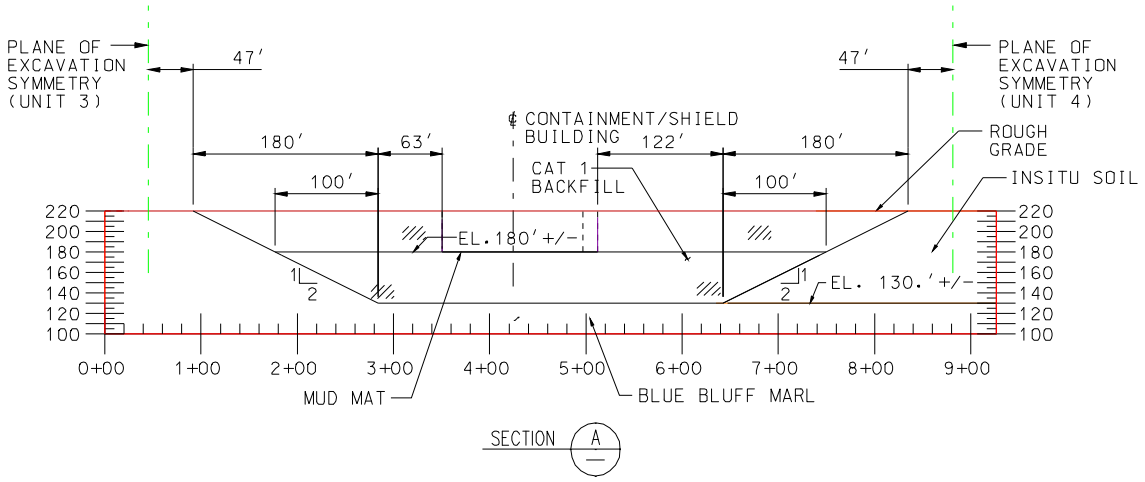

Figure 2.5.2-53 Cross Section A

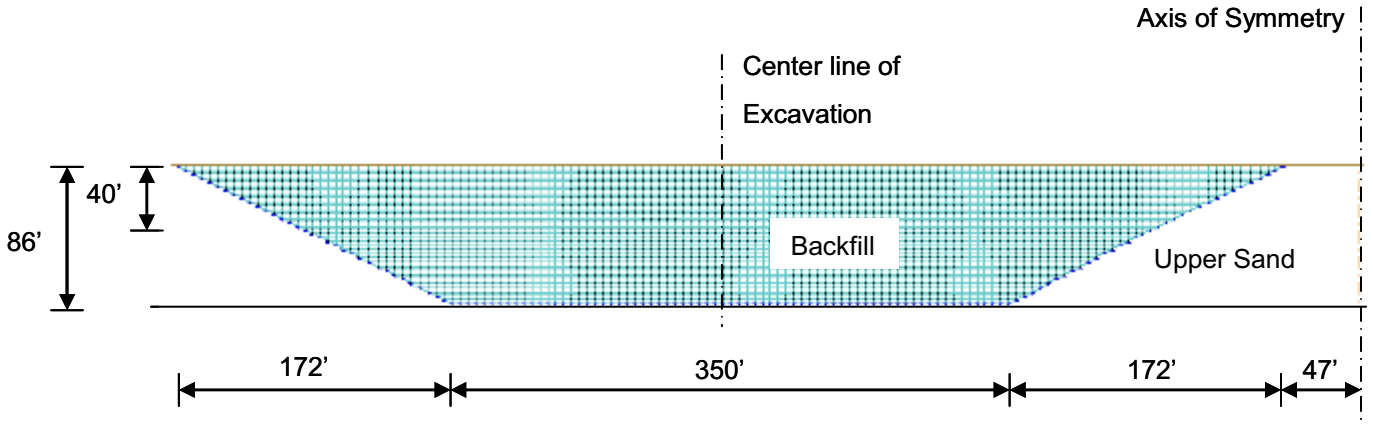

Figure 2.5.2-54 SASSI 2D-Model

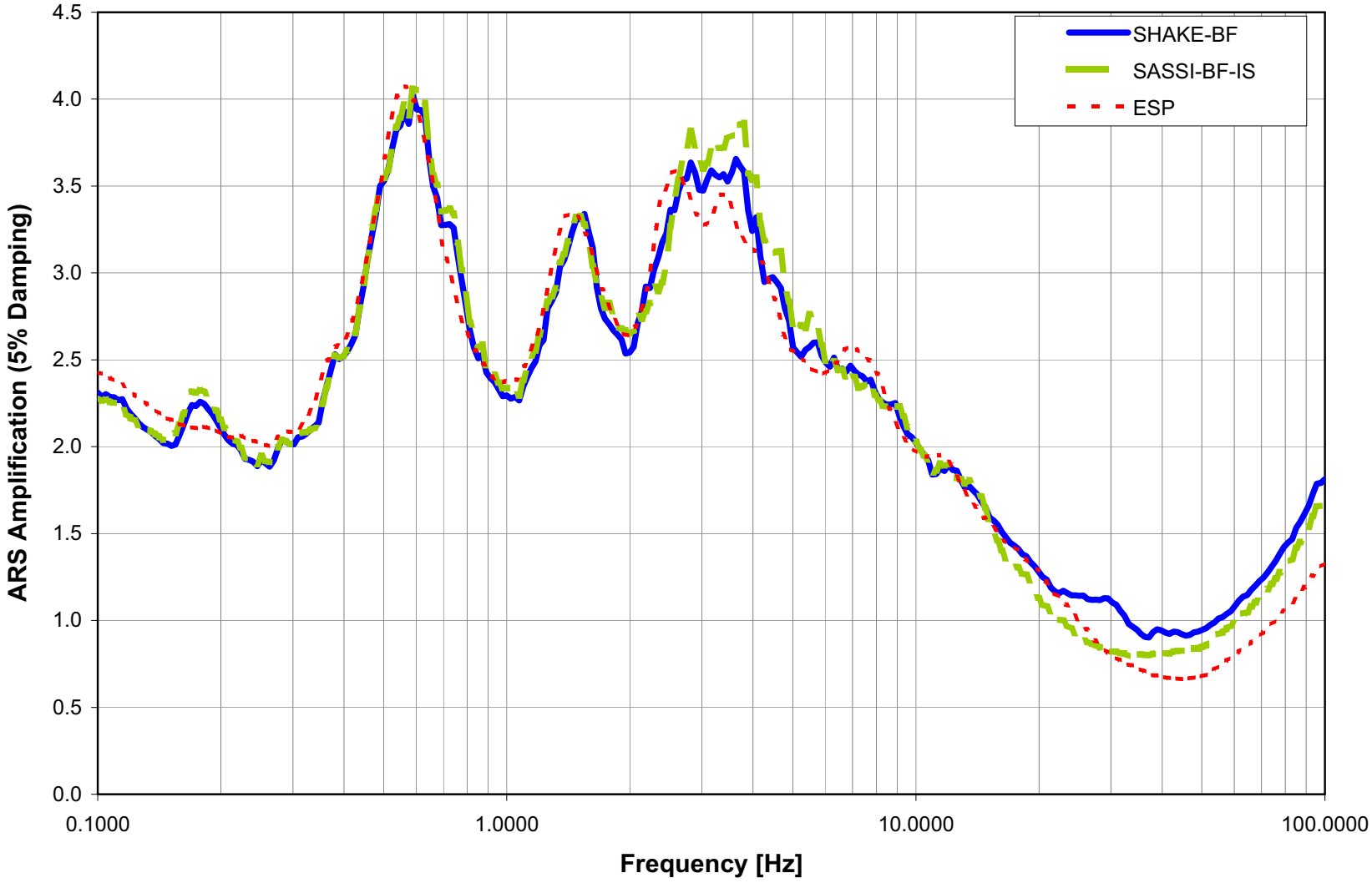

Figure 2.5.2-55 Amplification at 0 ft (GMRS Horizon)

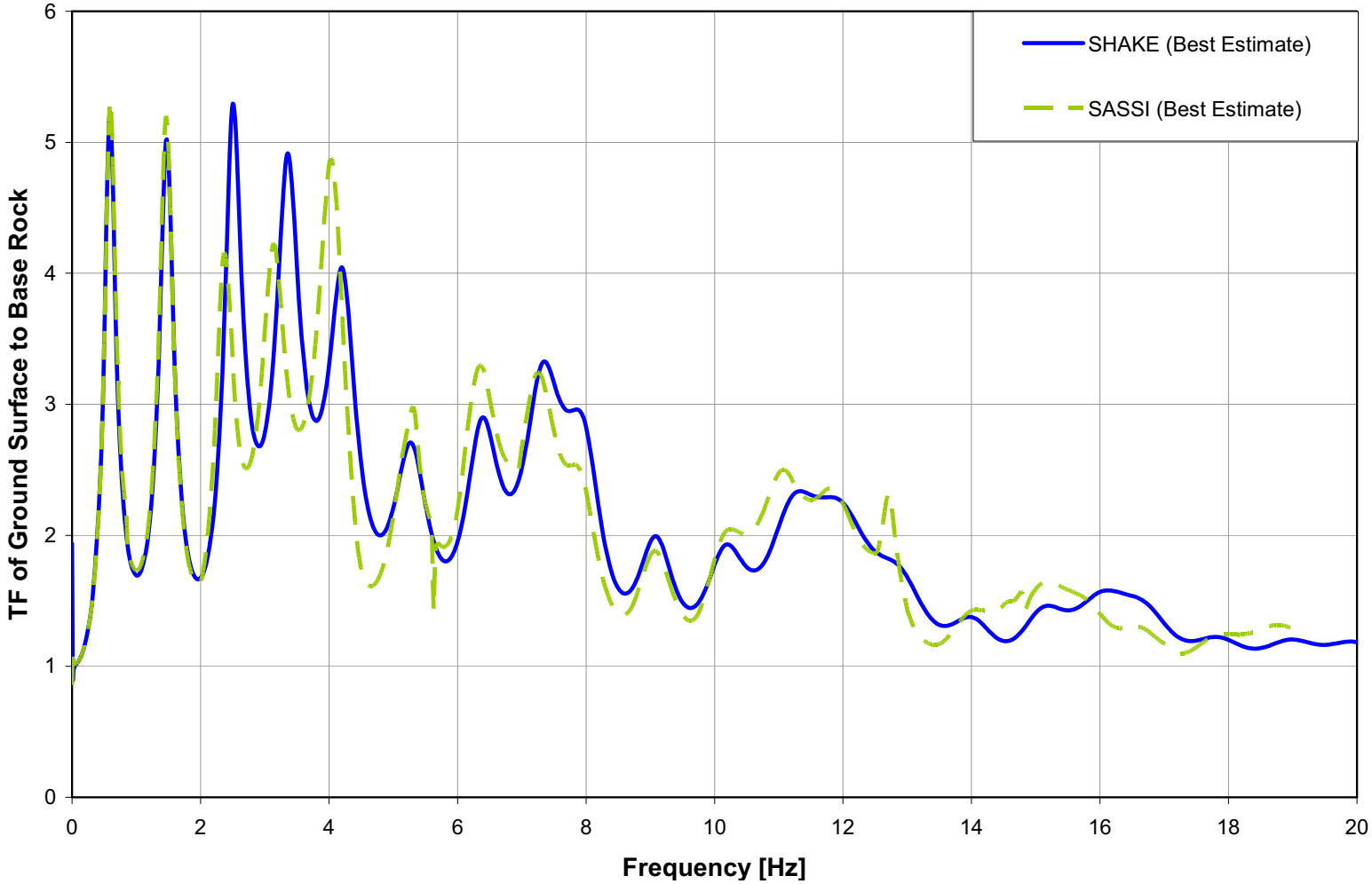

Figure 2.5.2-55a Transfer Functions at 0 ft (GMRS Horizon)

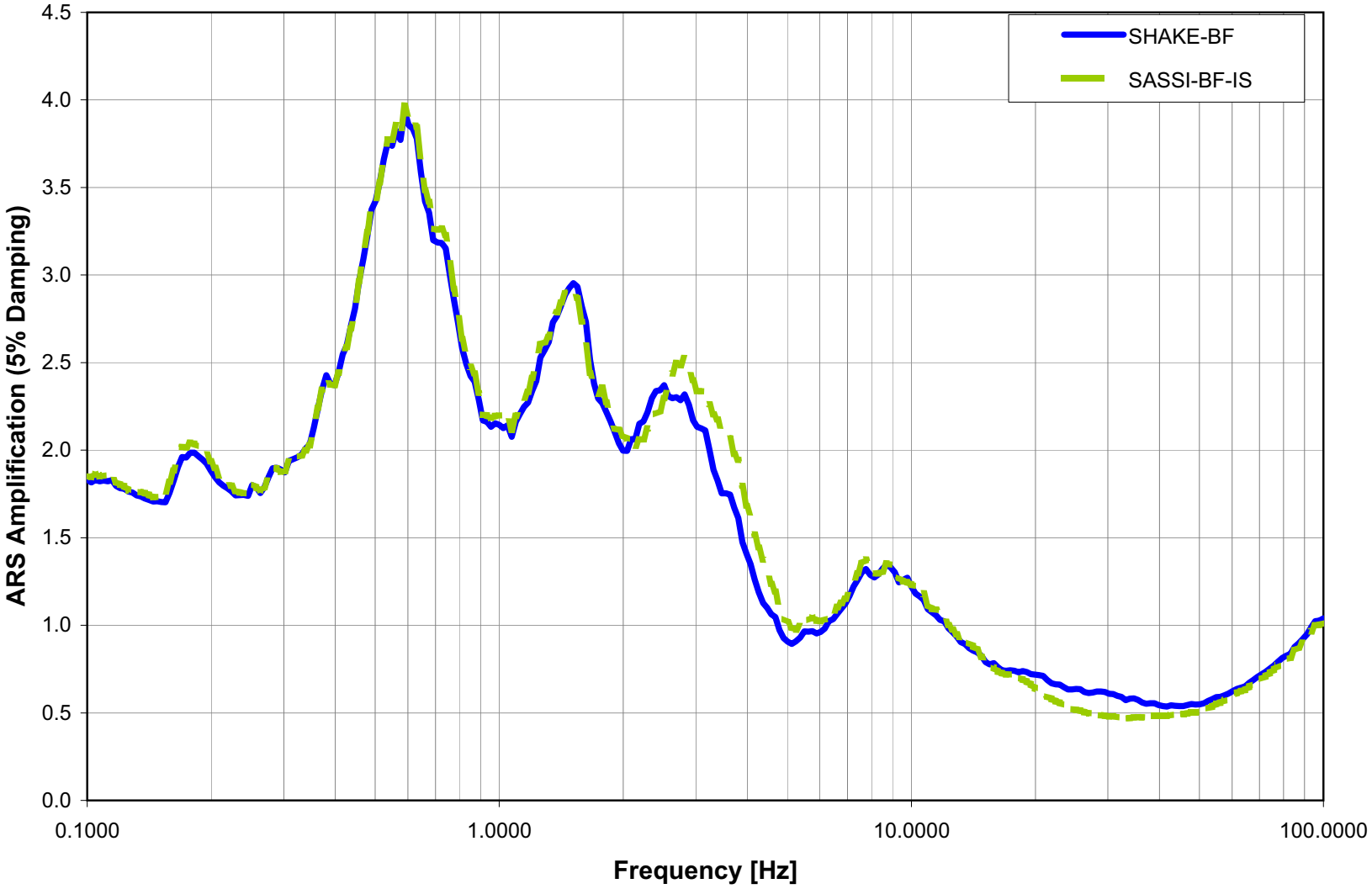

Figure 2.5.2-56 Amplification at 40 ft depth (FIRS horizon)

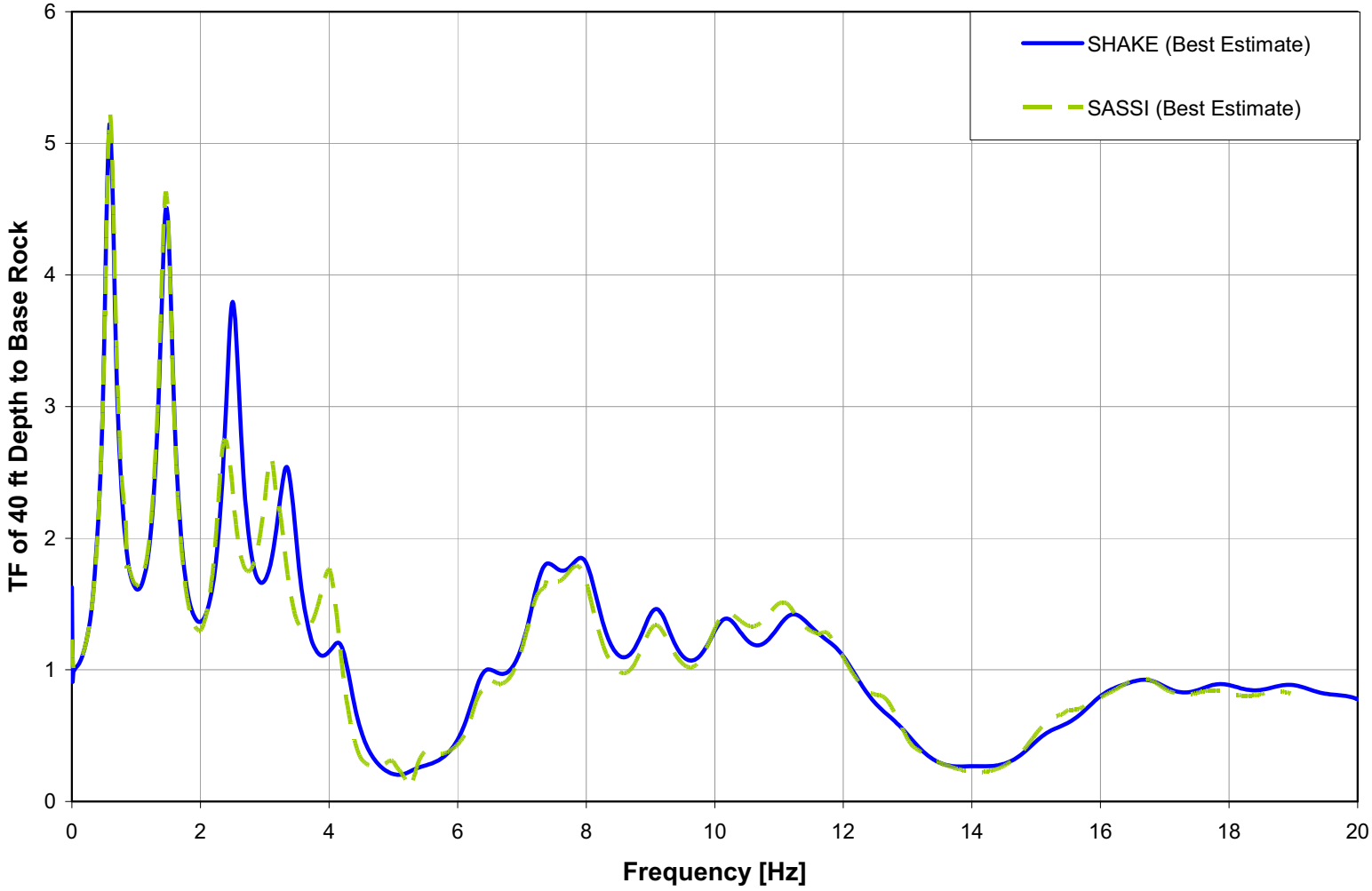

Figure 2.5.2-56a Transfer Functions at 40 ft (FIRS Horizon)

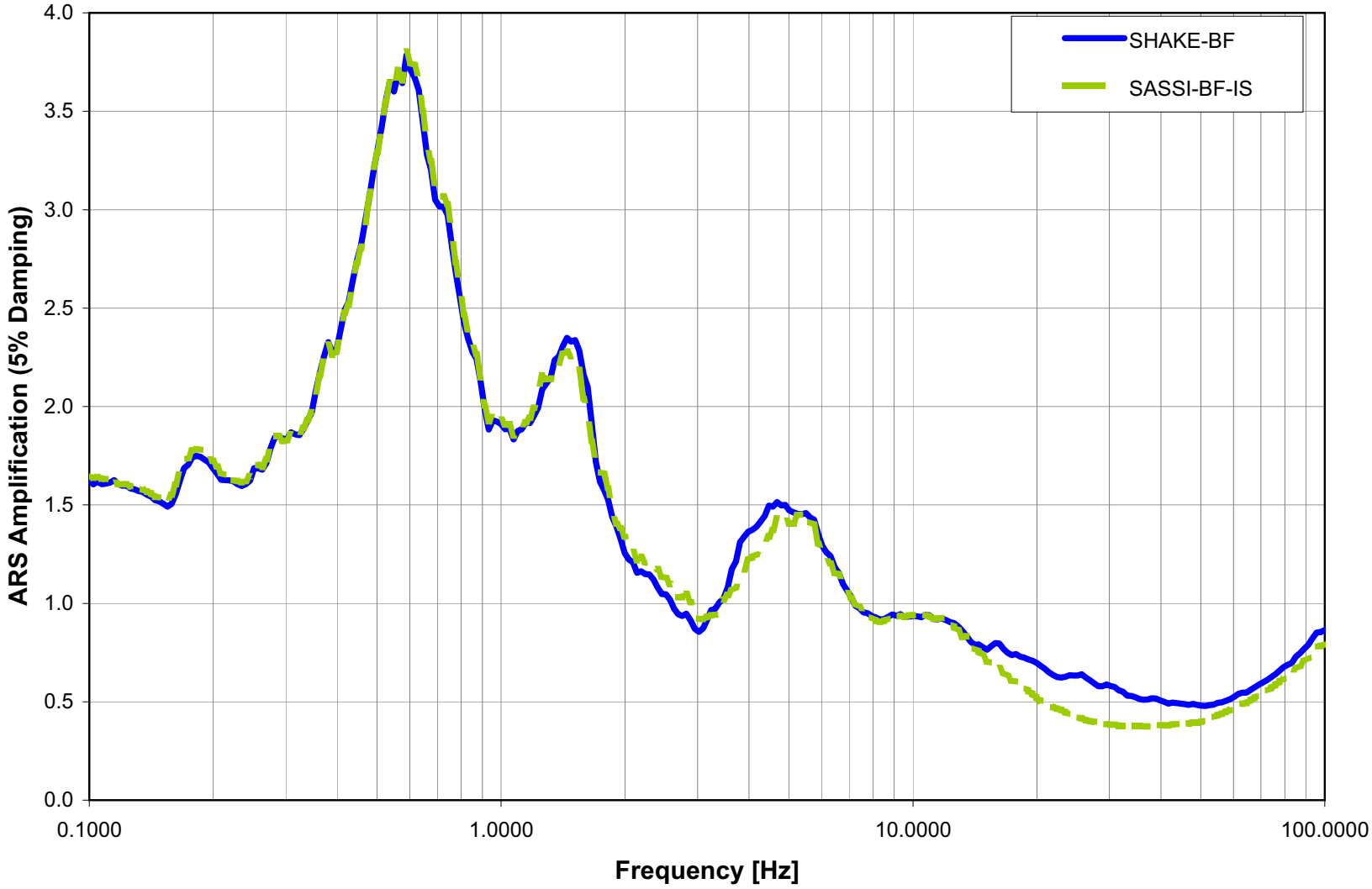

Figure 2.5.2-57 Amplification at 86 ft depth (Top of Blue Bluff Marl)

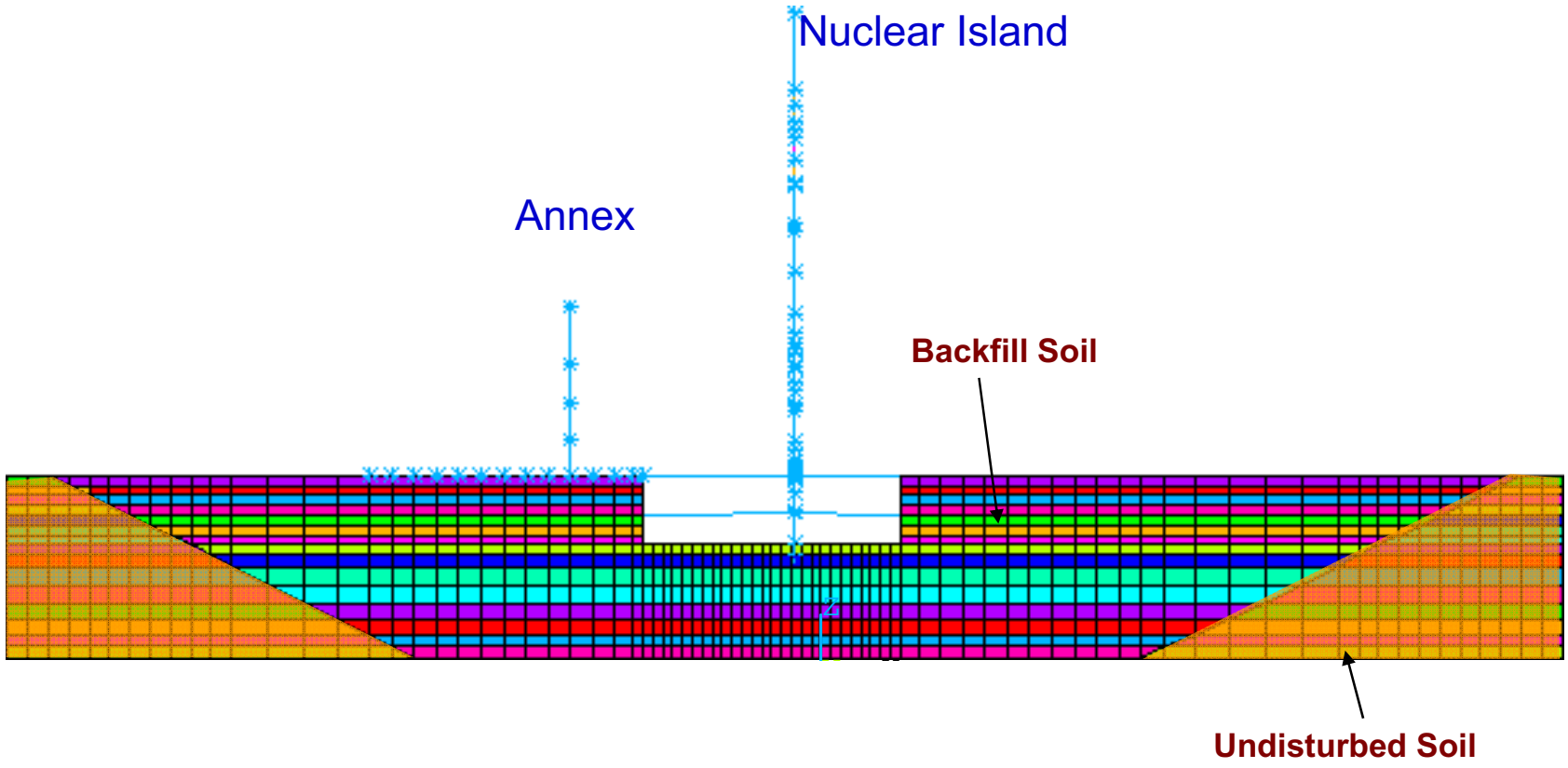

Figure 2.5.2-58 2D SASSI Backfill Model

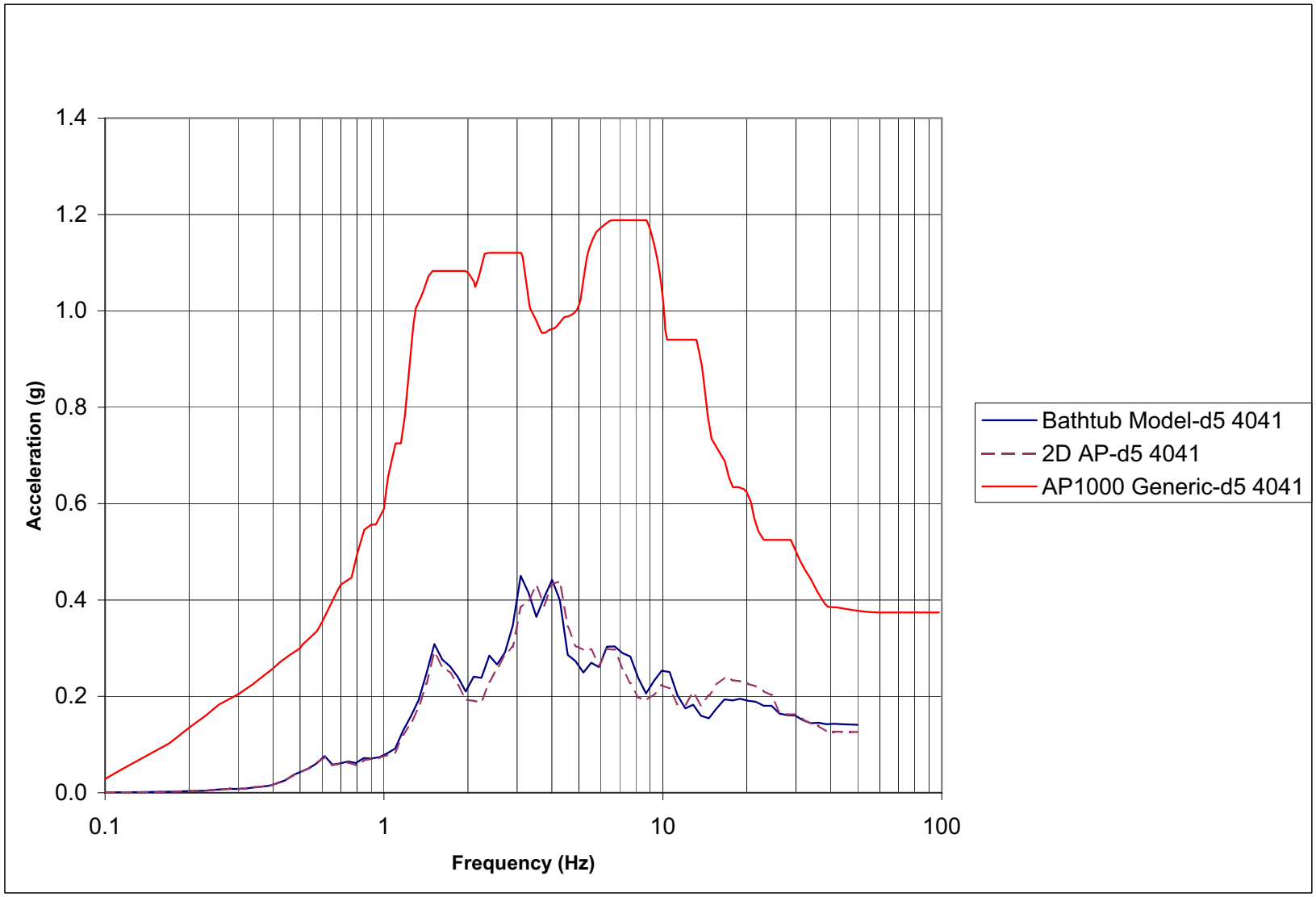

Figure 2.5.2-59 Node 4041 — EL 99.00 NI at Reactor Vessel Support Elevation

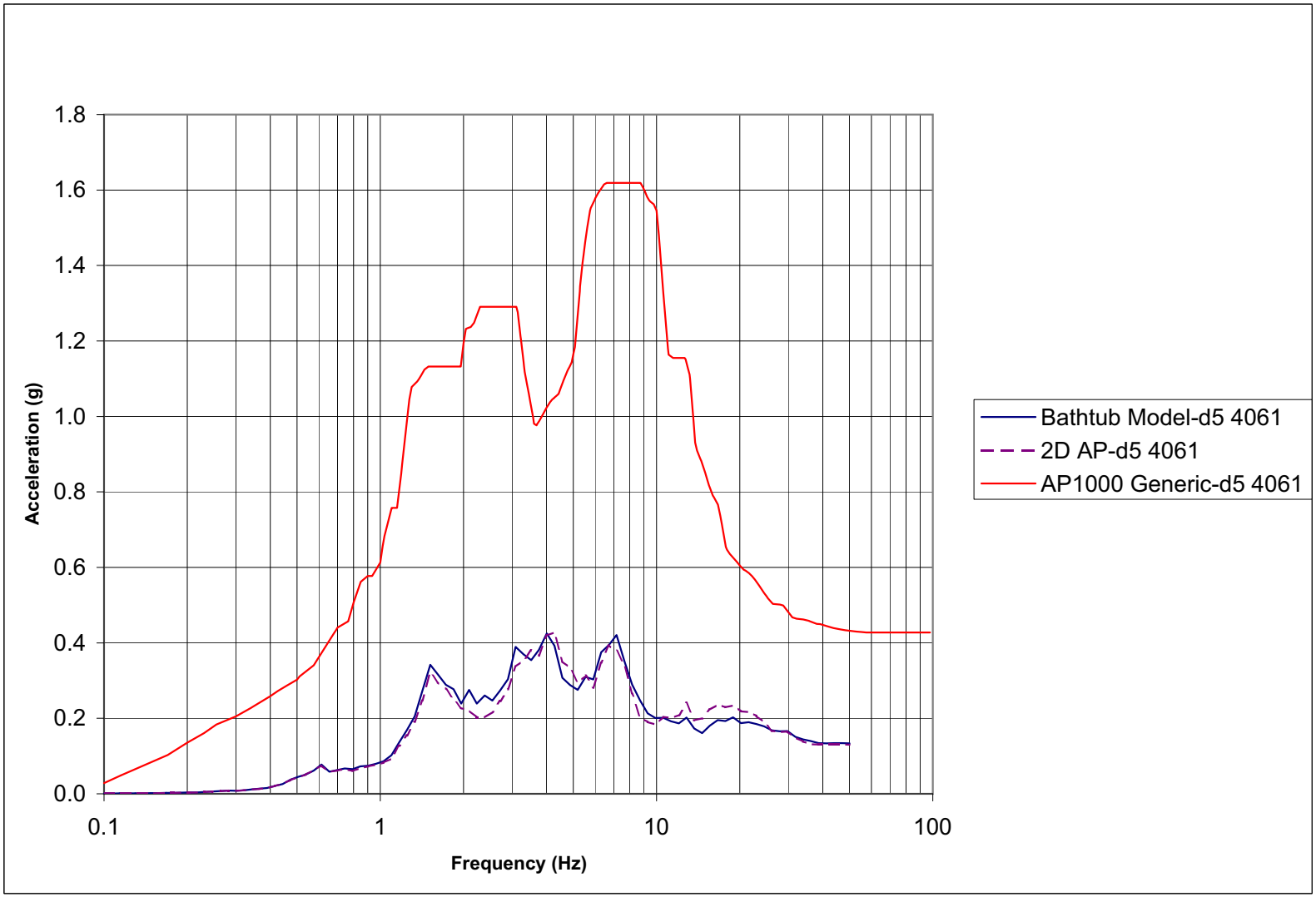

Figure 2.5.2-60 Node 4061 — EL 116.5 Auxiliary Shield Building at Control Room Floor

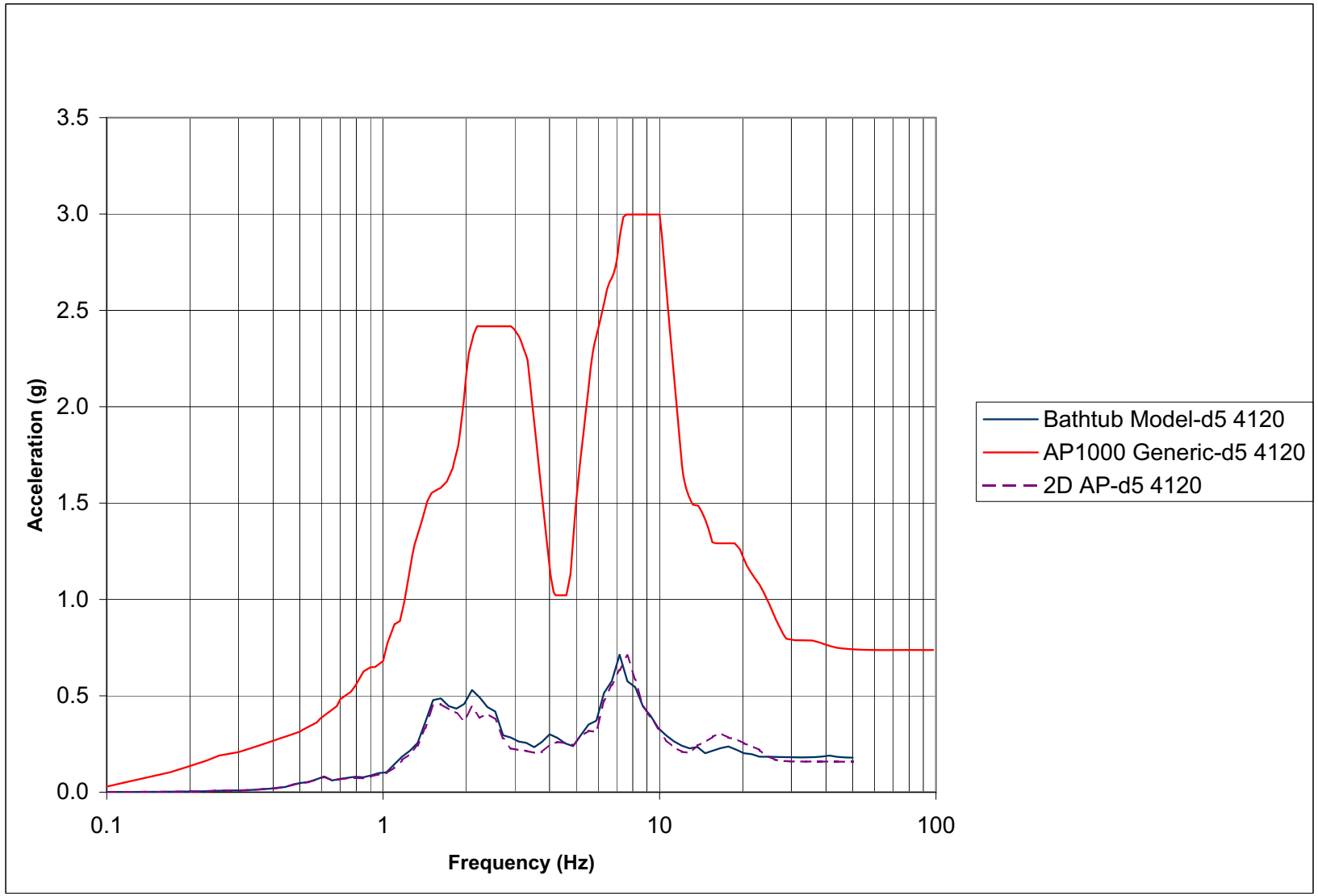

Figure 2.5.2-61 Node 4120 — EL 179.56 ASB Auxiliary Building Roof Area

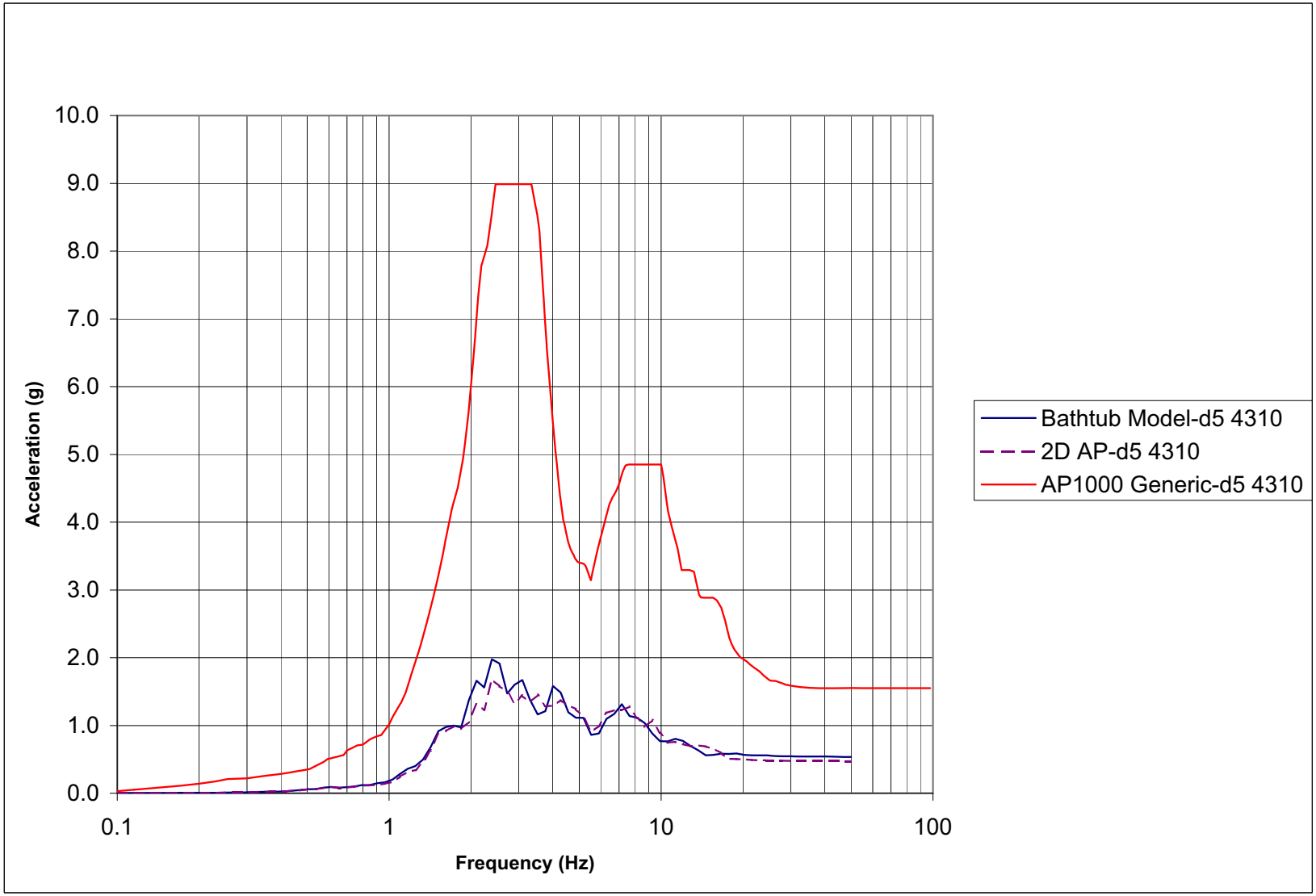

Figure 2.5.2-62 Node 4310 — EL 327.41 ASB Shield Building Roof Area

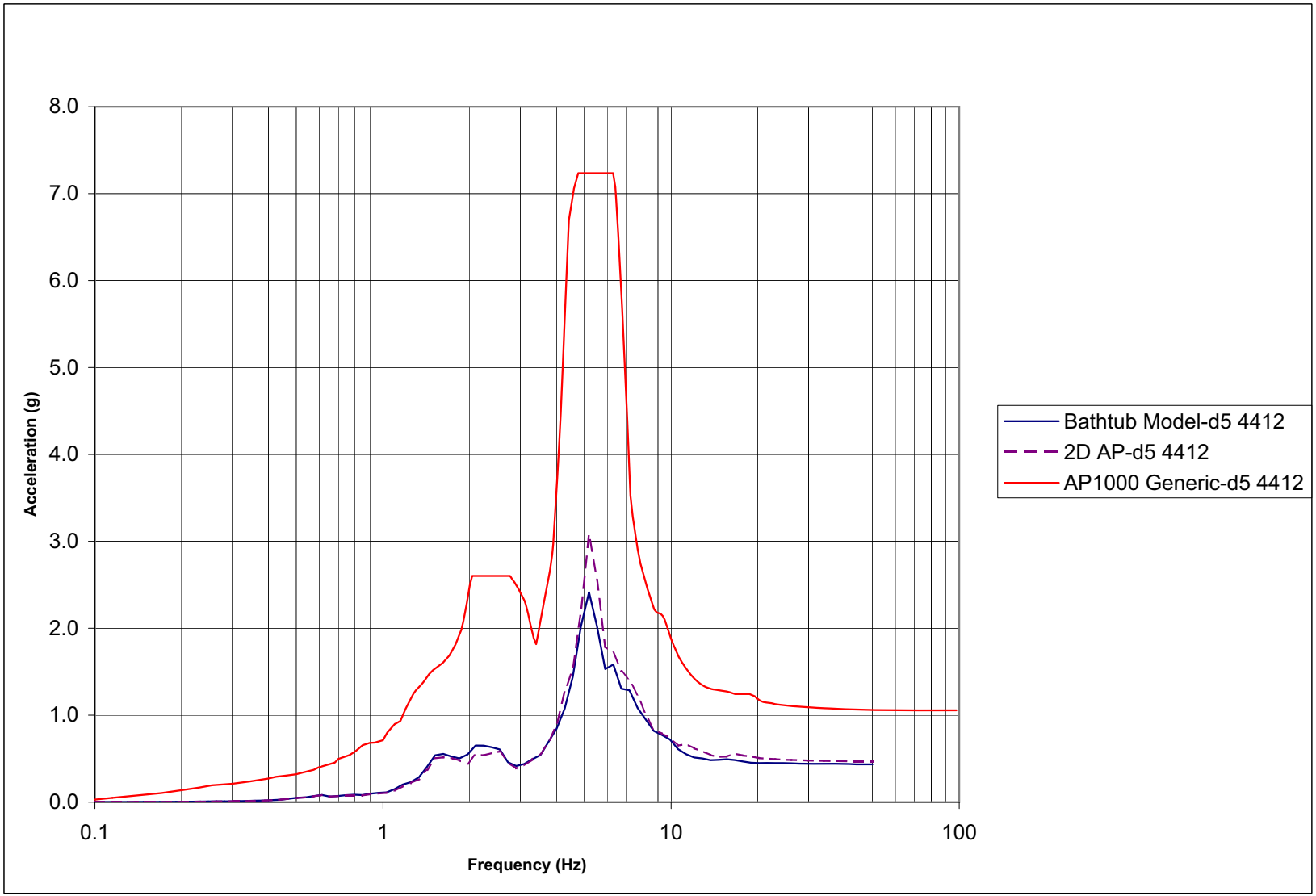

Figure 2.5.2-63 Node 4412 — EL 224 Steel Containment Vessel Near Polar Crane

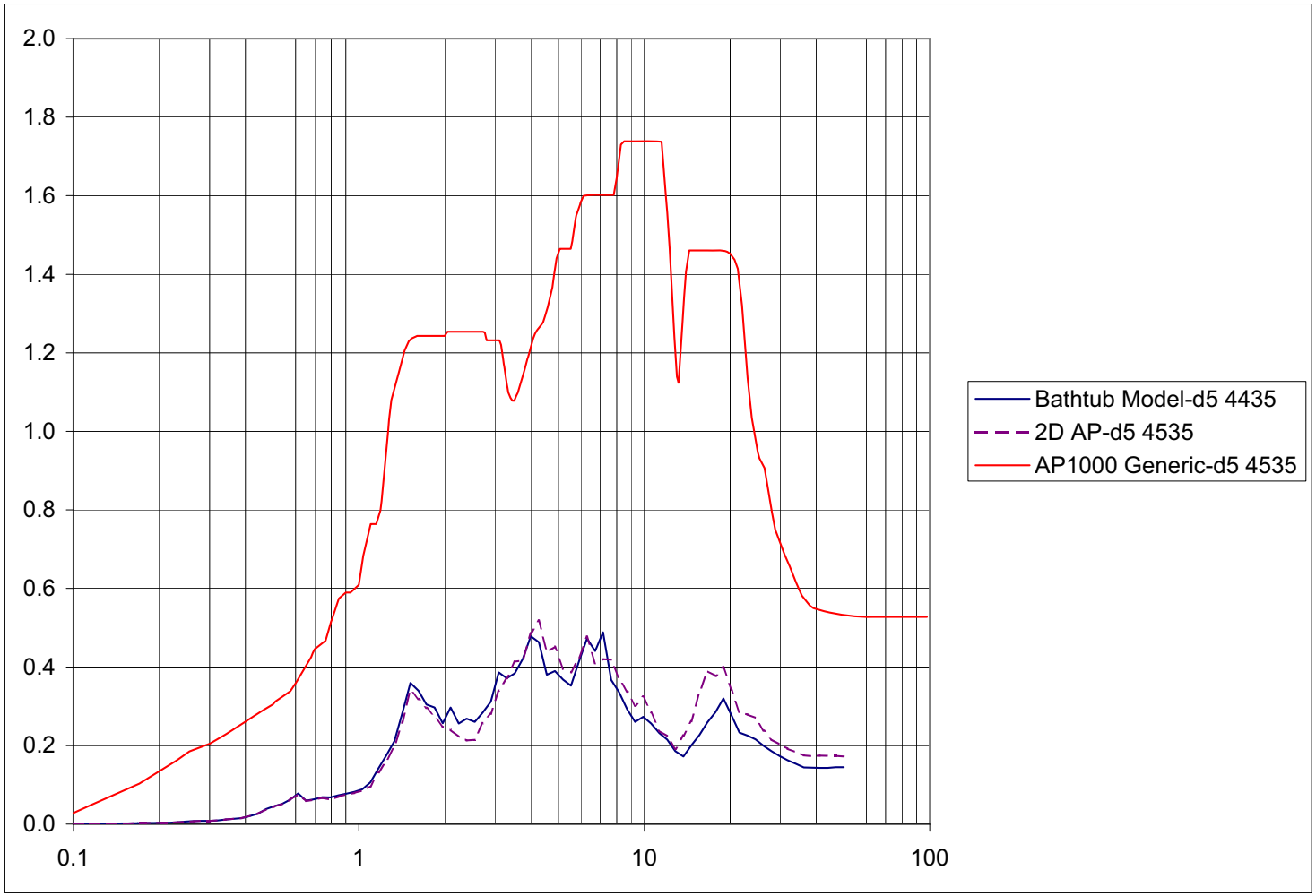

Figure 2.5.2-64 Node 4335 — EL 135.25 Containment Internal Structure at Operating Deck

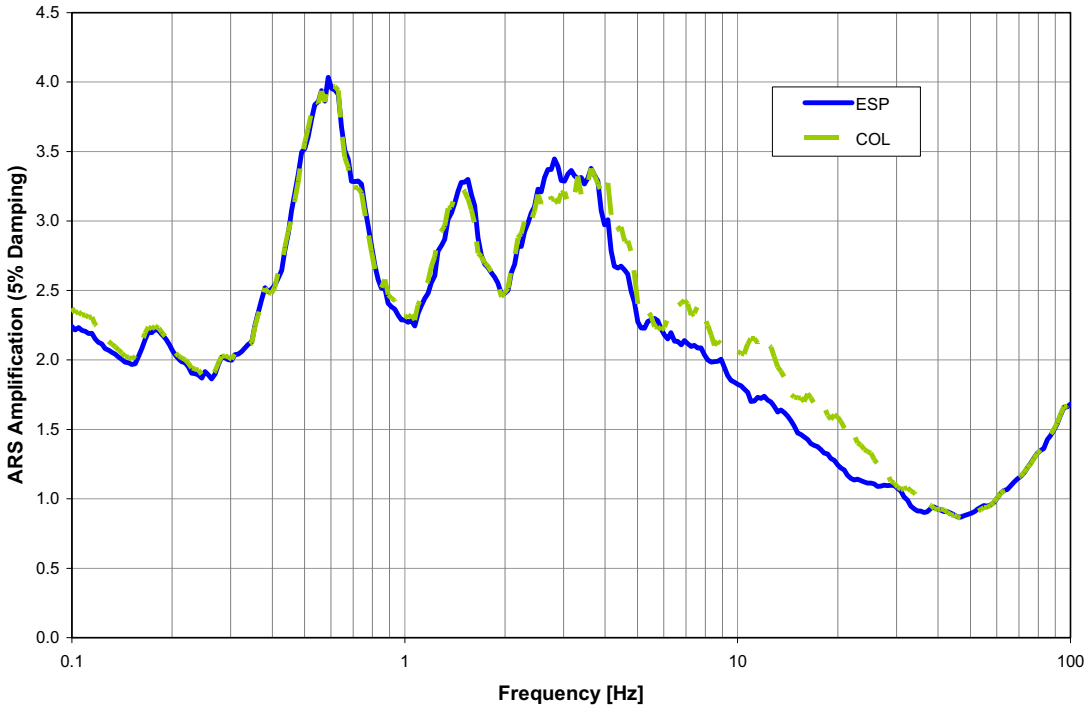

Figure 2.5.2-65 Amplification at 40-ft Outcrop Depth (FIRS Horizon)

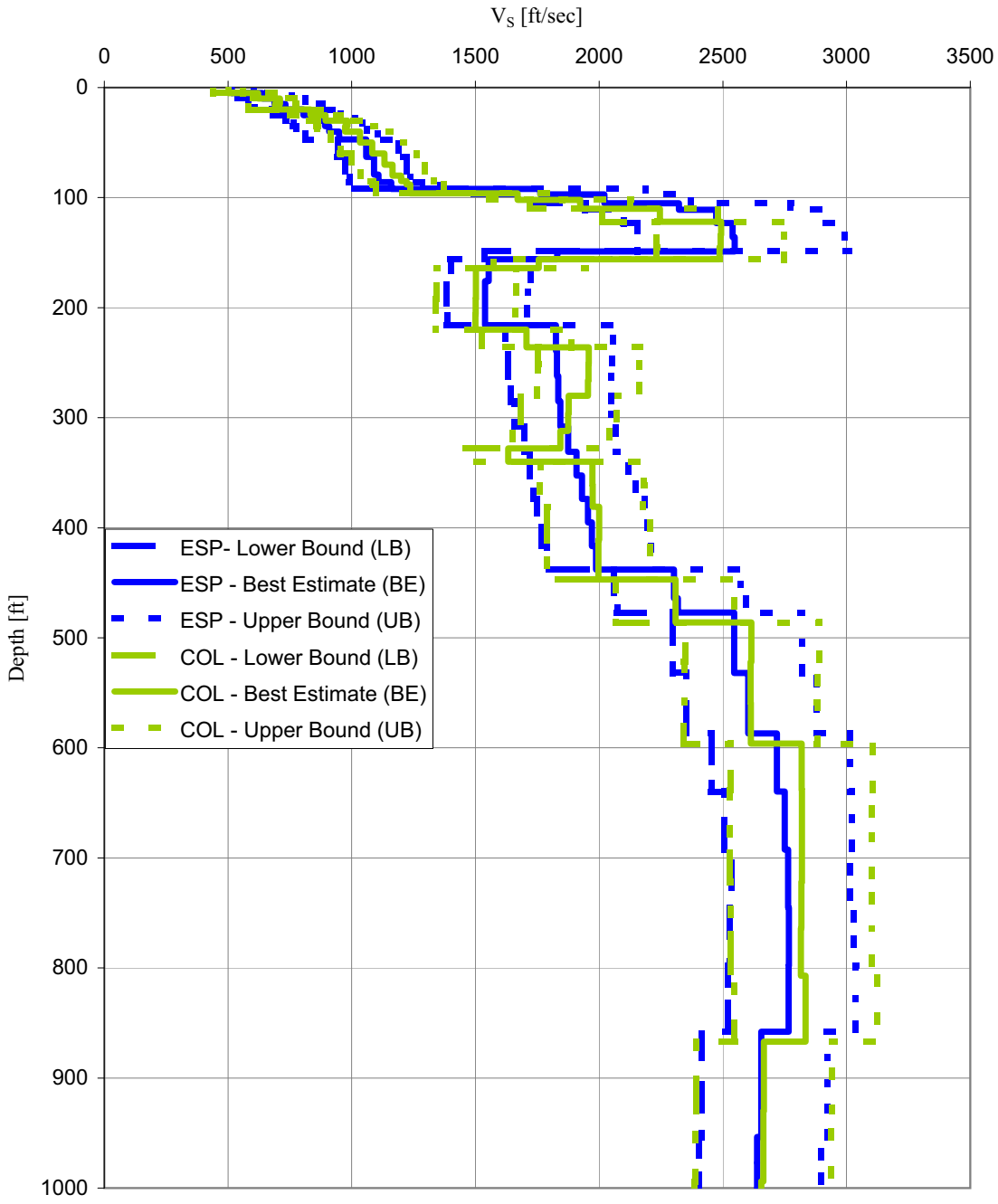

Figure 2.5.2-65a Vogtle Strain Compatible Profiles (S-Wave Velocity)

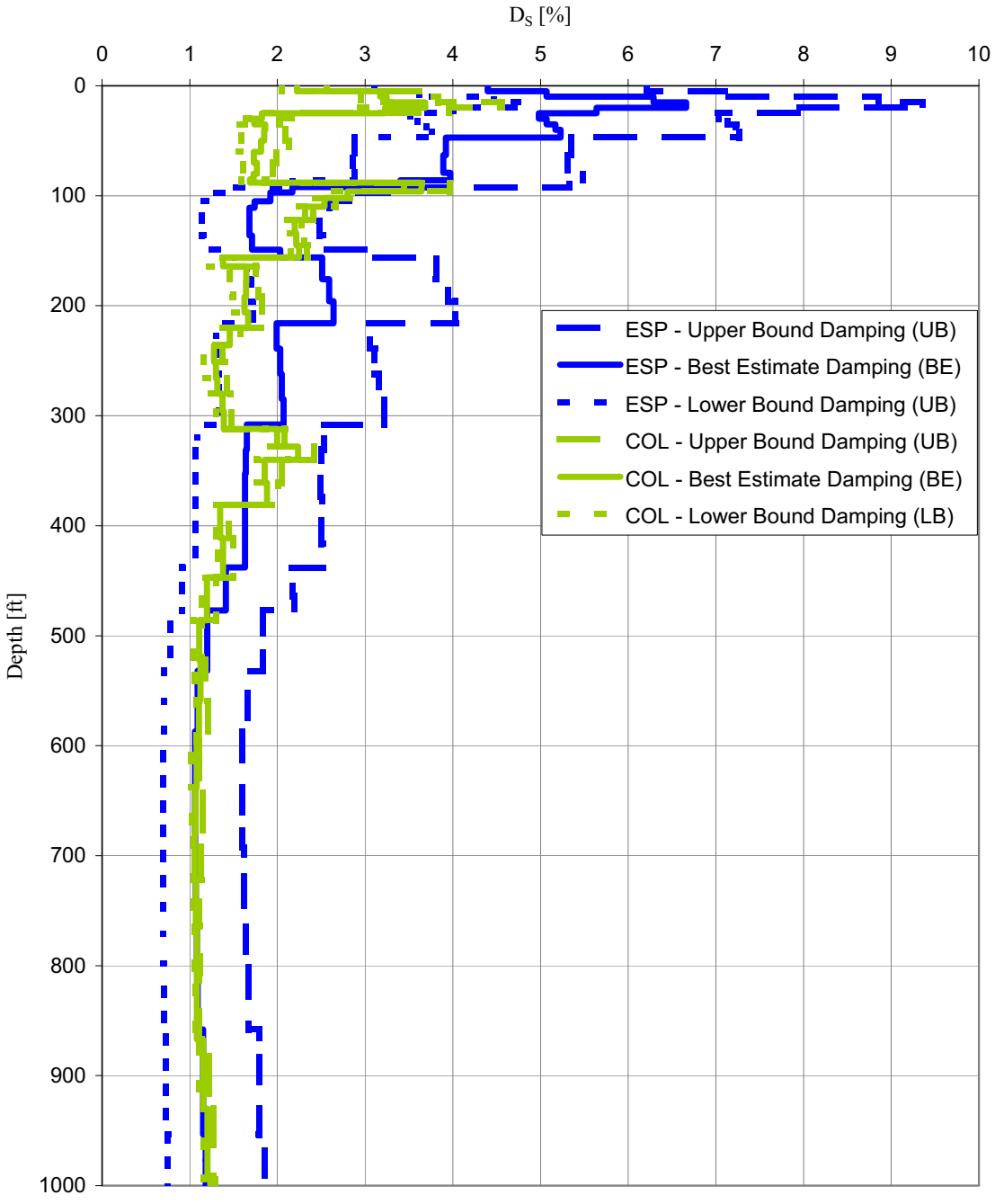

Figure 2.5.2-65b Vogtle Strain Compatible Profiles (S-Wave Damping)

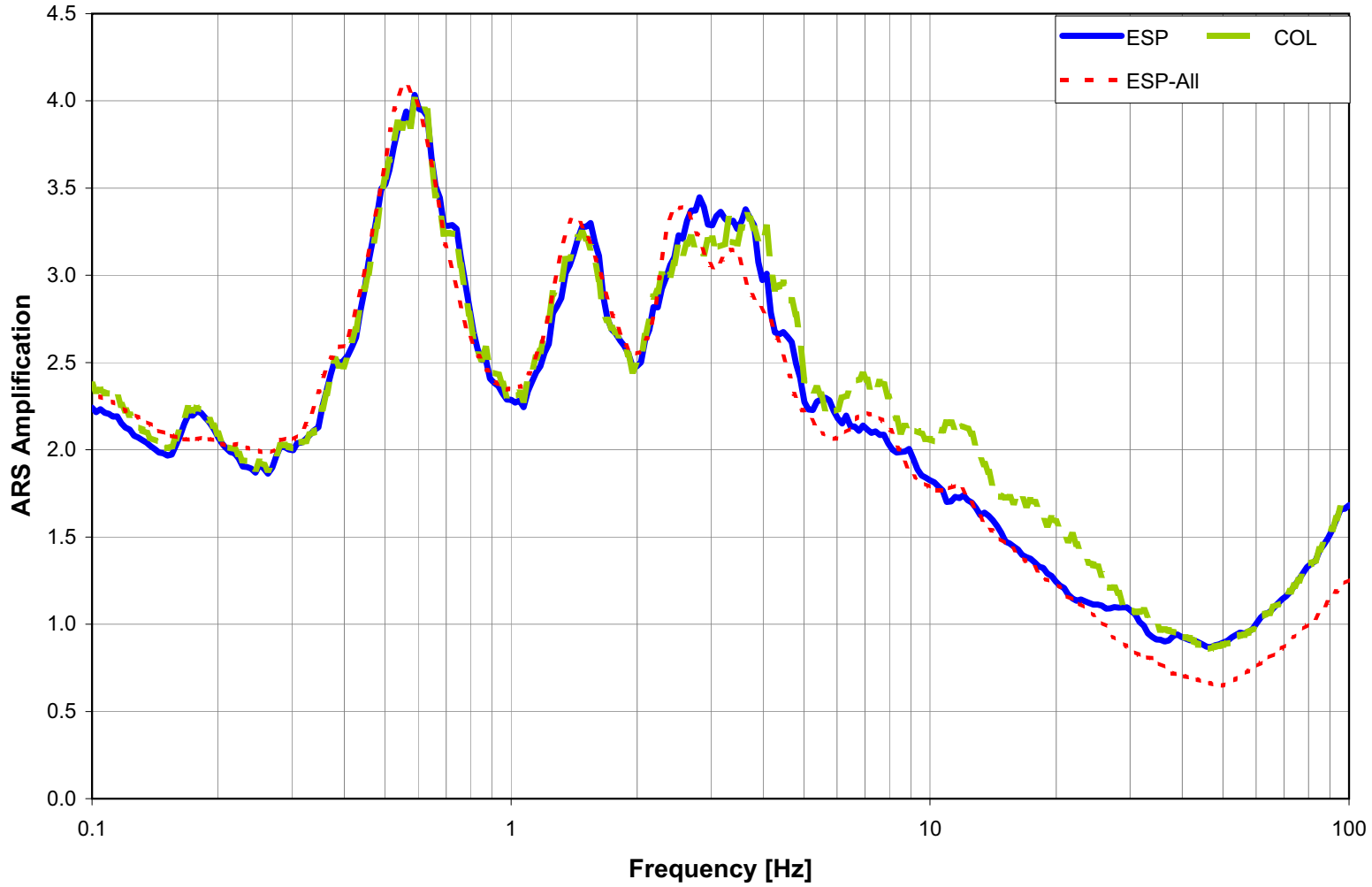

Figure 2.5.2-65c Envelope at 40 ft Depth (FIRS Horizon)

Section 2.5.2 References

(Abrahamson and Silva 1997) Abrahamson, N. N.,A. and W. J. Silva. “Empirical response spectral attenuation relations for shallow crustal earthquakes,” Bull. Seism. Soc. Am.,Empirical Response Spectral Attenuation Relations for Shallow Crustal Earthquakes, Seismological Research Letters, v. 68, n. 1, 94-127, Jan/Feb 1997.

(Amick 1990) Amick, D., Paleoliquefaction Investigations Along the Atlantic Seaboard With Emphasis on the Prehistoric Earthquake Chronology of Coastal South Carolina, unpub. Ph.D. dissertation, University of South Carolina, selected pages, 1990.

(Amick et al. 1990a) Amick, D., Gelinas, R., Maurath, G., Cannon, R., Moore, D., Billington, E., and Kemppinen, H., Paleoliquefaction Features Along the Atlantic Seaboard, U.S. Nuclear Regulatory Commission Report, NUREG/CR-5613, 147p., 1990a.

(Amick et al. 1990b) Amick, D., Maurath, G., and Gelinas, R., Characteristics of Seismically Induced Liquefaction Sites and Features Located In the Vicinity of the 1886 Charleston, South Carolina Earthquake, Seismological Research Letters, v. 61, no. 2, p. 117-130, 1990b.

(ANSS 2005) The Advanced National Seismic System catalog is website: http:// quake.geo.berkeley.edu/anss/catalog-search.html. Catsearch.16391.txt, 27 pages, downloaded on June 3, 2005.

(ASCE 2005) American Society of Civil Engineers, “Seismic Design Criteria for Structures, Systems, and Components in Nuclear Facilities”, ASCE/SEI 43-05, 2005.

(Atkinson and Boore 1995) Atkinson, G. M. and D. M. Boore, Ground-Motion Relations for Eastern North America. Bull. Seism. Soc. Am., v. 85, n. 1, 17-30 (1995).

(Bakun and Hopper 2004) Bakun, W. H. and Hopper, M. G., Magnitudes and Locations of the 1811-1812 New Madrid, Missouri, and the 1886 Charleston, South Carolina, Earthquakes, Bulletin of the Seismological Society of America, v. 94, no. 1, p. 64-75, 2004.

(Bechtel 1984) Bechtel Power Corporation, Seismic Analysis Report, Vogtle Nuclear Generating Plant Units 1 and 2, October 1984.

(Bechtel 2000) Bechtel Corporation, *Theoretical and User’s Manual for SHAKE 2000*, prepared by N Deng and F Ostadan, San Francisco, CA, 2000.

(Bechtel 2006d) Lindvall, S. C. and Hartleb, R. D., Update of Charleston Seismic Source and Integration with EPRI Source Models, Bechtel engineering study report 25144-006-V14-CY06-00006, revision 001, 2006.

(Behrendt and Yuan 1987) Behrendt, J. C. and Yuan, A., The Helena Banks Strike-slip (?) Fault Zone in the Charleston, South Carolina, Earthquake Area: Results From a Marine, High-resolution, Multichannel, Seismic-reflection Survey, Geological Society of America Bulletin, v. 98, p. 591-601, 1987.

(Behrendt et al 1981) Behrendt, J. C., Hamilton, R. M., Ackermann, H. D., and Henry, V. J., Cenozoic Faulting in the Vicinity of the Charleston, South Carolina, 1886 Earthquake: Geology, v. 9, no. 3, p. 117-122, 1981.

(Behrendt et al 1983) Behrendt, J. C., Hamilton, R. M., Ackermann, H. D., Henry, V. J., and Bayer, K. C., Marine Multichannel Seismic-reflection Evidence for Cenozoic Faulting and Deep Crustal Structure Near Charleston, South Carolina: U. S. Geological Survey Professional Paper 1313-J, p. J1-J29, 1983.

(Behrendt et al 1988) Behrendt, J. C., Klitgord, K. D., and Hutchinson, D. R., Reactivated Boundary Fault Zones of Buried Early Mesozoic Basins as Possible Sources of Seismicity in the Charleston, S.C. Region: Abstracts with Programs - Geological Society of America Southeastern Section, v. 20, no. 4, p. 253, 1988.

(Bollinger 1977) Bollinger, G. A., Reinterpretation of the Intensity Data for the 1886 Charleston, South Carolina, Earthquake in Studies Related to the Charleston, South Carolina, Earthquake of 1886- A Preliminary Report (D. W. Rankin, ed.), U. S. Geological Survey Professional Paper 1028, p. 17-32, 1977.

(Bollinger 1992) Bollinger, G. A. Specification of Source Zones, Recurrence Rates, Focal Depths, and Maximum Magnitudes for Earthquakes Affecting the Savannah River Site in South Carolina, U.S. Geological Survey Bulletin 2017, 1992.

(Bollinger et al. 1985) Bollinger, G. A., Chapman, M. C., Sibol, M. S., and Costain, J. K., An analysis of earthquake focal depths in the southeastern U. S., Geophysical Research Letters, v. 12, no. 11, p. 785-788, 1985.

(Bollinger et al. 1991) Bollinger, G. A., Johnston, A. C., Talwani, P., Long, L. T., Shedlock, K. M., Sibol, M. S., and Chapman, M. C., Seismicity of the Southeastern United States; 1698-1986 in Neotectonics of North America, Decade Map Volume to Accompany the Neotectonic Maps (D. B. Slemmons, E. R. Engdahl, M. D. Zoback, D. B. Blackwell, eds.), p. 291-308, 1991.

(Bronk Ramsey 1995) Bronk Ramsey, C., Radiocarbon calibration and analysis of stratigraphy: the OxCal program, Radiocarbon, v. 37, no. 2, p. 425-430, 1995.

(Bronk Ramsey 2001) Bronk Ramsey, C., Development of the radiocarbon program OxCal: Radiocarbon, v. 43, no. 2A, p. 355-363, 2001.

(Chapman 2005b) Chapman, M., Personal Communication, 2005.

(Chapman and Talwani 2002) Chapman, M. C. and Talwani. P., Seismic Hazard Mapping for Bridge and Highway Design in South Carolina, South Carolina Department of Transportation Report, 2002.

(Chapman et al. 2002) Chapman, M. C., Munsey, J. W., Powell, C. A., Whisner, S. C., and Whisner J., The Eastern Tennessee Seismic Zone - Summary after 20 Years of Network Monitoring: Seismological Research Letters, v. 73, no. 2, p. 245, 2002.

(Colquhoun et al. 1983) Colquhoun, D. J., Woollen, I. D., Van Nieuwenhuise, D. S., Padgett, G. G., Oldham, R. W., Boylan, D. C., Bishop, J. W., and Howell, P. D. Surface and Subsurface Stratigraphy, Structure and Aquifers of the South Carolina Coastal Plain: SCDHEC Report ISBN 0-9613154-0-7, 78 p., 1983.

(Cook et al. 1979) Cook, F. A., Albaugh, D. S., Brown, L. D., Kaufman, S., Oliver, J. E., Hatcher, R. D. Jr., Thin-skinned Tectonics in the Crystalline Southern Appalachians: COCORP Seismic Reflection Profiling of the Blue Ridge and Piedmont. Geology, vol. 7, p. 563-567, 1979.

(Cook et al. 1981) Cook, F.A., L.D. Brown, S. Kaufman, J.E. Oliver, and T.A. Petersen, COCORP Seismic Profiling of the Appalachian Orogen Beneath the Coastal Plain of Georgia, Geological Society of America Bulletin, v. 92, no. 10, p. 738-748, 1981.

(Costantino, 1996) Costantino, C. J. (1996). Recommendations for Uncertainty Estimates in Shear Modulus Reduction and Hysteretic Damping Relationships. Published as an appendix in Silva, W. J., N. Abrahamson, G. Toro and C. Costantino (1997). "Description and validation of the stochastic ground motion model." Report Submitted to Brookhaven National Laboratory, Associated Universities, Inc. Upton, New York 11973, Contract No. 770573.

(Cornell 1968) Cornell, C. A., Engineering Seismic Risk Analysis, Bulletin of the Seismological Society of America, v. 58, no. 5, p. 1583-1606, 1968.

(Cornell and Winterstein 1988) Cornell, C. A. and Winterstein, S. R., Temporal and Magnitude Dependence in Earthquake Recurrence Models, Bulletin of the Seismological Society of America, v. 79, p. 1522-1537, 1988.

(Cramer 2001) Cramer, C. H., A Seismic Hazard Uncertainty Analysis for the New Madrid Seismic Zone, Engineering Geology, v. 62, p. 251-266, 2001.

(Ellsworth et al. 1999a) Ellsworth, W. L., Matthews, M. V., Nadeau, R. M., Nishenko, S. P., Reasenberg, P. A., and Simpson, R. W., A Physically-Based Earthquake Recurrence Model for Estimation of Long-Term Earthquake Probabilities, U.S. Geological Survey Open-File Report 99-522, 22p., 1999.

(EPRI NP-4726 1986) Electric Power Research Institute (EPRI), Volumes 5–10, Seismic Hazard Methodology for the Central and Eastern United States, Tectonic Interpretations, July 1986.

(EPRI NP-4726-A 1988) Seismic Hazard Methodology for the Central and Eastern United States, Volume 1, Part 2: Methodology (Revision 1). EPRI NP-4726-A, Rev. 1, dated November 1988.

(EPRI NP-6452-D 1989) Electric Power Research Institute (EPRI), EQHAZARD Primer, Prepared by Risk Engineering for Seismicity Owners Group and EPRI, June 1989.

(EPRI NP-6395-D 1989) Probabilistic seismic hazard evaluation at nuclear plant sites in the central and eastern United States, resolution of the Charleston Earthquake issue, EPRI Rept. 6395-D, Palo Alto, CA, April 1989.

(EPRI TR-102293 1993) Electric Power Research Institute. Guidelines for Determining Design Basis Ground Motions. Volume 5: Quantification of Seismic Source Effects. EPRI Report TR-102293, Project 3302, Final Report, November 1993.

(EPRI 1009684 2004) Electric Power Research Institute, CEUS Ground Motion Project Final Report, Elec. Power Res. Inst, Technical Report 1009684, dated December 2004.

(Fletcher et al. 1978) Fletcher, J. B., Sbar, M. L., and Sykes, L. R., Seismic Trends and Travel-time Residuals in Eastern North America and Their Tectonic Implications: Geological Society of America Bulletin, v. 89, p. 1656-1676, 1978.

(Frankel et al. 1996) Frankel, A., Barnhard, T., Perkins, D., Leyendecker, E. V., Dickman, N., Hanson, S., and Hopper, M., National seismic-hazard maps: documentation, U.S.G.S. Open-File Report 96-532, 1996.

(Frankel et al. 2002) Frankel, A. D., Petersen, M. D., Mueller, C. S., Haller, K. M., Wheeler, R. L., Leyendecker, E. V., Wesson, R. L., Harmsen, S. C., Cramer, C. H., Perkins, D. M., and Rukstales, K. S., Documentation for the 2002 Update of the National Seismic Hazard Maps, U.S. Geological Survey Open-File Report 02-420, 2002.

(Grant and Sieh 1994) Grant, L. B. and Sieh, K., Paleoseismic Evidence of Clustered Earthquakes on the San Andreas Fault in the Carrizo Plain, California, Journal of Geophysical Research, v. 99, n. B4, p. 6819-6841, 1994.

(Hamilton et al 1983) Hamilton, R. M., Behrendt, J. C., and Ackermann, H. D., Land multichannel seismic-reflection evidence for tectonic features near Charleston, South Carolina, Studies Related to the Charleston, South Carolina, Earthquake of 1886- Tectonics and Seismicity, U.S. Geologic Survey Professional Paper 1313-I, p. I1-I18, 1983.

(Johnston 1996) Johnston, A. C., Seismic Moment Assessment of Earthquake in Stable Continental Regions – III. New Madrid 1811-1812, Charleston 1886 and Lisbon 1755, Geophysical Journal International, v. 126, p.314-344, 1996.

(Lee 1996) Lee, R., “Investigations of Nonlinear Dynamic Properties at the Savannah River Site,” *Report No. WSRC-TR-96-0062, Rev. 1*, Aiken, SC, 1996.

(Lee 2001) Lee, R.C., “Development of MFFF-Specific Vertical-to-Horizontal Seismic Spectral Ratios,” Report No. WSRC-TR-2001-00342, Rev. 0, Westinghouse Savannah River Co., Aiken, SC, 2001.

(Lennon 1986) Lennon, G., Identification of a Northwest Trending Seismogenic Graben Near Charleston, South Carolina, U. S. Nuclear Regulatory Commission Report, NUREG/CR-4075, 43p., 1986.

(Madabhushi and Talwani 1993) Madabhushi, S. and Talwani, P., Fault Plane Solutions and Relocations of Recent Earthquakes in Middleton Place-Summerville Seismic Zone near

Charleston, South Carolina, Bulletin of the Seismological Society of America, v. 83, no. 5, p. 1442-1466, 1993.

(Marple and Talwani 1990) Marple, R. T., and Talwani, P., Field investigations of the Woodstock Lineament: Seismological Research Letters, v. 61, no. 3-4, p. 156, 1990.

(Marple and Talwani 1993) Marple, R. T. and Talwani, P., Evidence for possible tectonic upwarping along the South Carolina coastal plain from an examination of river morphology and elevation data: Geology, v. 21, p. 651-654, 1993.

(Marple and Talwani 2000) Marple, R. T. and Talwani, P., Evidence for a Buried Fault System in the Coastal Plain of the Carolinas and Virginia - Implications for Neotectonics in the Southeastern United Sates, Geological Society of America Bulletin, v. 112, no. 2., p. 200-220, 2000.

(Marple and Talwani 2004) Marple, R. T. and Talwani, P., Proposed Shenandoah Fault and East Coast-Stafford Fault System and Their Implications for Eastern U. S. Tectonics, Southeastern Geology, v. 43, no. 2, p. 57-80, 2004.

(Martin and Clough 1994) Martin, J. R. and Clough, G. W., Seismic Parameters from Liquefaction Evidence, Journal of Geotechnical Engineering, v. 120, no. 8, p. 1345-1361, 1994.

(Matthews et al. 2002) Matthews, M. V., Ellsworth, W. L., and Reasenberg, P. A., A Brownian model for recurrent earthquakes, Bulletin of the Seismological Society of America, v. 92, p. 2233-2250, 2002.

(McGuire et al. 2001) McGuire, R.K., W. J. Silva, and C. J. Costantino. Technical Basis for Revision of Regulatory Guidance on Design Ground Motions, Hazard- and Risk-Consistent Ground Motion Spectra Guidelines. prepared for Nuclear Regulatory Commission, NUREG/CR-6728, 2001.

(McGuire et al. 2002) McGuire, R. K., W. J. Silva, and C. J. Costantino, Technical Basis for Revision of Regulatory Guidance on Design Ground Motions: Development of Hazard- & Risk-Consistent Seismic Spectra for Two Sites, Revision 0, prepared for Nuclear Regulatory Commission, NUREG/CR-6769, 2002.

(NIST/SEMATECH 2006) NIST/SEMATECH, e-Handbook of Statistical Methods, http://www.itl.nist.gov/div898/handbook/, accessed 11 January 2006.

(Obermeier 1996) Obermeier, S., Liquefaction-induced features: in Paleoseismology, J. McCalpin (ed.), Academic Press, San Diego, p. 331-396, 1996.

(Obermeier 2005) Obermeier, S., personal communication, September 2, 2005.

(Obermeier et al. 1989) Obermeier, S. F., Weems, R. E., Jacobson, R. B., and Gohn, G. S., Liquefaction evidence for Repeated Holocene Earthquakes in the Coastal Region of South Carolina, Annals of the New York Academy of Sciences, v. 558, p. 183-195, 1989.

(Rockwell et al. 2000) Rockwell, T. K., Lindvall, S., Herzberg, M., Murbach, D., Dawson, T., and Berger, G., Paleoseismology of the Johnson Valley, Kickapoo, and Homestead Valley faults:

clustering of earthquakes in the Eastern California shear zone, Bulletin of the Seismological Society of America, v. 90, no. 5, p. 1200-1236, 2000.

(Savage 1991) Savage, J. C., Criticism of Some Forecasts of the National Earthquake Evaluation Council, Bulletin of the Seismological Society of America, v. 81, n. 3, p. 862-881, 1991.

(Savy et al. 2002) Savy, J. B., Foxall, W., Abrahamson, N., and Bernreuter, D., Guidance for Performing Probabilistic Seismic Hazard Analysis for a Nuclear Plant Site: Example Application to the Southeastern United States, U.S. Nuclear Regulatory Commission, NUREG/CR-6607, 2002.

(Seeber and Armbruster 1981) Seeber, L., and Armbruster, J. G., The 1886 Charleston, South Carolina earthquake and the Appalachian detachment: Journal of Geophysical Research, v. 86, no. B9, p. 7874-7894, 1981.

(SEUSSN 2005) The South Eastern United States Seismic Network catalog is available from the Virginia Tech Seismic Observatory FTP site: http://www.geol.vt.edu/outreach/vtso/anonftp/catalog/susn2003cat.txt, (266 pages), Susn2003cat.txt, bulletin.txt and catalog.txt, downloaded on June 3, 2005.

(Sieh et al. 1989) Sieh, K., Stuiver, M., and Brillinger, D., A More Precise Chronology of Earthquakes Produced by the San Andreas fault in Southern California, Journal of Geophysical Research, v. 94, n. B1, p. 603-623, 1989.

(Smith and Talwani 1985) Smith, W. A., and Talwani, P., Preliminary interpretation of a detailed gravity survey in the Bowman and Charleston, S.C. seismogenic zones: Abstracts with Programs - Geological Society of America southeastern section, v. 17, no. 2, p. 137, 1985.

(SSHAC 1997) SSHAC, Recommendations for Probabilistic Seismic Hazard Analysis: Guidance on Uncertainty and Use of Experts, Prepared by Senior Seismic Hazard Analysis Committee (SSHAC), NUREG/CR-6372, 1997.

(Sykes 1978) Sykes, L. R., Intraplate Seismicity, Reactivation of Preexisting Zones of Weakness, Alkaline Magmatism, and Other Tectonism Postdating Continental Fragmentation: Reviews of Geophysics, v. 16, p. 621-688, 1978.

(Talwani 1982) Talwani, P. An internally consistent pattern of seismicity near Charleston, South Carolina, Geology, Volume 10, 655–658, 1982.

(Talwani 1999) Talwani, P., Fault Geometry and Earthquakes in Continental Interiors, Tectonophysics, v. 305, p. 371-379, 1999.

(Talwani 2000) Talwani, P., Macroscopic Effects of the 1886 Charleston Earthquake, A Compendium of Field Trips of South Carolina Geology, South Carolina Geological Survey, p. 1-6, 2000.

(Talwani 2005) Talwani, P., Personal Communication, September 8, 2005.

(Talwani and Katuna 2004) Talwani, P. and Katunam M., Macroseismic effects of the 1886 Charleston earthquake: Carolina Geological Society field trip guidebook, p. 18, 2004.

(Talwani and Schaeffer 2001) Talwani, P. and Schaeffer, W. T., Recurrence Rates of Large Earthquakes in the South Carolina Coastal Plain Based on Paleoliquefaction Data, Journal of Geophysical Research, v. 106, no. B4, p. 6621-6642, 2001.

(Tarr and Rhea 1983) Tarr, A. C. and Rhea, S., Seismicity Near Charleston, South Carolina, March 1973 to December 1979 in Studies Related to the Charleston, South Carolina Earthquake of 1886: Tectonics and Seismicity, G. S. Gohn (ed.), U. S. Geological Survey Professional Paper 1313, R1-R17, 1983.

(Tarr et al. 1981) Tarr, A. C., Talwani, P., Rhea, S., Carver, D., and Amick, D., Results of recent South Carolina seismological studies: Bulletin of the Seismological Society of America, v. 71, no. 6, p. 1883-1902, 1981.

(Toro 1996) Toro, G. R. (1996). Probabilistic Models of Site Velocity Profiles for Generic and Site-Specific Ground-Motion Amplification Studies. Published as an appendix in Silva, W. J., N. Abrahamson, G. Toro and C. Costantino (1997). "Description and validation of the stochastic ground motion model." Report Submitted to Brookhaven National Laboratory, Associated Universities, Inc. Upton, New York 11973, Contract No. 770573.

(Toro 1997) Toro, G.R. (1997). Probabilistic Models of Site Velocity Profiles at the Savannah River Site, Aiken, South Carolina. Report by Risk Engineering, Inc. to Pacific Engineering and Analysis, April. Published as an appendix in Lee, R.C.; Maryak, M.E.; and McHood, M.D. 1997. SRS Seismic Response Analysis and Design Basis Guidelines. WSRC-TR-97-0085, Rev. 0. Aiken, South Carolina: Westinghouse Savannah River Company.

(Toro 2005) Toro, G.R. (2005). Site-Wide Probabilistic Model of Shear-Wave Velocity Profiles at the Savannah River Site, Aiken, South Carolina. Report by Risk Engineering, Inc. to Bechtel Savannah River Co., October.

(Tuttle 2001) Tuttle, M. P., The Use of Liquefaction Features in Paleoseismology: Lessons Learned in the New Madrid Seismic Zone, central United States, Journal of Seismology, v. 5, p. 361-380, 2001.

(Weems and Lewis 2002) Weems, R. E., and Lewis, W. C., Structural and tectonic setting of the Charleston, South Carolina, region; evidence from the Tertiary stratigraphic record: Geological Society of America Bulletin, v. 114, no. 1, p. 24-42, 2002.

(Weems et al 1997) Weems, R. E., Lemon, E. M., Jr., and Nelson, M. S., Geology of the Pringletown, Ridgeville, Summerville, and Summerville Northwest 7.5-minute quadrangles, Berkeley, Charleston, and Dorchester counties, South Carolina: Miscellaneous Investigations Series - U. S. Geological Survey, 1997.

(Wells and Coppersmith 1994) Wells D.L. and K.J. Coppersmith. New Empirical Relationships Among Magnitude, Rupture Length, Rupture Width, Rupture Area, and Surface Displacement," Bulletin Seismological. Society of America, 84, 4, 974-1002, August 1994.

(Wentworth and Mergener-Keefer 1983) Wentworth, C.M., and Mergener-Keefer, M., Regenerate Faults of the Southeastern United States, in Studies Related to the Charleston, South Carolina, Earthquake of 1886: Tectonics and seismicity, Gohn, G. S. (ed., US Geological Survey Professional Paper 1313, pp. S1-S20, 1983.

(Wheeler 2005) Wheeler, R. L., Known or Suggested Quaternary Tectonic Faulting, Central and Eastern United States- New and Updated Assessments for 2005: U. S. Geological Survey Open-File Report 2005-1336, 2005.

(WGCEP 1995) Working Group on California Earthquake Probabilities, Seismic Hazards in Southern California: Probable earthquakes, 1994 to 2024, Bulletin of the Seismological Society of America, v. 85, p. 379-439, 1995.

(WGCEP 2003) Working Group on California Earthquake Probabilities, Earthquake Probabilities in the San Francisco Bay region: 2002-2031, U. S. Geological Survey Open-File Report 03-2134, 2003.

(WSRC 1998) General SRS Strain Compatible Soil Properties for 1886 Charleston Earthquake (U), Calculation K-CLC-G-0060, McHood, M.D, October 29, 1998.